

**Design, Synthesis and Biological Evaluation of Retinoid and
Non-Retinoid Mimetics of Fenretinide as Chemotherapeutic
Agents**

Rachael Elizabeth Tennant

Submitted in accordance with the requirements for the degree of
Doctor of Philosophy

The University of Leeds

School of Chemistry

September, 2014

The candidate confirms that the work submitted is her own and that appropriate credit has been given where reference has been made to the work of others.

This copy has been supplied on the understanding that it is copyright material and that no quotation from the thesis may be published without proper acknowledgement.

© 2014 The University of Leeds and Rachael Elizabeth Tennant.

The right of Rachael Elizabeth Tennant to be identified as Author of this work has been asserted by her in accordance with the Copyright, Designs and Patents Act 1988.

Acknowledgements

Firstly, I would like to thank my supervisors, Dr Richard Foster and Prof. Sue Burchill. It has been an honour to be Richard's first PhD student and I am very grateful for the opportunity to work on this project. I greatly appreciate his invaluable knowledge, support and guidance throughout my experimental work and write-up. Sue's enthusiasm and passion for research has inspired me greatly and I appreciate her boundless patience, knowledge and encouragement. I am very proud of what we have achieved together, thank you both.

I would also like to thank Prof. Colin Fishwick, Dr Shireen Gopaul and Dr Helen Payne for providing insightful discussions about the research throughout the project.

I'd like to thank the EPSRC and the Charles Brotherton Trust for making this research possible by financially supporting the project.

Thank you to the Foster research group within the School of Chemistry, particularly Dr Jeff Plante and Dr Jayakanth Kankanala who are two of the nicest, most helpful guys imaginable who are both extremely knowledgeable in just about everything! Also to the past and present group members over the last few years who have made my time in Leeds hugely enjoyable. Jeff also contributed to this project by carrying out the deprotection and coupling of affinity chromatography ligand **354** to Sepharose (Chapter 5). Non-retinoid hybrid molecules (**350-352**) were synthesised by Lewis Turner when he worked with me as part of his undergraduate summer-student placement. Thank you both for these contributions.

I'd like to thank the Lab 4 group at LICAP for all of their help; particularly Andrea Berry for teaching me several invaluable biological techniques and never tiring of my 'daft' questions! Thank you to Dr Paul O'Regan for contributing to the project by carrying out the affinity chromatography studies (Chapter 5).

Thanks also go to the technical staff within the School of Chemistry (Tanya Marinko-Covell, Simon Barrett, Martin Huscroft) and LICAP (Liz Straszynski) for their support and advice.

On a more personal note I would like to thank my friends, especially Sarah and Natalie, for reminding me there is a world outside of my PhD! I am forever grateful to my family- my parents Sharon and Paul, Grandma, Auntie Sue and John. Thank you for your endless support and encouragement.

Abstract

Fenretinide is a potent chemotherapeutic and chemopreventive against a range of cancer tumour cell lines, namely Ewing's Sarcoma Family of Tumours (ESFT) which is an aggressive malignant tumour primarily affecting children and young adults. The mechanism of action of the drug is not known. The major disadvantage to fenretinide as a treatment for cancer is its poor *in vivo* efficacy due to poor oral bioavailability, requiring the patient to take many tablets per day regularly in order to achieve an adequate plasma concentration.

By use of computational drug design and medicinal chemistry-led design, we have identified both novel retinoid and non-retinoid mimetics of fenretinide, which demonstrate comparable *in vitro* activity to fenretinide against ESFT cell types. This research has investigated the molecular features of fenretinide which contribute to its inhibition of cell growth in order to establish structure-activity relationships (SAR). We have also investigated the mechanism of cell death for a number of compounds and have identified molecules which appear to induce cell death *via* a similar mechanism to fenretinide as well as those which function *via* an alternative mechanism. Additional studies aimed at understanding the mechanism of action of fenretinide through affinity chromatography studies, have implicated several proteins as potential binding partners for further investigation.

The outcomes of the current project may aid the design of future retinoid or non-retinoid analogues of fenretinide with improved efficacy, whilst retaining the minimal toxicity profile of fenretinide as well as to better understand the mechanism of the chemotherapeutic induction of the cell death process in ESFT cells.

Abbreviations

%	percent
°C	degrees celsius
1D	one-dimensional
3D	three-dimensional
4'-MPR	4'-methoxyphenylretinamide
4-HBR	4-hydroxybenzylretinone
4-HPROG	<i>N</i> -(4-hydroxyphenyl) retinamide- <i>O</i> -glucuronide
ACR	acyclic retinoic acid
ADME	adsorption, distribution, metabolism and excretion
ANP32	acidic (leucine-rich) nuclear phosphoprotein 32 family
app.	apparent
Ar	aromatic
ASK1	apoptosis signal-regulating kinase 1
BAK	BCL2-antagonist/killer
BAX	BCL2-associated X protein
BCL-2	B-cell lymphoma 2
Bn	benzyl
Boc	<i>tert</i> -butoxycarbonyl
br	broad
BSA	bovine serum albumin
Bu	butyl
<i>ca.</i>	<i>circa</i> ; approximately
CDR	coding region determinant

ClogP	calculated logarithm (base 10) of partition coefficient
c-Myc	v-myc avian myelocytomatosis viral oncogene homolog
CNS	central nervous system
CRABP	cellular retinoic acid binding protein
CYP	cytochrome P450
δ	chemical shift
d	doublet
DCC	dicyclohexylcarbodiimide
DCFDA	2',7' –dichlorofluorescein diacetate
DCM	dichloromethane
dd	doublet of doublets
DIPEA	N,N-Diisopropylethylamine
DMAP	4-dimethylamino pyridine
DMBA	7,12-dimethylbenz[α]anthracene
DMF	dimethylformamide
DMSO	dimethyl sulphoxide
DNA	deoxyribose nucleic acid
DNA-PK	deoxyribose nucleic acid-dependent protein kinase
DR	death receptor
<i>E</i>	<i>entgegen</i>
<i>e.g.</i>	<i>exempli gratiā</i> ; for example
EC ₅₀	half maximal effective concentration
EDCI	1-ethyl-3-(3-dimethylaminopropyl) carbodiimide
EDTA	ethylenediaminetetraacetic acid
EF1a1	elongation factor 1-alpha 1
eHiTS	electronic high-throughput screening

EI	electron impact
equiv.	equivalent
ER	endoplasmic reticulum
ESFT	Ewing's sarcoma family of tumours
ESI	electrospray ionisation
Et	ethyl
EtOAc	ethyl acetate
EtOH	ethanol
EWS	Ewing's Sarcoma
FACS	fluorescence-activated cell sorting
FCS	fetal calf serum
flex-hets	flexible heteroarotinoids
g	G-force
GTP	guanosine-5'-triphosphate
h	hour
HBTU	<i>O</i> -Benzotriazole- <i>N,N,N',N'</i> -tetramethyl-uronium-hexafluorophosphate
HEPES	4-(2-hydroxyethyl)-1-piperazineethanesulfonic acid
HPLC	high-performance liquid chromatography
HRMS	high-resolution mass spectrometry
hTERT	telomerase reverse transcriptase
HTS	high-throughput screening
Hz	Hertz
IC ₅₀	half maximal inhibitory concentration
<i>i.e.</i>	<i>id est</i> ; that is
IGF	insulin-like growth factor

IGF1R	insulin-like growth factor 1 receptor
IGF2BP1	insulin-like growth factor 2 mRNA binding protein 1
<i>in silico</i>	performed by computer simulation
<i>in vitro</i>	process taking place outside a living organism
<i>in vivo</i>	process taking place within a living organism
ⁱ Pr	<i>iso</i> -propyl
IR	infrared
<i>J</i>	coupling constant
JNK	c-Jun N-terminal kinases
KO	knock-out
LCMS	liquid chromatography mass spectrometry
LDA	lithium diisopropylamide
logS	logarithm (base 10) of solubility
LXS	Lym-X-Sorb
m	multiplet
MAPK	mitogen-activated protein kinases
Me	methyl
Ms	mesyl
Mel	methyl iodide
MeOH	methanol
mg	milligram
MHz	megahertz
ml	millilitre
μl	microlitre
mM	millimolar
mmol	millimole

mol	mole
MP	melting point
mRNA	messenger ribonucleic acid
MsCl	methanesulfonyl chloride
MSCs	mesenchymal stem cells
MTS	(3-(4,5-dimethylthiazol-2-yl)-5-(3-carboxymethoxyphenyl)-2-(4-sulfophenyl)-2H-tetrazolium)
MTT	3-(4,5-dimethylthiazol-2-yl)-2,5-diphenyltetrazolium bromide
MW	molecular weight
n	number
N/A	not applicable
NADPH	nicotinamide adenine dinucleotide phosphate-oxidase
NaHMDS	sodium hexamethyldisilazide
NaOH	sodium hydroxide
NCI	National Cancer Institute
ND	not determined
NEt ₃	triethylamine
NMR	nuclear magnetic resonance
nOe	nuclear Overhauser effect
PAGE	polyacrylamide gel electrophoresis
PBS	phosphate buffered saline
PDB	Protein Data Bank
Ph	phenyl
pH	power of hydrogen
pK _a	acid dissociation constant
PMSF	phenylmethylsulfonyl fluoride

PP2A	phosphatase 2A inhibitor
Pr	propyl
q	quadruplet
r.t.	room temperature
RA	retinoic acid
Rac1	Ras-related C3 botulinum toxin substrate 1
RAMBAs	retinoic acid metabolism blocking agents
RAR	retinoic acid receptor
RBP4	retinol binding protein 4
RIPA	radioimmunoprecipitation
RNA	ribonucleic acid
ROCS	rapid overlay of chemical structures
ROS	reactive oxygen species
RPMI	Roswell Park Memorial Institute medium
RPSA	ribosomal protein SA
RT	retention time
RXR	retinoid X receptor
s	singlet
SAR	structure-activity relationship
SDS	sodium dodecyl sulfate
SEM	standard error of the mean
STRA6	stimulated by retinoic acid 6
t	triplet
T3P [®]	propylphosphonic anhydride solution
TBAF	tetra-n-butylammonium fluoride
TBDMSCI	tert-butyldimethylsilyl chloride

<i>tert</i>	<i>tertiary</i>
TFA	trifluoroacetic acid
TFAA	trifluoroacetic anhydride
THF	tetrahydrofuran
TLC	thin layer chromatography
TMS	tetramethylsilane
TMSCl	trimethylsilyl chloride
TMSCN	trimethylsilyl cyanide
TOF	time of flight
TRAIL	tumour necrosis factor-related apoptosis-inducing ligand
tris	2-amino-2-hydroxymethyl-propane-1,3-diol
tRNA	transfer ribonucleic acid
TRX	thioredoxin
TsCl	4-toluenesulfonyl chloride
TTNBP	4-[(E)-2-(5,6,7,8-Tetrahydro-5,5,8,8-tetramethyl-2-naphthalenyl)-1-propenyl]benzoic acid
UniProt	Universal Protein Resource
v/v	volume/volume
<i>via</i>	by way of
<i>vs</i>	<i>versus</i>
w/v	weight/volume
WT	wild-type
WT1	Wilm's tumour 1
Z	<i>zusammen</i>

Table of Contents

1. Introduction	1
1.1 Cancer	1
1.2 Ewing's sarcoma family of tumours.....	2
1.3 Drug discovery process	3
1.4 Preclinical testing	4
1.5 Fenretinide background	7
1.6 Mechanism of action of fenretinide	8
1.6.1 Retinoid-receptor mediated pathways.....	8
1.6.2 Retinoid receptor-independent mechanisms.....	9
1.7 Pharmacokinetics of fenretinide	13
1.7.1 Absorption.....	13
1.7.2 Distribution and intracellular delivery	14
1.7.3 Metabolism	15
1.7.4 Limiting the rate of metabolism of fenretinide and analogues	16
1.8 Clinical Efficacy of fenretinide	20
1.9 Side effects of fenretinide	22
1.10 Structure Activity Relationship (SAR) of fenretinide	23
1.10.1 SAR of the phenyl ring	25
1.10.2 SAR for the amide.....	31
1.10.3 SAR for cyclohexene derivatives	32
1.10.4 SAR of the central scaffold	34
1.11 Ligand-based design.....	42
1.11.1 Rapid Overlay of Chemical Structures (ROCS)	43
1.12 Target Validation.....	44
1.12.1 Affinity chromatography	44
1.12.2 Affinity chromatography for retinoid-based ligands	46
1.13 Aims of this Thesis.....	48
2. SAR for fenretinide in ESFT cells	49
2.1 Introduction	49
2.2 SAR study	49
2.2.1 SAR for the 4-hydroxyphenyl group	50

2.2.2	Synthesis of 4-hydroxyphenyl variants.....	50
2.2.3	Biological evaluation of 4-hydroxyphenyl variants.....	51
2.2.4	para-hydroxy and para-amino isosteric replacement	54
2.2.5	Synthesis of para-hydroxy and para-amino isosteres	55
2.2.6	Biological evaluation of the para-hydroxy and para- amine isosteres.....	58
2.2.7	Substitution in the 4-hydroxyphenyl ring	60
2.2.8	Synthesis of substituted 4-hydroxyphenyl analogues	60
2.2.9	Biological evaluation of substituted 4-hydroxyphenyl analogues	62
2.2.10	Additional phenyl analogues	64
2.2.11	Synthesis of additional phenyl analogues	64
2.2.12	Biological evaluation of additional phenyl analogues	66
2.3	Amide isosteres	68
2.3.1	Variation at the N-H position of the amide group	68
2.3.2	Variation at the carbonyl group	71
2.3.3	In vitro activity of amide isosteres	74
2.4	Central scaffold analogues	75
2.4.1	Synthesis of central scaffold analogues.....	76
2.4.2	Biological evaluation of central scaffold analogues.....	76
2.5	Substituted cyclohexyl analogues.....	78
2.5.1	Synthesis of substituted cyclohexyl analogues	78
2.5.2	Biological evaluation of substituted cyclohexyl analogues	80
2.6	Summary of SAR for fenretinide in ESFT cells	82
3.	Non-retinoid mimetics of fenretinide	84
3.1	General strategy	85
3.2	Identification of non-retinoid mimetics of fenretinide by ligand- based design.	85
3.2.1	Hit identification by ligand-based searches using ROCS ...	85
3.2.2	Biological evaluation	86
3.2.3	Optimisation of the rhodanine (251) and bis-amide (252)	89
3.2.4	Summary of results	94
3.3	Identification of non-retinoid mimetics of fenretinide by substructural search.....	94

3.3.1 Substructural search	94
3.3.2 Biological evaluation	95
3.4 Identification of non-retinoid mimetics of fenretinide with novel polar head-units	98
3.4.1 Substructural searches	98
3.4.2 Biological evaluation of compounds containing the 4-aminophenyl substructure	99
3.4.3 Biological evaluation of compounds containing the 4-pyridyl substructure	101
3.4.4 Summary of results	102
3.5 Optimisation of compounds 272-274, 276 and 299	103
3.5.1 Substructural searches of compounds compounds 272-274, 276 and 299	104
3.5.2 Biological evaluation of compounds bearing the substructure of compound 274	105
3.5.3 Biological evaluation of compounds bearing the 276 substructure	106
3.5.4 Biological evaluation of compounds bearing the 4-pyridyl substructure of compound 299	107
3.5.5 Biological evaluation of compounds bearing the 272 and 273 substructures	109
3.5.6 Summary of results	109
3.6 Validation of the hit compounds	110
3.6.1 Resynthesis of selected hits	111
3.6.2 Biological evaluation of resynthesised hits	112
3.7 Hybrid analogues	114
3.7.1. Design and synthesis of hybrid analogues	114
3.7.2 Biological evaluation of the 'hybrid' compounds	115
3.8 Conclusions	116
4. Preclinical evaluation of hit compounds	119
4.1 Concentration response studies	121
4.1.1 Concentration response of fenretinide	121
4.1.2 Concentration response of compound 200	122
4.1.3 Concentration response of compound 199	123
4.1.4 Concentration response of compound 58	124
4.1.5 Concentration response of compound 299	125
4.1.6 Concentration response of compound 276	126

4.2 Caspase-3 activation	127
4.3 Generation of ROS	129
4.4 ADME properties.....	130
4.5 Conclusion	131
5. Target identification by affinity chromatography.....	134
5.1 Design of Sepharose-supported ligands for affinity chromatography	134
5.2 Synthesis and biological affirmation of solid supported ligands for affinity chromatography	135
5.2.1 Design of solid supported ligands	135
5.2.2 Synthesis of the oxime linkered solid supported ligand (353)	136
5.2.3 Affirming biological activity of the oxime linkered ligand ...	139
5.2.4 Synthesis of the acyl-hydrazone linkered solid supported ligand	140
5.2.5 Affirming biological activity of the acyl-hydrazone linkered solid supported ligand 354	142
5.3 Negative controls	142
5.3.1 Synthesis of the benzylamine linkered solid supported ligand (365).....	144
5.3.2 Affirmation of absence of biological activity of the benzylamine solid supported ligand.....	144
5.3.3 Synthesis of the para-methoxy oxime solid supported ligand	145
5.3.4 Affirmation of absence of biological activity of the para-methoxy oxime solid supported ligand.....	146
5.4 Affinity chromatography	147
5.4.1 Isolation of membrane proteins binding to fenretinide.....	147
5.4.2 Literature review of binding fragments	149
5.5 Conclusion	152
6. Discussion and future work.....	154
7. Experimental	160
7.1 Materials	160
7.2 Methods	160
7.3 Synthesis	161
7.3.1 Phenyl analogues	161
7.3.2 Central scaffold analogues	192

7.3.3 Amide isosteres	194
7.3.4 Cyclohexyl analogues	203
7.3.5 Non-retinoid analogues	216
7.4 ROCS ligand-based database search.....	225
7.5 Biological evaluation	225
7.5.1 Cell lines and tissue culture	225
7.5.2 Preparation of stock solutions	226
7.5.3 Seeding of cells.....	226
7.5.4 Effect of compounds on viable cell number	227
7.5.5 Statistical analysis of data.....	227
7.6 ROS studies.....	228
7.7 Caspase-3 activation	228
7.7.1 Protein extraction	228
7.7.2 Protein assay	229
7.7.3 SDS-Polyacrylamide Gel Electrophoresis (SDS-PAGE) ...	229
7.7.4 Western blot.....	230
7.8 Affinity chromatography	230
7.8.1 Preparation of Sepharose affinity chromatography resin ..	230
7.8.2 Enrichment of cellular protein extracts for membrane proteins.....	231
7.8.3 Pull down assay	232
7.8.4 Identification of proteins	232
References.....	234
Appendix A – compound activity in TC32 cells.....	248
Appendix B – concentration response by cell line	250
Appendix C – mass spectroscopy analysis of binding proteins	253

1. Introduction

1.1 Cancer

Cancer is a term which covers a broad class of diseases that arise leading to abnormal cells which divide uncontrollably and have aberrant cell survival pathways. Cancer cells emerge from normal tissue as a result of the accumulation of unchecked mutations in genes within the cell.¹ These could be mutations in genes that enhance proliferation (*e.g.* oncogenes such as Ras, receptor tyrosine kinases) or inhibit the tumour suppressor function (*e.g.* tumour suppressor genes such as p53, p16).² The abnormal cells build up resistance to the regulatory pathways that maintain the tissue microenvironment, therefore allowing them to rapidly grow and resist apoptosis by programmed cell death. Six key biological features of cancer cells, described in the majority of cancer types, are known as the ‘hallmarks of cancer’ and include the ability to invade adjacent tissues and metastasise by inducing angiogenesis (forming new blood vessels from pre-existing vessels, therefore creating its own independent microenvironment).³ Cancer cells are self-sufficient in growth signals, with an ability to sustain unlimited proliferation, resist sensitivity to growth inhibitory signalling and evade apoptosis, leading to replicative immortality.⁴

Although 90–95 % of cancers are attributed to environmental factors (for example, cigarette smoking, obesity, alcohol, sun exposure, environmental pollutants, infections), 5–10 % of all cancer cases are a result of somatic or germline genetic defects.^{1,5} Cancer is a major disease globally which is on the rise; as of 2012 there were 14 million new cases reported annually, predicted to increase to 22 million over the next two decades. In which time, deaths from the disease are predicted to escalate from *ca.*8 million to *ca.*13 million annually.⁶ Furthermore, cancer is the most common disease responsible for mortality among children in developed countries.⁷

1.2 Ewing's sarcoma family of tumours

Although rare, Ewing's sarcoma family of tumours (ESFT) and other small round cell tumours (e.g. neuroblastoma) account for approximately 15 % of known childhood cancers.⁸ Primarily affecting children and young adults, ESFT includes Ewing's sarcoma, peripheral primitive neuroectodermal tumours and Askin's tumour. This family of tumours is defined by non-random gene rearrangements between the *EWS* gene and members of the *ETS* gene family. The majority of ESFT cell types contain a tumour-specific t(11;22)(q24;q12) chromosomal rearrangement, resulting in a EWS-Fli1 (type 1 or type 2) or EWS-ERG fusion transcript.⁹ Ewing's sarcoma is one of the most frequently encountered types of malignant bone tumour and was initially identified and characterised in 1921 by James Ewing as a small round blue cell tumour (*Figure 1.1*) emerging from endothelial cells.¹⁰ However, it has since been identified as a neuroectodermal tumour arising from cells in the early stages of differentiation, most likely mesenchymal stem cells of the mesoderm or neural crest.¹¹ The tumours arise in the majority of skeletal sites but predominate in long bones of the leg, the pelvis, arms and ribs and occasionally in soft tissues.^{12,13} Symptoms caused by the presence of the tumour can include pain and swelling in the region of the tumour, as well as weight loss and fever. The aetiology of ESFT is thought to

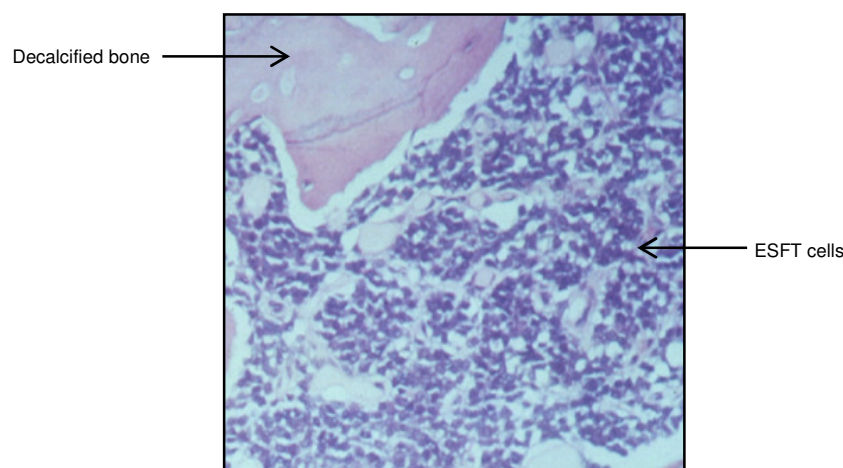


Figure 1.1 Histology of Ewing's sarcoma of the bone. The nuclei of tumour cells are stained blue with haematoxylin and the scant cytoplasm stained pink with eosin. The decalcified bone also takes up the eosin and so appears pink when examined by light microscopy.

be a consequence of several contributing factors, both environmental and genetic.¹³

Current treatment for ESFT typically includes local control of the tumour by radiotherapy and surgery, as well as essential systemic chemotherapy when there is disease at multiple sites. However, the disease is currently extremely difficult to cure, reflecting high local and systemic relapse rates even after an initial response to treatment.¹⁴ For those patients that present with localised disease, the disease free 5 year survival rate is *ca.* 45-60 %. In *ca.* 30 % of patients the disease will be metastatic at diagnosis, reducing 5 year survival rates to *ca.* 20-40 %; the 5 year disease free survival rate for patients with metastasis to the lungs is *ca.* 40 % and to the bone and/or bone marrow *ca.* 20 %. Even when disease is localised at diagnosis *ca.* 50 % of patients experience recurrence of the tumour which is likely to be caused by minimal disease remaining at the treated site or that which has spread to multiple sites.¹⁵ These poor survival rates emphasise the need for new, more effective, therapeutic agents to treat patients with ESFT.

1.3 Drug discovery process

The discovery of drugs, validation and introduction into clinical practice is a long process with a high attrition rate. Development of anticancer drugs takes on average 10-15 years, with less than 7 % successfully progressing from phase 1 toxicity studies to approval.^{16,17,18} The drug discovery process starts by identifying molecules, called hits or leads, that demonstrate a phenotype appropriate for treatment of the disease in question. Hits or leads can be identified by a variety of methods including structure-based design (where the nature and structure of the biological target is known), ligand-based design and high-throughput screening (HTS) of large libraries of compounds. Once a hit or lead is identified, extensive studies of its biological properties are performed in order to understand its pharmacology, pharmacokinetics and toxicology (preclinical testing, see Section 1.4). Over a long process iterative optimisation of these properties by structural modification of the hit or lead allows generation of a preclinical candidate suitable for progression into clinical trials.

1.4 Preclinical testing

Preclinical testing is important to gain sound reassurance that potential drug-like compounds are likely to have good efficacy and safety in clinical trials; indeed it is a prerequisite of law that a compound has been preclinically tested in an animal model before entering human clinical trials.¹⁹ Unfortunately, many compounds fail during clinical trials, unduly costing lives of some patients.²⁰ There is also a huge investment of time and money by pharmaceutical companies to enter a drug candidate into clinical trials which will often fail.^{20,21}

In vitro cell line screening is primarily used as an initial assay to identify compounds which have significant activity against a panel of cell lines.²² However, this method has several drawbacks. Firstly, for many cancer types it can be difficult to establish a tumour cell line. Secondly, tumour cell lines will most likely consist of selected cells that survive under culture conditions and thirdly cell lines that have been in culture for many years are likely to have adapted. Consequently, most tumour cell lines lack particular tumour characteristics and do not truly represent the cancer type which they propose to model.²² Furthermore, where cell lines have been established they will lack supportive interactions from the host such as a stromal environment.²⁰ Factors which are not taken into account and tested in the *in vitro* model include tumour cell heterogeneity, pharmacokinetics and pro-drug bio-activation; such *in vitro* assays are also unable to provide an indication of therapeutic index.²³ Nevertheless, these high throughput and low-cost tests provide information on the activity of a compound *in vitro* and are frequently used as a first screen to identify compounds with the potential to be effective *in vivo*.

A particularly high-throughput method for identifying hit compounds is to screen using the National Cancer Institute 60 (NCI60) anticancer drug screen. This consists of panels of cell lines that essentially represent a range of nine major tumour types: leukaemia, colon, lung, CNS, renal, melanoma, ovarian, breast and prostate.²⁴ However, the panel primarily focuses on adult tumour types therefore ESFT and neuroblastoma cell lines are not included.

Compounds are screened over a 5-log concentration range over 48 h using the sulphorhodamine B assay. Although this colorimetric assay is less accurate at predicting cytotoxicity than measuring cell viability (*i.e.* using the trypan blue exclusion assay), it allows for high-throughput screening of large batches of compounds. The compound screening service is available free of charge and the results are publically available for 43,000 out of *ca.*85,000 that have been screened.²⁵ The database provides the largest source of cell-based anticancer testing data to date which is accessible through PubChem.²⁶ Using this database, it is also possible to identify compounds which may exhibit a similar mechanism of action by comparing patterns of activity across the cell line panel; this is achieved using a computerized pattern recognition programme known as the 'COMPARE algorithm'. This method has proven successful in positively correlating the phenotype produced by compounds with known inhibitors to identify the target that the compound interacts with.²⁷ The NCI60 drug evaluation programme remains an invaluable tool for identification of novel anticancer agents, with around 2 % of the hit compounds proceeding from the *in vitro* screen to *in vivo* studies.

Subcutaneous tumour growth in immune-compromised mice is used for initial toxicity and activity studies *in vivo*. Animal models provide vital information on how a potential drug compound may perform in living organisms and provide an invaluable bridge between *in vitro* studies to *in vivo* patient trials.²⁸ As well as potentially predicting the *in vivo* efficacy of the compound in humans, informative pharmacological and toxicological data can be obtained.²¹ As they possess genomes over 95 % identical to humans, mice are primarily used for *in vivo* studies of potential anti-cancer drugs.²⁸ Human tumour xenografts can be easily formed in mice by injection of human tumour cells subcutaneously, which is the most widely employed method due to the reliability, reproducibility and predictions of efficacy in man are most accurate.^{21,28} Alternatively, an orthotopic model can be employed whereby a human tumour is implanted into the mouse at the site equivalent to where the tumour would arise in man. This method may possess benefit in that the tumour is in an environment that more closely represents the site in which the original tumour arose, and therefore may better represent the original

human tumour. However, insertion of the tumour into some anatomically relevant sites is often impractical and certainly more challenging than subcutaneous injection of tumour.²⁸ Another possibility is to utilise genetically engineered mice that are susceptible to development of cancer that recapitulates the human disease. Such models are thought to have great potential in screening of target-based therapies which induce cytotoxicity through changes in the tumour or its microenvironment.²¹ However, this method is not routinely used in preclinical testing and may be the least reproducible across different laboratories as tumour location, metastasis and onset varies greatly between the mice used in any group.²⁸

Although *in vivo* studies benefit from providing a more realistic environment for the cells compared to *in vitro* studies, as the tumour is able to form interactions with surrounding microenvironment, this may differ considerably between the mouse model and humans. Therefore it cannot be assumed that this is an accurate prediction of how the drug candidate may perform in a human model. In man, the complexity of the human tumour can be much greater and many factors will differ to the mouse model, such as the size, position and stromal interactions with the tumour. Therefore there is doubt over the predictive value of preclinical tests. Speculation over reliability arose when analysis of both xenograft data and Phase II clinical trial results by Johnson *et al.* found that data collected in *in vitro* studies did not correlate with activity in subcutaneously grown tumour models, which in turn was not reflected in clinical activity.²⁹ However, there is strong evidence to support the reliability of the subcutaneous tumour model for prediction clinical activity. A study carried out by Fiebig *et al.*, consisting of 80 comparisons between subcutaneous tumours in mice and clinical studies, found that clinical efficacy was correctly predicted in 90 % of tests for tumour sensitivity and 97 % for tumour resistance.³⁰ Even with these limitations, preclinical testing is an important pathway to identify lead agents for evaluation in man; maybe most importantly identifying agents and agent combinations that are toxic and have poor bioavailability that should not be taken forward.

An understanding of the pharmacokinetic properties of the drug candidate, can be assessed *in vitro* (e.g. permeability, solubility, metabolic stability) and

in *in vivo* animal models (*e.g.* clearance rate, half life and volume of distribution).^{31,32} These studies can support the pharmacological investigation by correlating predicted drug concentrations in plasma or tissue with predicted efficacy in man.

1.5 Fenretinide background

Vitamin A (retinol) was identified to have significant chemopreventive effects, due to observation of epithelial abnormalities that could progress to neoplastic lesions in retinol-deficient animals.³³ However, the toxicity of vitamin A at the therapeutic dose has prevented it from being a successful treatment. Fenretinide (1) (*Figure 1.2*), an analogue of vitamin A, is a synthetic amide formed from all-*trans*-retanoic acid and 4-aminophenol and was first synthesised by Johnson & Johnson in the 1970s. It was initially patented as a potential sunscreen agent owing to its ultraviolet absorption properties³⁴ and was later identified and patented as a potential chemotherapeutic agent for epithelial and breast cancer.^{35,36} However, the drug was not brought to market and is now out of patent.

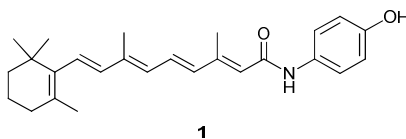


Figure 1.2 Molecular structure of fenretinide.

Fenretinide has since been found to have effective chemotherapeutic and chemopreventive activity in a wide range of human tumour cell lines by inducing apoptosis and growth inhibition.³⁷ Clinical data suggests that it is one of a few retinoids which shows great potential as a chemotherapeutic agent due to its potent apoptosis-inducing properties, low off-target toxicity and favourable biological activity in a wide range of targets.³⁸ It has been, and continues to be, evaluated in clinical trials where it has also been identified to be effective towards several cancer cell lines, including lung, breast, head and neck, prostate and skin cancer.^{39,40,41,42} Previous trials have evaluated fenretinide in children diagnosed with neuroblastoma as both a

maintenance therapy as well as a primary anti-tumour agent in patients in early-stages of the disease (see Section 1.8).

The major limitation which prevents fenretinide from being a successful chemotherapeutic agent is its poor oral bioavailability. The drug is not easily absorbed into the body due to the high lipophilicity of the compound, requiring administration of large quantities of the drug to achieve required plasma levels for effective activity.^{43,44}

1.6 Mechanism of action of fenretinide

Although the intracellular pathways executing the effects of fenretinide have been well described in different cancer types, how fenretinide initiates cell death remains controversial.^{40,45,46} Potential mechanisms of action are cell-type specific and can be retinoid-receptor mediated or non-receptor mediated.

1.6.1 Retinoid-receptor mediated pathways

A receptor-mediated pathway was identified by suppression of fenretinide-induced apoptosis in the presence of a nuclear retinoic acid receptor-specific antagonist, indicating that retinoic acid receptors (RAR) may play an important role in apoptosis of a range of cancer cells (*e.g.* head and neck squamous cell carcinoma, non-small-lung cell carcinoma and human prostate cancer carcinoma cells).^{40,46}

In a study of the effect of fenretinide on a panel of F9 murine embryonal carcinoma cell lines, which includes wild-type (F9-WT) and mutant cells (F9-KO) that have disrupted genes for both RXR- α and RAR- γ retinoid receptors, two distinct effects were identified. Firstly, inhibition of cell-growth is induced rapidly at higher concentrations in both F9-WT and F9-KO cells. Secondly, a slower induction of cell cycle arrest and accumulation in the G₁ phase was observed at lower concentrations in F9-WT cells only.³⁸ This indicates that fenretinide may function differently at varying concentrations (*i.e.* RAR/RXR-dependent mechanism at lower concentrations and independent at higher concentrations).⁴⁷ Transactivation assays have identified that fenretinide upregulates both RAR- β and RAR- γ gene expression at concentrations as

low as 1 μM , which is thought to be a contributor to its apoptotic effects.^{48,49} However, the induction of apoptosis through this mechanism is not the predominant route to cell death in most cell lines due to the low affinity for binding of fenretinide to RARs. Fenretinide binds to RARs and activates these receptors much less strongly than the native ligand, all-*trans*-retinoic acid, and therefore exhibits significantly lower toxicity than the parent compound.^{43,50}

1.6.2 Retinoid receptor-independent mechanisms

There are alternative mechanisms, independent of RAR activation, through which fenretinide initiates cell death in cancer but not in normal cells, although these are poorly understood.^{51,52}

A range of cell types have shown suppression of fenretinide-induced apoptosis upon pre-treatment with an oxidising agent, consistent with the hypothesis that the mechanism is dependent upon reactive oxygen species (ROS). The generation of ROS gives rise to an important retinoid receptor-independent mediated pathway for fenretinide-induced cell death which has been described in several cell lines.^{40,45,46,49,53}

ROS are highly reactive activated species of oxygen in the reduced state. Examples of ROS measured within the cell include superoxide ($\text{O}_2^{\cdot-}$), hydroxyl radicals (OH^{\cdot}), singlet oxygen (O_2^*) and hydrogen peroxide (H_2O_2).⁵⁴ ROS are generated through multiple mechanisms which can be specific to cell type. A major source of ROS generation is NADPH complexes (primarily complexes I and III) and several additional sites located in cell mitochondria.^{55,56}

Although cellular functions of ROS remain largely unknown, they have been reported to drive cell signalling and cell death pathways.^{57,58,59} Elevated levels of production are known to play a role in tumour biology, with oxidative stress causing damage to DNA which can contribute to cancer initiation and progression.⁶⁰

Despite their frequent involvement in the development of cancers, ROS are also known to have therapeutic effects by induction of necrosis and apoptosis. It is thought that the ROS can initiate several independent cell-death cascades, for example, mitochondrial membrane permeability transition, caspase activation, protein degradation, DNA damage and extensive oxidation of cellular components, which leads to subsequent cell-death.^{61,62,63} Oxidative stress resulting from accumulation of ROS in the cell is thought to activate sphingomyelinases and increase ceramide production, which in turn promotes apoptosis in response to secretion of inflammatory cytokines.⁶⁴ Metabolism of ceramide to glycosphingolipid GD3 increases cellular levels of GD3, which is thought to increase the activity of 12-lipoxygenase and has been shown to induce apoptosis through oxidative stress-dependent induction of the transcription factor GADD153 and pro-apoptotic protein BAK.^{63,64,65}

Fenretinide is known to generate mitochondrial ROS, this being critical for induction of apoptosis in neuroblastoma cells.⁶⁶ Previous research within our group has demonstrated that increased levels of ROS are observed in all substrate adherent ESFT cell lines compared to neuroblastoma cell lines, which correlated with the increased sensitivity of the ESFT cells towards fenretinide induced cell death.⁶⁷ Furthermore, cell death of ESFT cells was rescued by co-treatment with antioxidant vitamin C which eliminates ROS, indicating that ROS play an important role in the initiation of cell death. Several possible co-factors for fenretinide-induced cell death by ROS-dependent mechanisms have been identified within the group (*Figure 1.3*). p38^{MAPK} is activated by release of apoptosis signal-regulating kinase 1 (ASK1) from its complex with theoredoxin (TRX). TRX binds ASK1 in its reduced form but upon oxidation by ROS a disulphide bridge forms between two cysteine residues within the active site and releases ASK1.⁶⁸ ASK1 becomes activated by phosphorylation, which in turn leads to phosphorylation and activation of p38^{MAPK}.⁶⁹ Activated p38^{MAPK} induces mitochondrial membrane depolarisation and subsequent release of cytochrome C into the cytoplasm; the release of cytochrome C can be regulated by pro- and anti-apoptotic mitochondrial membrane proteins such

as BAX and BCL-2.^{70,71} These are critical components of the cell death cascade which are downstream of elevated ROS levels. Activation of c-Jun N-terminal kinase (JNK) was also observed, although it is unclear as to whether this is dependent upon ROS production and if this is an essential component in the cell death cascade in all cell types. Finally, caspase-9 followed by caspase-3 activation was observed, which was found to be dependent on ROS generation, p38^{MAPK} activation and mitochondrial membrane depolarisation ($\Delta\Psi_m$). Caspase activation is a critical step that marks the point of no return in the cell death cascade. Caspases are a family of cysteine proteases for which sequential activation leads to initiation of cell death *via* apoptosis. Full length caspases exist in the inactive form as proenzymes which undergo proteolytic cleavage at specific aspartate residues, to yield two sub-units (large and small), which upon dimerisation form the active enzyme.^{72,73} Caspase-3, for example, is cleaved from a 32 kDa zymogen into 17 kDa and 12 kDa subunits upon activation by either intrinsic (pro-apoptotic intracellular mediated) or extrinsic (receptor-mediated) pathways.

ROS dependent cell death is consistent with findings made by other groups

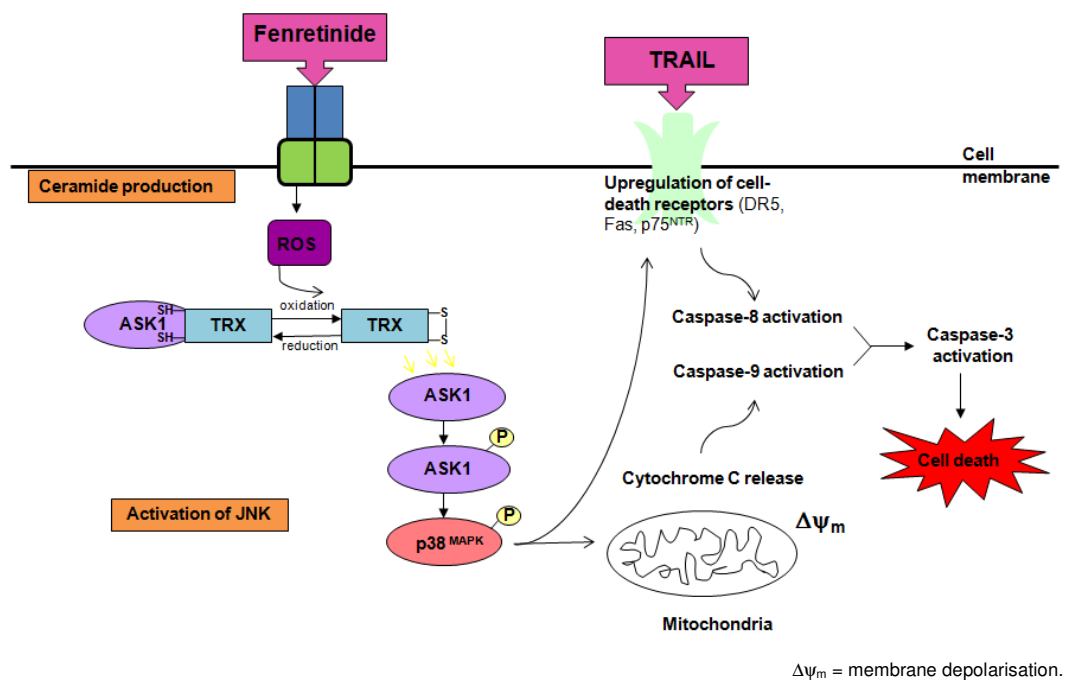


Figure 1.3 Intracellular signalling cascades of fenretinide-induced apoptosis.^{67,68,69,77}

against a range of cancer types. For example, a stress response to an increase in cellular ROS has been observed to induce the elimination of ovarian cancer cells. This was also determined by the observation of inhibition of fenretinide-induced apoptosis upon pre-treatment of the cells with the antioxidant vitamin C, which quenches the ROS therefore blocking this mechanism of action.⁷⁴ In this cell line, ROS were shown to activate the endoplasmic reticulum (ER) stress response, which subsequently induces JNK activation, consequently leading to apoptosis.³⁰ Other cancer types for which fenretinide-induced ROS production is critical for cell death include selected cell lines of human prostate cancer,⁴⁶ human leukemia,⁷⁵ cervical carcinoma,⁷⁶ head and neck, and lung cancer.⁴⁶

Another pathway of fenretinide-induced apoptosis, independent of mitochondrial membrane depolarisation but dependent on ROS generation, has been identified within the Burchill group. This is dependent on upregulation of cell surface death receptor (DR) proteins (DR5, Fas and p75^{NTR}) in an ASK1- and p38^{MAPK}-dependent manner.⁷⁷ Our group investigated co-treatment of ESFT cells with fenretinide and TRAIL, a cell death ligand which induces caspase-dependent apoptosis. Activation of caspase-8 was observed upon co-treatment, but was not activated by the respective ligands independently. Fenretinide therefore appears to upregulate cellular DRs, enhancing the caspase-dependent apoptosis of TRAIL.

Ulukaya *et al.* also recently investigated the application of fenretinide (due to its known ROS generation activity) in combination with caspase-activating TRAIL.⁷⁸ Caspase-3 activation was not observed upon treatment of the MDA-MB-231 breast cancer cell line with fenretinide but was upon treatment with TRAIL. The IC₅₀ values of fenretinide and TRAIL in this cell line were 2.7 µM and 19.5 ng/ml respectively. It is therefore thought that fenretinide induces cell death *via* a caspase-3 independent mechanism in this cell line (*e.g.* ROS-dependent mechanism). Strikingly improved activity was observed at a combined dose of 2.5 µM fenretinide and 20 ng/ml TRAIL, where cell viability was reduced to *ca.* 25 %. At the same concentrations, cells treated with fenretinide or TRAIL separately demonstrated *ca.* 80 % and *ca.* 60 %

viability respectively. This suggests that fenretinide may act through different mechanisms in different cell lines and combining fenretinide treatment with a compound that activates a complementary cell death mechanism to itself may induce additive or synergistic cell death.

1.7 Pharmacokinetics of fenretinide

The pharmacokinetics (known as absorption, distribution, metabolism and excretion (ADME)), of fenretinide has been extensively studied. To be a useful clinical agent, a drug must not only elicit a potent and selective biological effect, but also demonstrate a good pharmacokinetic profile in order to have the potential for sufficient exposure at the target site. Ideally a drug will have a long half-life, low clearance and good oral bioavailability in order to limit the dosing requirements.

1.7.1 Absorption

The main disadvantage of fenretinide as a therapeutic agent is its poor bioavailability due to poor oral absorption of the drug. This could be due to several possible factors, including poor aqueous solubility (< 10 ng/ml), accumulation in lipophilic cell membranes, inadequate absorption in the gastrointestinal tract and poor metabolic stability.^{44,79,80,81,82} Reflecting the poor ability of fenretinide to pass through the gut wall, it is excreted primarily in faeces.⁴⁴

A study of transport of fenretinide across Caco-2 cell monolayers was carried out and the drug was found to permeate the membrane by passive diffusion, moving from a region of high concentration to a region of lower concentration, at a poor rate.⁴⁴ After 3 h, there was a 16 % decrease in the initial fenretinide concentration in the donor well; however only 0.12 % of this diffused into the receiver well, indicating that the majority of the transported fenretinide was remaining within the cell bilayer. Accumulation of the drug in the lipid cell bilayer, commonly observed for highly hydrophobic molecules, is therefore a limitation to the rate of transport *via* the transcellular route. Tight junctions and a small surface area cause the paracellular route through the gut wall to be inefficient in comparison, and transport through the water-filled

pores is not considered to be a significant pathway for highly lipophilic species such as fenretinide.

1.7.2 Distribution and intracellular delivery

Using current oral formulations of fenretinide it is possible to achieve plasma concentrations of *ca.*10 μM , which may be effective for some cancer types.^{14,82} Unfortunately, the highly lipophilic nature of fenretinide results in accumulation of the drug in fatty tissue which is likely to hinder the distribution process and prevent high enough concentrations of the drug from reaching a specific target.⁴⁵ In certain cases this property may also be a benefit, where the cancer is formed in an area with a high density of fatty tissue. For example, this may contribute to its effectiveness against breast cancer, for which a series of phase III trials proved that fenretinide significantly reduced the risk of recurrence of breast cancer in premenopausal women.⁸³ However, this property is a disadvantage for many other targets as the effective concentration at the required site can be significantly reduced.

Fenretinide has been shown to bind to the retinol binding protein 4 (RBP4) in a similar manner to retinol, leading to suggestions that RBP4 is likely to be responsible for the transport of the drug in blood around the body and potentially a cofactor to its transport into the cell.^{84,85} It is thought that fenretinide is able to penetrate the cell membrane of ESFT cells through a cell surface receptor, STRA6, in a similar fashion to retinol; this hypothesis is currently being investigated by Dr Helen Payne and Professor Sue Burchill.⁸⁶ The STRA6 transmembrane protein is encoded by the gene *STRA6* which is part of a collection of genes that are activated by retinoic acid. This extensive group of genes are known to encode many transmembrane proteins and other proteins for which their purpose is unknown.⁸⁷ The STRA6 receptor is known to bind to the retinol-RBP4 complex at the cell surface with high affinity, aid removal of retinol from RBP4 and transport the molecule across the cell membrane.⁸⁷

1.7.3 Metabolism

As the liver metabolises foreign chemicals to more favourable compounds for excretion from the body, metabolism of fenretinide may be disadvantageous owing to a lowering of the plasma concentrations of the compound.⁴⁷ Two metabolites of fenretinide have been described : 4'-methoxyphenylretinamide (4'-MPR) (**2**), containing a methoxy substituent in place of the hydroxy group of fenretinide and 4-oxo-fenretinide (**3**), which contains a carbonyl group at the 4-position of the cyclohexene ring of fenretinide (*Figure 1.4.*)³⁷ 4'-MPR is reported to be the most abundant metabolite in human plasma following fenretinide administration. However, this metabolite is biologically inactive.³⁷ This is thought to reflect the lack of an ionisable substituent on the phenylamine ring which may reduce binding affinity to a relevant receptor site(s) and also inhibit ROS formation, therefore preventing apoptosis *via* this mechanism.^{37,38,45} Breakdown of fenretinide to 4'-MPR may therefore be a disadvantage and it could be favourable to block the degradation of fenretinide *via* this route.

4-Oxo-fenretinide (**3**) (*Figure 1.4.*) was later identified in the plasma and has been found to have significantly higher biological activity, including higher growth-inhibitory and apoptotic effects, than the parent drug.³⁷ The IC₅₀ concentrations of 4-oxo-fenretinide are significantly (*ca.*2-4 times) lower than those for fenretinide in an *in vitro* cell proliferation assay against neuroblastoma cell lines,⁴⁷ and are at least equivalent to the IC₅₀ for fenretinide in ESFT cell lines.⁸⁶ However induction of apoptosis by 4-oxo-fenretinide induced cell cycle arrest in the G₂-M phase, rather than the G₁

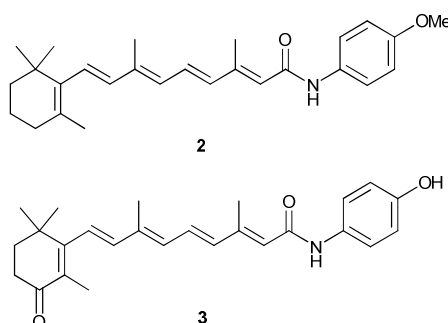


Figure 1.4 Molecular structures of metabolites methoxyphenylretinamide (**2**) and 4-oxo-fenretinide (**3**).

phase as for fenretinide, resulting in lack of cross-resistance and synergy when combined with fenretinide.³⁷ The formation of 4-oxo-fenretinide was identified to be due to induction of expression of a retinoic acid-metabolising enzyme, cytochrome P450 26A1, which catalyses the specific hydroxylation of fenretinide at the 4-position of the cyclohexene ring.⁸⁰

The observed C_{max} observed for both metabolites was lower than that for fenretinide, indicating that they may be excreted from the blood more readily than the parent drug. Therefore, despite 4-oxo-fenretinide having higher biological activity, the lower achievable concentration *in vivo* could reduce the effective activity due to a significantly lower amount reaching the target.

1.7.4 Limiting the rate of metabolism of fenretinide and analogues

This section describes approaches to reduce the rate of metabolism of fenretinide and analogues *in vivo*. These methods include the inhibition of enzymes responsible for metabolism of fenretinide (using metabolism blocking agents), as well as the synthetic variation of fenretinide to generate analogues with an improved metabolically stability profile.

1.7.4.1 Metabolism blocking agents

Roberts *et al.* originally identified the cytochrome P450 enzymes (CYPs) to be primarily responsible for oxidative metabolism of retinoic acid (**6**). The group's experiments concluded that the microsomal location of these enzymes, in addition to the requirement for NADPH and oxygen, suggested a CYP-dependent enzyme system.⁸⁸ CYPs metabolise all-*trans*-retinoic acid *via* several routes leading to a mixture of polar metabolites. Initially, 4-hydroxy-all-*trans*-retinoic acid (**4**) is formed; this is thought to be the physiologically most favourable pathway and rate-limiting step to alternative metabolites. Other metabolism products identified are 4-oxo-all-*trans*-retinoic acid 18-hydroxy-all-*trans*-retinoic acid (**5**), and 5,6- epoxy-all-*trans*-retinoic acid (**8**) by epoxidation and radical oxidation (*Figure 1.5*).⁸⁹

As discussed above, CYPs have also been reported to be responsible for oxidation of fenretinide to the polar metabolites 4-oxo-fenretinide and 4-OH-fenretinide.⁹⁰

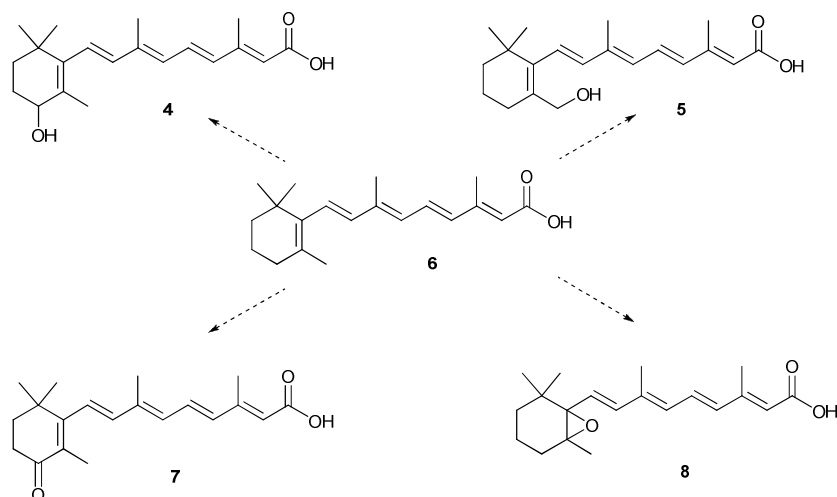


Figure 1.5 Known oxidative metabolites of retinoic acid.

There have been successful attempts at blocking undesired metabolism of retinoids in order to increase the effective concentration of the drug in the blood plasma. Extensive research into blocking of retinoic acid metabolism has been carried out by the Janssen Research Foundation (now Johnson and Johnson Pharmaceutical Research and Development). Initial compounds tested for a reduction in metabolism of retinoic acid include known CYP inhibitors; ketoconazole (**9**), liarozole (**10**) (*Figure 1.6*), aminoglutethimide, cimetidine, itraconazole, metyrapone and saperconazole.⁹¹ Pretreatment with ketoconazole or liarozole (40 mg/kg), when administered orally 1 h before intravenous retinoic acid treatment, reduced the elimination of retinoic acid from plasma and extended the half-life in control-treated animals from 27 min to 43 min and 76 min, respectively. No significant effect was observed upon co-treatment with the remaining CYP inhibitors. Furthermore, ketoconazole (**9**) (*Figure 1.6*) has been

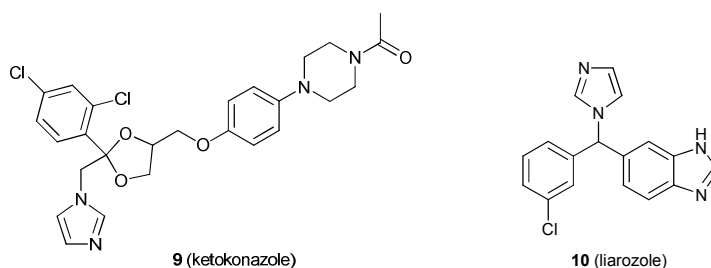


Figure 1.6 The chemical structure of fenretinide metabolism-blocking agent, ketoconazole.

demonstrated to successfully reduce fenretinide metabolism *in vivo*. One example is detailed in a patent application from the Children's Hospital Los Angeles Research Institute, in which *in vivo* screening in mouse models looking at the effect of ketoconazole on plasma fenretinide levels found that the compound successfully increased fenretinide plasma levels.⁹²

Liarozole (**10**) (*Figure 1.6*) was subsequently approved in Europe and USA (2004) as an orphan drug for the treatment of congenital ichthyosis, providing therapeutic effects by slowing down metabolism of the body's own retinoic acid.⁹³ As an anti-cancer agent, it has been shown to demonstrate promising inhibition of metabolism of retinoic acid in MCF-7 human breast cancer cells and rat Dunning R3327G prostate tumours.^{94,95} However, Liarozole was found to lack CYP specificity and inhibited the CYP-mediated bio-synthesis of steroid hormones.^{96,97} The Janssen Research Foundation subsequently identified two novel benzothiazolamine retinoic acid metabolism blocking agents (RAMBAs), R115866 (**11**) and R116010 (**12**) (*Figure 1.7*), as highly potent and selective second-generation RAMBAs. R115866 (**11**) is a nanomolar (IC_{50} 4 nM) inhibitor of the CYP26-dependent retinoic acid conversion, making it 750 times more potent than liarozole (IC_{50} 3 μ M).⁹⁸ *In vivo* studies found R116010 (**12**) potently inhibits retinoic acid metabolism in TA3-Ha murine mammary carcinoma cells (IC_{50} 8.7 nM), making it over 100-fold more potent than liarozole (IC_{50} value 1.4 μ M).⁹⁹ In addition, R116010 is a selective inhibitor for several CYPs.

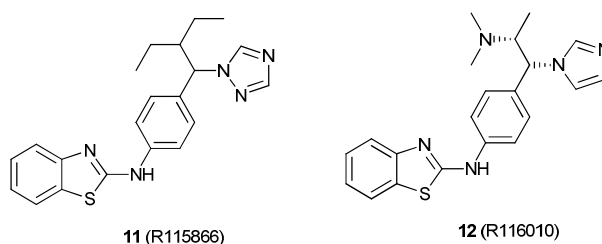


Figure 1.7 RAMBAs identified by the Janssen Research Foundation.

Human liver microsomes, along with CYPs, are known to metabolise retinoic acid (**6**) by oxidation of the 4-position.⁹⁰ Based on the retinoic acid scaffold, Patel *et al.* successfully synthesised a range of analogues which effectively inhibited hamster liver microsomal *all-trans*-retinoic acid metabolism

enzymes.¹⁰⁰ Compounds including **(13)** and **(14)** (*Figure 1.8.*), were designed to include a metabolically robust imidazole substituent at the 4-position of the cyclohexene ring. In addition to enhancing the activity of retinoic acid in an MCF-7 cellular assay, the compounds were found to also display potent antiproliferative effects and induction of apoptosis and differentiation was observed in several human cancer cell lines, giving these particular compounds an advantage of multiple mechanisms of action not observed in this model for fenretinide.

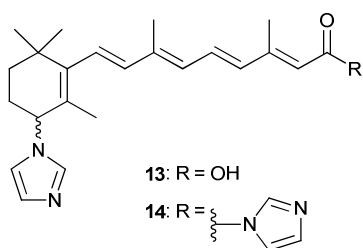


Figure 1.8 Retinoic acid metabolism blocking agent and cyclohexyl analogues of retinoic acid.

1.7.4.2 Fenretinide analogues with improved metabolic stability

Dawson *et al.* originally suggested that D-glucosiduronate analogues of fenretinide may be active *in vivo* due to metabolism of the phenol moiety by *O*-conjugation to D-glucuronic acid.¹⁰¹ The group detailed the synthesis of the proposed metabolism products, *N*-(4-hydroxyphenyl) retinamide-*O*-glucuronide (**15**) and 2-retinamidoethyl-*O*-glucuronide (**16**) (*Figure 1.9*). Swanson *et al.* subsequently found that synergistic metabolism of fenretinide with dietary glucurate (D-glucuronic acid salt) provided an active compound which inhibited 7,12-dimethylbenz[*a*] anthracene (DMBA)-

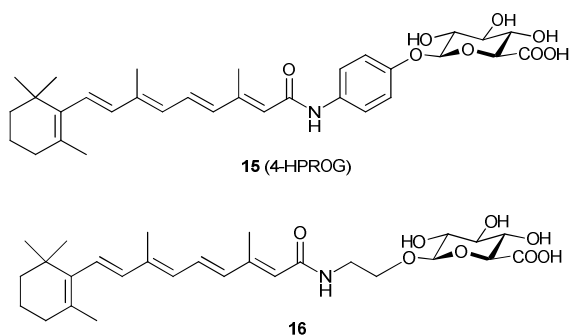


Figure 1.9 Structures of *N*-(4-hydroxyphenyl) retinamide-*O*-glucuronide (**15**) and 2-retinamidoethyl-*O*-glucuronide (**16**).

induced mammary cancer in a rat model.¹⁰² Metabolism by β -glucuronidation improves solubility and detoxifies a compound by reducing its lipophilicity.¹⁰³ This finding was further investigated by Curley *et al.*, whereby the stability of 4-HPROG (**15**) was evaluated in MCF-7 cells.¹⁰⁴ The group confirmed that the compound demonstrated good stability and interconversion to fenretinide was not observed over 24 h, concluding that this is an active species and not a pro-drug which yields fenretinide. The Curley group went on to develop additional analogues of 4-HPROG, whereby the hydrolysable *O*-glycosyl bond was replaced with a less hydrolysable CH₂ group (compound **17**) (Figure 1.10), and its biological activity was evaluated.¹⁰⁵ Compound **17** was found to induce cell death in an *in vivo* rat mammary tumour model and displayed improved toxicity *in vitro* compared to fenretinide. Additionally, these non-hydrolysable analogues of 4-HPROG demonstrated good activity in the rat tumour model, confirming that the metabolite molecules induce activity and that conversion to fenretinide is not necessary for activity. However, activity of these metabolites was marginally reduced compared to the activity of fenretinide in MCF-7 breast cancer cells.

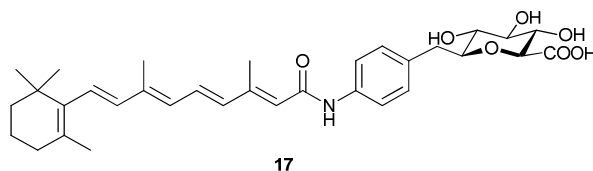


Figure 1.10 A non-hydrolysable analogue of *N*-(4-hydroxyphenyl) retinamide-*O*-glucuronide, whereby the *O*-glycosyl bond was replaced with a CH₂ group.

Several modifications to the lipophilic *trans*-alkene portion of fenretinide have been made to increase the metabolic stability. This research will be discussed in Section 1.10.4.

1.8 Clinical Efficacy of fenretinide

In phase I clinical trials fenretinide has been well tolerated in both adults and children. A phase I trial in children with neuroblastoma was carried out in order to determine the maximum tolerated dose, toxicity and pharmacokinetics.¹⁰⁶ Doses between 100 and 4,000 mg/m²/day were administered orally as an oil formulation in gelatine capsules. It was

concluded that 4,000 mg/m²/day was well tolerated over 28-day courses when followed by a 7-day drug-free interval. Additional dose escalation was not possible due to large amounts of capsules (ca.40 per day) being unpalatable for the patient; therefore the maximum tolerated dose could not be established in this study. The same trial identified that the peak plasma concentration of fenretinide was achieved approximately 4-5 h after administration of the drug, and that peak levels and absolute bioavailability was increased 2-fold by day 28. Out of 53 patients treated for progressive disease, 88 % underwent further progression and died. However, prolonged disease stabilisation was observed in the majority of patients showing early progression, with some showing regression of neoplastic lesions.

Subsequent phase II and III trials have confirmed that fenretinide does not demonstrate clinical efficacy at lower dose levels (600-900 mg/m²/day).^{107,108,109} It is stated that higher dose levels and prolonged treatment are required to obtain blood plasma concentrations to achieve a clinical benefit. Oral administration of a dose range between 300-4000 mg/m²/day maintains plasma concentration levels of fenretinide between 0.7-10 µM. The achieved plasma concentrations of the drug were found to be sufficient for required pharmacological activity and were successfully maintained for 24 h between dosing intervals, as supported by the calculation of an elimination half-life of 22 h.⁴⁷

Continuous administration of the drug over a longer period of time also improves growth inhibitory effects in solid tumours compared to shorter courses of treatment followed by a drug-free interval.⁴⁷ This is likely to be a consequence of the significant reduction in half-life from ca.22 h to ca.12 h when a drug-free interval is incorporated into the scheduling, therefore reducing the exposure of the tumour to fenretinide and the active metabolite 4-oxo-fenretinide. Unfortunately, continuous administration of fenretinide results in an unfavourable toxicity profile. Where side effects are minimal and reversible when a drug-free period is taken, they are likely to become unmanageable upon continuous administration where the maximal tolerated dose of 2,475 mg/m²/day can be exceeded.⁸²

Co-treatment with Lym-X-Sorb (LXS), a novel lipid matrix drug delivery formulation, has been evaluated in an *in vivo* mouse model, where an increase in fenretinide plasma concentration of up to 4-fold and an increase in tissue concentrations of up to 7-fold compared with similar doses of fenretinide alone was observed.¹¹⁰ This therefore has potential for improving fenretinide plasma concentrations and increasing bioavailability and is currently being evaluated in two phase I clinical trials; 'Intravenous Fenretinide in Treating Young Patients With Recurrent or Resistant Neuroblastoma' and 'Fenretinide LXS in Treating Patients With Recurrent, Refractory, or Persistent Neuroblastoma'.¹¹¹

Early trials on topical drug delivery of fenretinide have also been investigated in various cancer cell types including oral lichen planus, leukoplakias and facial actinic keratoses.¹¹² Although topical administration is only possible for a narrow range of cancer types, this appears to be a highly effective treatment for the aforementioned cell types, with a high percentage of patients showing complete or partial regression. However, only a small number of patients were monitored in these trials therefore further investigation into this route is required to confirm findings.¹¹²

1.9 Side effects of fenretinide

Several toxicities have been observed upon administration of fenretinide in patients at the higher dose levels which exhibit a higher absolute bioavailability. There are several minor side effects associated with fenretinide, including skin xerosis, fatigue, nausea and diarrhoea. The most commonly encountered side effect associated with the drug is impairment to visual dark adaptation (night-blindness), which increases in severity with dose level. This is likely to be due in part to inhibition of binding of retinol to RBP4 caused by a similar mode of binding of fenretinide to the protein, therefore reducing the transport of retinol around the body and consequently the retinol plasma concentration.¹¹³ However, a phase I clinical trial showed that all of the adverse reactions were reversible upon discontinuation of the drug and that night-blindness significantly diminished upon reduction of dose

level. This effect can therefore be minimised by taking a 7-day drug-free interval after each 28-day treatment period.¹⁰⁶

Night-blindness may also be brought on by hydrolysis of fenretinide to retinoic acid, which has been found to inhibit ocular retinol dehydrogenases *in vitro* leading to a reduction in formation of 11-*cis*-retinal (a visual chromophore).^{114,115} In an attempt to reduce night-blindness *via* this mechanism, Anding *et al.* investigated the possibility of reduction of the *in vivo* generation of retinoic acid from fenretinide by design of a hydrolytically stable version of fenretinide, 4-hydroxybenzylretinone (4-HBR) (**18**) (Figure 1.11).¹¹⁴ As predicted, it was found that this compound was not hydrolysed *in vivo* to all-*trans*-retinoic acid, thus eliminating night-blindness induced by retinoic acid generation. Furthermore, 4-HBR was found to prevent a decrease in circulating retinol levels, also eliminating the risk of night-blindness.

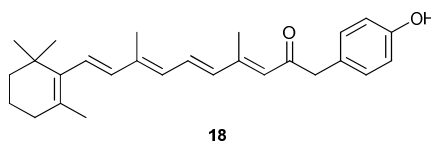


Figure 1.11 Molecular structure of 4-hydroxybenzylretinone.

Systemic side effects were eliminated upon topical administration as the drug was not absorbed into the circulation and no local side-effects were observed.¹¹² Topical drug delivery or lower-dosage oral administration may therefore provide an alternative treatment with significantly lower toxicity. However, these may have limited application in the treatment of cancer due to the relatively high plasma concentration required to provide chemotherapeutic effects and sufficient activity to combat systemic metastasis, with the possible exception of those where you could apply fenretinide topically (*e.g.* melanoma, oral cancer, cervical cancer).

1.10 Structure Activity Relationship (SAR) of fenretinide

A structure activity relationship (SAR) is the relationship between the hit, lead or drug and its biological activity. The analysis of the SAR for a hit, lead or

drug enables the understanding of the chemical groups on the molecule which are responsible for evoking the biological activity. Hence, knowledge about the SAR allows for the predictive and rational modification of chemical structure in order to appropriately fine-tune the biological response.

Very little is known about the SAR for fenretinide in cancer cell lines, including for the ESFT cell lines. Surprisingly few studies have been directed towards development of SAR, despite the fact that the cytotoxic properties of fenretinide have been known since the 1970s.³⁶ This lack of investigation into the SAR for fenretinide is probably, at least in part, due to the fact that the biomolecular target of fenretinide is unknown, making structure-based design of new analogues impossible. The few analogues of fenretinide which have been generated to date have been screened using a range of cell lines, from a variety of different cancer types for induction of cell death. This has made it difficult to build up a coherent SAR for fenretinide as it is possible that different cell lines are affected differently and cell death could be initiated by different mechanisms of action. Equally, experimental methods within different laboratories vary, for example by treatment times, concentrations and assay types.

This section describes the SAR for fenretinide and fenretinide analogues as chemotherapeutics. For organisation of this section, it has been divided into four parts based on substructures of fenretinide, to include the phenyl ring, the cyclohexene ring, the central scaffold, and the amide (*Figure 1.12*). Although this review is aimed primarily at discussion of the SAR of fenretinide, some of the discussion, particularly around the cyclohexene and central scaffold sub-sites, focuses on the SAR of alternative retinoids (retinoic acid and retinol) owing to their commonality of structure at this site and their common use as chemotherapeutics.

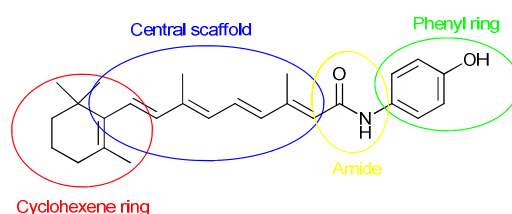
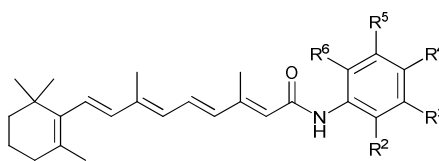


Figure 1.12 A schematic outlining the 4 regions of variation of the fenretinide scaffold.

1.10.1 SAR of the phenyl ring

Of the substructures highlighted in Figure 1.12, synthetic variation at the phenyl portion of fenretinide has been the most widely studied. This is presumably due to the relative simplicity of the chemistry involved in generation of analogues for variation at this site.

A library of fenretinide-like compounds with variation on the phenyl ring was prepared by Sabichi *et al.*³⁸ The group focussed on investigation of the effect of *ortho*-, *meta*- and *para*- ring substitution using a set of hydroxyl, carboxyl and methoxy substituents. Six compounds (**19-24**) (Table 1.1) were synthesised and tested *in vitro* for both cell growth inhibition and retinoid X receptor- (RXR) or RAR-dependence. To test RXR/RAR dependence, the group analysed the activity of the compounds on a panel of F9 murine embryonal carcinoma cell lines, which includes wild-type (F9-WT) and mutant cells (F9-KO) that have disrupted genes for both RXR- α and RAR- γ retinoid receptors. They found that all 6 compounds induced cell growth inhibition against both cell lines in an MTT assay, with 3 of the compounds (**20**, **21** and **24**) inducing similar levels of activity to fenretinide at 10 μ M (70-80 % inhibition of cell viability vs > 80 % for fenretinide). The results suggested that, although relocation of the OH around the phenyl ring or its replacement with a carboxylic acid or methoxy group was tolerated, the *para*-hydroxy substitution was still favoured. The activity of the compounds was



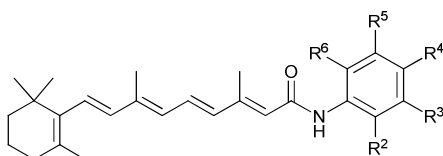
Compound	R ²	R ³	R ⁴	R ⁵	R ⁶	Growth inhibition*
1 (fenretinide)	H	H	OH	H	H	+++
19	OH	H	H	H	H	+
20	H	OH	H	H	H	++
21	CO ₂ H	H	H	H	H	++
22	H	CO ₂ H	H	H	H	+
23	H	H	CO ₂ H	H	H	+
24	H	H	OCH ₃	H	H	++

* + ca.30-65% growth inhibition; ++ ca.70-80% growth inhibition; +++ ca.80% growth inhibition of F9-WT/F9-KO cells at 10 μ M.

Table 1.1 Analogues of fenretinide with varying phenylamine substituents synthesised by Sabichi *et al* and their effects on F9 murine embryonal carcinoma cell growth.³⁸

similar in both the F9-WT and F9-KO cell lines, indicating a RXR/RAR-independent mechanism. Retinoic acid displayed reduced activity in F9-KO compared to F9-WT, confirming its retinoid-receptor dependence which is associated with accumulation of cells in the G₁ phase of the cell cycle. The group concluded that a polar substituent is necessary on the phenylamine ring to induce RAR-dependent G₁ accumulation. This could be a hydroxyl (any position) or carboxyl substituent (*ortho*/*para*-) to the alkyl chain. Unlike the compounds bearing a charged moiety, 4'-MPR (**24**) displayed an inability to induce RAR-dependent actions in cotransfection reporter assays, indicating that an alternative mechanism of action is responsible for activity of this compound. When tested against a panel of cell lines, 4'-MPR also failed to induce significant growth inhibition, suggesting that the high levels of inhibition observed upon treatment of F9-WT and F9-KO is cell-line specific.³⁸

Mershon *et al.* went on to prepare a library of 49 fenretinide analogues, 43 of which were substituted phenyl analogues representing a wider variation of substitution at the phenyl ring (**21** and **24-65**) (*Table 1.2*).¹¹⁶ Screening of this library using a cell viability assay against the MCF-7 human mammary tumour cell line identified 12 active analogues of fenretinide (with 25-100 % the activity of the fenretinide standard). The most active compound from the library, compound **42**, displayed comparable levels of activity compared to fenretinide (activity ≥ 100 % the activity of the fenretinide standard), closely followed by compound **31** which displayed activity approaching that of fenretinide. Compound **42** contains a 2-hydroxy and 4-nitro substitution pattern on the phenyl ring, implying that a charged substituent on the ring is important for growth inhibition. However, relocation of the OH or NO₂ groups to alternative positions around the ring (compounds **40**, **41** and **43**) significantly reduced activity, implying that the position of the polar moieties is important for activity for this compound series. It is noteworthy that the OH group was tolerated in a variety of positions around the phenyl ring. This was demonstrated for a series of compounds where the phenyl ring was substituted with both OH and CH₃, Cl or NO₂ group at the *ortho*-, *meta*- and/or *para*- positions; for instance, compounds **31** (3-OH, 4-CH₃) and **42** (2-



Compound	R ²	R ³	R ⁴	R ⁵	R ⁶	MCF-7 growth inhibition*
1 (fenretinide)	H	H	OH	H	H	+++
25	CH ₃	H	OH	H	H	-
26	CH ₃	H	OH	CH ₃	H	-
27	OH	H	CH ₃	H	H	++
28	OH	H	H	CH ₃	H	-
29	OH	H	H	C(CH ₃) ₂	H	-
30	OH	H	H	H	CH ₃	-
31	H	OH	CH ₃	H	H	+++
32	CH ₃	OH	H	H	H	-
33	H	OH	OCH ₃	H	H	-
34	Cl	H	OH	H	H	-
35	H	Cl	OH	H	H	++
36	OH	H	H	Cl	H	++
37	H	Cl	OH	Cl	H	-
38	H	Br	OH	Br	H	-
39	OH	Cl	CH ₃	Cl	H	-
40	NO ₂	H	OH	H	H	-
41	H	NO ₂	OH	H	H	-
42	OH	H	NO ₂	H	H	+++
43	OH	H	H	NO ₂	H	+
44	OH	CO ₂ CH ₃	H	H	H	-
45	OH	CO ₂ H	H	H	H	-
46	OH	H	CO ₂ CH ₃	H	H	+
47	OH	H	CO ₂ H	H	H	-
48	OH	H	H	H	CO ₂ CH ₃	-
49	OH	H	H	H	CO ₂ H	-
50	H	OH	CO ₂ CH ₃	H	H	-
51	H	OH	CO ₂ H	H	H	-
52	H	CO ₂ CH ₃	OH	H	H	+
53	H	CO ₂ H	OH	H	H	-
54	OH	H	H	CO ₂ CH ₃	H	-
55	OH	H	SO ₂ CH ₂ CH ₃	H	H	-
56	CH ₂ OH	H	H	H	H	ND
57	H	CH ₂ OH	H	H	H	+
58	H	H	NH ₂	H	H	++
59	CO ₂ CH ₃	H	H	H	H	ND
21	CO ₂ H	H	H	H	H	+
60	H	H	OCH ₂ CH ₃	H	H	-
61	H	H	H	H	H	+
62	H	H	Cl	H	H	+
24	H	H	OCH ₃	H	H	+
63	H	H	CH ₃	H	H	-
64	H	Cl	Cl	H	H	+
65	H	H	N(CH ₃) ₃	H	H	-

*-, activity equivalent to the vehicle; +, ≥ 25% the activity of; ++, ≥ 50% the activity; +++, ≥ 100% the activity of the fenretinide standard at 1 μM; ND, not determined. ^a at 0.59 μM; ^b at 0.39 μM; ^c at 0.66 μM; ^d at 0.74 μM.

Table 1.2 Analogues of fenretinide with varying phenylamine substituents synthesised by Mershon *et al.* and the effects on MCF-7 human mammary tumour cell growth.¹¹⁶

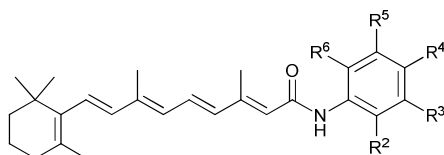
OH and 4-NO₂) demonstrated comparable activity to fenretinide and **27** (2-OH, 4-CH₃), **35** (3-Cl, 4-OH) and **36** (2-OH, 5-Cl) over 50 % the activity of

fenretinide. Good activity ($\geq 50\%$ fenretinide control) was also retained upon substitution of the *para*-OH with NH₂ (compound **58**), indicating that a hydroxy to amino substitution at this site can be tolerated.

The inactive compounds from the set included a range of alkyl/OH, halogen/OH, nitro/OH, carboxyl/OH, di/tri-substituted analogues (e.g. compounds **25**, **26**, **34**, **40** and **51**). Addition of more steric bulk around the phenyl ring (e.g. C(CH₃)₂, CO₂CH₃, SO₂CH₂CH₃, OCH₂CH₃ groups, compounds **29**, **54**, **55** and **60** respectively) significantly reduced or abolished activity, indicating the possibility of a sterically constrained binding pocket at this site on a hypothetical biological target.

Although the authors were unable to identify a robust SAR for substitution at the phenyl ring, they were able to conclude that substitution both *ortho*- and *meta*- to the amide, as well as substitutions and/or a change in the position of the hydroxyl group, can be tolerated for activity against the breast cancer cell line, MCF-7. Highest activity was observed for compounds containing a charged substituent on the phenyl ring, which reaffirms the findings made by Sabichi *et al.*³⁸

Das *et al.* synthesised a library of 14 substituted phenylamides (**24**, **35**, **41**, **62** and **66-74**) as agents to inhibit proliferation of rhabdoid tumour cells (Table 1.3).¹¹⁷ Of the *para*-hydroxy containing analogues, substitution *meta*- to the amide with a halogen (compound **70**, F; compound **35**, Cl; compound **71**, I) was well tolerated in an MTS cell proliferation assay against rhabdoid tumour cells. Specifically, the *meta*-fluoro and chloro analogues (**70** and **35**) displayed a similar level of activity (IC₅₀ 8.0 and 12.5 μ M respectively) to fenretinide (19 μ M), and the *meta*-iodo analogue (**71**) displayed significantly increased activity (IC₅₀ 3 μ M). Substitution *ortho*- to the amide with a second OH group (compound **74**) also resulted in an encouraging level of cytotoxicity (IC₅₀ 8 μ M, compared to fenretinide 19 μ M). Conversely, a *meta*-NO₂ substituent (compound **41**) eliminated cytotoxic activity, suggesting that a weak electron donating group at this position (*i.e.* a halogen) is more favourable than a strong electron withdrawing group. An *ortho*-halogen substituent increases the hydrogen bond donor capabilities of the adjacent



Compound	R ²	R ³	R ⁴	R ⁵	R ⁶	IC ₅₀ (μM)
1 (fenretinide)	H	H	OH	H	H	9-19
66	H	H	F	H	H	150
62	H	H	Cl	H	H	>200
67	H	H	Br	H	H	150
68	H	H	I	H	H	N/A
69	H	H	NO ₂	H	H	>200
24	H	H	OCH ₃	H	H	N/A
70	H	F	OH	H	H	8
35	H	Cl	OH	H	H	12.5
71	H	I	OH	H	H	3
41	H	NO ₂	OH	H	H	>200
72	H	H	CH ₂ OH	H	H	25
73	H	H	(CH ₂) ₂ OH	H	H	>50
74	OH	H	OH	H	H	8

Table 1.3 Structures and biological activity of fenretinide analogues with varying phenylamine substituents synthesised by Das *et al.*¹¹⁷

OH moiety compared to the phenol, potentially aiding an important interaction with the target. The *meta*-nitro substituent will increase the *pi*-orbital stacking capabilities of the phenyl group which could account for the insolubility of this compound that the group observed.

It is noteworthy that all of the most active compounds from the library share a *para*-hydroxy group, which supports the findings of Sabichi *et al.*, and in part, those of Mershon *et al.* which suggest that a *para*-hydroxy group may be an important moiety for biological activity, perhaps by forming hydrogen-bonding interactions with a biological target or enabling ROS production. Replacement of the OH with halogens (compounds **62** and **66-78**), NO₂ (compound **69**) and OMe (compound **24**) was found to significantly reduce or eliminate cytotoxic activity. Supporting the hypothesis for requirement of hydrogen-bonding at this site, extension of the OH group to the benzyl alcohol at the *para*-position (compound **72**) resulted in a similar IC₅₀ (25 μM) compared to fenretinide (19 μM) although the IC₅₀ was increased (> 50 μM) when substituted with a hydroxyethyl group at the same site (compound **73**).

Um *et al.* designed and synthesised a range of retinamide and retinoate derivatives containing butyryl derivatives of the aminophenol moiety

(compounds **75-79**) (Figure 1.13), based on butyric acid having been previously identified as an anticancer agent.⁵⁰ Two retinamide derivatives (compounds **75** and **76**) with IC_{50} of 1.67 μ M and 3.15 μ M respectively and three of the retinoate derivatives (compounds **77**, **78** and **79**) with IC_{50} of 0.65 μ M, 3.01 μ M and 4.08 μ M respectively were found to have an increased cytotoxicity compared to fenretinide (IC_{50} 8.21 μ M) against HCT116 colon cancer cells. All of the active compounds contain an ester linkage either at the retinoate or the butyrate site. This may help to explain the improvement in activity of these compounds in comparison to fenretinide owing to cellular hydrolysis of the ester resulting in liberation of a cytotoxic agent, either retinoic acid or butyric acid. It is also noteworthy that each of the active compounds contains a hydrogen-bond donor at the *para*-position of the phenyl ring in accordance with the findings of Sabichi *et al.* previously.³⁸

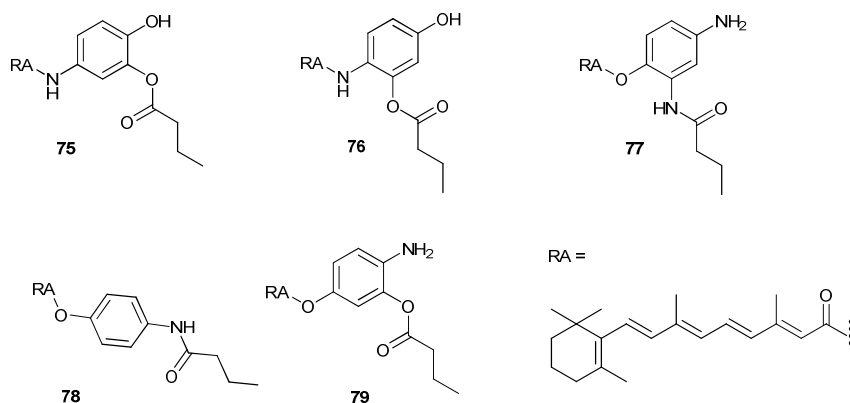


Figure 1.13 Retinamide (**75** and **76**) and retinoate (**77-79**) butyryl derivatives of fenretinide synthesised by Um *et al.*⁵⁰

Sadikoglou *et al.* reported a synthesis of a series of conjugates of amino acids with retinoic acid (Figure 1.14) by succinimidyl activated coupling reactions.¹¹⁸ It was shown that those analogues containing α -amino acids with a lipophilic (valine) side chain (**80**) or linear (β -alanine) amino acids (**81**) successfully induced cell death in a human prostate cancer cell line, whilst that bearing a highly polar carboxylic acid (aspartic acid) side chain (**82**) displayed no apoptotic effects, possibly due to a lack of cell penetration.

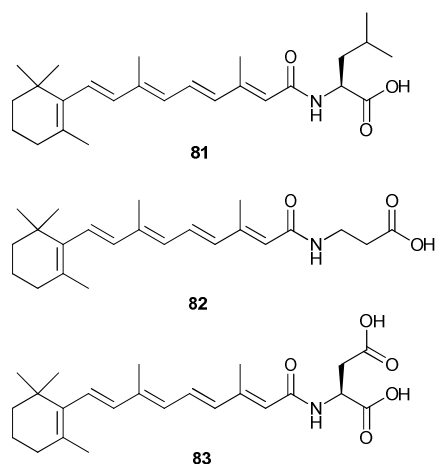


Figure 1.14 α -amino acid-containing analogues of retinoic acid synthesised by Sadikoglou *et al.*¹¹⁸

Supporting the hypothesis that a *para*-hydroxy group is essential for cytotoxic activity of fenretinide and fenretinide analogues in a range of cell lines, the hydroxyl group on the phenylamine ring has been identified as an essential substituent for recognition by retinol binding proteins, particularly RBP4, a major transport protein for fenretinide in blood plasma.^{84,119} The crystal structure of the fenretinide-RBP4 complex has been solved, confirming this specific interaction (*Figure 1.15*).¹²⁰

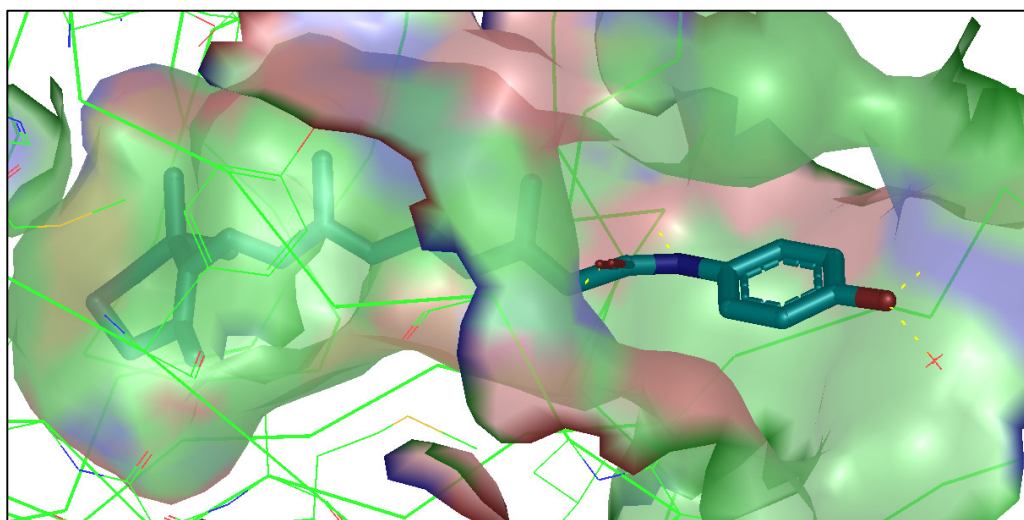


Figure 1.15 The crystal structure of fenretinide (cyan sticks) bound to RBP4 (PDB: 1FEL).¹²⁰

1.10.2 SAR for the amide

A small number of isosteres and analogues of the amide linkage in fenretinide have been investigated for their anti-cancer properties. Firstly,

Weiss *et al.* described the synthesis and biological evaluation of 4-HBR (**18**) (*Figure 1.11*, page 23), whereby the NH group was replaced with a methylene linkage.¹²¹ Weiss hypothesised that fenretinide may act as a pro-drug, which liberates retinoic acid *in vitro*, and wished to investigate the possibility of this using the non-hydrolysable methylene variant (**18**). 4-HBR was found to induce comparable activity to fenretinide (77 % and 85 % decrease in tumour volume respectively, over 21 days treatment at 2 mmol/kg) in DMBA-induced mammary tumours in rats. This suggested that the NH group was not important for the biological response in this assay, suggesting perhaps that the NH group does not interact with a target to elicit its biological effect. 4-HBR induced apoptosis was shown to be independent of the RAR signalling pathway. However, the presence of a ketone may result in additional toxicity compared to the amide variant due to its increased susceptibility towards nucleophilic attack and also an increased rate of metabolism owing to the newly exposed methylene group.

Mershon *et al.* synthesised the *N*-methylated amide fenretinide (**83**) (*Figure 1.16*).¹¹⁶ This compound demonstrated ≥ 25 % activity compared to the fenretinide control at 1 μ M in a fluorescein diacetate cell viability assay against MCF-7 cells. The significant reduction in activity observed for this compound in comparison to the fenretinide control might suggest that the NH group is beneficial for activity in this cell type and/or that the *N*-Methyl group confers a negative steric or electronic effect impacting the pharmacology and/or pharmacokinetics of this compound.

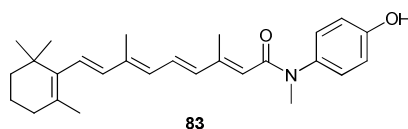


Figure 1.16 Molecular structure of *N*-methyl fenretinide analogue.

There is no evidence in the literature for modification of the carbonyl of the amide to understand its effects on SAR.

1.10.3 SAR for cyclohexene derivatives

A limited number of analogues of the cyclohexene ring of retinoids have been synthesised and investigated for their biological properties. Those that

have been prepared to date have focussed exclusively on investigation of variation at the 4-position (*Figure 1.17*), presumably due the ease of synthetic accessibility. Substitution at the 4-position of the cyclohexene ring of retinoic acid has been investigated with molecules initially synthesised to function as retinoic acid metabolism blocking agents (as previously discussed in Section 1.7.4.1). These compounds were also found to induce significant levels of apoptosis and differentiation.¹⁰⁰ Two compounds (**13** and **14**) (*Figure 1.8*, page 19) with comparable activity to fenretinide were identified; both compounds are retinoic acid analogues containing an imidazole-substitution at the 4-position of the cyclohexene ring; compound **13** as the carboxylic acid and compound **14** as the acyl imidazole variant.

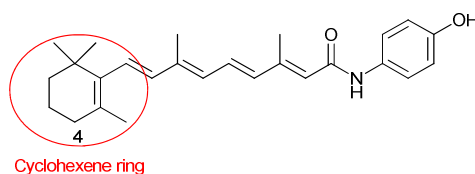


Figure 1.17 A schematic highlighting the cyclohexyl subunit of fenretinide and the synthetically accessible 4-position for modification.

The structure and biology of 4-oxo-fenretinide (**3**) (*Figure 1.4*, page 15), an active metabolite of fenretinide bearing a carbonyl modification at the 4-position of the cyclohexene ring, has also been previously discussed. When synthesised and tested *in vitro* by Villani *et al.*, 4-oxo-fenretinide was found to be more potent than the parent drug in 13 out of 16 of the cell lines tested (a range of ovarian, breast and neuroblastoma lines) for growth inhibition using the sulforhodamine B assay.^{37,47} In these cell lines, the IC₅₀ concentrations of fenretinide were found to be significantly (*ca.*2-4 times) higher than that for 4-oxo-fenretinide.

No other SAR for the cyclohexyl sub-site has been described, although an interesting acyclic variant of the cyclohexyl ring has been reported for the retinoic acid sub-structure. Suzui *et al.* originally identified that acyclic retinoic acid (ACR) (**84**) (*Figure 1.18*) inhibited growth in cell proliferation assays using human colon carcinoma cell lines.¹²² G₁-phase cell cycle arrest and apoptosis was confirmed to be induced by ACR in these cell lines.

However, Wada *et al.* found that the rigid cyclohexane group is favourable for activity in HL-60 cells, as acyclic derivatives (**85-90**) (*Figure 1.18*) (cleaved 1–6 single bond and saturated adjacent double bonds) reduced activity by *ca.*3-fold compared to retinoic acid.¹²³ This suggests that activity of acyclic analogues is cell line specific and, in this particular cell line, a rigid conjugated structure binds more efficiently to the target and therefore leads to an increase in potency.

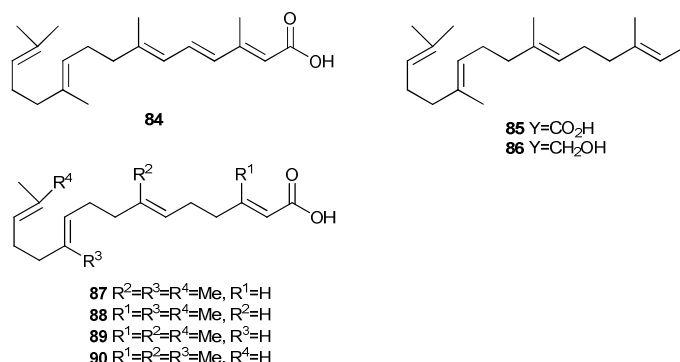


Figure 1.18 Chemical structures of acyclic retinoic acid analogues.

The cyclohexene ring may be important for *in vivo* biological activity as it has been proven to be a significantly important substituent in binding to the serum protein, RBP4, which may be a target for cell growth inhibition or transport of fenretinide.⁸⁴ The crystal structure of the fenretinide-RBP4 complex confirms this specific interaction (*Figure 1.15*, page 31); the cyclohexene ring of fenretinide is buried within a hydrophobic cavity in the protein, with the polar phenylamide group pointing towards the exterior of the protein.^{119,120}

1.10.4 SAR of the central scaffold

This section describes the known SAR for the central hydrophobic linker (central scaffold) of the fenretinide sub-structure (*Figure 1.19*). The number

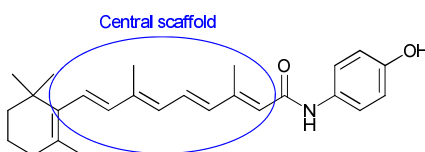


Figure 1.19 A schematic highlighting the central scaffold of fenretinide.

of synthetic variations of fenretinide at this site is rather limited, presumably due to the relative complexity of any chemistry involved in adapting this part of the molecule.

Takahashi *et al.* synthesised a range of *para*-acylaminophenol (**91** and **92**) and *para*-alkylaminophenol (**93-96**) compounds, replacing the fenretinide isoprene ring and alkene scaffold with lipophilic alkyl chains of varying lengths (*Figure 1.20*).^{124,125} The chain length of the *para*-alkylaminophenols was proven to be proportional to growth suppression in a range of cancer cell lines including some human leukaemia cell lines, with an elongated chain length identified as a more potent chemopreventative and antiproliferative agent than a shorter chain length.¹²⁴ Additionally, *para*-dodecylaminophenol (**94**) was found to show cell growth inhibition comparable/improved compared to fenretinide across several cell lines (HL60, HL60R, MCF7, HepG2, DU-145).¹²⁵ The *para*-acylaminophenols were weakly active or inactive, therefore, the presence of the carbonyl moiety is detrimental to activity of these compounds against the cell lines tested.

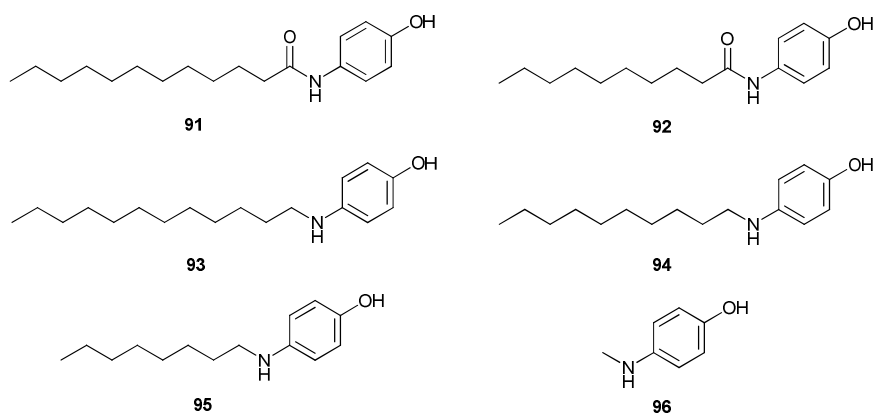
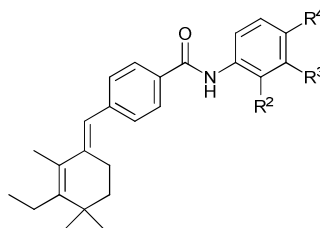


Figure 1.20 *para*-acylaminophenol (**91** and **92**) and *para*-alkylaminophenol (**93-96**) compounds synthesised by Takahashi *et al.*¹²⁴

Das *et al.* designed and synthesised a range of rigidified analogues of fenretinide which involved substitution of the alkene backbone with a rigid phenyl ring (**97-103**) (*Figure 1.21*).⁸³ It was found that incorporation of a phenyl ring into the alkene backbone did not reduce the activity compared to fenretinide in rhabdoid tumour cells at lower concentrations. However the compounds precipitated out in the cell culture medium at higher concentrations, preventing an IC₅₀ from being determined. Analogues

incorporating variation at the R²-R⁴ sites were synthesised. The most active compound amongst this set was compound **100** (R² = H, R³ = I, R⁴ = OH) (*Figure 1.21.*) which was found to have increased cell death (IC₅₀ 3 μM) *in vitro* compared to fenretinide (IC₅₀ 15 μM). This preference for a *para*-hydroxy, *meta*-iodo substitution pattern on the phenyl ring is consistent with previous studies carried out by Das of the retinoid substructure, as discussed previously (Section 1.10.1).¹¹⁷



Compound	R ²	R ³	R ⁴	IC ₅₀ (μM)
1 (fenretinide)	-	-	-	15
97	H	H	OH	N/A
98	H	Cl	OH	10
99	H	F	OH	13
100	H	I	OH	3
101	OH	H	OH	47
102	H	H	-CH ₂ OH	29
103	H	H	-CH ₂ CH ₂ OH	N/A

Figure 1.21 Structure and biological activity of rigidified derivatives of fenretinide synthesised by Das *et al.*¹³⁵

No further variations on the central scaffold of fenretinide have been described to date. However, several interesting variants of the central scaffold of retinoic acid have been reported which are worthy of comment.

Simoni *et al.* synthesised a range of central scaffold variants of retinoic acid containing a 1,1,4,4-tetramethyl-1,2,3,4-tetrahydronaphthalene moiety and replacing a portion of the conjugated alkene with a phenyl (TTNBP, compound **104**) or an isoxazole ring (**105** and **106**) (*Figure 1.22*)^{126,127}. They found that the *trans*-phenyl and *trans*-isoxazole variant, **104** and **105**, to be largely inactive in cytotoxicity assays in the HL-60 promyelocytic cell line using a trypan blue exclusion assay. However, the *cis*-isoxazole **106** was found to have 6.5 times increased apoptosis inducing activity compared to 13-*cis*-retinoic acid. Although the *trans*-isoxazole analogue (**105**) displayed no

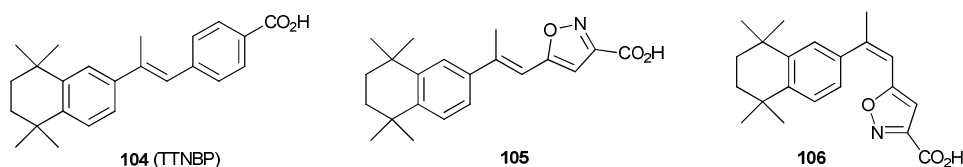


Figure 1.22 The scaffold of retinoid analogues synthesised by Simoni *et al.*¹²⁷

significant apoptotic activity some differentiating activity was observed, whereby differentiation of cancer cells into benign cells is induced by the compound. The group concluded that the *cis*- and *trans*- forms of retinoic acid and their isoxazole analogues are able to induce cell death through different mechanisms, apoptotic and differentiating mechanisms respectively.

Baraldi *et al.* went on to design a range of heteroatom-containing retinol analogues (*Figure 1.23*) comprising of an isoxazole ring tethering the C10 and C12 atoms of the central scaffold (compounds **107-112**), OH and carbonyl functionalisation at C7 (compounds **107-110**) and saturation of the C7/C8 double bond (compounds **109**, **110** and **112**).¹²⁸ Compound **112** differs from compounds **107-111** in that the double bonds are shifted from the 2- to 3-position of the cyclohexene ring and 7/8- to 6/7-position of the backbone. It was hypothesised that incorporation of the isoxazole ring in this compounds may increase potency by restricting the confirmation of the molecule and by also reducing the rate of metabolism in comparison to the parent alkene. The *in vitro* activity of the analogues was evaluated against a panel of cancer cell lines including erythromyeloid, erythroleukemic and B-lymphoid cells. All of the compounds were seen to display comparable or improved toxicity compared to retinol across the panel of cell lines, with compound (**111**) displaying markedly improved inhibition of cell proliferation (IC_{50} of 2-15 μ M compared to that of retinol, 18-55 μ M). This indicates that quite drastic modification of the central scaffold is well tolerated and further

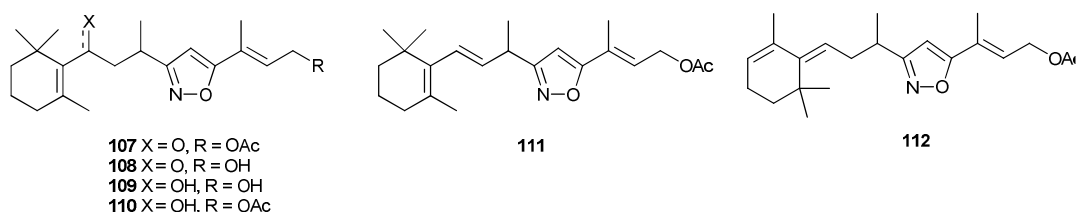


Figure 1.23 Central scaffold derivatisation of retinol by Baraldi *et al.*¹²⁸

restriction of the alkene chain by tethering with heteroatomic rings may improve selectivity and activity.

Others have taken the approach of replacing the retinoid substructure with a more metabolically stable backbone. As well as oxidation at the 4-position of the cyclohexyl ring (as for fenretinide), retinoic acid is known to be metabolised to two additional products, 18-hydroxy-retinoic acid (**5**) and 5,6-epoxy-retinoic acid (**8**) (*Figure 1.5*, page 17), by epoxidation and radical oxidation.⁸⁹ Barnard *et al.* demonstrated that TTNBP (**104**) (*Figure 1.22*) (previously synthesised by Simoni *et al.*), incorporating replacement of the cyclohexyl ring/isoprene region with the non-oxidisable 1,1,4,4-tetramethyl-1,2,3,4-tetrahydronaphthalene moiety, was less liable to metabolism by epoxidation and radical oxidation in a hamster trachea organ culture (TOC) assay.⁸⁹ Additionally, incorporation of diphenylacetylene or biaryl moieties into the central scaffold provided robust structures which retained significant activity, for example EC23 (**113**) and TTNN (**114**) respectively (*Figure 1.24*).

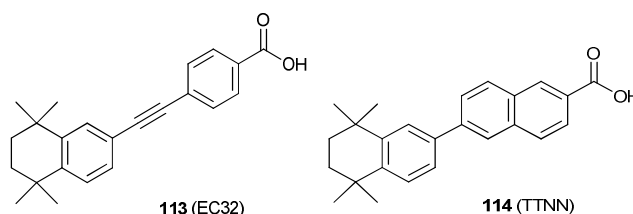


Figure 1.24 Chemical structures of EC23 and TTNN synthesised by Barnard *et al.*⁸⁹

Further modifications of the TTNBP structure were investigated by the group (*Figure 1.25*). However, they were unable to improve upon the activity observed for TTNBP in RXR/RAR binding studies. Selective removal of one (**115** and **116**) or both (**117**) of the methyl substituents required to block oxidation from the C4 position on the cyclohexene ring and substitution with a benzonorbornenyl analogue (**118**) resulted in loss of activity in varying magnitudes.

Aromatization of the cyclohexyl ring to the naphthalene ring (**119**) resulted in loss of activity by over two orders of magnitude, indicating that it is more favourable for the methyl groups to lie out of the plane of the ring. A C11-C14 benzofused retinoic acid analogue (**120**) showed reduced activity to both

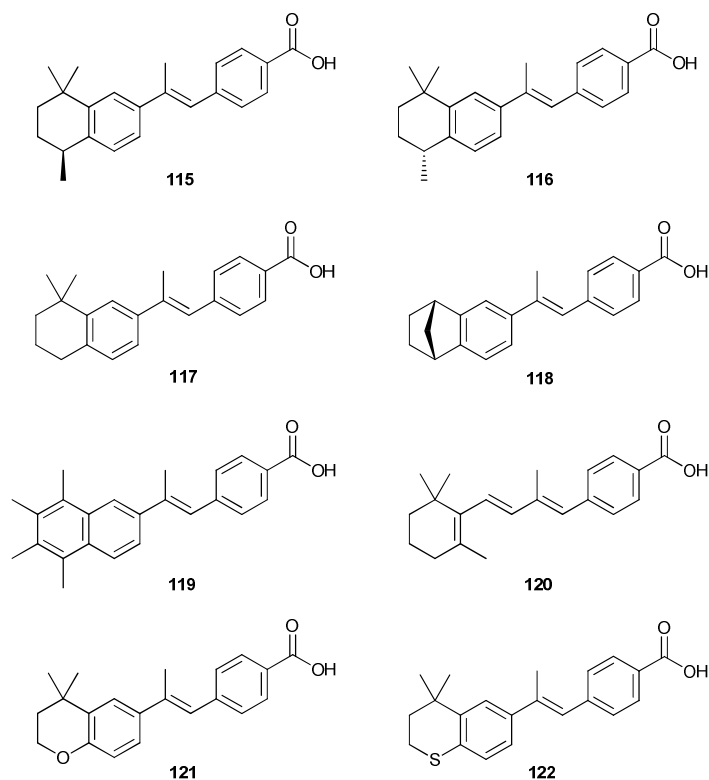


Figure 1.25 Chemical structures of heteroarotinoids designed to block oxidative metabolism by Barnard, *et al.*⁸⁹

retinoic acid (**6**) and TTNBP (**104**), as well as its de-methylated analogue (**117**), indicating that incorporation of the naphthalene moiety in place of the isoprene ring, in addition to the C4 methyl groups, is favourable for activity. Incorporation of heteroatoms designed to prevent oxidation at the 4-position also lacked activity (compounds **121** and **122**). This is likely to be due to removal of lipophilic bulk at this position, as well as the presence of polar heteroatoms which would reduce any hydrophobic interactions important for activity, since the more electronegative oxygen analogue displayed reduced activity compared to the sulphur analogue.

Benbrook *et al.* have carried out extensive research to identify heteroarotinoid derivatives of TTNBP (**104**), in collaboration with Berlin *et al.*^{126,129,130} They reported that the arotinoid TTNBP (**104**) (*Figure 1.22*), previously reported to be inactive in the HL-60 promyelocytic cell line by Simoni *et al.*, displays significant anticancer activity a human cervical cell line (CC-1) but demonstrated a highly unfavourable toxicological profile in a mouse model. In an attempt to optimise the pharmacological and toxicological profile of TTNBP, Benbrook designed and synthesised a library

of 21 heteroarotinoid variants. Screening of this library identified two compounds (**123** and **124**) (*Figure 1.26*) out of the library of 21 compounds which displayed much more acceptable toxicity levels (mean tolerated dose 34 and 32 mg/kg/day respectively; and 3000-fold reduced toxicity compared to TTNBP (**104**) as well as 3-fold reduced toxicity compared to retinoic acid (**6**)).¹²⁶ Although cell-based assays demonstrated growth inhibition was reduced by 27 % in cervical carcinoma cell line treated with compounds (**123**) and (**124**) compared to TTNBP (**104**), the significantly reduced toxicity profile is much more favourable therefore they have greater potential to become successful anticancer agents. The group subsequently synthesised a wide range of sulphur- and oxygen-containing heteroarotinoids primarily linked *via* an ester (*e.g.* Compounds **126** and **127**) or (*E*)-2-methylthienyl moiety (*e.g.* Compound **129**) to a *para*-carboxylic acid (*e.g.* Compounds **125** and **129**) or *para*-ethyl ester (*e.g.* Compounds **126** and **128**) phenyl moiety (*Figure 1.27*). Analogue **128**, displaying an amide linker moiety, demonstrated the most activity (37 - 64 % growth inhibition), closely followed by the ester linked compound **127** (6-52 % growth inhibition), in mouse xenograft models of two head and neck cancer cell lines.¹²⁹

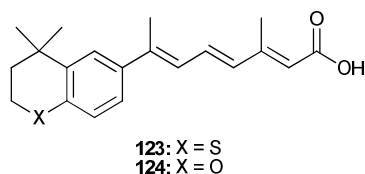


Figure 1.26 Heteroarotinoids designed and synthesised by Benbrook *et al.*^{126,129}

More recently, the group have synthesised a library of heteroarotinoid compounds containing urea and thiourea linker moieties, termed flexible heteroarotinoids (flex-hets) (*Figure 1.28*).¹³¹ All compounds demonstrated potent growth inhibition in ovarian cancer cell lines (EC_{50} 0.2 ± 5 to 10.2 ± 0.7 μ M), many of which were comparable to fenretinide (3.7 ± 0.2 μ M). In particular, compound **130** (*Figure 1.28*) demonstrated activity (37-84 % proliferation inhibition) which exceeded that of retinoic acid (7-52 % proliferation inhibition) and other analogues in the library across the majority

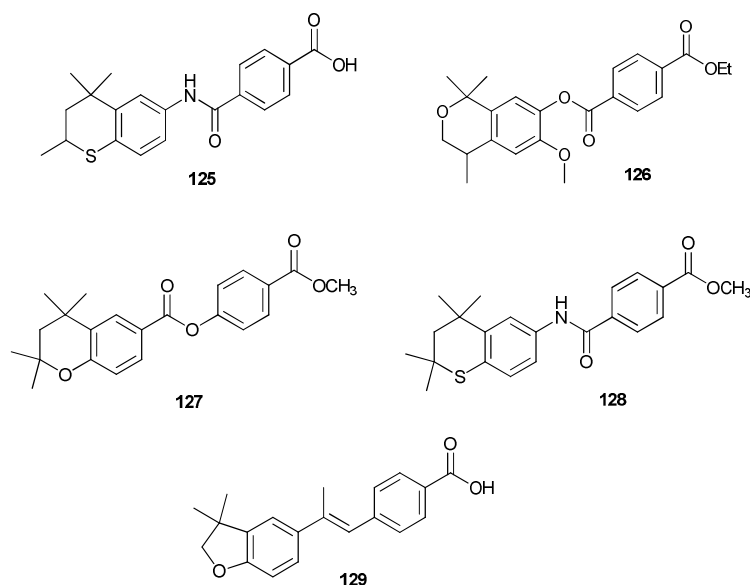
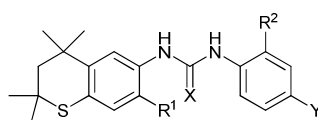


Figure 1.27 Further heteroarotinoids designed and synthesised by Benbrook, *et al.*¹³³



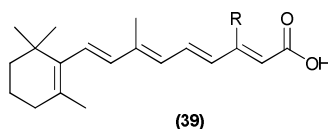
Compound	R ¹	X	R ²	Y
130	H	S	H	NO ₂
131	H	S	H	CO ₂ Et
132	H	O	H	CO ₂ Et
133	H	S	CH ₃	NO ₂
134	H	S	H	SO ₂ NH ₂
135	CH ₃	O	H	CO ₂ Et
136	CH ₃	S	H	CO ₂ Et
137	CH ₃	S	H	SO ₂ NH ₂

Figure 1.28 Potent flexible heteroarotinoid synthesised by Benbrook *et al.*¹³⁰

of the cell lines tested. This compound was proceeded to further biological evaluation; it was found to be active against all cell lines in the NCI60 cell line panel as well as cervical and head and neck cancer cell lines at 10 μ M, where it displayed improved activity compared to retinoic acid.^{132,133} Mechanistic studies identified that ‘flex-hets’ induce activity through a RAR-independent mechanism by directly targeting the mitochondria.¹³⁰

Wada *et al.* identified the size of the group at position 3 of retinoic acid (**6**) to be of significant importance for biological activity, as substitution with hydrogen (Compound **138**) resulted in a 10-fold decrease in activity

compared to the parent compound (**6**) (*Figure 1.29*).¹³⁴ Substitution of the methyl with an ethyl moiety (compound **139**) approximately halved the antiproliferative activity compared to retinoic acid (**6**). Addition of further steric bulk (*e.g.* Pr, Bu groups (compounds **140** and **141**, respectively)) led to a dramatic loss of activity rendering them inactive.



Compound	R	Relative antiproliferative activity (%) ^a	Apoptosis-inducing activity ^b
6 (retinoic acid)	Me	100	+
138	H	11	-
139	Et	43	-
140	Pr [†]	1	-
141	Bu [†]	< 0.3	-
142	PhCH ₂ CH ₂	6	-

^a The potency of retinoic acid (**6**) at ED₅₀ was normalized to 100%.

^b + positive; - negative. [†] Actual isomer not specified.

Figure 1.29 Investigation of substitution of position 13 of retinoic acid by Wada *et al.*¹³⁴

Das *et. al.* have synthesised a range of central scaffold variants of retinoic acid replacing a portion of the *trans*-alkene skeleton with a phenyl ring (compound **143** and **144**) (*Figure 1.30*).¹³⁵ The biological evaluation of these compounds is as yet unpublished.

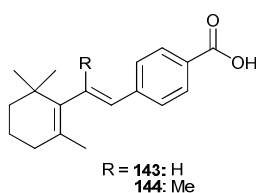


Figure 1.30 Constrained retinoic acid derivatives synthesised by Das *et al.*¹³⁵

1.11 Ligand-based design

Ligand-based design is a powerful technique for computer-aided drug design of new chemical entities.¹³⁶ Ligand-based design relies on the knowledge of the chemical structure of a molecule or molecules that bind to the biological target of interest or produce the desired phenotype. Such molecule(s) may then be used to derive a pharmacophore model that defines the minimum

necessary structural characteristics a molecule must possess in order to bind to the target. In other words, a model of the biological target may be built based on the knowledge of what binds to it, and this model in turn may be used to design new molecular entities that interact with the target. The generation of the pharmacophore takes into account the molecular shape of the query molecule(s), as well as properties such as hydrogen-bond donors and acceptors, positive and negative charges, rings and hydrophobic groups. At a minimum, a single query molecule can be used to define a pharmacophore; although the more active compounds that can be used to build the model the more reliable it will typically be. Ligand-based design can be used to identify new molecules which are either sub-structurally related or sub-structurally distinct to the query molecule(s). For those searches which generate molecules which are structurally distinct we term the technique 'scaffold hopping' as the substructure for a key unit in the molecule has been replaced with a pharmacophorically similar, but sub-structurally different unit. Ligand-based design has been shown to be as powerful as structure-based design for the design of new bioactive molecules.^{137,138} A number of different software packages are available to perform ligand-based design, including ROCS (Rapid Overlay of Chemical Structures, OpenEye Scientific)¹³⁹ and Phase (Schrodinger).¹⁴⁰

1.11.1 Rapid Overlay of Chemical Structures (ROCS)

ROCS performs ligand-based virtual screening of large databases of compounds, requiring only the structure of a single known active compound (the query) as a starting point.¹³⁹ ROCS works by measurement of the 3D 'similarity' of chemical compounds measured by tanimoto comparison and chemical features (*e.g.* electrostatic/hydrogen bonding properties). A score (0-2) based on the similarity between each compound and the query molecule is calculated, allowing the compounds to be ranked in order of their 'likeness' to the query. This score is called the ComboScore, which takes into account the shape-tanimoto (shape similarity) and scaled colour score (chemical similarity). The larger the number for the ComboScore score, the more similar the compound is to the query. On this scale if the molecules

being compared are the same then the ROCS ComboScore will give a score of 2.

1.12 Target Validation

Very little is known regarding the mechanism of action of fenretinide. Identification of a biological target responsible for the cell death process in ESFT cell lines and other cell lines is an attractive objective which may also aid in the design of future inhibitors. Although target identification is often challenging and time-consuming, knowledge of the actual biological target for a bioactive compound is fundamental objective for drug discovery. There are several methods available for the identification of the biological target of a bioactive molecule, including isolation of binding-proteins by use of affinity chromatography, drug affinity responsive target stability (DARTS), radioisotope-labelling, ion exchange chromatography and gel filtration.^{141,142}

1.12.1 Affinity chromatography

Affinity chromatography is a well established method for protein purification, developed in the 1960s, and remains the most frequently utilised method for target validation due to a relatively short number of steps compared to other methods and comparable yields.¹⁴³ The technique is unique in that it relies on the specificity of the binding interaction between a known inhibitor and the target protein. The inhibitor molecule is immobilised covalently on a solid resin. The amount of inhibitor that is successfully coupled to the Sepharose beads can be estimated by calculating the amount of the ligand (measured spectroscopically) recovered in the final washings. Alternatively, the loaded quantity can be measured by acid hydrolysis of the Sepharose and subsequent analysis of the recovered ligand.¹⁴⁴ A schematic diagram depicting the affinity chromatography process is shown (*Figure 1.31*). Cell lysates of cells under investigation are passed over the resin, under low pressure in a suitable buffer at around physiological pH. Binding components are adsorbed onto the bead by interaction with the ligand. The column is washed to remove any non-binding components, and those fragments with a specific binding affinity to the ligand are subsequently dissociated and eluted, usually using a high salt buffer. The purified proteins can be analysed by

SDS-PAGE and protein bands identified by mass spectrometry. A simultaneous negative control, preferably utilising a 'deactivated' ligand (*e.g.* activity eliminated by removal of an essential binding region such as a hydrogen-bond donor, as confirmed by SAR studies), is essential to distinguish between potential targets and non-specific binders. Affinity chromatography has been used extensively in the past and has been optimised to successfully provide high selectivity, resolution and yields of target proteins in a relatively short amount of time.

Several types of solid support for affinity chromatography studies are available, including cross-linked cellulose, Trisacryl, Fractogel and silica. However, the most widely used resin is an agarose, commonly known as Sepharose, due to its desirable qualities (*i.e.* good chemical stability, high surface:volume ratio, easy binding of ligand to linker moiety and good flow properties) and reliability over the years. Sepharose is a polysaccharide polymer extracted from seaweed which is bound in a cross-linked bead formation of approximately 50-400 μm diameter.^{143,144}

The importance of the length of the hydrocarbon chain linking the ligand to a Sepharose bead was highlighted by Cuatrecasas *et al.*¹⁴⁵, who demonstrated that steric hindrance could be reduced, subsequently increasing the protein-binding capacity of the gel, by placing the ligand a moderate distance from the gel (*ca.*7 atoms) compared to a ligand directly bound to the gel. However,

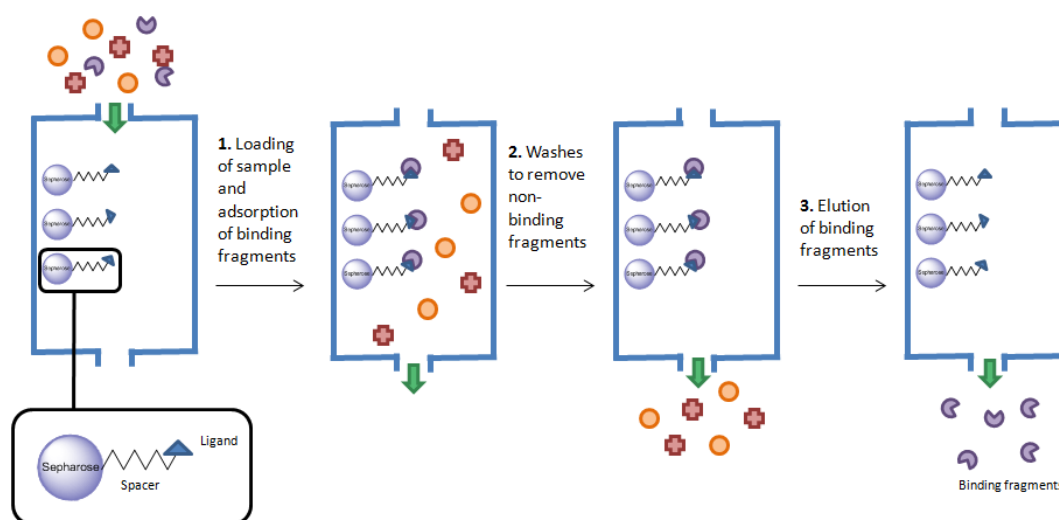


Figure 1.31 A schematic diagram depicting the affinity chromatography process.
(Adapted²²¹)

the protein-binding capacity was not increased further by further extension of the hydrocarbon chain past this optimum length. Furthermore, O'Carrar *et al.* have subsequently demonstrated that the hydrophilicity of the linker moiety between the bead and ligand is significant, where highly hydrophobic chains result in an increase in non-specific binding to a wide range of enzymes.¹⁴⁵ It is important that a more hydrophilic linker moiety is incorporated which, as observed by O'Carrar *et al.*, results in elimination of the majority of the interfering adsorptions.

Identification of an appropriate attachment point for a linker moiety onto the ligand is often the primary limitation of affinity chromatography, requiring extensive SAR studies which can be time consuming. Furthermore, many ligands may not allow for attachment of the linker moiety, as doing so impedes binding to the biological target and results in loss of activity.¹⁴¹

1.12.2 Affinity chromatography for retinoid-based ligands

Affinity chromatography has been a preferable method in the past for purification of RBP4 using retinoid ligands, due to its relative simplicity and similar yields in comparison to alternative methods (*e.g.* ion exchange, gel filtration).^{142,146} Sepharose was regularly used as the solid matrix to which the retinoid ligands were bound. First reported by Fex and Hansson in 1978, retinoic acid was linked to Sepharose *via* the carboxylic acid moiety.¹⁴⁶ Attempts to couple the preferred ligand, retinol, to Sepharose failed, therefore retinoic acid was used as an alternative due to the ease of coupling of a carboxyl group to the matrix and it is known to display similar binding properties to RBP4. Very strong binding was observed between RBP4 and retinoic acid-Sepharose and the protein was successfully purified from both serum and urine, with *ca.* 80 % apo-RBP4 recovered from the sample. Interestingly, predicted binding of cellular retinoic acid binding protein (CRABP) was not observed. This could possibly due to disruption of an important binding interaction between the protein and the carboxylic acid of retinoic acid, as this moiety is incorporated into the linker moiety and therefore unavailable.¹⁴²

Chapman and Curley utilised an alternative approach, whereby two novel retinoids (**145** and **146**) based on β -ionone, bearing amino and chloride warheads at the allylic 4-position for attachment to Sepharose (*Figure 1.32*) were designed and synthesised.¹⁴² The design of these ligands avoided the use of the relatively unstable retinol and retinol derivatives. Initial attempts to couple compound (**146**) to the terminal amino group of AH-Sepharose 4B were unsuccessful. The group subsequently found that a catalytic amount of sodium iodide aided coupling to Sepharose, by displacement of the chloride by the iodide, but only *ca.* 50 % of available binding sites were found to be occupied by the ligand. However, compound (**146**) was successfully coupled to the terminal carboxyl group of CH-Sepharose 4B, with virtually all possible binding sites occupied. The matrix proved to isolate apo-RBP4 selectively from rabbit serum with a yield of 11 % and 900-fold amplification.

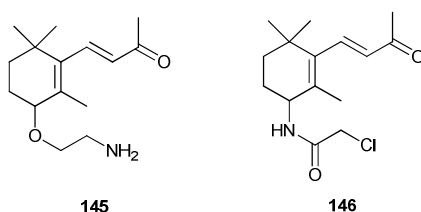


Figure 1.32 Two novel retinoid affinity chromatography ligands based on β -ionone, synthesised by Chapman and Curley.¹⁴²

1.13 Aims of this Thesis

This research aims to apply classical medicinal chemistry and ligand-based approaches to identify and develop novel, potent and selective chemotherapeutics which may have improved efficacy compared to fenretinide. Screening of the compounds using biological assays will identify new potential anti-cancer leads with improved activity in Ewing's Sarcoma Family of Tumours (ESFT).

Through consideration of the molecular structure of both retinoid and non-retinoids, a SAR for fenretinide in ESFT cells will be established. Understanding of the molecular features of fenretinide responsible for biological activity will guide the design of further analogues which should have improved potency compared to fenretinide, whilst retaining its minimal toxicity profile. The *in vitro* pharmacokinetic profile of new compounds will also be studied.

Through mechanistic studies, the project will identify whether retinoid and non-retinoid fenretinide analogues induce cell death by induction of similar cell death pathways to fenretinide, or whether the compounds may activate novel pathways.

Additionally, target validation studies using affinity chromatography methods will identify potential targets to which fenretinide may bind to initiate cell death which may inform the development of novel targeted therapeutics.

2. SAR for fenretinide in ESFT cells

2.1 Introduction

It was of interest to perform a molecule-wide systematic study of atom and functional group replacements on the structure of fenretinide to understand the molecular basis of its cytotoxic activity and identify the structural moieties critical for fenretinide-induced cell death in ESFT cells. This structure-activity relationship (SAR) study will help to determine whether it is possible to improve the biological effects of fenretinide in ESFT cell types by synthetic modification and to appropriately guide the design of new cytotoxic agents with improved pharmacological properties over fenretinide. Through these studies, and by comparing observed results with those of the published literature, it will be possible to establish and understand the molecular features required for activity in different cell types/assays.

The SAR study will also allow the design of target-capture probes for affinity chromatography to support identification of the biological target(s) responsible for initiation of the cell death process (Chapter 5) as well as guide the design of non-retinoid mimetics of fenretinide as novel cytotoxic agents (Chapter 3).

2.2 SAR study

Various structural analogues of fenretinide were designed and synthesised to probe the SAR for fenretinide in inducing cytotoxicity in ESFT TC32 cells. To ensure a systematic approach to structural modification, the structure of

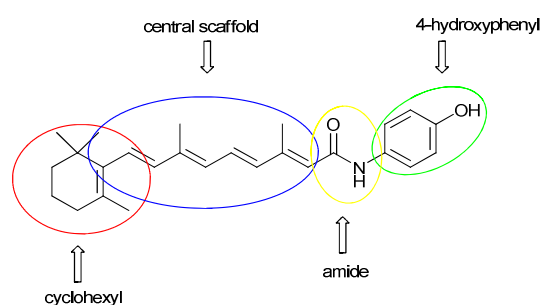


Figure 2.1 Fenretinide structure divided into four synthetically accessible regions.

fenretinide was subdivided into four discrete substructures for study; the 4-hydroxyphenyl, amide, cyclohexyl and central scaffold (*Figure 2.1*).

2.2.1 SAR for the 4-hydroxyphenyl group

Since a polar *para*-substituent on the phenyl ring of fenretinide is reported to be important for cell death activity in F9 murine embryonal carcinoma and breast cancer cells^{38,116} and, more specifically, the *para*-hydroxy substitution is essential for cell death activity in rhabdoid tumour cell line¹¹⁷, it was of interest to investigate the hydroxy group to better understand its role in promoting cell death in ESFT cells. Additionally, since phenols are widely known to suffer high phase II metabolism by glucorinidation¹⁴⁷, including that of fenretinide¹⁰⁴, it would be desirable to identify a moiety that could replace the hydroxy group whilst retaining activity which might lead to an increase in bioavailability.

For the SAR study, a number of variants of the *para*-hydroxyl group were designed; replacement of the OH with a OMe, NH₂ or H, and movement of the polar group (OH or NH₂) to the *ortho*- and *meta*- positions (*Figure 2.2*).

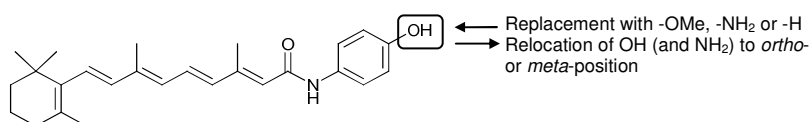
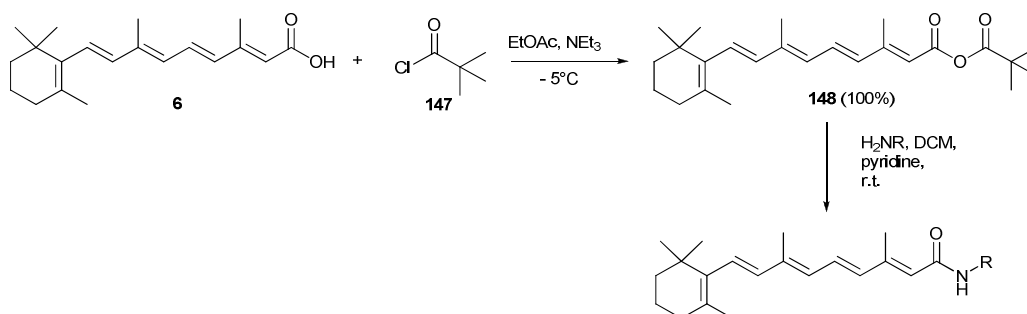


Figure 2.2 SAR study for the importance of the *para*-hydroxy group for induction of cell death in cancer cells.

2.2.2 Synthesis of 4-hydroxyphenyl variants

The designed *para*-hydroxyl variants were all synthesised by amide coupling chemistry from the aniline containing the desired 4-hydroxyphenyl variant to retinoic acid (**6**). The preferred method involved the formation of a pivalic mixed anhydride intermediate (**148**), derived from retinoic acid (**6**), followed by reaction with the substituted aniline to generate the desired amide (*Scheme 2.1*). Using this methodology, seven substituted amides were synthesised in variable yields (28-61 %) (*entries 1-7, Scheme 2.1*). The purity of the final compounds obtained *via* this method was significantly improved in comparison to a previously investigated method involving use of

DCC/EDCI or HBTU mediated coupling reaction, which generated by-products that were difficult to separate from the desired products.



Entry number	H ₂ NR	Product	Yield (%)
1			30
2			35
4			61
3			50
5			42
6			28
7			35

Scheme 2.1 Synthesis of 4-hydroxyphenyl analogues of fenretinide *via* a mixed anhydride intermediate.

2.2.3 Biological evaluation of 4-hydroxyphenyl variants

To determine the biological activity of the 4-hydroxyphenyl variants synthesised above, the compounds were screened against a single ESFT cell line (TC32) at 10 μM over 24 h (*Table 2.1*). Each compound was screened in triplicate and each independent experiment was repeated at least three times ($n \geq 9$). Cell viability was measured on a ViCell machine which utilises the trypan blue exclusion assay¹⁴⁸ to measure viable cell number; viable cell number was expressed as a percentage of that obtained

from cells treated with the vehicle control. Statistical analysis was evaluated by 1-way ANOVA with Dunnetts post hoc tests using GraphPad InStat 3.¹⁴⁹ Compounds were deemed to display statistically significant activity when $p < 0.05$ compared to the vehicle control cell viability, and comparable activity to fenretinide when $p > 0.05$ compared to the fenretinide control cell viability.

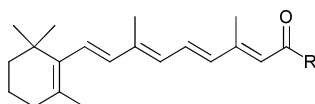
Any hit compounds were screened against a normal cell line, mesenchymal stem cells (MSCs), using the same assay, to identify compounds with *in vitro* activity in cancer cells but not in normal cells. Although this is a rudimentary measurement of potential toxicity and may not accurately reflect *in vivo* toxicity, which can be assessed more accurately using animal models (as described in Section 1.4), a significant decrease in the viable cell number of MSCs may identify compounds that are likely to have unfavourable toxicity and should not progress further. MSCs were treated with compounds at 10 μM for 24 h and cell viability was analysed using the trypan blue exclusion assay, as described for the ESFT cells above.

For each compound the ClogP and aqueous solubility was calculated using ChemBioDraw Ultra (PerkinElmer)¹⁵⁰ and an estimation of solubility ($\log S$), in a unit stripped logarithm (base 10) of the solubility measured in mol/litre, was calculated using OSIRIS property explorer.¹⁵¹ An estimated $\log S > -4$ is favourable, which accounts for more than 80 % of the drugs on the market. The ClogP and solubility values can be used to support the understanding of the SAR.

Initial screening confirmed that the hydroxy group at the *para*-position of fenretinide is important for activity in ESFT cells (*Table 2.1*). Removal of the hydroxy (*i.e.* replacement with H, compound **61**) or its methylation (compound **24**) resulted in loss of activity (90 ± 4 and 93 ± 2 % cell viability, respectively) compared to the fenretinide control (43 ± 2 % cell viability). Movement of the hydroxy group to the *ortho*- (**19**) and *meta*-positions (**20**) also resulted in loss or a significant decrease in activity (93 ± 3 and 83 ± 2 % cell viability respectively) compared to the *para*-hydroxy version (the fenretinide control) (43 ± 2 % cell viability). The results suggest the importance of a polar (hydroxy) group at the *para*-position. Consistent with

these findings, replacement of the *para*-hydroxy with H was found to be detrimental to cytotoxic activity in MCF-7 breast cancer cells reported by Mershon *et al.*, where only weak activity (≤ 50 % activity of the fenretinide standard) was observed in a fluorescein diacetate cell viability assay.¹¹⁶

In contrast, for the methoxy compound (**24**), Sabichi *et al.*³⁸ reported cytotoxic activity approaching that of fenretinide when using F9 murine embryonal carcinoma cells in an MTT assay, suggesting that the biological activity of this compound may be cell line specific. Sabichi *et al.* also reported that the *ortho*- and *meta*-OH compounds (**19** and **20**) were weakly active in the same assay, although a similar trend in activity was observed to ours (*para*-OH > *meta*-OH > *ortho*-OH) suggesting that the *para*-position is favoured for biological activity, perhaps mediated by a H-bond interaction from the ligand to the protein at this site.



Compound number	R	% TC32 cell viability*	% MSC cell viability*	ClogP	Predicted logS (mol/litre)
1 (fenretinide)		43 ± 2	88 ± 5	7.1	-4.6
61		90 ± 4	-	7.8	-5.0
24		93 ± 2	-	7.9	-5.0
19		93 ± 3	-	7.4	-4.7
20		83 ± 2	-	7.1	-4.7
58		60 ± 3	101 ± 7	6.6	-5.1
156		83 ± 3	-	6.6	-5.1
157		80 ± 4	-	6.6	-5.1

*Toxicity in TC32 cells and MSC cells treated at 10 μ M for 24 h; Cell viability is expressed as the mean viable cell count as a % of the DMSO control \pm SEM; -, not measured.

Table 2.1 Chemical structures, biological activity and physicochemical properties of the 4-hydroxyphenyl analogues of fenretinide.

The most active compound from the set was the *para*-amino-containing compound (**58**) which displayed good activity (60 ± 3 % cell viability) compared to the fenretinide control (43 ± 2 % cell viability). As this compound displayed an encouraging level of activity, it was screened against the MSC cell line. The compound was inactive against MSCs (101 ± 7 % cell viability), indicating that the observed activity is specific to the cancer cells. The activity observed for this compound supports the conclusions made for the hydroxy-containing compounds above, possibly suggesting that relocation of the amino group to the *ortho*- (**156**) and *meta*- (**157**) positions significantly reduced activity (83 ± 3 and 80 ± 4 % cell viability respectively), suggesting that *para*-substitution is preferred, consistent with the observation for the hydroxy group. The activity observed for the *para*-amino containing compound is consistent to that described by Mershon *et al.* for this compound against the MCF-7 breast cancer cells (≥ 50 % activity compared to the fenretinide control).¹¹⁶

A possible explanation for the reduced activity observed for the *ortho*-hydroxy and amino substituted analogues (**19** and **156**) is the increased level of planarity associated with these compounds, owing to an intramolecular hydrogen bond extending from the H atom of the *ortho*-hydroxy or amino group to the oxygen atom of the carbonyl of the amide, forming a pseudo 7-membered ring which cannot be present in the *para/meta*-substituted analogues.¹⁵² An increase in planarity might adversely affect physicochemical properties associated with the cell death response, including the aqueous solubility (planar compounds are typically less soluble than structurally related non-planar compounds¹⁵³), as well as disrupt any hypothetical binding interactions to the target associated with a change in conformation of the molecule. It is noteworthy that the predicted aqueous solubility of the *ortho*- substituted molecules is roughly equivalent to that of the *meta*- and *para*- analogues (*Table 2.1*); however, aqueous solubility is a very difficult metric to predict accurately.

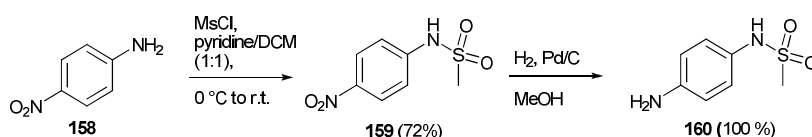
2.2.4 *para*-hydroxy and *para*-amino isosteric replacement

Since the *para*-hydroxy and *para*-amino moieties were found to be important for activity, a range of *para*-hydroxy or *para*-amino isosteres were

synthesised to investigate whether bioisosteric substitution at this position was tolerated. A range of classical isosteres of the phenol (or aniline)¹⁵⁴, including phenyl sulfonamide/acetamide, indole and benzimidazolinone, and a range of substituted phenyls including hydroxymethyl, aminomethyl and a carboxylic acid were selected for investigation.

2.2.5 Synthesis of *para*-hydroxy and *para*-amino isosteres

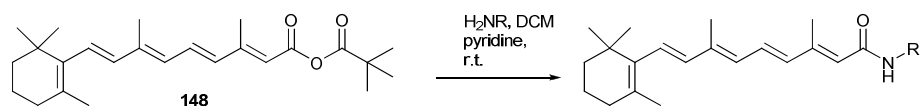
The *para*-hydroxy and *para*-amino isosteres planned for synthesis all relied on an amide coupling chemistry from the aniline containing the desired *para*-hydroxy and *para*-amino isostere to the pivalic mixed anhydride intermediate (**148**) (prepared from retinoic acid (**6**) as described previously, see page 50) (*Scheme 2.3*). Most of the anilines selected for use in this study were commercially available. However, one non-commercially available aniline was required for synthesis. The *para*-aminosulfonamide (**160**) was synthesised from *para*-nitroaniline (**158**) by addition of methanesulfonyl chloride in a 1:1 pyridine:DCM solution to generate the nitro sulfonamide (**159**) which was then reduced to the desired aniline (**160**) in excellent yield over two steps (*Scheme 2.2*).



Scheme 2.2 Synthesis of the aniline precursor of the methylsulfonamido phenol isostere.

The amide coupling reactions to generate the desired amides progressed without incident for all but three of the library reactions (*entries 8-10, Scheme 2.3*). The reaction of methylamine (**170**) generated the undesired *N*-methylamide regioisomer (**179**) as the exclusive product rather than the desired NH-amide (**178**) (*Scheme 2.4*), as confirmed by ¹H NMR based on the observed chemical shift of the *N*-methyl protons (δ 3.3) (predicted shift of the amide being higher (δ 3.4) than for the the amine variant (δ 2.7)).

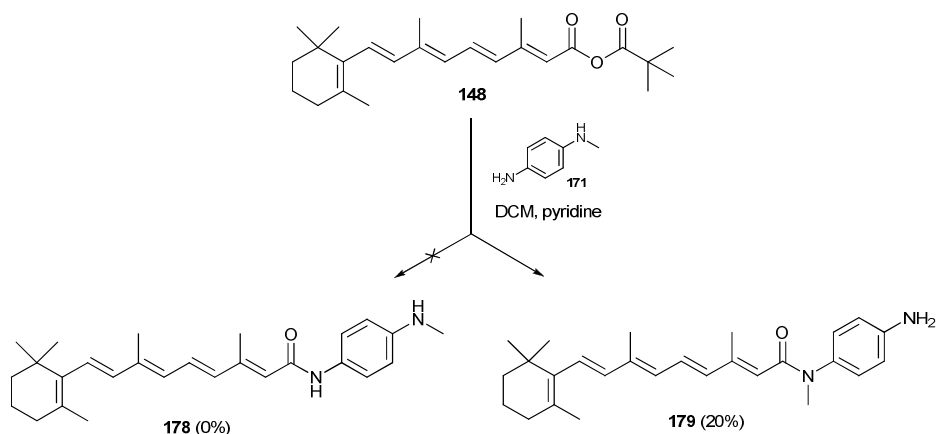
In an effort to generate the the desired regioisomer (**178**), the secondary amine was protected using a Boc-protection strategy. *N*-methyl-4-nitroaniline (**180**) was Boc-protected and the nitro group reduced to give the aniline (**182**) in excellent yield over two steps (*Scheme 2.5*). The aniline (**182**) was then



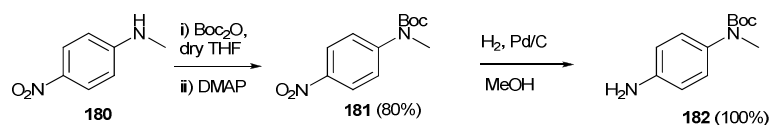
Entry number	H ₂ NR	Product	Yield (%)
1			16
2			41
3			53
4			7
5			11
6			33
7			22
8			0
9			0
10			0

Scheme 2.3 Synthesis of *para*-hydroxy and *para*-amino isosteres of fenretinide using the mixed anhydride method.

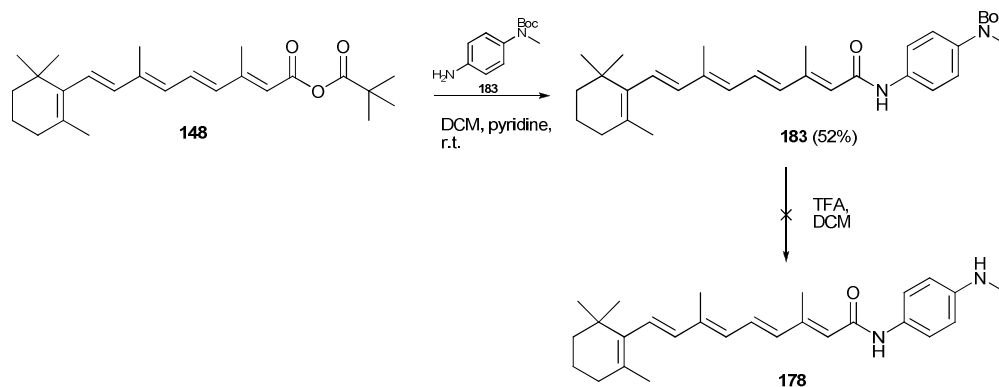
coupled to the mixed anhydride of retinoic acid (**148**) using the standard method to yield the Boc-protected amide (**183**) (Scheme 2.6). Unfortunately, upon attempted liberation of the desired *N*-methylamine (**178**) using TFA or 2M HCl at varying concentrations and timescales, an uncharacterisable product was generated with only trace-quantities of the desired product visible as indicated by LCMS.



Scheme 2.4 Coupling of *N*-methyl *para*-phenylenediamine (**170**) to the mixed anhydride (**148**) formed the methylamide (**179**) as the only regioisomer.



Scheme 2.5 Synthesis of the Boc-protected *N*-methylbenzene-1,4-diamine precursor.



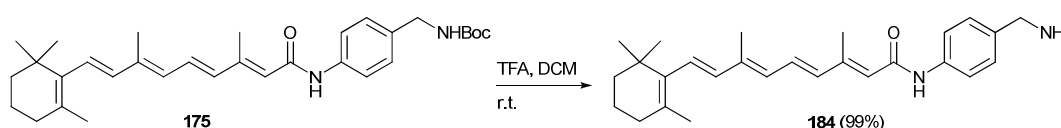
Scheme 2.6 Synthesis of the Boc-protected *N*-methyl amine (**183**). Deprotection of the Boc group was unsuccessful.

For the hydroxymethyl variant (**72**), a single regioisomer was obtained, which was confirmed as the amide (rather than the ester originating from coupling of the OH to the activated carboxylic acid) due to the observed chemical shift of the CH_2 protons adjacent to the hydroxyl (observed: δ 4.44; predicted: δ 4.16, compared to ester predicted: δ 5.16) in the ^1H NMR spectrum. The preference for reactivity of the NH_2 over the OH for this class of substrate is

consistent with that observed in the literature for amide bond formation using similar conditions.¹⁵⁵

The synthesis of the the sulfonamide (**176**) and benzimidazole (**177**) were also unsuccessful. In both cases the desired products were generated as observed by both NMR and LCMS but, upon standing, an impurity developed indicative of cleavage of the amide bond to retinoic acid.

The desired final compound, aminomethyl derivative (**184**), was generated from the Boc-protected benzylamine (**175**) (*entry 6, Table 2.2*), by stirring in TFA/DCM for 1 h at room temperature (*Scheme 2.7*).



Scheme 2.7 deprotection of the Boc-protected benzylamine (**175**).

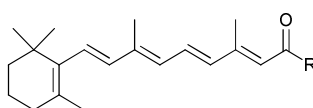
2.2.6 Biological evaluation of the para-hydroxy and para-amine isosteres

The nine compounds prepared above were screened in the TC32 cell viability assay, using the method as described previously (see page 51). The compounds demonstrated a range of activities from 62 ± 2 to 106 ± 6 % cell viability compared to the vehicle control, with three compounds (**171**, **172**, and **174**) demonstrating a statistically significant response (*Table 2.2*).

The most potent compound from the set - the acetamide (**172**) – demonstrated good activity (62 ± 2 % cell viability) compared to the vehicle control, but reduced activity compared to fenretinide (43 ± 2 % cell viability). The next most active compound, the sulfonamide isostere (**171**), also displayed statistically significant activity (71 ± 2 % cell viability) compared to the vehicle control. As both the acetamide and sulphonamide are isosteres of phenol in which the NH can mimic the OH group, it may be that the OH (or NH) is acting as a hydrogen bond participator to a macromolecular target responsible for eliciting the biological effect. As the *NH*-acetamide is a weaker H-bond donor than the *OH* of the phenol (increase in pK_a from *ca.*10 to *ca.*16 from *OH* of a phenol to *NH*-acetamide) this may correlate to a

weaker polar interaction.¹⁵⁶ Weak but statistically significant activity was also observed for the benzimidazolinone (**174**) (82 ± 3 % cell viability).

Of the inactive compounds, a consistent feature is the presence of a methylene spacer between the phenyl ring and the functional group, *i.e.* the hydroxymethyl (**72**) and aminomethyl variants (**175** and **184**). The loss of activity for these compounds may be the result of a range of steric, electronic and/or hydrophobic factors associated with incorporation of the methylene spacer between the functional group and the aromatic ring. For instance, the incorporation of the methylene spacer will decrease the electron density of



Compound number	R	TC32 cell viability*	ClogP	Predicted logS (mol/litre)
1 (fenretinide)		43 ± 2	7.1	-4.7
171		71 ± 2	6.6	-6.1
172		62 ± 2	6.8	-5.3
72		88 ± 3	6.8	-4.9
173		87 ± 4	7.8	-5.5
174		82 ± 3	6.8	-5.9
175		106 ± 6	8.5	-6.2
23		100 ± 6	7.8	-5.0
183		88 ± 3	8.4	-8.4
184		99 ± 10	6.8	-4.9

*Toxicity in TC32 cells treated at 10 μ M for 24 h; Cell viability is expressed as the mean viable cell count as a % of the DMSO control \pm SEM; -, not measured.

Table 2.2 Chemical structures, biological activity and physicochemical properties of *para*-hydroxy isosteres of fenretinide.

the phenyl ring compared to the phenol, possibly disrupting any *pi*-orbital interactions to a potential target. Also, the acidity and hydrogen bond donor/acceptor capability of the functional groups attached to a methylene or phenyl ring will vary owing to delocalisation. The loss of activity observed for compounds containing the methylene spacer is consistent with the earlier studies suggesting the importance of a hydroxy or amino group at the *para*-position of the phenyl ring (Section 2.2.3). Interestingly, the loss of activity for the hydroxymethyl substitution (**72**) is consistent with that observed by Das *et al.* when this compound was screened against rhabdoid tumour cells using an MTS cell viability assay.¹¹⁷

Completing this set of compounds, the Boc-protected *N*-methylamine (**183**), the NH-indole (**173**) and the carboxylic acid (**23**) were inactive. The lack of activity for the carboxylic acid is probably the result of the reduced ability of the compound to penetrate the cell membrane. The inactivity of the indole may be attributed to the increase in hydrophobicity in comparison to the 4-aminophenyl variant (**58**) (ClogP 7.8 vs 6.6) or possibly the differing hydrogen-bonding capability of the NH.

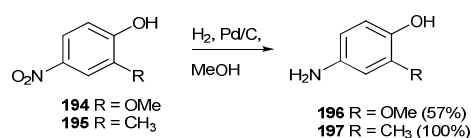
2.2.7 Substitution in the 4-hydroxyphenyl ring

A range of molecules were designed to probe the relative importance of substitution of the 2- and 3-positions of the 4-hydroxyphenyl ring of fenretinide. The substituent groups were selected to encompass a range of substituents with varying hydrophobicity, size and electron withdrawing/donating parameters.

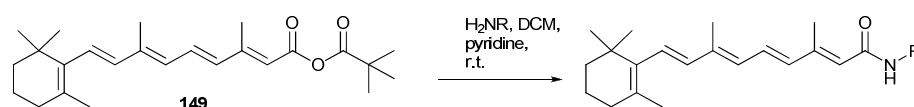
2.2.8 Synthesis of substituted 4-hydroxyphenyl analogues

A range of compounds was planned based on the investigation of a range of substituted 4-hydroxyphenyl variants. Each of the proposed compounds was synthesised using amide coupling chemistry from the aniline containing the desired substituted 4-hydroxyphenyl variant to the pivalic mixed anhydride intermediate (**148**) (prepared from retinoic acid (**6**) as described previously, see page 50). Most of the anilines were commercially available although two, the methoxyaniline (**196**) and the methyl aniline (**197**), were required in order to synthesise the desired 3-methoxy and 3-methyl fenretinide variants (**192**

and **193**). These anilines were prepared from the parent nitro compounds **194** and **195** using hydrogenation to give the anilines **196** and **197**, respectively, in variable yields (*Scheme 2.8*). Using the pool of anilines assembled and the amide coupling chemistry described, six 4-hydroxyphenyl variants were synthesised in modest yields (24-57 %) (*entries 1-6, Scheme 2.9*).



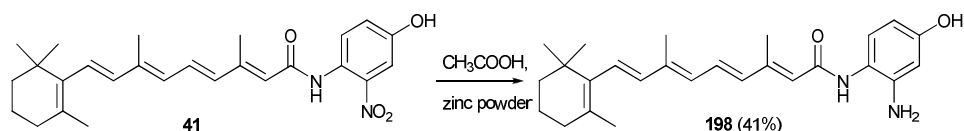
Scheme 2.8 Hydrogenation of compounds **194** and **195** to form the anilines **196** and **197**.



Entry number	H ₂ NR	Product	Yield %
1			40
2			27
3			57
4			24
5			29
6			33

Scheme 2.9 Synthesis of substituted phenyl analogues of fenretinide from the mixed anhydride intermediate.

An additional compound, the aniline (**198**), was synthesised by reduction of the nitro group of compound **41** to the primary amine using zinc powder in acetic acid in reasonable yield (*Scheme 2.10*).

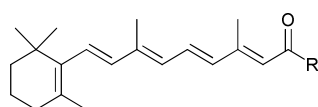


Scheme 2.10 Zinc reduction to generate the anilino analogue (**198**) of the nitro compound (**41**).

2.2.9 Biological evaluation of substituted 4-hydroxyphenyl analogues

The seven compounds prepared above were screened in the TC32 cell viability assay, using the method as described previously (see page 51).

Only one compound from the set demonstrated a significant induction of cell death in the TC32 assay (compound **198**, 35 ± 3 % cell viability) which was statistically comparable to fenretinide (compound **1**, 43 ± 2 % cell viability) (*Table 2.3*). This compound contains an amino group at the 2-position of the



Compound number	R	% TC32 cell viability*	% MSC cell viability*	ClogP	Predicted logS (mol/litre)
1 (fenretinide)		43 ± 2	88 ± 5	7.1	-4.6
70		70 ± 7	-	7.5	-5.0
191		92 ± 3	-	8.1	-5.5
41		94 ± 4	-	7.2	-5.3
198		35 ± 3	93 ± 3	5.9	-4.8
192		87 ± 3	-	7.0	-4.7
25		90 ± 2	-	7.0	-5.0
193		84 ± 2	-	7.6	-5.0

*Toxicity in TC32 cells and MSC cells at 10 μ M at 24 h. – not measured. Cell viability is expressed as the mean viable cell count as a % of the DMSO control.

Table 2.3 Chemical structures, biological activity and physicochemical properties of substituted 4-hydroxyphenyl analogues of fenretinide.

phenyl ring of the fenretinide structure. The compound also failed to induce cytotoxicity when tested in the MSC cell assay (93 ± 3 % cell viability), therefore the activity for this compound is likely to be specific to the cancerous TC32 cells. Although the TC32 cell activity for this compound is not significantly better than for fenretinide, the compound is less hydrophobic (ClogP 5.9 vs 7.1 for fenretinide), suggesting the possibility that compound **198** may be more water soluble, although this is not truly reflected in the calculated aqueous solubility values (*Table 2.3*).

Of the inactive compounds, the electron donating *meta*-OMe (**192**) and *ortho*- and *meta*-Me groups (**25** and **193**) were very weakly active or inactive (87 ± 3 , 90 ± 2 and 84 ± 2 % cell viability respectively) compared to the vehicle control. The electron withdrawing substituents, Br at the 3-position (**191**), and nitro at the 2-position (**41**) resulted in complete loss of activity (92 ± 3 and 94 ± 4 % cell viability respectively), whilst 3-fluoro substitution (**70**) resulted in a significant reduction in activity (70 ± 7 % cell viability) compared to that of fenretinide (43 ± 2 % cell viability). The biological data for the range of inactive substituents suggests that the 4-hydroxyphenyl ring is highly sensitive to structural modification, although some of the data may be cell line specific. For instance, the same fluoro analogue (**70**) has been shown to demonstrate significant activity (IC_{50} 8 μ M) which was similar to fenretinide (IC_{50} 19 μ M) when tested in a different cell line (rhabdoid tumour cells) as reported by Das *et al.*¹¹⁷

The change from an electron withdrawing substituent (nitro **41**) at the 2-position to an electron donating (amino **198**) at the same site was particularly interesting as the biological data demonstrated a steep SAR for this modification. The influence of the amino and nitro groups on the electronic and hydrophobic properties of the molecule will be different, which will influence the biological data obtained. The hydrophobicity of the nitro compound (**41**) is higher than the amino compound (**198**) (ClogP 5.9 vs 7.2) owing to the increased hydrophilicity of the amino substituent. The significant difference in the electronic properties of the substituents may influence the ability of the molecule to bind to a macromolecule either directly (hydrogen-bonding site from or to the amino or nitro group), or indirectly (electronic

influence to interactions mediated through the amide, aromatic ring, or indeed the OH). Additionally, the nitro group is predicted to have a more significant influence on the pK_a of the OH group than for the amino group (*ca.*8 vs *ca.*10). Additionally, the difference in biological activity observed for the nitro- and amino-substituted compounds could be a steric effect, either directly blocking binding to a macromolecule, or through a conformational change. For instance, the *ortho*-NO₂ group may form an intramolecular 6-membered ring hydrogen-bonding interaction between the δ^+ nitrogen (which is not present in the amino variant) and the adjacent amide-carbonyl group¹⁵⁷, therefore restricting flexibility and hindering a possible binding interaction. It is noteworthy that the same 2-nitro substituted fenretinide analogue (**41**) was found to be inactive against MCF-7 breast cancer cells by Mershon *et al.*¹¹⁶

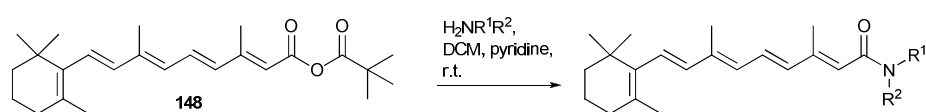
2.2.10 Additional phenyl analogues

A range of additional analogues of the 4-hydroxyphenyl moiety were synthesised to further explore the SAR within this region. Designed analogues, all based on the aniline template, contained a range of functional groups; substituent heterocycles as well as saturated variants of the phenyl ring were investigated. In general the designed analogues were more diverse and less focused on specific atom replacements than those analogues selected for the two previous rounds of synthesis and biological testing.

2.2.11 Synthesis of additional phenyl analogues

Each of the proposed compounds was synthesised using amide coupling chemistry from the aniline (or amine) containing the desired substituted 4-hydroxyphenyl variant to the pivalic mixed anhydride intermediate (**148**) (prepared from retinoic acid as described previously) (*Scheme 2.11*). Using this method, the eight amides (**199-207**) were synthesised in varying yields (12-95 %) and without incident except for the nitro substituted compound (**207**) (*Scheme 2.11*). The reaction between *para*-nitroaniline and the mixed anhydride (**148**) failed to generate any evidence of the desired product, even when the temperature of the reaction was raised to reflux for 48 h. This is likely due to the deactivating nature of the *para*-NO₂ substituent on the reactivity of amino group. No further efforts were made to synthesise this

compound. For the pyrazole (**204**), a mixture of inseparable regioisomers was obtained. The major product (> 70 % by ^1H NMR) was tentatively assigned as the NH-amide due to the characteristic chemical shift of the carbon of the pyrazole bonded directly to the amide in the ^{13}C NMR spectrum (observed: δ 135.7; predicted: δ 135.4), compared to that for the carbon bonded directly to the primary amine of the acylpyrazole (predicted: δ 149.5). A preference for the same regiochemical outcome, *i.e.* reactivity from the NH_2 rather than the NH of the imidazole to form the secondary amide instead of the acylpyrazole from carboxylic acids has been reported by others.¹⁵⁸

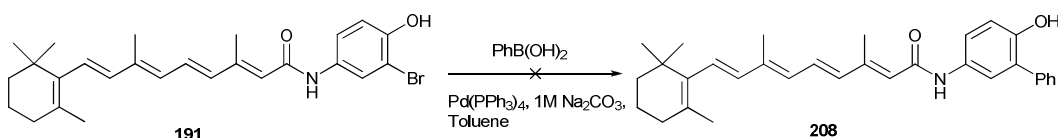


Entry number	R ¹	R ²	Product	Yield %
1	H			37
2	H			48
3	H			12
4	H			44
5	H			31
6 [†]	H			26
7				95
8	H			36
9	H			0

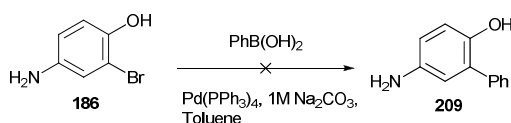
[†] Exists as a mixture of inseparable regioisomers (major isomer reported).

Scheme 2.11 Synthesis of selected phenyl analogues of fenretinide from the mixed anhydride.

An additional analogue (the *meta*-phenyl analogue, **208**) was designed based on a Suzuki reaction of the *meta*-Br substituted compound (**191**) (prepared previously; *Scheme 2.9*, page 61) and phenylboronic acid. Unfortunately, the reaction failed to provide sufficient quantities of the desired product for purification (*Scheme 2.12*). As only small quantities of the bromide (**191**) were available an alternative approach was adopted, whereby the Suzuki coupling would be performed at an earlier stage for later coupling to retinoic acid, to generate the target compound. Following this strategy, the attempted Suzuki coupling of the bromoaniline (**186**) with phenyl boronic acid to form the aniline **209** was also unsuccessful (*Scheme 2.13*).



Scheme 2.12 Failed synthesis of the biphenyl analogue (**208**).



Scheme 2.13 Failed Suzuki coupling of bromophenol (**186**) to generate 5-aminobiphenyl-2-ol (**209**).

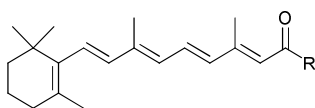
2.2.12 Biological evaluation of additional phenyl analogues

The compounds prepared above were screened in the TC32 cell viability assay as described previously (see page 51).

Only one compound (the 4-pyridyl variant, **199**) out of the eight compounds tested demonstrated a significant induction of cell death in the assay (50 ± 2 % cell viability) which was comparable to that of fenretinide (43 ± 2 % cell viability) (*Table 2.4*). As this is contrary to our hypothesis that a hydrogen bond participator (possibly a donor) at the *para*-position is likely to be required for activity, it is possible that this analogue initiates cell death through an alternative mechanism to the parent compound. Alternatively, the nitrogen atom may form an interaction with a target through a water-mediated hydrogen bond. The nitrogen may also form interactions directly

with the target by acting as a hydrogen-bond acceptor, potentially forming a similar interaction to the oxygen atom of the *para*-hydroxy moiety in the parent compound. This compound also lacked activity in the MSCs (94 ± 7 % cell viability), therefore the observed activity in TC32 cells is likely to be specific to the cancerous cells.

Interestingly, the pyridinone (**200**) displayed only weak activity (82 ± 2 % cell viability). Of the inactive compounds, the saturated ring variants of fenretinide, the hydroxycyclohexyl (**205**) and hydroxypiperidine (**206**) displayed no activity (90 ± 5 % and 98 ± 6 % cell viability, respectively), indicating that the aromatic or planar nature of the phenyl ring could be



Compound number	R	% TC32 cell viability*	% MSC cell viability*	ClogP	Predicted logs (mol/litre)
1 (fenretinide)		43 ± 2	88 ± 5	7.1	-4.6
199		50 ± 2	94 ± 7	7.1	-4.2
200		82 ± 2	-	5.6	-4.4
201		82 ± 2	-	6.9	-4.5
202		105 ± 3	-	7.8	-5.5
203		88 ± 4	-	7.9	-5.1
204 [†]		97 ± 6	-	6.7	-4.1
205		90 ± 5	-	5.8	-4.6
206		98 ± 6	-	5.3	-3.7

*Toxicity in TC32 cells and MSC cells treated at 10 μ M for 24 h; Cell viability is expressed as the mean viable cell count as a % of the DMSO control \pm SEM; -, not measured. [†] Compound exists as mixture of inseparable regioisomers (major isomer reported).

Table 2.4 Chemical structures, biological activity and physicochemical properties of the additional phenyl analogues of fenretinide.

important for biological activity, or that the donor/acceptor capability of the hydroxyl group is playing a role. Furthermore, the amide of the hydroxypiperidine (**206**) is tertiary. The indole and indazole analogues (**202** and **203**) displayed no significant activity (105 ± 3 and 88 ± 4 % cell viability, respectively) consistent with attempts to incorporate other heterocyclic variants (indole (**173**), and benzimidazolinone (**174**), *Table 2.2*) in the previous round of testing, although the position of the NH on the phenyl ring is altered between these structures. The pyrazole analogue (**204**) was also inactive (97 ± 6 % cell viability). The hydroxybenzylamide (**201**) was weakly active (82 ± 2 % cell viability).

2.3 Amide isosteres

This section describes the synthesis and biological evaluation of isosteres of the amide of fenretinide. The aim was to synthesise variants by strategic replacement of the N-H and carbonyl moieties, with for instance an *N*-methyl (as replacements for the N-H) and a methylene group (as replacement for the carbonyl) to better understand the importance of the N-H and carbonyl groups for the activity of fenretinide (*Figure 2.3*).

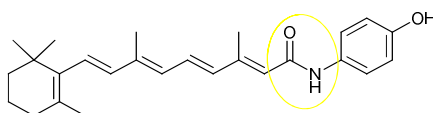
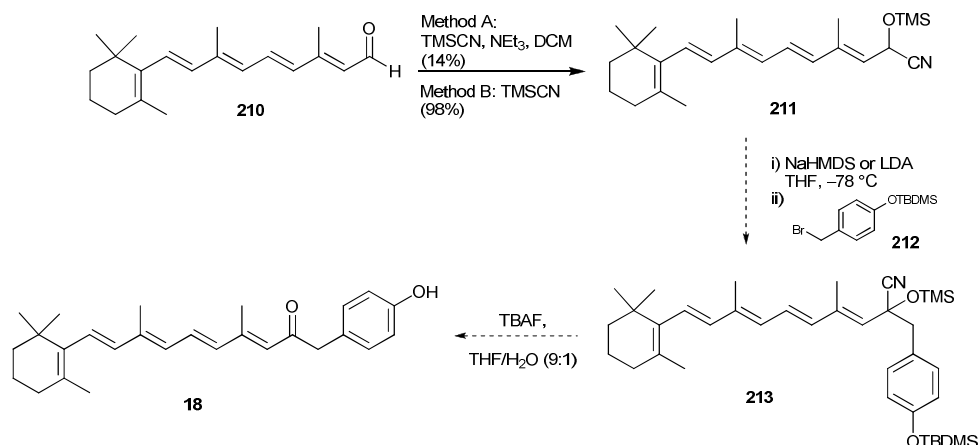


Figure 2.3 The amide group of fenretinide selected for isosteric replacement.

2.3.1 Variation at the N-H position of the amide group

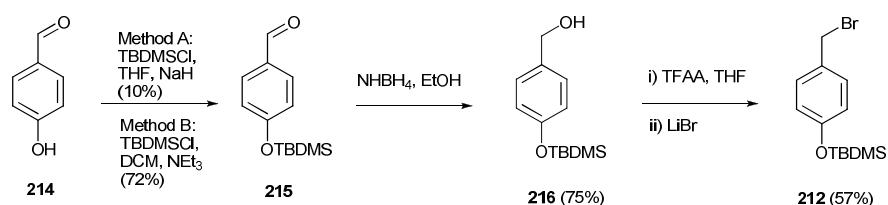
The keto isostere of fenretinide (the N-H of fenretinide replaced with a methylene spacer, compound **18**) was proposed for synthesis. The methylene group was proposed for introduction to fenretinide by benzylation of retinal (**210**) at the 1-position, mediated by a transient nitrile group (*Scheme 2.14*).

The nitrile group was incorporated into retinal (**210**) using a method described by Kobayashi *et al.*,¹⁵⁹ involving substitution of retinal (**210**) with TMSCN in DCM in the presence of triethylamine in poor yield (14 %) (*Method A, Scheme 2.14*). Owing to the low yield obtained for this reaction,



Scheme 2.14 Protocol for synthesis of the keto isostere of fenretinide.¹⁶¹

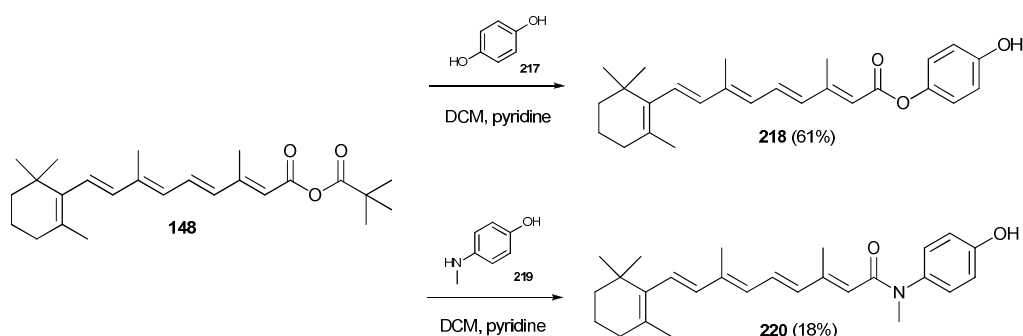
an alternative method involving a solvent-free protocol catalysed by triethylamine (as described by Baesa *et al.*¹⁶⁰) was attempted, providing compound **211** in excellent yield (98 %) with no need for purification (*Method B*, *Scheme 2.14*). The next step involved alkylation of the site of the acidic proton with a silyl protected benzyl bromide (**212**). The silyl protected benzyl bromide (**212**) was prepared from 4-hydroxybenzaldehyde using the protocol described by Olszewski *et al.*¹⁶¹ (*Scheme 2.15*). The hydroxyl group of the aldehyde (**214**) was protected with TBDMSCl in dry THF and sodium hydride, to generate the silyl protected compound (**215**) in low yield (10 %) (*Method A*, *Scheme 2.15*). Owing to the poor yield obtained, an alternative method for synthesis of this compound was attempted employing the same phenolic aldehyde (**214**) and silyl chloride but this time in dry DCM in the presence of triethylamine (*Method B*, *Scheme 2.15*). This efficiently generated the desired product (**215**) in 72 % yield. The incorporation of the organic base may aid formation of a very reactive pentavalent silica intermediate with TBDMSCl.¹⁵⁹ Reduction of the aldehyde (**215**) to the benzylalcohol (**216**) using NaBH₄ was achieved in 75 % yield, followed by activation of the hydroxyl group with TFAA and displacement of the



Scheme 2.15 Synthesis of benzyl bromide (**212**) from 4-hydroxybenzaldehyde (**214**).

trifluoroacetate with lithium bromide to form the benzylbromide (**212**) in 57 % yield. Returning to the synthesis of the ketone (**18**), deprotonation of the cyanohydrin (**211**) with NaHMDS at $-78\text{ }^{\circ}\text{C}$ and alkylation with the silyl-protected benzyl bromide (**212**) was unsuccessful, yielding retinoic acid as the major product (*Scheme 2.14*). Repeating the reaction using LDA as base was also unsuccessful. Although the synthesis of ketone (**18**) from retinal (**210**) has previously been reported (by Weiss *et al.*¹²¹), the specific experimental conditions were not detailed and no further efforts were made to synthesise the compound.

Instead, two further isosteres of the amide were investigated for synthesis, the analogue containing an oxygen atom in place of the N-H group (**218**) (*i.e.* the ester variant of fenretinide) and the *N*-methyl variant (**220**) (*Scheme 2.16*). The compounds were synthesised in each case by reaction of the 4-hydroxyphenol (**217**) or 4-methylamino phenol (**219**), as appropriate, with the mixed anhydride (**148**) (prepared from retinoic acid as described previously, see page 50) to generate the desired ester (**218**) and amide (**220**) in acceptable yields (*Scheme 2.16*). For the *N*-methyl variant, evidence for formation of the preferred regioisomer (*N*-linked amide rather than *O*-linked ester) was confirmed by the characteristic chemical shift of the *N*-methyl amide protons (δ 3.4 predicted vs 3.3 observed, compared to the predicted amine δ 2.7), indicative of a *N*-methyl amide rather than a *N*-methyl aniline. Additionally, the preferred reactivity for the NH_2 over the OH is consistent

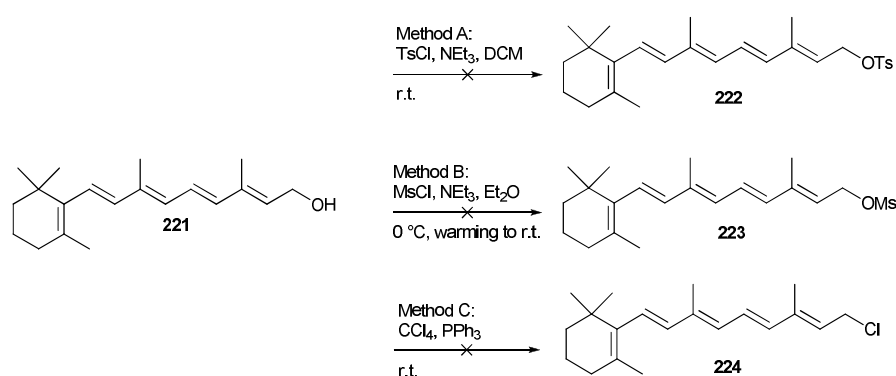


Scheme 2.16 Synthesis of ester (**218**) and *N*-methyl amide (**220**) from the mixed anhydride of retinoic acid. (Physicochemical property profile for compound **218**: ClogP 7.9, predicted logS -4.6 ; **220**: ClogP 8.0, predicted logS -4.7 .)

with that reported in the literature for formation of amides using this reagent.¹⁶²

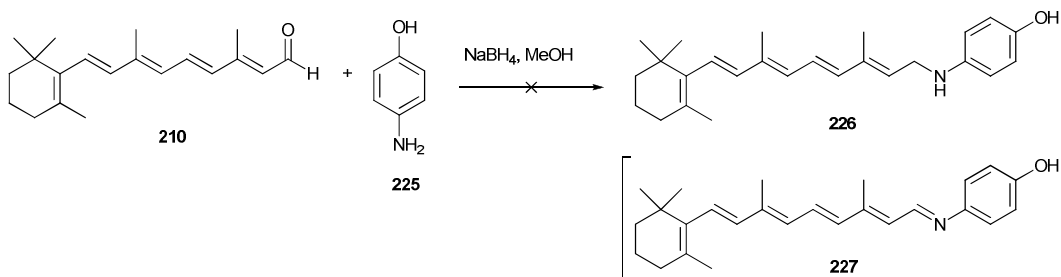
2.3.2 Variation at the carbonyl group

The amino variant of the amide of fenretinide (*i.e.* where the carbonyl of the amide has been reduced to a methylene group) was proposed for synthesis. Various attempts at synthesis of this compound were attempted. The first method involved preparation of an activated retinol for displacement with 4-aminophenol. Synthesis of the tosyl- (**222**) (Method A), mesyl- (**223**) (Method B) or chloro-retinol (**224**) (Method C) was attempted, but in each case the activated retinol was not observed (*Scheme 2.17*).



Scheme 2.17 Unsuccessful activation of the retinol hydroxyl group.

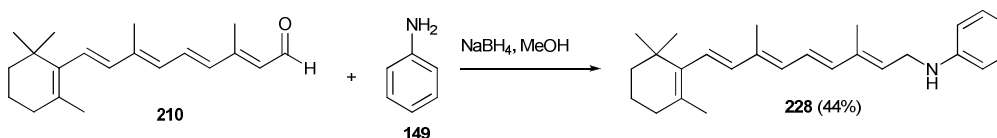
The next method involved reductive amination of 4-aminophenol (**225**) and retinal (**210**) using sodium borohydride as a reducing agent (*Scheme 2.18*). This provided trace quantities of the desired product (**226**) (6.5 % by LCMS) and the unreduced imine (**227**) as the major product. Attempts to force the reaction to completion by addition of additional quantities of sodium



Scheme 2.18 Failed reductive amination reaction to form the amino variant of the amide of fenretinide. Formation of the imine was observed.

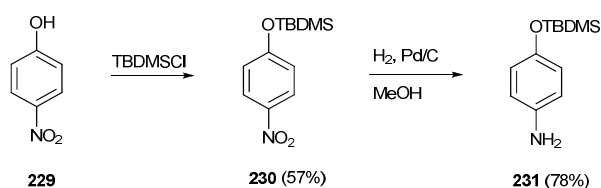
borohydride were unsuccessful. Use of sodium triacetoxyborohydride, borane (1M in THF) under reflux and Red-Al in toluene at room temperature was also unsuccessful.

Owing to the failure of the above reductive amination reactions, a model reaction was carried out in which the 4-aminophenol was replaced with aniline to test whether the hydroxy group was interfering with the reaction. Aniline (**149**) and retinal (**210**) were mixed and then reduced using sodium borohydride to deliver the desired amine (**228**) in modest yield (44 %) (*Scheme 2.19*). Evidently the OH of 4-aminophenol in the previous synthesis was interfering with reaction.

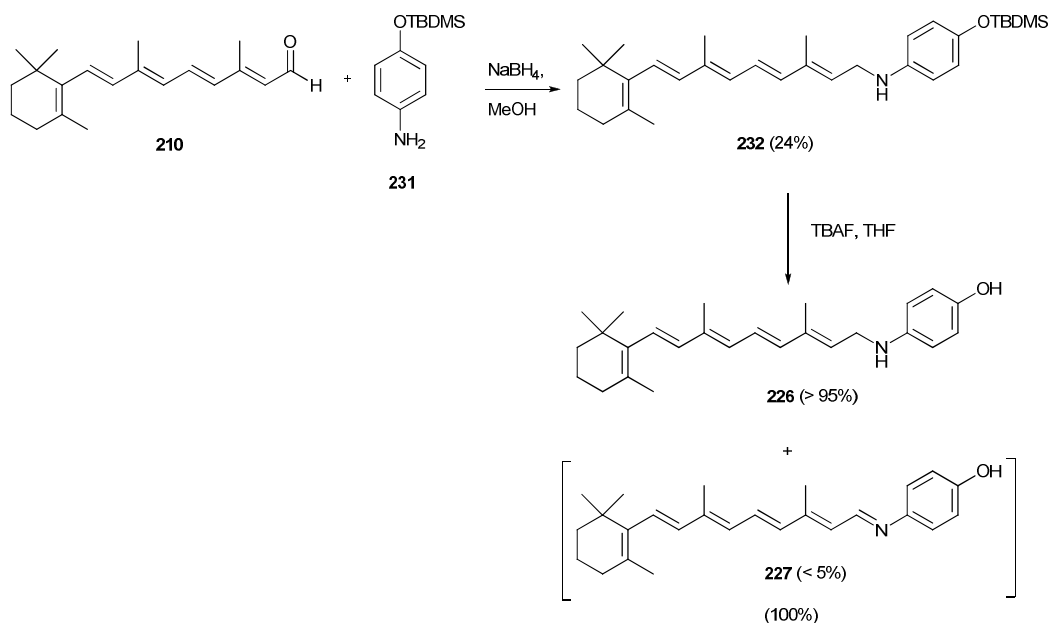


Scheme 2.19 Synthesis of the reduced amide variant of fenretinide. (Physicochemical property profile for compound **228**: ClogP 8.8, predicted logS -5.0.)

The required hydroxyaniline (**226**) was eventually synthesised *via* protection of the hydroxyl group with a silyl ether. Reaction of 4-nitrophenol (**229**) with TBDMSCl yielded the protected phenol (**230**) in moderate yield (*Scheme 2.20*). The nitro group was then reduced by palladium catalysed hydrogenation to generate the primary amine (**231**) in modest yield. The amine was then exposed to retinal (**210**) in the presence of sodium borohydride to generate the desired secondary aniline (**232**) in good yield (*Scheme 2.21*), consistent with the hypothesis that the hydroxy group was inhibiting the previous reaction. Upon deprotection with TBAF, the aniline (**226**) was obtained in excellent yield, together with a small amount of the imine (**227**) as an inseparable contaminant (< 5 %).

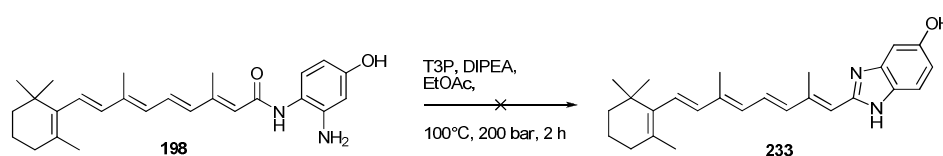


Scheme 2.20 Synthesis of the TBDMS-oxyaniline precursor to the aniline analogue of fenretinide.



Scheme 2.21 Synthesis of the aniline analogue of fenretinide. (Physicochemical property profile for compound **226**: ClogP 8.1, predicted logS -4.7 .)

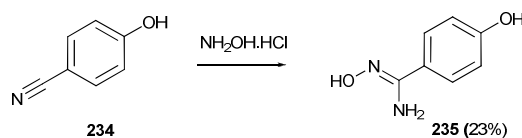
It was also of interest to synthesise a cyclic isostere of the amide – firstly the benzimidazole **233**. This was attempted by a T3P[®]/DIPEA promoted aromatisation of the amino variant (**198**) of fenretinide prepared previously (Section 2.2.8) upon microwave radiation (100 °C, 200 bar) but the reaction led to an uncharacterisable single product and no further efforts were made to synthesise this compound (*Scheme 2.22*).



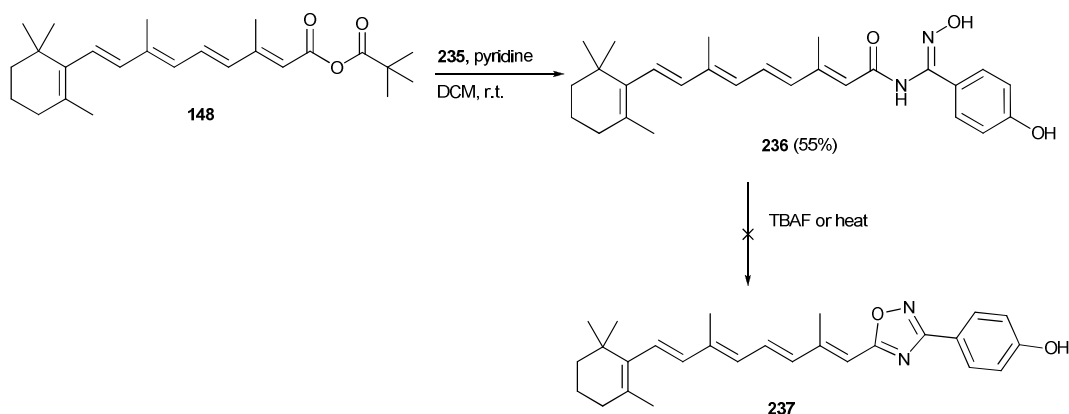
Scheme 2.22 Failed T3P[®]-catalysed synthesis of a benzimidazole isostere of the amide.

Synthesis of another amide isostere - an oxadiazole - was also attempted. For this, the amidoxime (**235**) required for synthesis of the planned oxadiazole was synthesised by reaction of benzonitrile (**234**) with hydroxylamine hydrochloride (*Scheme 2.23*). This amidoxime was then reacted with the mixed anhydride of retinoic acid (**148**) to generate the acylamidoxime (**236**). However, attempted cyclisation of this using both TBAF to catalytically aid cyclisation and by heating to reflux in DMF failed to

yield the expected oxadiazole containing compound (**237**), instead generating a mixture of uncharacterisable reaction products (*Scheme 2.24*).



Scheme 2.23 Synthesis of *N*,4-dihydroxybenzimidamide from 4-hydroxybenzonitrile.



Scheme 2.24 Failed synthesis of the oxadiazole (**237**) from the amidoxime intermediate (**235**). (Physicochemical property profile for compound **236**: ClogP 7.5, logS -5.0 .)

2.3.3 In vitro activity of amide isosteres

The six amide isosteres prepared above were screened in the TC32 cell viability assay, as described previously (see page 51).

The ester isostere (**218**) was statistically inactive (89 ± 2 % cell viability), suggesting that the hydrogen-bond donor capability of the NH of fenretinide could be important for activity. The loss of activity for the ester may also be explained by the potential for hydrolysis of the ester in the cell to the carboxylic acid (hence retinoic acid (**6**)). Previous studies have shown that retinoic acid does not induce cell death or decrease viable cell number in TC32 cells.⁸⁶

The *N*-methylamide (**220**) was weakly active (81 ± 5 % cell viability). Similarly the *N*-methylated amide (*para*-amino version) (**179**) (synthesised as a by-product of the reaction in Scheme 2.6, Section 2.2.5), lacked any significant activity (96 ± 5 % cell viability) suggesting that a H-bond donor at

this position may be important for activity. Alternatively, the additional hydrophobicity or a steric effect associated with the *N*-methyl group may hinder any interaction with a target. These findings are consistent with Mershon *et al.* for the *N*-methylanilide (**220**) where only weak activity was observed for induction of cell death in MCF-7 breast cancer cells in comparison to fenretinide.¹¹⁶

The 4-hydroxyphenyl amine (**226**) showed some activity *in vitro* (74 ± 3 % cell viability) but this was not comparable to fenretinide (43 ± 2 % cell viability). The data may suggest that the oxygen of the carbonyl may act as a hydrogen bond acceptor.

Both the amidoxime (**236**) (Scheme 2.24) and the phenylamine (**228**) (Scheme 2.19) showed little or no activity (92 ± 6 % vs 102 ± 6 % cell viability). The lack of activity for the phenylamine (**228**) was perhaps not unexpected as the molecule does not possess a polar substituent (*e.g.* a *para*-hydroxy group) on the phenyl ring.

2.4 Central scaffold analogues

Two isosteres of the central repeating isoprenoid scaffold of fenretinide were proposed for synthesis in order to identify whether the shape and rigidity at this region of the molecule was important for activity. The two isosteres planned for synthesis were a simple unsaturated variant of the isoprenoid scaffold (**91**) and the geometric isomer (**238**) (Figure 2.4).

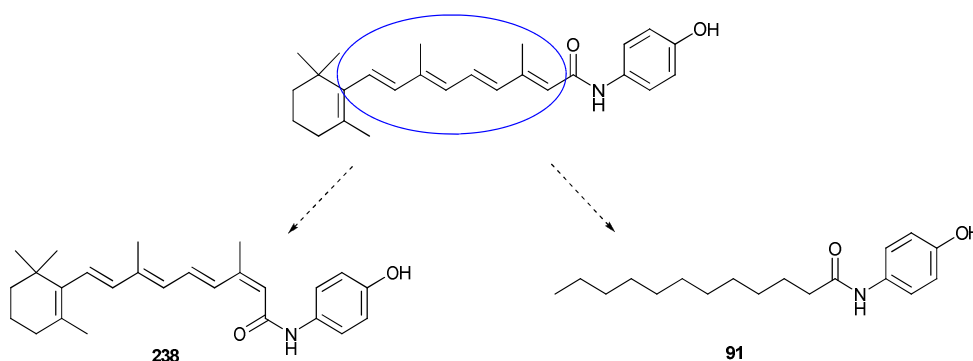
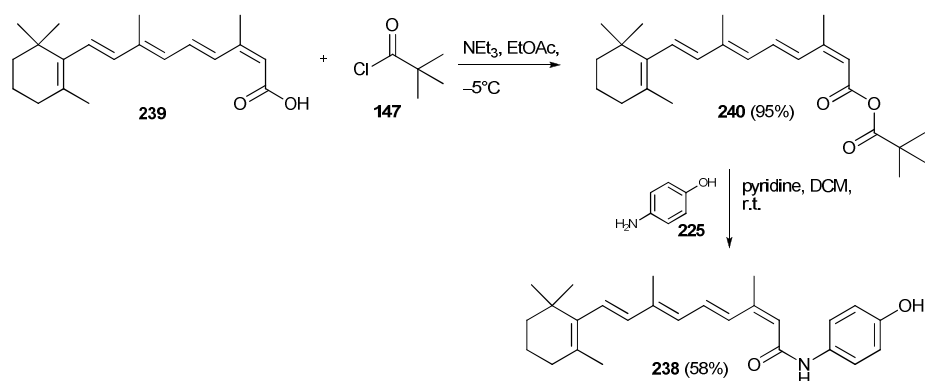


Figure 2.4 Proposed adaptations to the central scaffold of fenretinide.

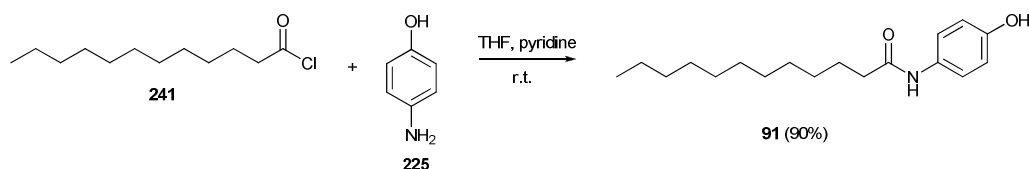
2.4.1 Synthesis of central scaffold analogues

13-*Cis*-fenretinide (**238**) was synthesised from 13-*cis*-retinoic acid (**239**) via a mixed anhydride intermediate from trimethyl acetyl chloride (**147**) and 4-amino phenol (**225**) in moderate yield (58 %) (*Scheme 2.25*).



Scheme 2.25 Synthesis of 13-*cis*-fenretinide from 13-*cis*-retinoic acid via a mixed anhydride intermediate. (Physicochemical property profile for compound **238**: ClogP 7.1, predicted logS -4.7.)

The proposed alkyl variant (**91**) was synthesised by coupling of 4-aminophenol (**225**) to lauroyl chloride (**241**) (*Scheme 2.26*).



Scheme 2.26 Reaction of lauroyl chloride (**241**) with 4-aminophenol (**225**) to form the alkyl chain derivatives (**91**). (Physicochemical property profile for compound **91**: ClogP 5.8, predicted logS -4.4.)

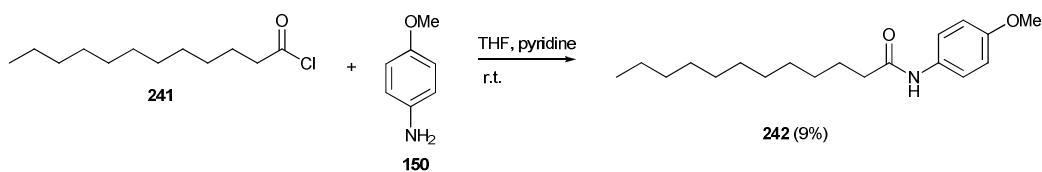
2.4.2 Biological evaluation of central scaffold analogues

The central scaffold analogues were screened in the TC32 cell viability assay (as described previously, see page 51).

The 13-*cis*-fenretinide (**238**) largely showed weak activity *in vitro*. However the standard error of the mean of the viable cell count for this particular compound was relatively large (76 ± 10 % cell viability). This could be a consequence of slow isomerisation to all-*trans*-fenretinide (**1**), initiated by warming in the incubator to 37.5 °C and exposure to light. Armstrong *et al.* reported that isomerisation of *cis*-retinoic acid to the *trans*- isomer to be heat

and light activated, leading to the hypothesis that 13-*cis* retinoic acid is likely to act as a prodrug for *trans*-retinoic acid.¹⁶³ Previously, *cis*-fenretinide has been found to be significantly less active as a cytotoxic than *trans*-fenretinide in squamous metaplasia in hamster trachea organ cultures¹⁶⁴ but showed comparable activity to fenretinide in urinary bladder carcinogenesis in mice.¹⁶⁵

In screening of the alkyl chain analogue (**91**), cell death was also somewhat variable across the nine experiments carried out in triplicate (ranging from 35-117 % cell viability compared to the vehicle control, n=27), with an average cell viability of 76 ± 5 %. This could be due to the ability of the compound to form aggregates in media, with the flexible alkyl chain and polar phenylamine groups ideal structures for forming micellar assemblies. This may remove some of the compound from solution and therefore reduce the effective concentration. The compound was screened against MSC cells where no significant activity was observed (95 ± 7 % cell viability), therefore the activity observed in TC32 cells is likely to be specific to the cancer cells. Takahashi *et al.* also found this compound to demonstrate activity against breast cancer, leukaemia and prostate cancer cell lines.¹²⁴ To identify the importance of the OH group for activity of this compound, a methylated analogue (**242**) was synthesised as a negative control (based on the hypothesis that methylation of the hydroxy group should reduce activity consistent with the result for 4-methoxyfenretinide (**24**), *Table 2.1*). The compound was prepared using the same method as for the hydroxyl-containing compound above, substituting 4-aminophenol for 4-methoxyaniline (**150**) (*Scheme 2.27*). Screening of this compound resulted in loss of activity (95 ± 2 % cell viability) in comparison to the *para*-hydroxy compound (**91**) (76 ± 5 % cell viability), consistent with the result for the



Scheme 2.27 Reaction of lauroyl chloride (**241**) with 4-methoxyaniline (**150**) to form the alkylamide (**242**). (Physicochemical property profile for compound **242**: ClogP 6.5, predicted logS -4.7.)

methylated version of fenretinide and hence suggesting that the *para*-hydroxy analogue may be initiating activity in TC32 cells by interaction with the same target as fenretinide.

2.5 Substituted cyclohexyl analogues

Variants of the cyclohexyl group were designed based on compounds previously investigated within the Foster group. Unpublished research has identified a cyclohexyl-analogue of fenretinide (**243**) (*Figure 2.5*), containing a methyloxime group at the 4-position of the cyclohexyl ring, which has been found to induce cell death at a similar rate to fenretinide in six ESFT cell lines at 5 μ M over 48 h (screening performed by Dr Helen Payne). A good therapeutic ratio was observed in TC32 and mesenchymal stem cells ($38 \pm 2\%$ vs $77 \pm 10\%$ cell viability, respectively). The compound has since progressed to *in vivo* studies to evaluate efficacy in a tumour regression model (data for this study is confidential). Based on the encouraging biological data obtained for this compound, further oxime (plus hydrazone) variants were designed for synthesis.

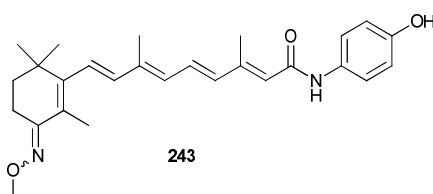
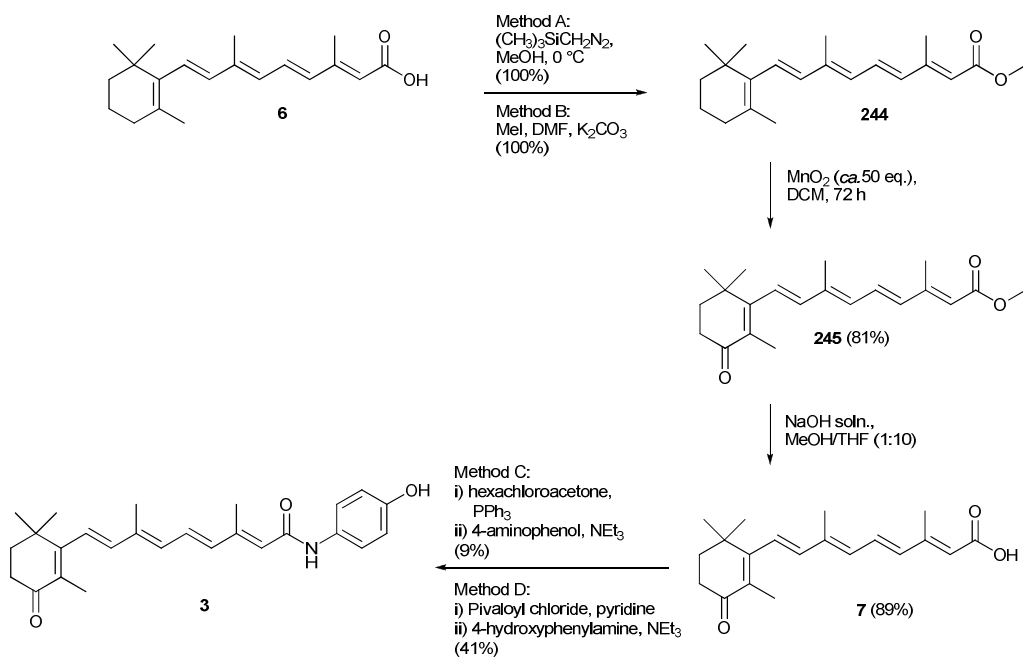


Figure 2.5 The chemical structure of an active cyclohexyl analogue of fenretinide.

2.5.1 Synthesis of substituted cyclohexyl analogues

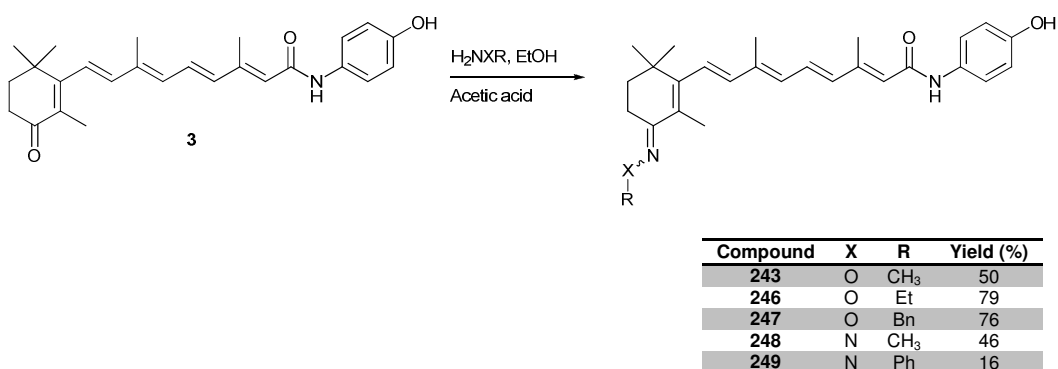
The proposed oxime and hydrazone variants were planned for synthesis by a condensation chemistry from the parent ketone, 4-oxo-fenretinide (**3**), which itself was synthesised in 4-steps from retinoic acid (**6**) (*Scheme 2.28*). Retinoic acid (**6**) was methylated using trimethylsilyl diazomethane, providing the methyl ester (**244**) in quantitative yield (*Method A, Scheme 2.28*). An excess of trimethylsilyl diazomethane (2.5 eq) was required to achieve completion of this reaction. This was undesirable as the reagent is both expensive and potentially hazardous for use on a larger scale (explosion risk). Fortunately, methylation of the carboxylic acid (**6**) with methyl iodide as replacement for trimethylsilyl diazomethane provided a safer alternative,

generating the desired ester (**244**) in quantitative yield (*Method B, Scheme 2.28*). Oxidation at the desired position of the cyclohexyl ring was achieved by stirring the methyl ester with a large excess of activated manganese dioxide for 72 h. Hydrolysis of the resulting ketone (**245**) with 10 % NaOH solution in MeOH/THF yielded 4-oxo-retinoic acid (**7**) in good yield (89 %). For formation of the desired amide (**3**), the acid-free synthesis of acyl chlorides described by Villeneuve *et.al.*⁴ was adapted (*Method C, Scheme 2.28*). Here, 4-oxo-retinoic acid (**7**) was mixed with hexachloroacetone/triphenylphosphine to form an acid chloride which was reacted *in situ* with *para*-aminophenol to give 4-oxo-fenretinide (**3**) in poor yield (9 %), owing to difficulties in purification due to co-elution of contaminants originating from the triphenylphosphine complex upon column chromatography. As multi-gram quantities of 4-oxo-fenretinide were required in order to synthetically elaborate the ketone functionality, an alternative method for synthesis of the compound was sought. As the mixed anhydride method had proved useful for synthesis of many of the amides prepared throughout this chapter, these conditions were adopted to the current scheme. Hence, 4-amino phenol was reacted with the pivalic mixed anhydride generated from 4-oxo-retinoic acid (**7**) to generate the desired product (**3**) in 41 % yield (*Method D, Scheme 2.28*).



Scheme 2.28 Synthesis of 4-oxo-fenretinide (**3**).

The synthesis of the planned oxime and hydrazone variants was then achieved by acid catalysed condensation of the respective hydroxylamine or hydrazine with 4-oxo-fenretinide (**3**) in variable yields (16-79 %) (*Scheme 2.29*). Three oximes (methyl **243**, ethyl **246** and benzyl **247**) and two hydrazones (methyl **248** and phenyl **249**) were synthesised. In each case a single regiosomer was obtained but attempts to characterise the stereochemistry for one of these products (the benzyl oxime, **247**) by nOe enhancement experiments was inconclusive.



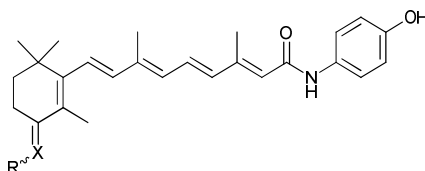
Scheme 2.29 Synthesis of substituted cyclohexyl analogues.

2.5.2 Biological evaluation of substituted cyclohexyl analogues

The oxime and hydrazone analogues plus 4-oxo-fenretinide (**3**) were screened in the TC32 cell viability assay, using the method as described previously (see page 51). Of the six compounds tested, three showed a statistically significant response when compared to vehicle control; two from the oxime series and 4-oxo-fenretinide (compounds **243**, **246** and **3**, respectively) (*Table 2.5*).

An interesting trend was observed for the oxime series, in which an increase in size of the R substituent (methyl (**243**) > ethyl (**246**) > benzyl (**247**)) corresponded to a decrease in activity (68 ± 2.7 , 79 ± 2 , 89 ± 2 % cell viability, respectively), suggesting that increase in hydrophobicity, either locally at the site of the oxime, or whole molecule (logP), was disfavoured for activity.

Conversely, the less hydrophobic methyl hydrazone (**248**) was found to be less active (94 ± 7 % cell viability) than for the more hydrophobic



Compound number	X	R	% TC32 cell viability*	% MSC cell viability	ClogP	Predicted logs (mol/litre)
1 (fenretinide)	H	-	43 ± 2	88 ± 5	7.1	-4.6
3 (4-oxo-fenretinide)	O	-	41 ± 1	58 ± 11	4.8	-4.3
243	N	OMe	68 ± 3	77 ± 10	5.8	-5.0
246	N	OEt	79 ± 2	-	6.3	-5.3
247	N	OBn	88 ± 2	-	7.5	-6.4
248	N	NMe	94 ± 7	-	6.3	-5.0
249	N	NPh	79 ± 4	-	7.1	-5.9

*Toxicity in TC32 cells and MSC cells treated at 10 μ M for 24 h; Cell viability is expressed as the mean viable cell count as a % of the DMSO control \pm SEM; -, not measured. Fenretinide control: 43 \pm 2 % cell viability; ClogP 7.1; predicted logS -4.7.

Table 2.5 Chemical structures, biological activity and physiochemical properties of substituted cyclohexyl compounds.

phenylhydrazine (**249**) (79 \pm 4 % cell viability). Taken together, the biological data for the oximes and hydrazones would appear to indicate that the nature of the R group has a significant influence on activity in the TC32 cells, although any detailed analysis of trends between the oxime and hydrazone series is complicated by the number of analogues prepared and screened from which to base a SAR.

The lack of activity in the MSC cell line observed for the methyloxime (**243**) (77 \pm 10 % cell viability) would imply that incorporation of an oxime functionality might offer some potential for the generation of compounds with a fold-differential toxicity between normal and cancerous cell death, assuming a similar trend for related analogues can be established. Owing to time constraints and lack of availability of MSC cells at the time of testing, no further oximes were investigated in the MSC assay, although further investigation of the normal and cancerous cell toxicity for oximes (and hydrazones) will be returned to in Chapter 5 (Target identification by affinity chromatography).

The 4-oxo-fenretinide (**3**) was the most active of the series of compounds tested, displaying impressive activity (41 \pm 1 % cell viability), comparable to fenretinide (43 \pm 2 % cell viability). However, unlike the methyloxime (**243**),

4-oxo-fenretinide also displayed significant activity in the MSCs (58 ± 11 % cell viability) indicating unfavourable toxicity which suggests that the ability of this compound to induce cell death may not be specific to the cancer cells.

2.6 Summary of SAR for fenretinide in ESFT cells

This chapter has investigated the SAR for modifications to the structure of fenretinide having evaluated the activity in ESFT cells. A systematic approach to structural variation was adopted in which synthetic variations were targeted at four sub-sites of the fenretinide structure. Although the 4-hydroxyphenyl site of fenretinide has proved quite resistant to structural modification, several interesting analogues have been identified which demonstrate fenretinide-like activity in TC32 cells and MSCs. Of these, the 4-aminophenyl (**58**, *Table 2.1*), the 4-pyridyl (**199**, *Table 2.3*) and 2-aminophenyl-4-hydroxyphenyl variants (**198**, *Table 2.4*) demonstrate the most interesting results in terms of activity in TC32 vs MSCs as well as structural variety. In terms of rationalisation of the SAR, it would appear that replacement of the 4-hydroxy group with a methoxy (**24**, *Table 2.1*) is not tolerated, consistent with the finding of others for this compound in related cell types. Conversely, replacement of the OH for the amino group is well tolerated, suggesting perhaps that the OH (and NH₂) act as hydrogen-bonding donors in a polar interaction to a protein. The activity observed for the acetamide (**172**, *Table 2.2*) also supports this hypothesis. In general, efforts to incorporate heterocycles and substituents other than a 2-amino group (compound **198**, *Table 2.4*) to the phenyl ring are not well tolerated. Attempts to improve the activity by modification of the amide portion of the molecule were met with little success, although weak activity of the 4-hydroxyphenyl amine (**226**, *Scheme 2.21*) showed some activity *in vitro*, suggests perhaps that some modification may be possible. Establishment of an SAR at the central scaffold is complicated by the fact that few compounds were synthesised and tested based on modification at this site. However, it would seem that an extended alkyl variation (compound **91**, *Scheme 2.26*) is tolerated, although structurally this molecule is quite distinct to the fenretinide structure. At the cyclohexyl ring, a number of variations were tolerated at the

4-position with an interesting SAR apparent for hydrophobicity of the oxime substituent (hydrophobicity of alkyl substituent correlates positively with activity). In general, an increase in hydrophobicity for the molecules investigated throughout this chapter appears to favour improved activity in TC32 cells, although it is difficult to correlate this trend to activity at a specific site of the molecule.

Although this work appears to show the development of a preliminary SAR for fenretinide activity in TC32 cells, it is important to state that the compounds investigated herein may be interacting at one or more targets and/or pathways to elicit the same phenotype which will naturally complicate any rationalisation of the SAR.

3. Non-retinoid mimetics of fenretinide

This chapter describes the design, synthesis, biological evaluation and optimisation of non-retinoid mimetics of fenretinide.

Non-retinoid mimetics of fenretinide can be described as molecules which share a similar 3-dimensional structure and pharmacophore to fenretinide, but pertain to a structurally distinct substructural class. This class of molecule may offer advantages over fenretinide as the basis of design of chemotherapeutics as they have potential for improved pharmaceutical properties, including improved solubility, permeability and metabolic stability, as well as the potential for novel composition of matter intellectual property. Additionally, non-retinoids may offer advantage as tools to support the understanding of the mechanism of action of fenretinide and analogues.

The highly hydrophobic nature of the retinoid substructure of fenretinide confers a number of inherent liabilities to the molecule, limiting the clinical development of drugs based on this scaffold. For instance, the poor solubility and high metabolic liability for fenretinide, has been ascribed, at least in part, to the molecule's high lipophilicity.^{44,79} Hence, we and others have hypothesised that replacement of the hydrophobic cyclohexyl/isoprenoid regions of the molecule with polar isosteres, by incorporating heteroatoms, may confer improved physicochemical and pharmaceutical properties for potential use as more effective pharmaceutical agents.^{126,127,128}

It is also of interest to use non-retinoid mimetics of fenretinide as tools to reaffirm findings from the earlier SAR study which may help to elucidate the molecular requirements and mechanism for fenretinide induced cell death. It may be possible to achieve this by development of chemical tools based on comparison to the retinoid SAR, by synthesis of non-retinoids containing elements of the retinoid SAR, so called 'hybrid' compounds.

3.1 General strategy

The identification and optimisation of non-retinoid mimetics of fenretinide was achieved by iterative compound purchase and biological screening employing ligand-based design and directed by the SAR identified for fenretinide as described in Chapter 2.

3.2 Identification of non-retinoid mimetics of fenretinide by ligand-based design.

This section describes the identification of non-retinoid mimetics of fenretinide *via* iterative virtual screening and biological evaluation.

3.2.1 Hit identification by ligand-based searches using ROCS

A flow diagram illustrating the process of identification of non-retinoid mimetics of fenretinide using a ROCS-based screening approach is described in *Figure 3.1*. The ligand-based search tool, ROCS (described in Chapter 1, Section 1.11.1), was used to search a library of compounds (the

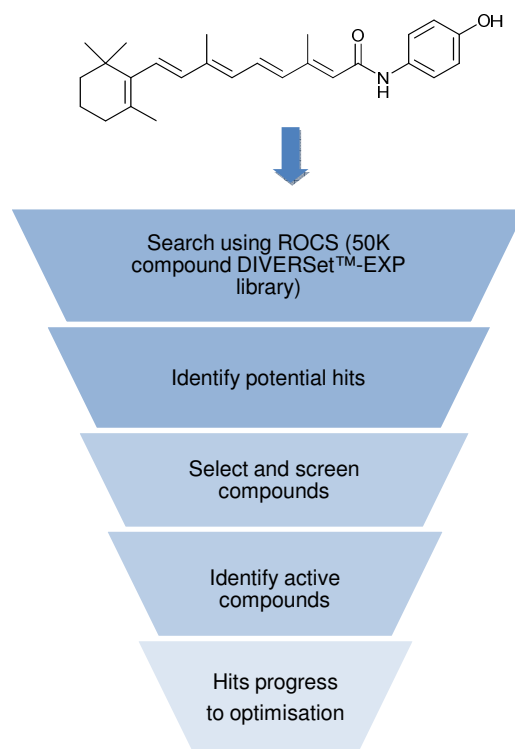


Figure 3.1 A flow diagram illustrating the process of hit identification of non retinoid analogues of fenretinide using ligand-based design (ROCS) and screening.

50,000 compound DIVERSet™-EXP library from the commercial vendor, ChemBridge¹⁵⁰) for those which exhibit a high similarity (assessed by ROCS Comboscore) to fenretinide.¹³⁹ The ROCS Comboscore takes into account the shape-tanimoto (shape similarity) and scaled color score (chemical similarity) between the query molecule (fenretinide) and the members of the library. The outcome of the search provided a 'hit list' of compounds ranked according to the ROCS Comboscore in order of their 'similarity' to fenretinide. The top 500 hits based on the ComboScore were filtered for visualisation using the molecular modelling software, VIDA (Visualization and Communication of Modeling, OpenEye Scientific).¹⁶⁶

Nine compounds were then chosen by eye for purchase and screening based on a requirement for the molecule to share a similar size or 'length' to fenretinide and to contain the 4-hydroxyphenyl moiety which was identified as an important feature of biological activity for fenretinide in the SAR study (Chapter 2) (*Table 3.1*). Additionally, the compounds were selected to ensure they had an improved predicted physicochemical property profile (ClogP, solubility) in comparison to fenretinide.

3.2.2 Biological evaluation

To determine the biological activity of the compounds selected from the above ROCS-based search, the compounds were screened against a single ESFT cell line at 10 µM over 24 h. Cell viability was analysed *via* the trypan blue exclusion assay, as previously described (see page 51), except that the compounds were screened against A673 cells rather than TC32 cells (TC32s were used for screening of all compounds described in Chapter 2) due to the unavailability of TC32 cells at the time of testing. A673 cells are a suitable alternative to TC32 cells as they demonstrate a similar response to fenretinide (mid-range cell-death compared to alternative ESFT cell lines) as well as similar genetic features associated with the ESFT phenotype (p16 expression, EWS-FL1 type 1 fusion type).⁸⁶ A673 cells differ from TC32 cells in that they do not express p53; however, fenretinide is known to initiate cell death independent of p53.¹⁶⁷

Of the nine compounds purchased, six compounds (**250-255**) demonstrated statistically significant activity ($< 71 \pm 10$ % cell viability) compared to the vehicle control (*Table 3.1*). Compounds **250** and **251** were the most active, achieving 41 ± 4 and 47 ± 12 % cell viability respectively, although this activity was reduced compared to fenretinide (6 ± 2 % cell viability). Compound **251** was also the most 'similar' of the selected nine compounds to fenretinide as ranked by ROCS Comboscore, but in general there was little correlation between the ROCS Comboscore and activity for these compounds. The ROCS derived overlays for compounds **250** and **251** are shown in *Figure 3.2*. The overlays demonstrate good shape and functional group complementarity between the compounds and fenretinide. It is noteworthy that three of the compounds (**250**, **254** and **258**) are based on a rhodanine substructure. Rhodanine-containing compounds are known to be highly promiscuous modulators of proteins and so it's perhaps not that surprising that two of these compounds promoted cell death in this assay.¹⁶⁸ However, it is interesting to note that only one of rhodanine-containing compounds (compound **250**) potently promoted cell death, suggesting that

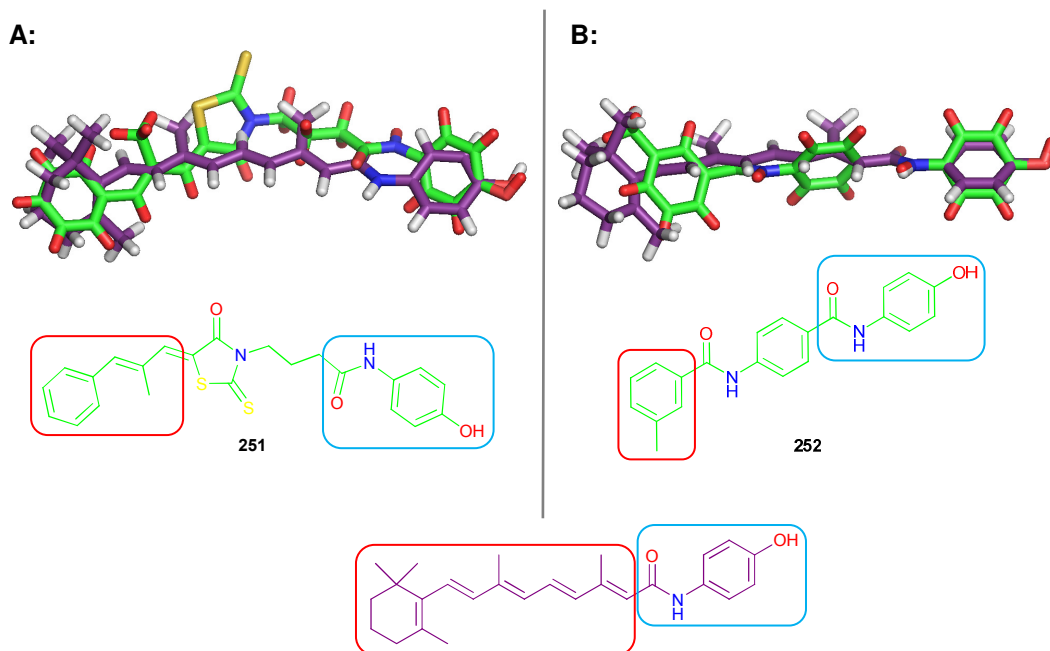
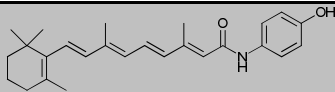
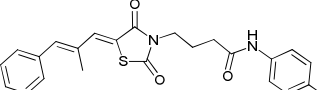
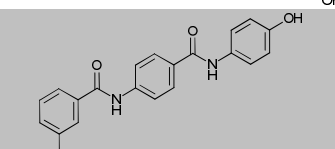
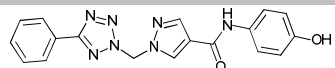
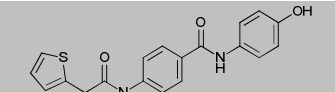
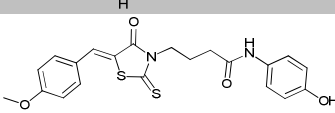
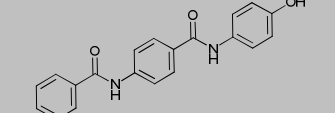
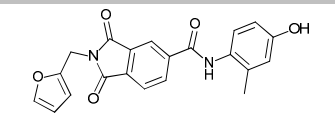
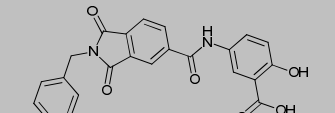
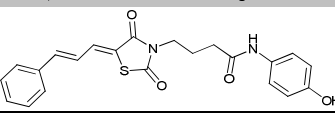


Figure 3.2 Panel A: ROCS overlay of compound **250** (green sticks) and fenretinide (**1**) (purple sticks). Panel B: ROCS overlay of compound **251** (green sticks) with fenretinide (**1**) (purple sticks). Both overlays demonstrate good overlap between the 4-hydroxyphenylamide (blue box) and lipophilic (red box) moieties of their respective substructures.

there may be a specific (*i.e.* non-promiscuous) effect associated with this compound.

For the two most active compounds from the screen (rhodanine **250** and bis-amide **251**), testing was continued using the normal cell line (MSCs) to ensure that any activity observed *in vitro* is cancer cell specific and the compound does not significantly decrease viable cell number in normal cells. The MSCs were treated with the two compounds at 10 μ M for 24 h and cell viability was analysed using the trypan blue exclusion assay, as described

Compound number	Structure	ROCS ComboScore	% A673 cell viability*	% MSC cell viability*	MW	ClogP
1 (fenretinide)		n/a	6 \pm 2	88 \pm 5	391	7.1
250		0.928	41 \pm 4	82 \pm 4	422	4.4
251		1.138	47 \pm 12	98 \pm 10	346	3.3
252		0.791	59 \pm 3	-	361	2.0
253		0.815	61 \pm 8	-	352	2.5
254		0.738	71 \pm 10	-	428	2.7
255		0.804	81 \pm 8	-	332	2.8
256		0.782	85 \pm 6	-	376	2.6
257		0.823	89 \pm 4	-	416	4.3
258		0.937	89 \pm 6	-	408	4.0

*Toxicity in A673 cells and MSC cells treated at 10 μ M for 24 h; Cell viability is expressed as the mean viable cell count as a % of the DMSO control \pm SEM; -, not measured.

Table 3.1 Chemical structures, biological and physicochemical properties of compounds identified by a ROCS search using fenretinide as the query.

previously (see page 51). Encouragingly, the compounds **250** and **251** did not display statistically significant activity (82 ± 4 and 98 ± 10 % cell viability, respectively) compared to the DMSO control. This indicates that the cytotoxicity maybe specific to the A673 cancer cells, and hence these compounds may demonstrate low toxicity *in vivo*.

The activity of the two most active compounds was subsequently confirmed in TC32 cells (as cells available again), to ensure consistency with the historical data. Gratifyingly, both compounds demonstrated statistically significant cytotoxicity in TC32 cells (64 ± 2 % and 63 ± 2 % cell viability for compounds **250** and **251** respectively), consistent with the result generated with the A673 cells. The activity of compounds **250**, **251** and fenretinide was reduced in TC32 cells, indicating that the compounds have increased specificity towards the A673 cell line.

As both of the compounds demonstrated an acceptable preliminary *in vitro* profile, they were progressed for chemical optimisation with the aim of improving the therapeutic ratio for TC32 vs MSC toxicity, as well as to develop a preliminary SAR for their respective compound class.

3.2.3 Optimisation of the rhodanine (**250**) and bis-amide (**251**)

This section describes the process of optimisation of the hits **250** and **251** from above using a combination of ROCS-based and 'SAR-by-catalogue' substructural searches using eMolecules¹⁶⁹, as illustrated by the process in *Figure 3.3*.

3.2.3.1 Optimisation using ROCS

The 50,000 compound DIVERSet™-EXP library from the commercial vendor, ChemBridge, was searched for compounds which exhibit a high ROCS Comboscore to either the rhodanine (**250**) or *bis*-amide (**251**). The outcome of the search provided a pooled 'hit list' of 500 compounds ranked according to the ROCS Comboscore in order of the similarity to their respective query compound. The results were visualised using VIDA, and prioritised by eye to give six compounds for purchase; three based on the structure of **250** and three based on **251**.

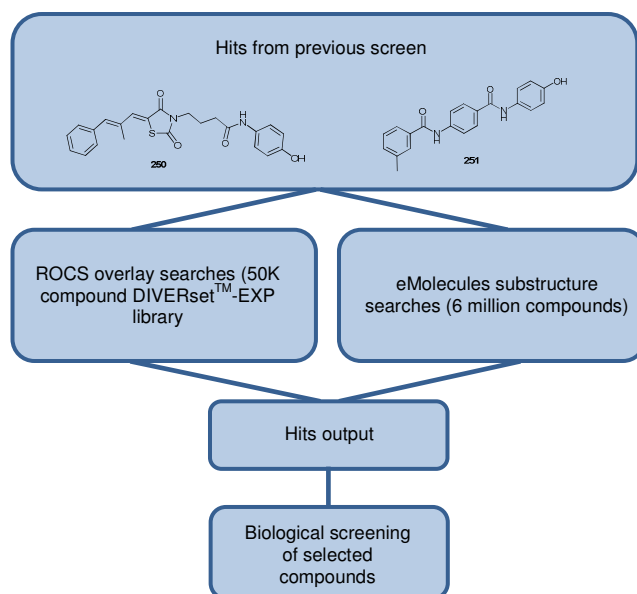


Figure 3.3 A schematic illustrating the process of identification of analogues of compounds **250** and **251** using ROCS overlay and substructure searches.

3.2.3.2 Optimisation using substructural searches

In parallel to the ROCS-based method above, substructure searches of the rhodanine (**250**) and *bis*-amide (**251**) were carried out using the website eMolecules to identify additional structural analogues for testing. eMolecules allows the user to perform a substructure search of a query molecule against a commercially available small molecule library comprising of 6 million compounds from multiple commercial vendors.¹⁶⁹ A substructure of each of the molecules, **250** and **251** (Figure 3.4), was queried in eMolecules to identify commercially available compounds containing the specified substructure. The substructure for each compound was selected to contain the *para*-hydroxyphenylamido moiety (identified as a key pharmacophore for fenretinide-like activity) and a ‘further portion’ of the active compound. This

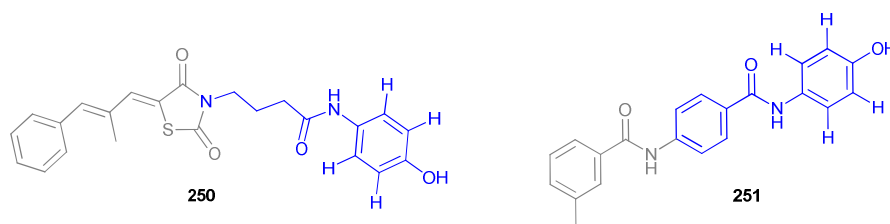


Figure 3.4 Chemical structures of compounds **250** and **251**, with substructures for the eMolecules search highlighted in blue.

'further portion' of each molecule was prescribed to maintain some potential for identification of substructurally similar molecules and to help support the development of a SAR for each new compound class. The searches provided *ca.*50-100 analogues of each compound, which were filtered by eye and any duplicates previously identified in the ROCS searches removed. Six compounds based on the substructural query of the *bis*-amide (**251**) were selected. These compounds were added to the pool of compounds previously selected from the above ROCS-based search for biological testing. No compounds based on the rhodanine (**250**) were selected owing to a significant overlap with the ROCS-based output for this query.

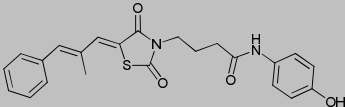
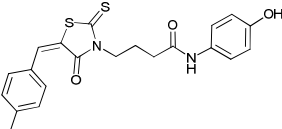
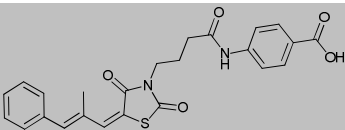
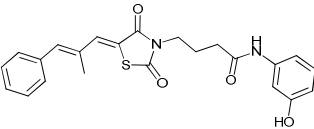
3.2.3.3 Biological evaluation of analogues of rhodanine 250

The three analogues of rhodanine **250** (all selected from the ROCS based searches, as described above) were screened in the TC32 cell viability assay at 10 μ M compound concentration over 24 h, as described previously (see page 51).

Of the three analogues, one compound (**259**) demonstrated statistically significant activity compared to the DMSO control (65 ± 6 % cell viability) which was comparable to the parent hit compound (**250**) (64 ± 2 % cell viability) (*Table 3.2*). Both compound **259** and its parent **250** share a common *N*-propyl linked thiazolidinedione ring with variation at the conjugated lipophilic moiety extending from the 5-position of the heterocycle.

It is interesting to note that the two inactive compounds (compound **260** and **261**) have groups other than a *para*-hydroxy at the phenyl ring (*para*-carboxyl and *meta*-hydroxyl for **260** and **261**, respectively), supporting our observation that a *para*-hydroxyphenyl is an important moiety for maintaining fenretinide-like activity.

The active compound **259** was screened against MSCs (assay as described previously) and no significant toxicity was observed (77 ± 10 % cell viability) (*Table 3.2*). This indicates that the activity of this compound may be specific to the cancer cells, although the therapeutic ratio observed is quite narrow (65 ± 6 % for TC32 and 77 ± 10 % for MSC cell viability respectively).

Compound number	Structure	Identified by ROCS (ComboScore)/ eMolecules	% TC32 cell viability*	% MSC cell viability*	MW	ClogP
251 (hit compound)		n/a	64 ± 2	82 ± 4	422	4.4
259		ROCS (1.375)	65 ± 6	77 ± 10	412	3.3
260		ROCS (1.764)	90 ± 6	-	450	5.1
261		ROCS (1.740)	95 ± 8	-	422	4.4

*Toxicity in TC32 cells and MSC cells treated at 10 μ M for 24 h; Cell viability is expressed as the mean viable cell count as a % of the DMSO control \pm SEM; -, not measured. Fenretinide control: 44 \pm 2 % TC32 cell viability; 88 \pm 5 % MSC cell viability; MW 391; ClogP 7.1.

Table 3.2 Chemical structure, biological activity and physicochemical properties of compounds identified by ROCS and substructural searches based on the non-retinoid rhodanine **250**.

3.2.3.4 Biological evaluation of analogues of bis-amide **251**

The nine analogues of *bis*-amide (**251**) (three selected based on ROCS and six based on the substructural searches, as described above) were screened in the TC32 cell viability assay at 10 μ M compound concentration over 24 h, using the method as described previously (see page 51). All nine compounds displayed statistically significant activity compared to the DMSO control, demonstrating < 86 \pm 3 % cell viability (*Table 3.3*). The most potent compound (**262**) displayed very good activity (38 \pm 4 % cell viability) that was statistically comparable to the fenretinide control (44 \pm 2 % cell viability) and more active than the parent hit compound **251** (63 \pm 2 % cell viability). The compounds **251** and **262-264** all share the common *bis*-benzamide scaffold, differing by a minor variation at the lipophilic tail, distal to the OH group. Compound **265** is a mono-sulfonamide variant of the *bis*-amide, suggesting that a sulfonamide may be a suitable isostere for the amide at this site in this class of molecule. The weak activity observed for compounds **268-270** may be attributed to the replacement of the amide *para*- to the hydroxy group with a dioxo-*iso*-indoliny group, reaffirming findings from the SAR study (Chapter

2) which suggest that a NH-amide at this site may be important for biological activity.

The top five compounds **262-266** were then progressed for screening against MSCs at 10 μ M compound concentration over 24 h (assay as described previously). Encouragingly, no significant toxicity was observed for any of the

Compound number	Structure	Identified by ROCS (ComboScore) / eMolecules	TC32 cell viability*	MSC cell viability*	MW	ClogP
251 (hit compound)		n/a	63 \pm 2	98 \pm 10	346	3.2
262		ROCS (1.547)	38 \pm 4	88 \pm 7	404	4.3
263		ROCS (1.729)	64 \pm 2	89 \pm 8	312	2.8
264		eMolecules	65 \pm 5	87 \pm 12	326	1.5
265		ROCS (1.297)	66 \pm 4	89 \pm 7	322	1.6
266		eMolecules	69 \pm 7	94 \pm 5	440	3.9
267		eMolecules	80 \pm 2	-	372	2.8
268		eMolecules	86 \pm 2	-	430	4.1
269		eMolecules	86 \pm 3	-	456	4.9
270		eMolecules	86 \pm 3	-	440	3.5

*Toxicity in TC32 cells and MSC cells treated at 10 μ M for 24 h; Cell viability is expressed as the mean viable cell count as a % of the DMSO control \pm SEM; -, not measured. Fenretinide control: 44 \pm 2 % TC32 cell viability; 88 \pm 5 % MSC cell viability; MW 391; ClogP 7.1.

Table 3.3 Chemical structure, biological activity and physicochemical properties of compounds identified by ROCS and eMolecules substructure searches based on the non-retinoid *bis*-amide (**251**).

compounds (*Table 3.3*), indicating that the activity of these compounds is specific to the cancer cells.

3.2.4 Summary of results

Two compounds (**250** and **251**) were identified from ROCS-based searches of fenretinide which demonstrated an acceptable preliminary *in vitro* profile of induction of cytotoxicity of TC32 cells with absence of significant toxicity in MSCs. These compounds were progressed for chemical optimisation with the aim of improving the therapeutic ratio for TC32 vs MSC toxicity, as well as to develop a preliminary SAR for their respective compound class. Several analogues were identified which displayed significant activity, with one compound from the *bis*-amide series (**262**) displaying comparable activity to that of fenretinide.

As the *bis*-amide series demonstrated an encouraging level of activity and some evidence for selectivity towards the TC32 cells, this series was selected for further optimisation (discussed later in Section 3.6). Despite the encouraging therapeutic ratio observed for the rhodanine-containing compounds (maximum therapeutic ratio observed for compound **250**, TC32 62 ± 2 % vs MSC 82 ± 4 % cell viability), this series was not progressed for optimisation owing to the well known potential for promiscuous modulation of proteins associated with this compound class.

3.3 Identification of non-retinoid mimetics of fenretinide by substructural search.

To investigate the potential to identify a range of other structurally distinct non-retinoid scaffolds, we returned to the fenretinide structure as a starting point to identify new analogues, this time employing a substructural search of the *para*-hydroxyphenyl fragment as an alternative to the ROCS-based search performed previously, see Section 3.2).

3.3.1 Substructural search

The polar head-unit (*para*-hydroxyphenyl group) of fenretinide was used as a substructural search query to identify structurally distinct analogues of fenretinide for screening (*Figure 3.5*). The eMolecules search returned a

large number of potential hits which was filtered down to 15 compounds for testing based on a qualitative assessment of diversity of the structures returned.

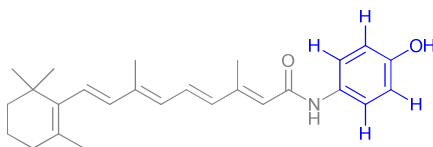


Figure 3.5 The chemical structure of fenretinide with the selected substructural search query highlighted in blue.

3.3.2 Biological evaluation

The 15 compounds containing the 4-hydroxyphenyl substructure (**271-285**) were screened in the TC32 cell viability assay at 10 μ M compound concentration over 24 h, as described previously (see page 51). The biological activity of the 15 compounds is detailed in *Table 3.4*. Of these, 12 displayed statistically significant activity with cell viability ranging from 59 ± 2 to 83 ± 4 % cell viability compared to the DMSO control. However, even the most potent compound (**271**), demonstrated a significant decrease in activity (59 ± 2 % cell viability) compared to the fenretinide control (44 ± 2 % cell viability).

Most of the active compounds from this set are highly structurally related, bearing a short aliphatic linker from the amide nitrogen to an aromatic ring. Many of the compounds contain minor variations in structure, for instance compounds **274**, **275**, **278** and **279** are related by the differing substitution pattern of the alkyl groups on the terminal aromatic ring. Gratifyingly, the TC32 cell viability observed for these compounds was similar (66 ± 2 , 69 ± 2 , 70 ± 4 and 79 ± 2 % cell viability for compounds **274**, **275**, **278** and **279**, respectively) indicative of some commonality of activity for this structural class, although it is not possible to identify a clear SAR for preference for substitution at the phenyl ring. The less active compounds from the set are typically based on structures with a significant structural or physicochemical property variation in comparison to the most active compounds. For instance, compound **285** contains no amide group, compounds **281**, **283** and **284** contain no aromatic region at the lipophilic side of the molecule, and the

hydrophobicity of compounds **281**, **282** and **285** (ClogP < 1) is significantly less than for the average of the set. A shift in hydrophobicity may be an important factor in modulating the activity of compounds in ESFT cells. Indeed, it is noteworthy that a reduction in hydrophobicity for a series of related alkylaminophenol analogues was also found to be detrimental to biological activity, where a decrease in activity was observed for shorter hydrophobic chain lengths when tested in human leukemia cell lines using the trypan blue exclusion assay.^{124,125} Compound **285**, bearing an oxadiazole ring at the site of the amide of fenretinide, was completely inactive which supports our understanding of the requirement for an amide for activity in TC32 cells (Chapter 2).

Four of the five most active compounds from the above studies (**271-273** and **275**) were progressed for toxicity screening against MSC cells (assay details described previously). Encouragingly, compounds **272**, **273** and **275** did not show statistically significant activity compared to the DMSO control (74 ± 7 , 75 ± 4 and 78 ± 5 % cell viability, respectively), indicating that the cytotoxicity of these compounds is statistically specific to the cancer cell line. The ester **272** showed marginally the greatest fold-differential over normal cell toxicity. In contrast, compound **273** demonstrated markedly significant activity (61 ± 4 % cell viability) indicating that cytotoxicity of this compound may be non-specific to the cancer cell line. The toxicity of compounds **272**, **273** and **275** was statistically comparable to fenretinide (88 ± 5 % cell viability) which has a favourable *in vivo* toxicity profile, therefore it is possible that the toxicity of these compounds may be tolerated *in vivo* and hence it might be of interest to investigate the potential for further development of these compounds.

Compound number	Structure	% TC32 cell viability*	% MSC cell viability*	MW	ClogP
1 (fenretinide, query compound)		44 ± 2	88 ± 5	391	7.1
271		59 ± 2	61 ± 4	297	4.3
272		59 ± 3	74 ± 7	406	2.9
273		63 ± 3	75 ± 4	294	3.3
274		66 ± 2	-	271	3.0
275		69 ± 2	78 ± 5	271	3.0
276		68 ± 4	-	241	2.6
277		68 ± 2	-	247	3.7
278		70 ± 4	-	299	3.8
279		79 ± 2	-	243	2.0
280		82 ± 3	-	313	4.4
281		82 ± 4	-	326	0.81
282		83 ± 4	-	309	0.38
283		86 ± 2	-	193	2.1
284		88 ± 4	-	290	2.8
285		95 ± 2	-	176	0.58

*Toxicity in TC32 cells and MSC cells treated at 10 μ M for 24 h; Cell viability is expressed as the mean viable cell count as a % of the DMSO control \pm SEM; -, not measured.

Table 3.4 Chemical structures, biological activity and physicochemical properties of compounds identified by substructural search of the para-hydroxyphenyl unit of fenretinide.

3.4 Identification of non-retinoid mimetics of fenretinide with novel polar head-units

This section describes an approach to identify non-retinoid-based molecules incorporating polar phenyl variants other than the *para*-hydroxyl group. The SAR studies in Chapter 2 identified three isosteres of the 'head-unit' (the *para*-phenol moiety) of fenretinide which were tolerated for induction of cytotoxicity in TC32 cells; the 4-aminophenyl-, the 2-amino-4-hydroxy- and the 4-pyridyl-groups (substructures of compounds **58**, **198** and **199**, respectively) (*Figure 3.6*). It was of interest to consider whether these isosteres could also be accommodated into non-retinoid-based molecules.

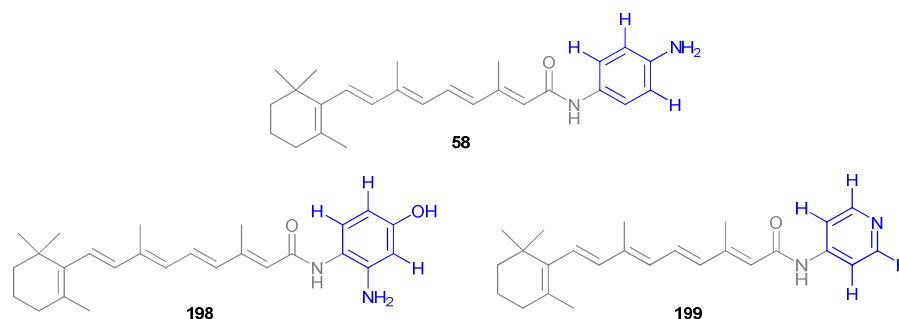


Figure 3.6 Active retinoids bearing novel head units identified in Chapter 2. (Substructure query for eMolecules search highlighted in blue).

3.4.1 Substructural searches

Substructural searches were performed to identify new compounds for testing based on the need to maintain both the 'active' head unit plus a novel, non-retinoid scaffold. The searches were performed in eMolecules using the substructures highlighted in *Figure 3.6*.

The outputs from the substructural searches were combined to generate a pool of virtual hits for selection of compounds for screening. A large number of potential hits was obtained containing the 4-aminophenyl- and 4-pyridyl-groups (substructures of compounds **58** and **199**, respectively) (*Figure 3.6*). However, the 2-amino-4-hydroxy fragment (substructure of compound **198**) returned no hits. The pool of virtual hits was filtered to a list of 500 compounds and then compounds were selected by eye for screening to represent both a diverse range of scaffolds as well as to incorporate examples based on each of the queried head units of compounds **58** and

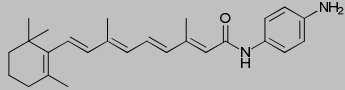
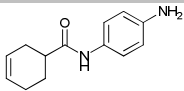
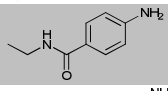
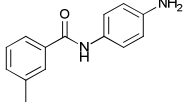
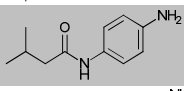
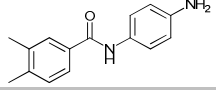
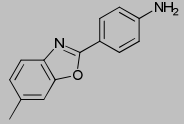
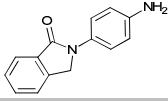
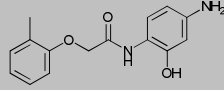
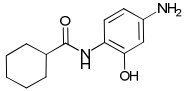
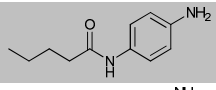
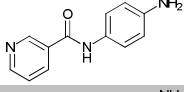
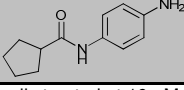
199. In total, 21 compounds were selected for screening; 12 based on the 4-aminophenyl substructure of compound **58** (**286-297**, *Table 3.5*) and nine based on the 4-pyridyl substructure of compound **199** (**298-306**, *Table 3.6*).

3.4.2 Biological evaluation of compounds containing the 4-aminophenyl substructure

The 12 compounds containing the 4-aminophenyl substructure (**286-297**) were screened in the TC32 cell viability assay at 10 μ M compound concentration over 24 h, as described previously (see page 51); the biological activity is detailed in *Table 3.5*. Out of the 12 analogues selected for screening, seven displayed statistically significant activity (compounds **286-292**), with cell viability ranging from 76 ± 3 to 86 ± 3 % compared to the DMSO control. However, there was a significant decrease in activity for these compounds compared to the fenretinide control (44 ± 2 % cell viability) as well as the parent compound (**58**) (60 ± 3 % cell viability). Although the activity observed for these analogues is quite weak in general, compounds containing the 4-aminophenyl moiety appeared to have the potential to show a desirable cytotoxic effect in TC32 cells and there is evidence that substitution of the *para*-hydroxy with an amino group may be tolerated, reaffirming findings from the SAR study (Chapter 2). The general decrease in activity observed for these compounds in comparison to fenretinide and compound **58** may be attributed to a general reduction in lipophilicity within the compound set, owing to the limited availability of suitable compounds for testing containing the appropriate 4-aminophenyl head-unit. Those compounds containing a 2-hydroxy-4-amino substituted phenyl group (**293** and **294**) were statistically inactive. Although the threshold for activity assessment for these compounds is narrow, it would appear that the addition of the additional hydroxy group at the 2-position is not well tolerated, although care needs to be observed when drawing conclusions from this result as the dataset is small and the compounds demonstrate some variation at the lipophilic side in comparison to compounds tested containing just the amino group, which may also be responsible for the drop in activity observed. Compound **291** is the most structurally distinct compound within the set, bearing a benzoxazole isostere for the amide group. The lack of

activity observed for this compound may support our hypothesis that an amide at this site is important for induction of cytotoxicity, as was suggested based on the studies from the retinoid SAR (Chapter 2).

Due to the relatively poor level of activity observed for the compounds from this set, none were taken forward for further screening in MSCs to determine comparable toxicity in normal cells.

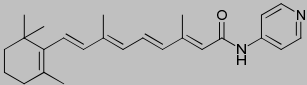
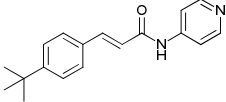
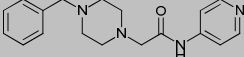
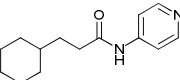
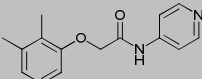
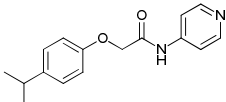
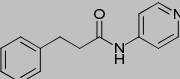
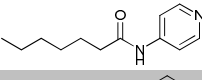
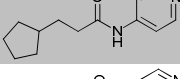
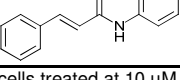
Compound number	Structure	% TC32 cell viability*	% MSC cell viability*	MW	ClogP
58 (query compound)		60 ± 3	101 ± 7	391	6.5
286		76 ± 3	-	216	1.5
287		76 ± 4	-	164	0.48
288		79 ± 5	-	226	1.9
289		80 ± 5	-	192	1.4
290		81 ± 4	-	240	2.4
291		82 ± 2	-	224	3.0
292		86 ± 3	-	224	1.9
293		88 ± 2	-	272	1.5
294		89 ± 5	-	234	1.5
295		91 ± 2	-	192	1.5
296		92 ± 5	-	213	0.76
297		95 ± 3	-	204	1.4

*Toxicity in TC32 cells and MSC cells treated at 10 μM for 24 h; Cell viability is expressed as the mean viable cell count as a % of the DMSO control ± SEM; -, not measured, Fenretinide control: 44 ± 2 % TC32 cell viability; 88 ± 5 % MSC cell viability; MW 391; ClogP 7.1.

Table 3.5 Chemical structures, biological activity and physicochemical properties of compounds identified by substructural search containing the 4-aminophenyl substructure of compound **58**.

3.4.3 Biological evaluation of compounds containing the 4-pyridyl substructure

The nine compounds containing the containing the 4-pyridyl substructure (**298-306**) were screened in the TC32 cell viability assay at 10 μ M compound concentration over 24 h, as described previously (see page 51); the biological activity is detailed in *Table 3.6*. Of the nine compounds screened, seven compounds (compounds **298-304**) displayed statistically significant activity with cell viability ranging from 60 ± 2 to 84 ± 4 % compared to the DMSO control. However, there was a statistically significant decrease in activity for these compounds compared to both the fenretinide control (44 ± 2 % cell viability) and the parent 4-pyridyl retinoid (**199**) (50 ± 2 % cell viability). The most active compound from the set (**298**) contains a lipophilic

Compound number	Structure	% TC32 cell viability*	% MSC cell viability*	MW	ClogP
199 (query compound)		50 ± 2	94 ± 7	377	7.1
298		60 ± 2	67 ± 3	280	4.8
299		70 ± 2	-	310	2.9
300		71 ± 3	-	232	3.7
301		74 ± 2	-	256	3.0
302		75 ± 4	-	270	3.4
303		80 ± 2	-	226	2.6
304		84 ± 4	-	206	3.1
305		88 ± 3	-	218	3.1
306		89 ± 5	-	224	3.0

*Toxicity in TC32 cells and MSC cells treated at 10 μ M for 24 h; Cell viability is expressed as the mean viable cell count as a % of the DMSO control \pm SEM; -, not measured. Fenretinide control: 44 ± 2 % TC32 cell viability; 88 ± 5 % MSC cell viability; MW 391; ClogP 7.1.

Table 3.6 Chemical structures, biological activity and physicochemical properties of compounds identified by substructural search based on the 4-pyridyl substructure of compound **199**.

conjugated amide in place of the repeating isprenoid unit of feneretinide and is structurally the most reminiscent of fenretinide of the analogues tested. Interestingly, the least active compound from this set (**306**) is a close variant of this compound containing the same conjugated amide and phenyl substituents, but no *tert*-butyl group in the *para*-position of the phenyl ring, implying that hydrophobicity in this region of the molecule might be important for activity. The rest of the compounds within the screening set contain various linear hydrophobic variants at the repeating isoprenoid region of fenretinide, except for compound **299** which contains two basic nitrogens. This compound is particularly interesting as it contains a significant hydrophilic character at the repeating isoprenoid region, suggesting that incorporation of polar groups at this site offers potential for development of retinoid mimetics with improved pharmacokinetic properties, assuming a general trend for tolerance of hydrophilic variation at this site can be established.

The most potent compound from this set (**298**) was selected for screening in MSCs to determine toxicity against normal cells (using the methods as described previously). Although this compound contains a Michael acceptor functionality - a moiety usually avoided in drug discovery for reasons of potential indiscriminate toxicity - it was deemed of sufficient interest to evaluate further due to its acceptable level of activity in TC32 cells. Despite our interest in the tertiary amine (**299**), restrictions to availability of cells at the time of screening meant that only one compound was selected for further screening. Using the standard MSC viability assay, compound **298** demonstrated significant activity (67 ± 3 % cell viability) compared to the DMSO control (*Table 3.6*); a relatively poor therapeutic ratio.

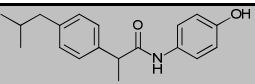
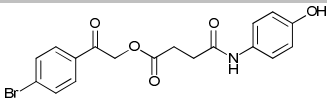
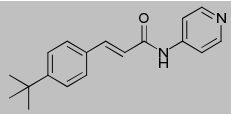
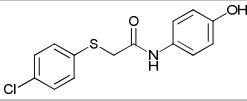
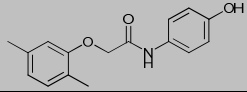
3.4.4 Summary of results

This section has investigated the potential to identify active compounds bearing a novel polar 'head-unit' identified from the retinoid SAR, and combining this with a non-retinoid scaffold. Significant activity was observed for a number of compounds bearing both of the selected polar head groups, indicating that a 4-aminophenyl or 4-pyridyl moiety may be a suitable alternative to the 4-hydroxyphenyl moiety as a general warhead for use as a

chemotherapeutic. A general theme throughout the results is that reduction in lipophilicity of the molecules often results in loss of activity, consistent with chain-length dependant activity of the *para*-alkylaminophenols observed by Takahashi et al.,¹²⁴ although there are clear exceptions to this, for instance for the tertiary amine **299** (*Table 3.6*) which has a significantly lower ClogP than for the majority of compounds tested. Additionally, those compounds containing anything other than a secondary amide at the central portion of the molecule were inactive.

3.5 Optimisation of compounds 271-273, 275 and 298

A subset of compounds from the most recent rounds of testing (encompassing the non-retinoid 4-hydroxyphenyl and polar head-unit variants, Sections 3.3 and 3.4, respectively) were prioritised for optimisation. The five compounds which showed the highest level of activity (59 ± 2 to 69 ± 2 % cell viability) and with some evidence for lack of induction of cytotoxicity in the MSC assay were selected to take forward for further optimisation (*Table 3.7*). The compound set comprised four compounds containing the 4-hydroxyphenyl group (from Section 3.3) (compounds **271**, **272**, **273** and **275**) and one containing the 4-pyridyl motif (from Section 3.4) (compound **298**). Although non-specific toxicity was a determinant in

Compound number	Structure	% TC32 cell viability*	% MSC cell viability*	MW	ClogP
271		59 ± 2	61 ± 4	297	4.3
272		59 ± 3	74 ± 7	406	2.9
298		60 ± 2	67 ± 3	280	4.8
273		63 ± 3	75 ± 4	294	3.3
275		69 ± 2	78 ± 5	271	3.0

*Toxicity in TC32 cells and MSC cells treated at 10 μ M for 24 h; Cell viability is expressed as the mean viable cell count as a % of the DMSO control \pm SEM; –, not measured. Fenretinide control: 44 ± 2 % TC32 cell viability; 88 ± 5 % MSC cell viability; MW 391; ClogP 7.1.

Table 3.7 Biological data of the 5 hit compounds selected for further optimisation.

selection of these compounds for optimisation, the level of non specific activity observed for these compounds (61 ± 4 to 78 ± 5 % cell viability in MSC) was less than ideal. In an effort to improve the specificity against MSCs as well as the activity to comparable or improved cytotoxicity compared to fenretinide, the five hits were taken forward for structural searches to identify close analogues for further biological investigation.

3.5.1 Substructural searches of compounds 271-273, 275 and 298

For each of the hit compounds (**271**, **272**, **273**, **275** and **298**), a substructure search was performed based on the apportioned substructure highlighted in blue in *Figure 3.7*. The substructure for each hit was selected based on the need for both availability of a certain number of substructural analogues, with the requirement for development of a SAR (*i.e.* not too broad a search to allow for positive development of SAR and not too narrow a search to return a minimum number of compounds to select for testing). For each of the selected substructures, a number of analogues were identified and pooled to generate a list of 500 compounds for selection. From this list, 29 compounds (11 analogues of **273**, 10 of **275**, 5 of **298**, two of **272**, one of **271**) were selected by eye to represent a range of structurally diverse analogues of each of the hits.

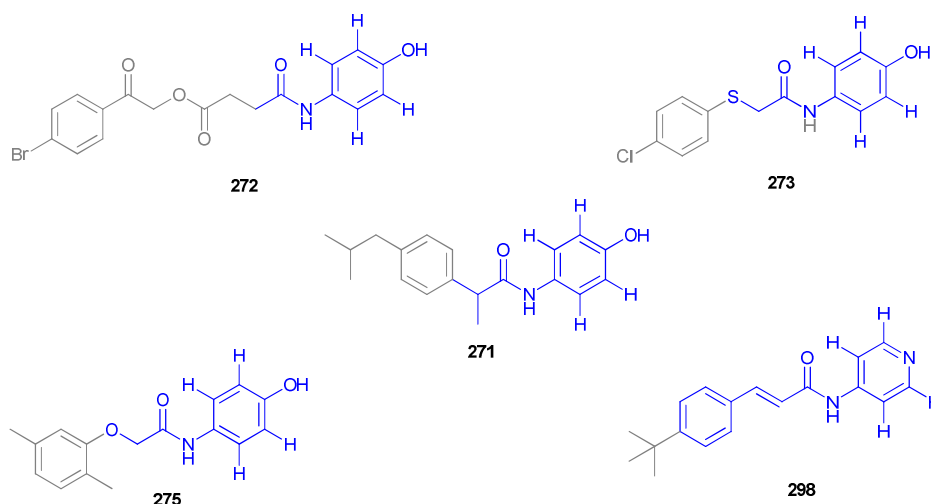
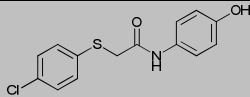
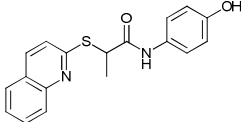
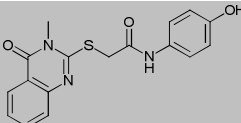
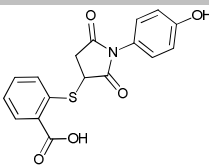
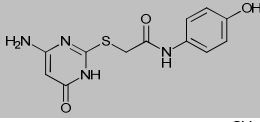
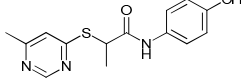
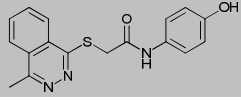
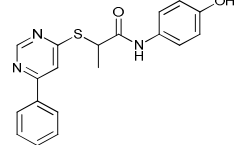
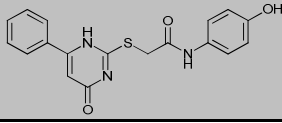
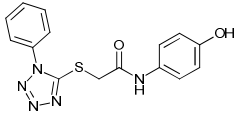
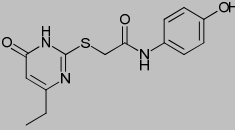
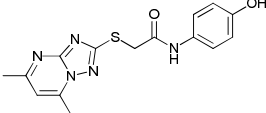


Figure 3.7 Substructures (highlighted in blue) of the active compounds selected for optimisation.

3.5.2 Biological evaluation of compounds bearing the substructure of compound 273

The 11 compounds bearing the **273** substructure (*Figure 3.7*) were screened in the TC32 cell viability assay at 10 μ M compound concentration over 24 h, as described previously (see page 51). Out of these, seven compounds (**307-313**) demonstrated significant activity compared to the DMSO control, ranging from 70 ± 2 to 81 ± 9 % cell viability (*Table 3.8*), although none achieved activity comparable to that of the fenretinide control (44 ± 2 % cell viability), or that of the parent compound (**273**) (63 ± 3 % cell viability). As a result, none of these compounds were taken forward for screening in MSCs or for further optimisation.

Compound number	Structure	% TC32 cell viability*	% MSC cell viability*	MW	ClogP
273 (hit compound)		63 ± 3	75 ± 4	294	3.3
307		70 ± 2	-	324	3.3
308		70 ± 3	-	341	1.7
309		76 ± 5	-	343	1.4
310		75 ± 7	-	292	-0.4
311		80 ± 5	-	298	1.6
312		87 ± 2	-	325	1.8
313		81 ± 9	-	351	3.2
314		92 ± 3	-	353	1.8

315		97 ± 2	-	327	1.7
316		95 ± 8	-	305	0.8
317		92 ± 8	-	329	1.4

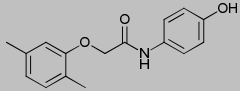
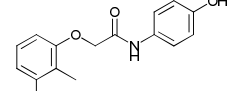
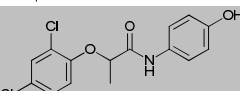
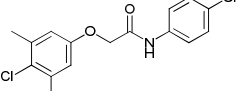
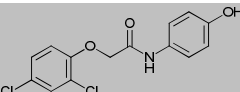
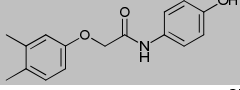
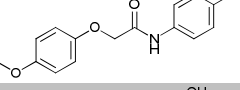
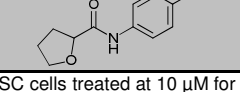
*Toxicity in TC32 cells and MSC cells treated at 10 μM for 24 h; Cell viability is expressed as the mean viable cell count as a % of the DMSO control ± SEM; -, not measured. Fenretinide control: 44 ± 2 % TC32 cell viability; 88 ± 5 % MSC cell viability; MW 391; ClogP 7.1.

Table 3.8 Chemical structures, biological activity and physicochemical properties of compounds identified by substructural search based on the substructure of compound **273**.

3.5.3 Biological evaluation of compounds bearing the **275** substructure

Ten compounds bearing the apportioned substructure of compound **275** (*Figure 3.7*) were screened at 10 μM compound concentration over 24 h using the TC32 cell viability assay, as described previously (see page 51). Of these, all except compound **327** demonstrated statistically significant activity compared to the DMSO control, ranging from 54 ± 3 to 84 ± 2 % cell viability (*Table 3.9*). The phenylether **318** was the most active compound, achieving activity statistically comparable (54 ± 3 % cell viability) to fenretinide (44 ± 2 % cell viability) and was marginally more active than the parent compound **275** (69 ± 2 % cell viability). Interestingly, this compound is the most structurally similar of all of the compounds of the set to the parent compound with only a variation in position of a methyl group on the phenyl ring. This and the next most active compound - the dichloro analogue (compound **319**) - were screened against MSCs to determine a therapeutic ratio. Unfortunately, both of these compounds displayed significant activity in this assay (70 ± 5 and 67 ± 3 % cell viability respectively) compared to the DMSO control, indicating that the compounds may be demonstrating unfavourable toxicity which is not specific to the TC32 cells. The compounds are also more toxic than the parent compound **275** (78 ± 5 % cell viability). However, *in vivo* assessment may provide a more accurate prediction as to the true toxicity for these compounds as the toxicity of the compounds was

statistically comparable to fenretinide (88 ± 5 % cell viability). Owing to the relatively poor activity and therapeutic ratio no compounds from this set were selected for further biological evaluation.

Compound number	Structure	% TC32 cell viability*	% MSC cell viability*	MW	ClogP
275 (hit compound)		69 ± 2	78 ± 5	271	3.0
318		54 ± 3	70 ± 5	271	3.0
319		60 ± 3	67 ± 3	326	3.7
320		65 ± 3	-	257	2.5
321		65 ± 6	-	293	3.2
322		66 ± 3	-	306	3.9
323		66 ± 3	-	312	3.4
324		73 ± 4	-	293	3.2
325		83 ± 2	-	271	3.0
326		84 ± 2	-	273	2.1
327		100 ± 2	-	207	0.7

*Toxicity in TC32 cells and MSC cells treated at $10 \mu\text{M}$ for 24 h; Cell viability is expressed as the mean viable cell count as a % of the DMSO control \pm SEM; -, not measured. Fenretinide control: 44 ± 2 % TC32 cell viability; 88 ± 5 % MSC cell viability; MW 391; ClogP 7.1.

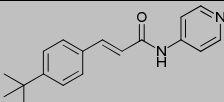
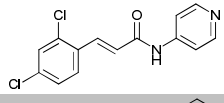
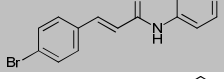
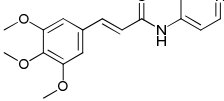
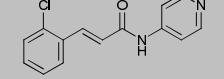
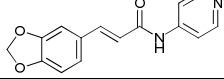
Table 3.9 Chemical structures, biological activity and physicochemical properties of compounds identified by substructural search based on substructure **275**.

3.5.4 Biological evaluation of compounds bearing the 4-pyridyl substructure of compound 298

Five compounds bearing the apportioned substructure of compound **298** (Figure 3.7) were screened at $10 \mu\text{M}$ compound concentration over 24 h using the TC32 cell viability assay, as described previously (see page 51). Of these, four compounds (**328-331**) demonstrated significant activity compared

to the DMSO control, ranging from 57 ± 2 to 84 ± 2 % cell viability (Table 3.10). The most active compound, the dichloro amide (**328**), displayed good activity (57 ± 2 % cell viability) which was approaching that of fenretinide (44 ± 2 % cell viability) and comparable to that of the parent compound (**298**) (60 ± 2 % cell viability). Interestingly, the mono-Cl analogue of this compound (**331**) is significantly less active (84 ± 2 vs 57 ± 2 % cell viability). This may be the result of loss of a specific halogen-mediated interaction to a target responsible for induction of cell death or more likely a general reduction of hydrophobicity of the molecule, a trend which is observed to generally correlate with reduction of activity within this set of compounds.

The dichloro amide (**328**) was taken forward for screening in MSCs, where significant activity was observed compared to the vehicle control (67 ± 3 % cell viability). However, this toxicity was statistically comparable to that of fenretinide, therefore further evaluation for toxicity (e.g. *in vivo* study) may provide a more accurate assessment of true toxicity.

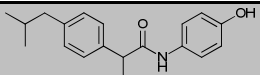
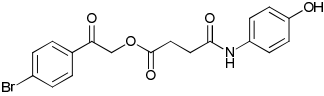
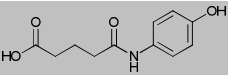
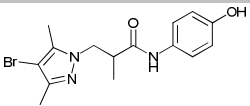
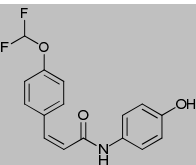
Compound number	Structure	% TC32 cell viability*	% MSC cell viability*	MW	ClogP
298 (hit compound)		60 ± 2	67 ± 3	280	4.8
328		57 ± 2	67 ± 3	293	4.4
329		71 ± 2	-	303	3.9
330		77 ± 2	-	314	2.3
331		84 ± 2	-	259	3.7
332		91 ± 1	-	268	3.0

*Toxicity in TC32 cells and MSC cells treated at 10 μ M for 24 h; Cell viability is expressed as the mean viable cell count as a % of the DMSO control \pm SEM; -, not measured. Fenretinide control: 44 ± 2 % TC32 cell viability; 88 ± 5 % MSC cell viability; MW 391; ClogP 7.1.

Table 3.10 Chemical structures, biological activity and physicochemical properties of compounds identified by substructural search of the 4-pyridyl unit of compound **298**.

3.5.5 Biological evaluation of compounds bearing the 271 and 272 substructures

A discussion of the screening results for the analogues selected from the substructural search of the 4-hydroxyphenyl amidoalkyl moiety of compounds **271** and **272**, has been grouped together as they are structurally related and only three analogues in total were identified for screening. The three compounds (**333-335**) were screened in the TC32 cell viability assay but none of the compounds displayed significant activity compared to the DMSO control (*Table 3.11*). This is perhaps not surprising given the significant variation of structure of these compounds to the parent compounds as a result of the rather limited availability of close structural analogues for selection. Additionally, compound **333** contains a carboxylic acid group which will be highly ionised at the pH of the assay (7.4), limiting uptake of the compound into the cell.

Compound number	Structure	% TC32 cell viability*	% MSC cell viability*	MW	ClogP
271 (hit compound)		59 ± 2	61 ± 4	297	4.3
272 (hit compound)		59 ± 3	74 ± 7	406	2.9
333		95 ± 2	-	223	0.7
334		99 ± 6	-	352	2.6
335		102 ± 5	-	305	3.4

*Toxicity in TC32 cells and MSC cells treated at 10 μM for 24 h; Cell viability is expressed as the mean viable cell count as a % of the DMSO control ± SEM; -, not measured. Fenretinide control: 44 ± 2 % TC32 cell viability; 88 ± 5 % MSC cell viability; MW 391; ClogP 7.1.

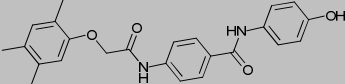
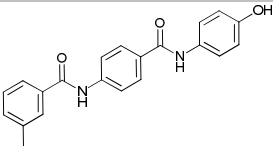
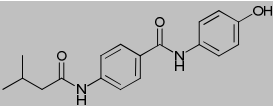
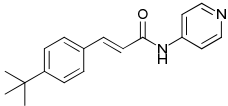
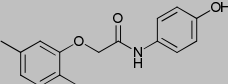
Table 3.11 Chemical structures, biological activity and physicochemical properties of compounds identified by substructural search based on compounds **271** and **272**.

3.5.6 Summary of results

Chemical optimisation of the five hits identified from the the most recent rounds of testing (encompassing the non-retinoid 4-hydroxyphenyl and polar head-unit variants) by use of 'SAR-by-catalogue' purchase and testing

identified a number of structurally diverse non-retinoids with an ability to induce cytotoxicity in TC32 cells and which demonstrate a lack of toxicity towards the normal cell type, MSCs. The activity in TC32 cells and therapeutic ratio in all cases was less than for fenretinide; as a result none of the compounds from this round of optimisation were progressed for further study.

Instead, the hit compounds originating from the original ROCS-based search and optimisation (Section 3.2) (compounds **251**, **262**, **263**) and substructural search of the 4-hydroxyphenyl (**275**) and 4-pyridyl (**298**) groups (*Table 3.12*) were selected for further biological evaluation, to include SAR studies, dose response studies across multiple cell lines and mechanistic studies. The compounds were selected for optimisation because in each case the hit compounds demonstrated good activity against TC32 cells and acceptable toxicity in the MSCs.

Compound number	Structure	TC32 cell viability*	MSC cell viability*	MW	ClogP
262		38 ± 4	88 ± 7	404	4.3
251		47 ± 12	89 ± 9	346	3.3
263		64 ± 2	98 ± 5	312	2.8
298		60 ± 2	67 ± 3	280	4.8
275		69 ± 2	78 ± 5	271	3.0

*Toxicity in TC32 cells and MSC cells treated at 10 μM for 24 h; Cell viability is expressed as the mean viable cell count as a % of the DMSO control ± SEM; -, not measured. Fenretinide control: 44 ± 2 % TC32 cell viability; 88 ± 5 % MSC cell viability; MW 391; ClogP 7.1.

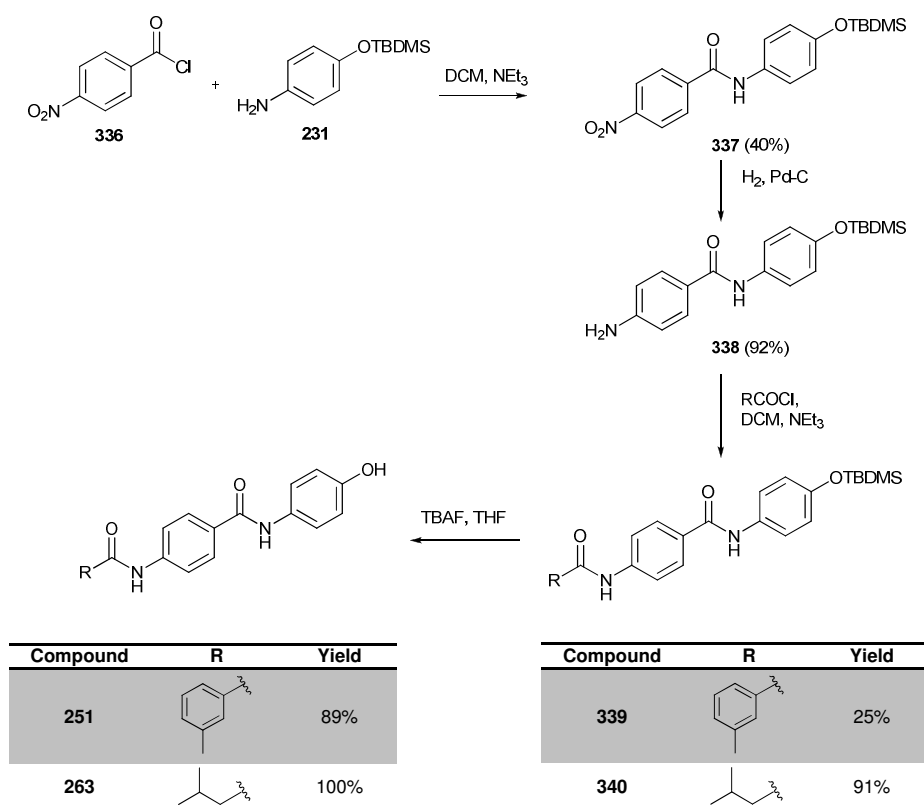
Table 3.12 Biological data of the five non-retinoid compounds selected for further biological evaluation.

3.6 Validation of the hit compounds

In this section, selected hit compounds were resynthesised in order to confirm the structure of the compounds and to provide sufficient quantity of each for thorough biological evaluation and re-screening.

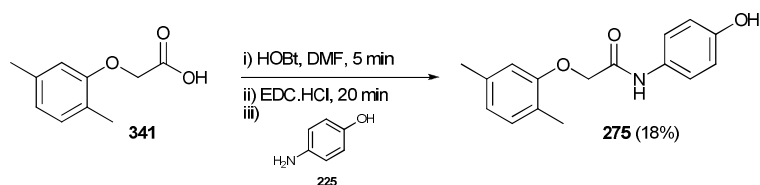
3.6.1 Resynthesis of selected hits

Compounds **251** and **263** (Table 3.12) are based on a common *bis*-benzamide scaffold with variation at the hydrophobic portion at the site distal to the OH group. The compounds were synthesised from a common intermediate (**338**), which itself was synthesised in a two-step process by amide coupling of TBDMS-protected *para*-aminophenol (**231**) with *para*-nitrobenzoyl chloride (**336**), followed by hydrogenation of the nitro group to afford the primary amine (**338**) (Scheme 3.1). Subsequent coupling of the amine with *meta*-toluoyl chloride or isovaleryl chloride, as appropriate, followed by silyl-deprotection using TBAF, yielded compounds **251** and **263**, respectively, in moderate to good yields over two steps.



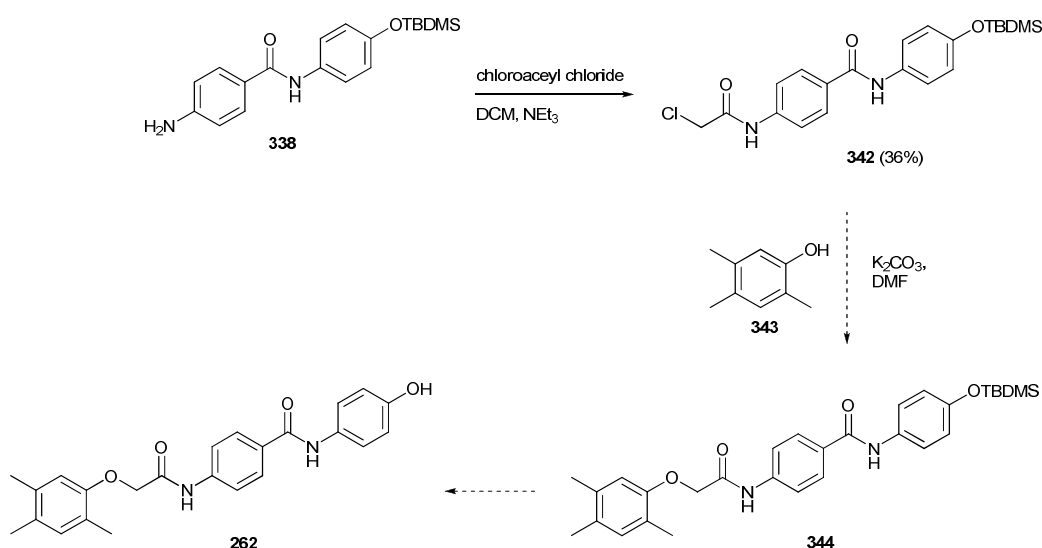
Scheme 3.1 Synthesis of non-retinoid compounds (**251**) and (**263**).

Compound **275** (Table 3.12) was synthesised by HOBt/EDC mediated coupling of 2,5-dimethylphenoxyacetic acid (**341**) to 4-aminophenol (**225**) (Scheme 3.2). Although the yield for the reaction was poor, the product was easily obtained by recrystallisation in excellent purity and in sufficient quantity for screening.



Scheme 3.2 Synthesis of compound **275** via a HOBt/EDC amide coupling reaction.

An attempt to synthesise the most active compound, amide **262** (Table 3.12) was unsuccessful. The aniline **338**, previously prepared as a precursor to compounds **251** and **263** (Scheme 3.1), was successfully coupled to chloroacetyl chloride to afford the activated chloride **342** in modest yield. However, attempts to alkylate the chloride with 2,4,5-trimethyl phenol generated a highly insoluble product which could not be characterised (Scheme 3.3).



Scheme 3.3 Proposed synthesis of compound **262**.

3.6.2 Biological evaluation of resynthesised hits

The three resynthesised compounds (**251**, **263**, **275**) were screened in the TC32 cell viability assay at 10 μ M compound concentration over 24 h, using the method as described previously (see page 51).

Screening of the resynthesised *bis*-amides **251** and **263** confirmed activity against TC32 cells. However, the activity was marginally reduced in both cases (73 ± 4 % and 76 ± 3 % cell viability, respectively) compared to the previously investigated (purchased) compounds (63 ± 2 % and 64 ± 2 % cell

viability compared to the DMSO control) (*Table 3.13*). This reduction in activity was statistically significant in the case of **263**, but not **251**. Further repeats of the experiment were carried out (total n = 18), in which the result was confirmed. When screened alongside each other in the same experiment there was a difference in activity of 30 % and 23 % between purchased and resynthesised compounds, **251** and **263** respectively (*Table 3.13*).

Compound	Overall average of TC32 cell viability (%, n ≥ 9)		TC32 cell viability within the same experiment (%, n = 9)	
	Purchased compound	Resynthesised compound	Purchased compound	Resynthesised compound
251	63 ± 2	73 ± 4	44 ± 1	74 ± 2
263	64 ± 2	76 ± 3	48 ± 2	71 ± 2
275	69 ± 2	54 ± 4	-	-

*Toxicity in TC32 cells and MSC cells treated at 10 µM for 24 h; Cell viability is expressed as the mean viable cell count as a % of the DMSO control ± SEM; -, not measured. Fenretinide control: 44 ± 2 % TC32 cell viability; 88 ± 5 % MSC cell viability; MW 391; ClogP 7.1.

Table 3.13 A table comparing the biological data of purchased and resynthesised non-retinoid. -, not screened within the same experiment.

The resynthesised phenylether **275** displayed considerably increased activity (54 ± 4 % cell viability) compared to the purchased compound (69 ± 2 % decrease in cell viability), which is statistically significant. Furthermore, the activity of the resynthesised compound demonstrated activity statistically comparable to fenretinide (44 ± 2 % cell viability).

The variation observed between purchased and resynthesised samples could possibly be due to discrepancies in aliquoting/weighing of the compounds or the presence of minor impurities in the purchased sample which were not detected upon analysis by LCMS or NMR. Although the resynthesised *bis*-amides **251** and **263** still demonstrate a significant response in comparison to the DMSO control, the variation in assay result between the purchased and resynthesised compound was somewhat concerning and hence these compounds were not progressed for further biological evaluation. Conversely, phenylether **275** demonstrated only a minor variation. The compound also consistently demonstrated very good activity in TC32 cells, as well as a good fold-differential of activity for the resynthesised compound in TC32 cells (54 ± 4 % cell viability vs MSC cells 78 ± 5 % cell viability). Therefore, this compound was taken forward for

further study (to dose response and mechanism of action studies, see Chapter 4).

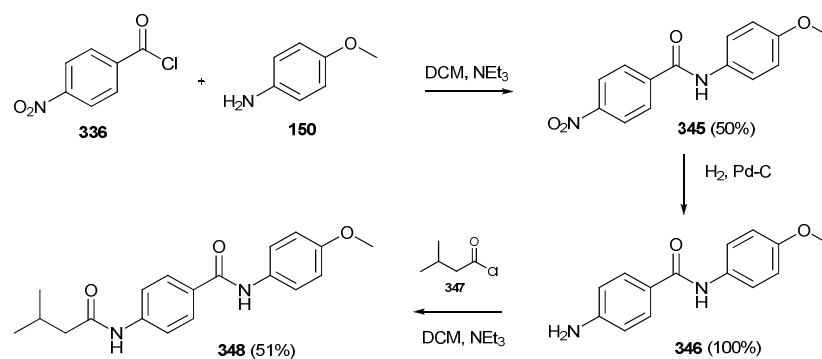
3.7 Hybrid analogues

In this section, analogues of the 4-hydroxyphenyl-containing hit compounds **263** and **275** were designed whereby the polar head group was substituted with alternative head groups previously investigated in the retinoid SAR study (Chapter 2) with the intention of either reducing activity (by selection of 'inactive' head groups from the SAR study), or retaining or improving activity (by selection of 'active' head groups). 'Inactive' head groups can be defined as the head groups which reduced or abolished activity when substituted into the fenretinide structure in place of the 4-hydroxyphenyl group, whereas 'active' head groups retained or promoted activity (4-pyridyl, 4-aminophenyl and 4-amino-2-hydroxyphenyl). Biological evaluation of these 'hybrid' analogues may help to elucidate the molecular requirements for retinoid/non-retinoid induced cell death, as well as to investigate whether these structurally disparate compounds (in comparison to fenretinide) may be acting *via* a similar mechanism to fenretinide.

3.7.1. Design and synthesis of hybrid analogues

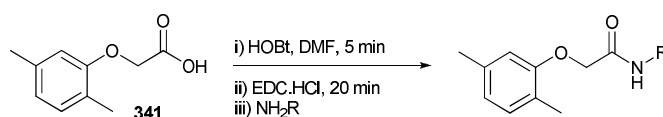
We hypothesised that introduction of a methoxy group at the OH site of the non-retinoid hits **263** and **275** should decrease or abolish activity based on our understanding of the SAR from the retinoid studies (OMe abolishes activity, Chapter 2). The *para*-methoxy analogue (**348**) of *bis*-amide **263** was synthesised over 3 steps in a similar manner as for the parent hydroxyl variant, by replacing TBDMS protected *para*-aminophenol for *para*-methoxyaniline. Using this method, *para*-methoxyaniline (**150**) was coupled to *para*-nitrobenzoyl chloride (**336**) and the resulting amide (**345**) reduced to the amine (**346**), followed by amide coupling to isovaleryl chloride (**347**) to generate the methoxy compound (**348**) (*Scheme 3.4*).

The *para*-methoxy analogue of the other hit, phenylether **275**, was also synthesised to further qualify the importance of the OH/OMe exchange for a structurally distinct non-retinoid scaffold. In addition, the influence of



Scheme 3.4 Synthesis of the *para*-methoxy analogue (**348**) of the *bis*-amide (**263**).

replacement of the 4-hydroxyphenyl group for 4-pyridyl and 4-aminophenyl was studied within this molecule to investigate whether modification for these variants was also tolerated (*para*-amino and 4-pyridyl retain activity, Chapter 2). These compounds were all synthesised using the same general method employing a HOBt/EDC mediated coupling of 2,5-dimethylphenoxyacetic acid (**341**) to the required aniline - 4-aminopyridine, *para*-phenylenediamine or *para*-methoxyaniline - to give the required amides **349**, **350** and **351**, respectively (*Scheme 3.5*). Although the yields of the reactions were quite poor in each case, the products were easily obtained by recrystallisation in excellent purity and in a sufficient quantity for screening.



Compound	R	Yield (%)
349		21
350		26
351		14

Scheme 3.5 Synthesis of three 'hybrid' analogues of compound (**275**) via a HOBt/EDC amide coupling reaction.

3.7.2 Biological evaluation of the 'hybrid' compounds

The four 'hybrid' compounds were screened in the TC32 cell viability assay at 10 μ M compound concentration over 24 h, as described previously (see page 51).

The methoxy analogue (**348**) of the *bis*-amide **263** showed no significant activity (98 ± 3 % cell viability) compared to the DMSO control. The lack of activity observed for this compound in comparison to the parent hydroxy compound (**263**) (70-76 % cell viability), suggests that the methoxy group is not tolerated and that compound **263** may be having a specific cytotoxic effect on TC32 cells. This lack of activity for the methoxy analogue is consistent with the SAR identified with the retinoids which might suggest that *bis*-amide (**263**) may be binding to the same target and/or acting *via* a similar mechanism to fenretinide.

Similarly, the methoxy analogue (**349**) of the phenylether **275** demonstrated no significant activity (95 ± 6 % cell viability) compared to the DMSO control, reaffirming our observation about the importance of the methoxy substitution to biological activity. Interestingly, the other 'hybrid' compounds based on compound **275** (4-aminophenyl analogue (**350**), and 4-pyridyl (**351**)) also demonstrated no significant activity (97 ± 7 % and 93 ± 5 % cell viability, respectively). This is contradictory to the SAR identified for the retinoids, whereby the 4-aminophenyl and 4-pyridyl isosteres demonstrated significant activity. This could imply that compound **275** is affecting a different target and/or acting *via* an alternative mechanism to fenretinide. It was therefore of interest to take this compound forward for further mechanistic studies (Chapter 4) in attempt to identify whether this compound initiates programmed cell death by the same pathways that are known to contribute to fenretinide induced cell death.

3.8 Conclusions

Through iterative ROCS shape- and electrostatic-based similarity and substructural searching methods, a range of novel and highly structurally diverse non-retinoid mimetics have been identified which demonstrate a significant cell death capability in TC32 cells, as well as evidence for an encouraging therapeutic ratio to normal MSCs. As these compounds have been designed to incorporate a more favourable predicted physicochemical profile, by reduction in the lipophilic capacity of the molecule, these compounds may also demonstrate more favourable pharmacokinetic

properties including improved metabolic stability and solubility, resulting in an improved bioavailability than that which is achieved by fenretinide. The actual physicochemical (and pharmacokinetic) properties of the non-retinoids will be returned to for discussion in Chapter 4.

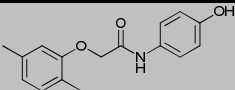
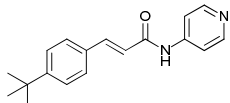
All active non-retinoids identified within this Chapter contained substructures of compounds found to display activity in the retinoid SAR study, namely a *para*-hydroxyphenyl, *para*-aminophenyl or 4-pyridyl substructure. Synthesis and screening of the methylated 'hybrid' analogues for two of the most interesting hits resulted in loss of activity. This indicates that these compounds may be binding to the same target and acting *via* a similar mechanism to the parent compound. Additionally, those compounds with reduced hydrophobicity in comparison to fenretinide generally exhibited reduced activity, indicating that hydrophobicity may be an important factor for binding or for delivery to the target.

Of the specific hits identified in this chapter, the hydroxyphenyl phenyl ether (**275**) and 4-pyridyl-containing compound (**298**) were of most interest based on a good, consistent activity against TC32 cells and represent a diverse set of structures for optimisation (*Table 3.14*). Compound **275** also did not demonstrate statistically significant activity in MSCs, hence the observed activity has the potential to be specific to the cancer cells. In contrast, compound **298** bearing the 4-pyridyl polar head group did demonstrate significant activity in MSCs. However toxicity in this cell line was statistically comparable to that of fenretinide and therefore a more substantive assessment of the toxicity is required. It was of particular interest to understand the biological activity of this compound due to its structural diversity in comparison to the other hit compounds which typically bear the fenretinide-like 4-hydroxyphenol moiety.

The 'hybrid' analogues of hydroxyphenyl phenyl ether **275**, whereby the *para*-hydroxyphenyl component was replaced with 4-pyridyl and 4-aminophenyl, were only weakly active or inactive, which is contradictory to the SAR identified for the retinoids, whereby the 4-aminophenyl and 4-pyridyl isosteres demonstrated significant activity. This could imply that

hydroxyphenyl phenyl ether **275** is affecting a different target and/or acting *via* an alternative mechanism to fenretinide.

Both of these compounds (**275** and **298**) were prioritised for optimisation and taken forward for further biological evaluation, including dose response studies across multiple cell lines and mechanism of action studies (Chapter 4).

Compound number	Structure	TC32 cell viability*	MSC cell viability*	MW	ClogP
275		54 ± 4 ^a 69 ± 2 ^b	78 ± 5	271	3.0
298		60 ± 2	67 ± 3	280	4.8

*Toxicity in TC32 cells and MSC cells treated at 10 μM for 24 h; Cell viability is expressed as the mean viable cell count as a % of the DMSO control ± SEM; –, not measured. Fenretinide control: 44 ± 2 % TC32 cell viability; 88 ± 5 % MSC cell viability; MW 391; ClogP 7.1. ^aresynthesised compound, ^bpurchased compound.

Table 3.14 Biological data of the two non-retinoid hits selected for further biological evaluation (Chapter 4).

4. Preclinical evaluation of hit compounds

The goal in this Chapter was to examine and compare the concentration-dependent activity of the fenretinide analogues and non-retinoid compounds of most interest and through mechanistic studies establish if these compounds might be effecting cell death through the intrinsic mitochondrial death pathway that is activated by fenretinide.

In addition to establishing the range of activity of the hit compounds across the heterogeneous tumour types, these studies may also highlight any genetic factors which might influence the activity of some compounds. p53 and p16 are tumour suppressor proteins which are responsible for the arrest of cell growth in DNA damaged cells. p53/p16 are capable of holding the damaged cell at the G₁ regulation point, where DNA repair proteins fix any damage before the cell is allowed to proceed to the S phase, or by induction of apoptosis through programmed cell death in irreparable cells. Most chemotherapeutic drugs cause DNA damage, which is sensed by p53 or p16 checkpoint proteins. Therefore mutations leading to loss of tumour suppressor protein expression can influence the response of cells to some therapeutics. Since cells which do not express p53/p16 are more resistant to apoptosis, it may be favourable to identify cytotoxic agents that induce cell death independently of these. Fenretinide is known to induce cell death independently of p53 and p16 in a wide range of cancer types, including ESFT.^{67,167}

ROS are species of reduced oxygen that are in a more reactive state than molecular oxygen. It was of interest to examine the effect of the most active compounds on ROS levels, as one of the earliest effects of fenretinide in cancer cells is a time and concentration dependent induction of ROS.^{40,67} Inhibition of ROS rescues cells from fenretinide-induced cell death in many cell lines, including ESFT cells, which is consistent with the hypothesis that elevated levels of ROS activate cell death in cancer cells.^{67,74,170,171} The intracellular levels and activity of ROS will be dependent on both the production and inhibition of ROS. Variation in both ROS production and

elimination most likely regulate the selective initiation of cell death in cancer cells by fenretinide. Consistent with this hypothesis, fenretinide fails to increase ROS in normal cells, which are resistant to fenretinide induced cell death.^{51,52} The lack of fenretinide toxicity in normal cells, substantiated in phase 1 clinical trials, is one of the reasons why fenretinide is such an attractive therapeutic candidate.¹⁰⁶ ROS modulate the activity of many cellular signalling molecules, and appears to mediate fenretinide induced cancer cell death through different cancer-type dependent pathways.^{67,74} However, the morphological cellular changes induced by fenretinide cell death are known to be a consequence of the activation of intracellular cysteine-aspartic proteases known as caspases.^{62,65,67} Therefore it was also of interest to examine the effect of the most active compounds on caspase 3 cleavage.

By screening against multiple cell lines and investigating cell-death pathways, these studies may help to further establish the SAR required for activity within individual cell lines. Identification of an important pathway in the cell death process may aid the design of future potentially active compounds. This chapter describes an investigation into the mechanism of initiation of cell death in ESFT cells for 5 active compounds (three retinoids identified by the SAR studies (**58**, **198** and **199**) and two non-retinoids (**275** and **298**) identified by *in silico* searches (*Figure 4.1*) following concentration

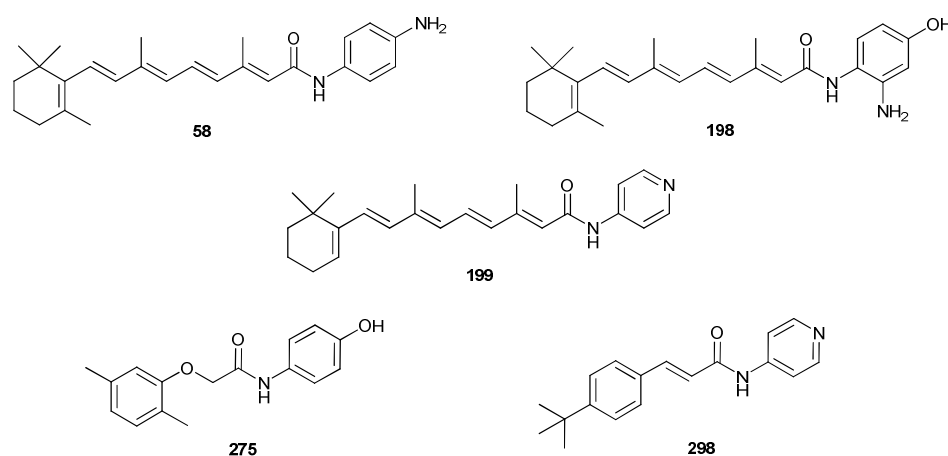


Figure 4.1 Three retinoids (**58**, **198** and **199**) and two non-retinoids (**275** and **298**) selected for further biological evaluation.

response studies across multiple cell lines. The 5 compounds were assessed for their ability to generate ROS and cleave caspase-3.

4.1 Concentration response studies

Prior to embarking on mechanistic studies, concentration response studies were carried out using the five compounds selected for further biological evaluation in order to determine whether activity reflects that of fenretinide across a wide concentration range and multiple cell lines.

Activity of the compounds was tested at 3, 6, 10, 20 and 40 μM against three ESFT cell lines (TC32, A673, SK-N-MC) and two neuroblastoma cell lines (SHEP-1 and SK-N-SH). ESFT cell lines were selected to represent the range of genetic features associated with the ESFT phenotype (*Table 4.1*).

Cell line	p53 expression	p16 expression	Fusion type
TC32	+	-	EWS-FL1 type 1
SK-N-MC	-	+	EWS-FL1 type 1
TTC466	+	+	EWS-ERG

Table 4.1 Characteristics of the three ESFT cell lines prioritised for the concentration response studies.

Cell viability was analysed using the trypan blue exclusion assay (as previously described, see page 51). Biological experiments consisted of three technical repeats per experiment and three independent experiments were carried out ($n = 9$). Statistical analysis was carried out as described previously. Compounds were deemed to display statistically significant activity or ROS production when $p < 0.05$ compared to that of the vehicle control viability, and comparable to fenretinide when $p > 0.05$ compared to the fenretinide control. Here, data is illustrated in charts displaying the activity of each respective compound against all five cell lines tested. Charts displaying all compounds against each respective cell line can be found in Appendix B.

4.1.1 Concentration response of fenretinide

As expected, fenretinide (**1**) demonstrated statistically significant activity across all cell lines tested (*Chart 4.1*). Activity was significant compared to the vehicle control across the concentration range (3-40 μM) in TC32 and SK-N-

SH cell lines, at concentrations $\geq 6 \mu\text{M}$ in TTC466 and SHEP-1 cells and $\geq 10 \mu\text{M}$ in SK-N-MC cells.

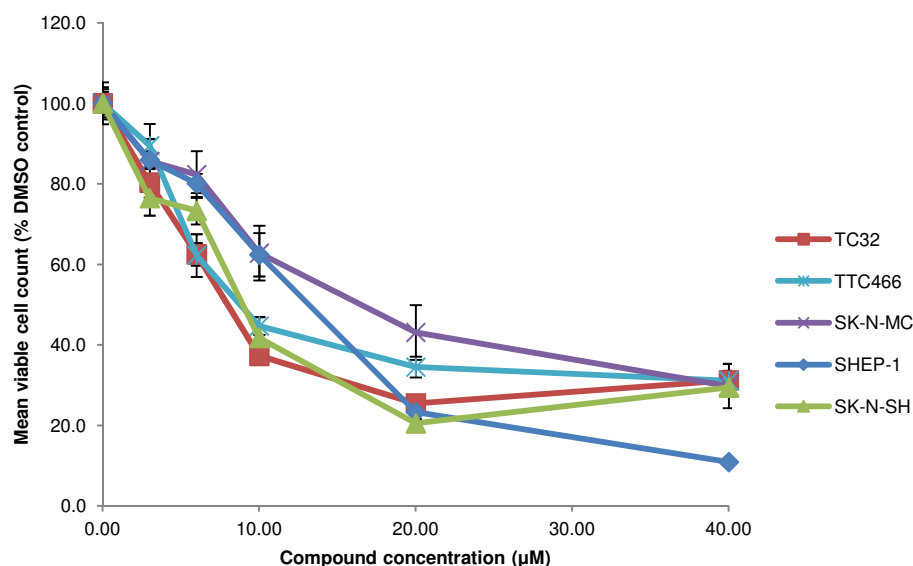


Chart 4.1 Effect of fenretinide (**1**) (3-40 μM) on ESFT (TC32, TTC466, SK-N-MC) and neuroblastoma (SHEP-1, SK-NS-H) viable cell number. Viable cell number was counted after treatment of cells for 24 hours. Results are shown as mean \pm SEM, n = 9.

4.1.2 Concentration response of compound 199

The 4-pyridyl analogue (**199**) demonstrated dose-dependent activity across all cell lines tested (*Chart 4.2*). Activity was significant compared to the DMSO control and comparable or approaching activity of fenretinide across the concentration range in SK-N-SH cells. Significant activity was observed at higher concentrations (20 and 40 μM) in SK-N-MC cell lines and activity was comparable to fenretinide at 20 μM . Activity in TC32 cells was significant at $\geq 6 \mu\text{M}$ concentrations compared to the DMSO control which was comparable to fenretinide at 6 μM ; however, activity was slightly reduced compared to fenretinide at $\geq 10 \mu\text{M}$ concentrations. TTC466 cell death was significant at 20-40 μM , but was also reduced compared to fenretinide, particularly at the lower concentrations. A considerable reduction in activity was observed in the SHEP-1 cell line; activity of compound **199** was only significant at 40 μM (63 ± 16 % cell viability) and this was markedly reduced compared to fenretinide (13 ± 2 % cell viability).

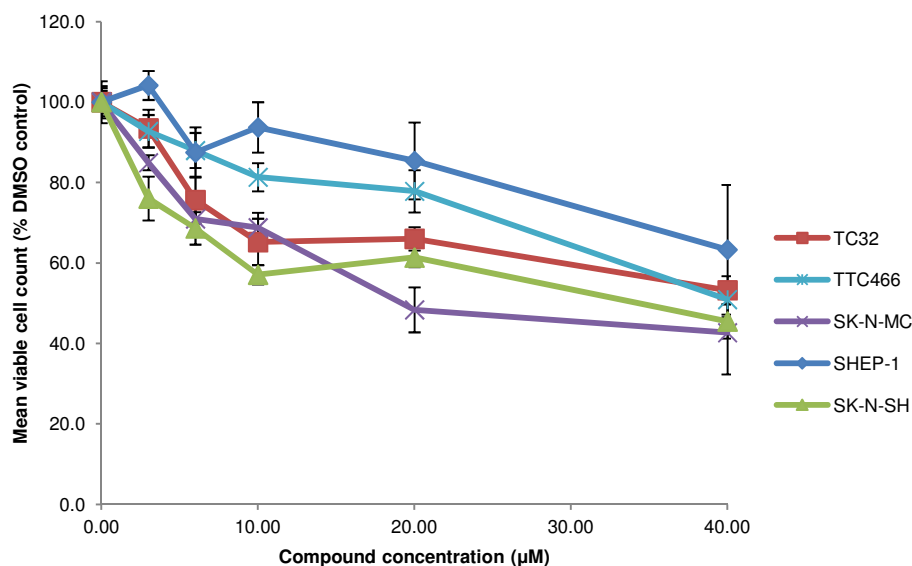


Chart 4.2 Effect of the 4-pyridyl analogue (**199**) (3-40 µM) on ESFT (TC32, TTC466, SK-N-MC) and neuroblastoma (SHEP-1, SK-N-SH) viable cell number. Viable cell number was counted after treatment of cells for 24 hours. Results are shown as mean ± SEM, n = 9.

4.1.3 Concentration response of compound 198

The *ortho*-amino substituted analogue (**198**) demonstrated activity comparable to fenretinide across the concentration range in the three EFST cell lines tested, and improved activity at 3 µM in TC32 and TTC466 cells (55 ± 3 and 68 ± 5 % cell viability) compared to fenretinide (80 ± 4 and 90 ± 5 % cell

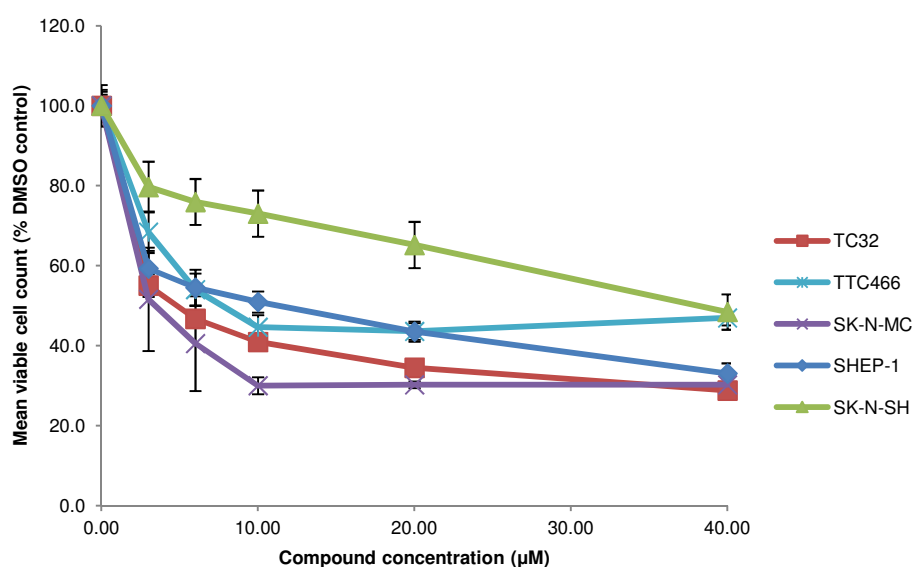


Chart 4.3 Effect of the *ortho*-amino substituted analogue (**198**) (3-40 µM) on ESFT (TC32, TTC466, SK-N-MC) and neuroblastoma (SHEP-1, SK-N-SH) viable cell number. Viable cell number was counted after treatment of cells for 24 hours. Results are shown as mean ± SEM. n = 9.

viability respectively) (*Chart 4.3*). In SHEP-1, activity was comparable to fenretinide at 10 μM but was improved compared to fenretinide at 3-6 μM . Although activity was reduced compared to fenretinide at 20 and 40 μM concentrations, good cytotoxicity was still observed (55 ± 5 and 59 ± 4 % cell viability respectively). Similarly, in SK-N-SH cells, reduced activity was observed at the higher concentrations (≥ 10 μM) but was comparable to fenretinide at 3 and 6 μM , although significant cytotoxicity was observed across the concentration range (48 ± 4 to 80 ± 6 % cell viability). Interestingly, this compound demonstrated a marked increase in activity compared to fenretinide in 3/5 of the cell lines tested (TC32, TTC466, SHEP-1) at 3 μM . Highest levels of activity induced by compound **199** were observed in the SK-N-MC cell line, closely followed by TC32, TTC466 and SHEP-1. The SK-N-SH cell line demonstrated the most resistance to this compound; however, significant activity was still observed across the concentration range.

4.1.4 Concentration response of compound 58

The *para*-amino analogue (**58**) demonstrated significant activity in all three ESFT cell lines at concentrations ≥ 10 μM and both neuroblastoma cell lines at ≥ 20 μM (*Chart 4.4*). In the ESFT cell lines, activity is approaching that of

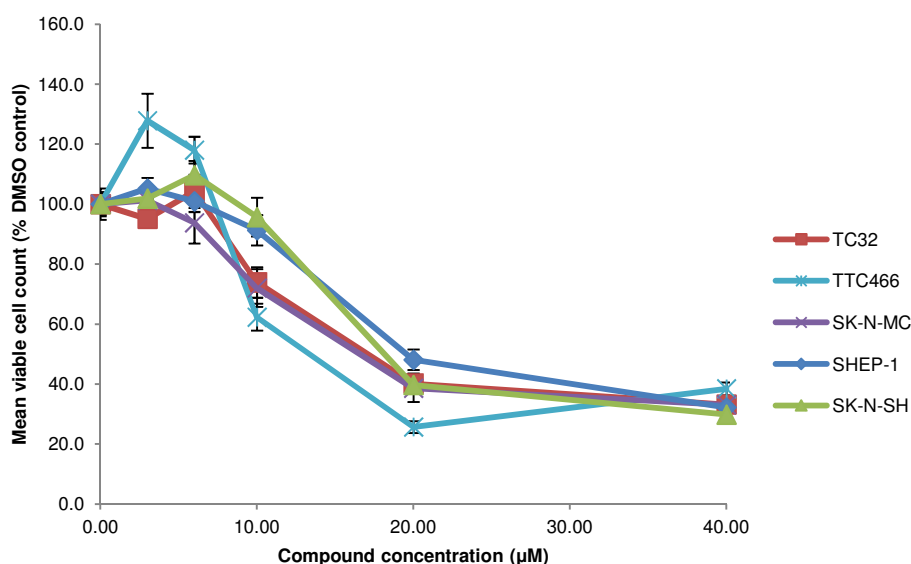


Chart 4.4 Effect of the *para*-amino analogue (**58**) (3-40 μM) on ESFT (TC32, TTC466, SK-N-MC) and neuroblastoma (SHEP-1, SK-N-SH) viable cell number. Viable cell number was counted after treatment of cells for 24 hours. Results are shown as mean \pm SEM, n = 9.

fenretinide at lower concentrations and comparable at higher concentrations. Although this compound consistently showed reduced activity to fenretinide across the concentration range in SHEP-1 cells, very good activity was still observed at 40 and 20 μM (32 ± 2 and 48 ± 3 % cell viability respectively) compared to fenretinide (11 ± 1 and 23 ± 2 % cell viability respectively). Similarly, good activity was observed in SK-N-SH cells at 20 and 40 μM (30 ± 1 and 40 ± 2 % cell viability respectively), which was comparable to fenretinide at 40 μM .

4.1.5 Concentration response of compound 298

The 4-pyridyl-containing non-retinoid compound (**298**) demonstrated significant activity in the TC32 and SK-N-SH cell lines across the concentration range, and in the TTC466, SK-N-MC and SHEP-1 cell lines at concentrations ≥ 10 μM (*Chart 4.5*). In all three ESFT cell lines and SK-N-H neuroblastoma cells, activity is comparable or approaching that of fenretinide across the concentration range. A reduction in activity compared to fenretinide was observed in the SHEP-1 cell line, particularly at higher concentrations (20 and 40 μM).

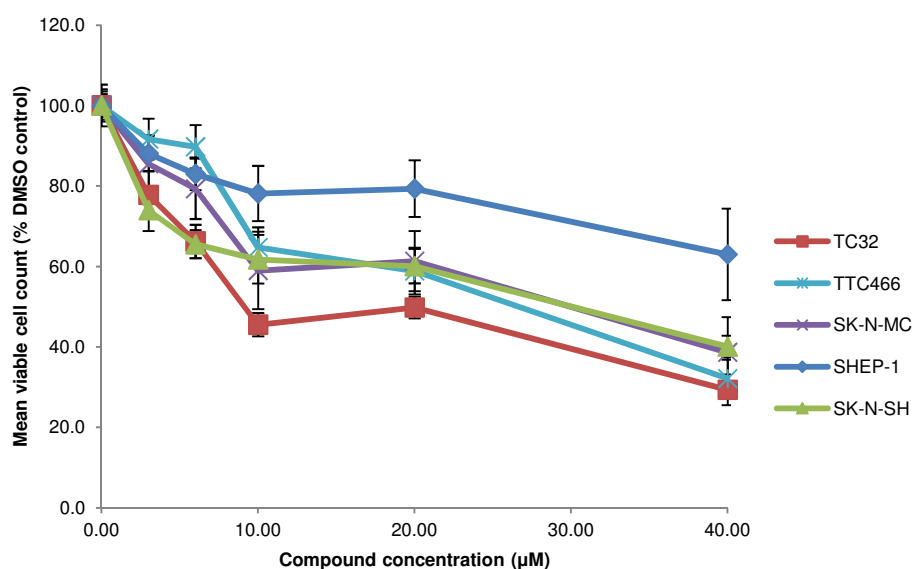


Chart 4.5 Effect of the 4-pyridyl-containing non-retinoid compound (**298**) (3-40 μM) on ESFT (TC32, TTC466, SK-N-MC) and neuroblastoma (SHEP-1, SK-N-SH) viable cell number. Viable cell number was counted after treatment of cells for 24 hours. Results are shown as mean \pm SEM, n = 9.

4.1.6 Concentration response of compound 275

The 4-hydroxyphenyl non-retinoid compound (**275**) demonstrated activity comparable to or approaching that of fenretinide in TC32 and SK-N-SH cell lines across the concentration range, which was significant at concentrations $\geq 6 \mu\text{M}$ (Chart 4.6). However, the compound was dramatically less active in the other four cell lines tested. At 10 μM in SHEP-1 cells, activity was comparable to fenretinide but a reduction in activity was observed at higher concentrations (possibly due to precipitation of the compound). Activity was significant at $\geq 20 \mu\text{M}$ in TTC466 cells; however, observed activity was markedly reduced compared to fenretinide. Interestingly, this compound did not induce cytotoxicity across the concentration range in SK-N-MC cells.

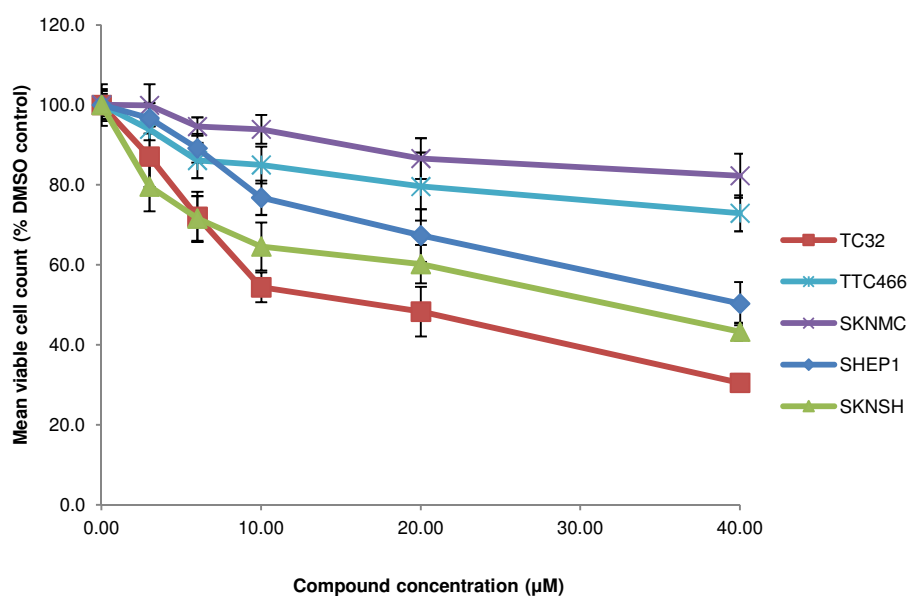
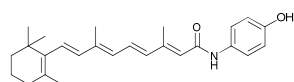


Chart 4.6 Effect of the 4-hydroxy-containing non-retinoid compound (**275**) (3-40 μM) on ESFT (TC32, TTC466, SK-N-MC) and neuroblastoma (SHEP-1, SK-N-SH) viable cell number. Viable cell number was counted after treatment of cells for 24 hours. Results are shown as mean \pm SEM, n = 9.

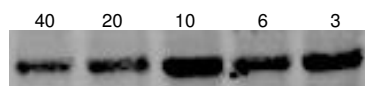
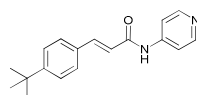
4.2 Caspase-3 activation

Caspase-3 is known to be activated by fenretinide, as well as other retinoids,^{172,173} and is an important effector of fenretinide-induced cell death in many cancer types including ESFT cells.⁶⁷ In order to determine whether the hit compounds identified in this study induce caspase-3 cleavage, TC32 cells were treated for 24 h with the five hit compounds (**58**, **198**, **199**, **275** and **298**). SDS-PAGE and western blot analysis were used to assess cleavage (activation) of caspase-3 from full length (35 kDa) to cleaved products (17 and 19 kDa) following treatment with the selected compounds. As expected, cleavage of caspase-3 by fenretinide was observed, with an increasing amount of cleaved product and decreasing amount of full length caspase-3 observed with increasing concentration of fenretinide (*Figure 4.2*). The same pattern of caspase-3 cleavage was observed for the *para*-amino isostere (**58**) and the *ortho*-amino substituted analogue (**198**) of fenretinide. This suggests that these compounds are effecting cell death through caspase-3 cleavage, which may be induced through the same programmed cell death signalling pathway as fenretinide. Interestingly, both of the non-retinoid-based compounds (**275** and **298**) and the 4-pyridyl fenretinide analogue (**199**) did not activate caspase-3. This was rather surprising as caspase-3 cleavage is a common effector of programmed cell death through apoptosis or autophagy; this suggests that these compounds may be killing cells through alternative non physiological mechanisms and requires further investigation. Two of the compounds that are unable to activate the caspase-3 cleavage mechanism (compounds **199** and **298**), bear a 4-pyridyl moiety in place of the *para*-hydroxyphenyl group. This might suggest that the *para*-hydroxy/amino group is important for initiating programmed cell death by interacting with a protein target facilitated through an OH/NH₂-mediated hydrogen bond interaction or by generation of reactive oxygen species mediated by the presence of the OH/NH₂ group. Proteins were not detected in cells treated with 40 μM of compounds **58** or **198**, which may reflect the low yield and poor quality of protein extracted due to high levels of toxicity at these concentrations.

A. Fenretinide



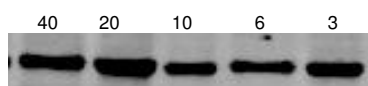
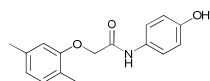
B. Compound 298



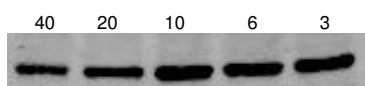
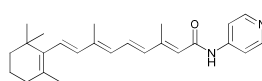
μM
tubulin (50 kDa)

full length caspase-3 (35 kDa)
caspase-3 cleavage products
(19, 17 kDa)

C. Compound 275



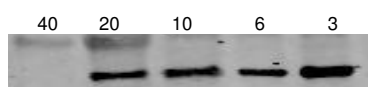
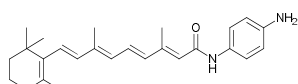
D. Compound 199



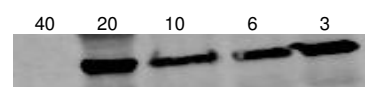
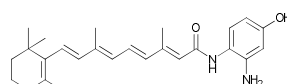
μM
tubulin (50 kDa)

full length caspase-3 (35 kDa)
caspase-3 cleavage products
(19, 17 kDa)

E. Compound 58



F. Compound 198



μM
tubulin (50 kDa)

full length caspase-3 (35 kDa)
caspase-3 cleavage products
(19, 17 kDa)

Figure 4.2 Western blot analysis of caspase-3 activation in TC32 cells after 24 h treatment with **A.** Fenretinide, **B.** Compound 298, **C.** Compound 275, **D.** Compound 199, **E.** Compound 58 and **F.** Compound 198 over a concentration range (3-40 μM). Tubulin was probed as a loading control. Compounds were labelled with Alexa fluorphore 680 and visualised using a LI-CORE Odyssey CLx Infrared Imaging System. These data are representative of two independent experiments.

4.3 Generation of ROS

Fenretinide is known to produce ROS in a dose-dependent manner in ESFT cells; this is thought to be a major factor in induction of cell death in the TC32 cell line.⁶⁷ In order to determine whether ROS are produced by the five selected compounds (**58**, **198**, **199**, **275** and **298**), TC32 cells were treated with each compound and fenretinide (the control) at a concentration of 3-40 μM for 30 minutes. ROS accumulation in cells, fluorescently labelled with a molecular probe, was detected by flow cytometry (see Chapter 8). ROS accumulation was measured at 30 minutes, as a prior time course study (between 15 to 60 minutes) had identified optimum levels of ROS accumulation after 30 minutes of exposure to fenretinide (*Chart 4.7*).

Consistent with previous data, fenretinide induced a concentration-dependent increase in ROS (*Chart 4.8*). However, there was a drop in ROS levels when cells were exposed to 40 μM of fenretinide; this may reflect the increased amount of cell death that was observed after 30 minutes exposure to fenretinide at this concentration. At this high concentration, fenretinide appeared to be toxic to the cells and consequently the dye (DCFDA) might be leaking from cells that were not intact, therefore leading to a false decrease in ROS levels.

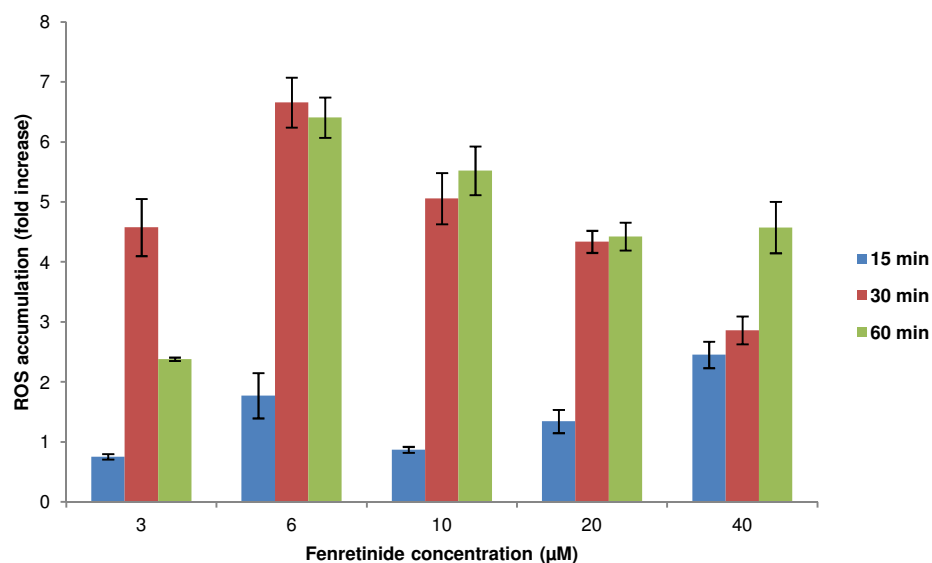


Chart 4.7 ROS levels upon treatment of TC32 cells with fenretinide (3-40 μM) at 15, 30 and 60 minute timepoints (n = 3).

None of the test compounds produced ROS across the concentration range of 3-40 μM (Chart 4.8).

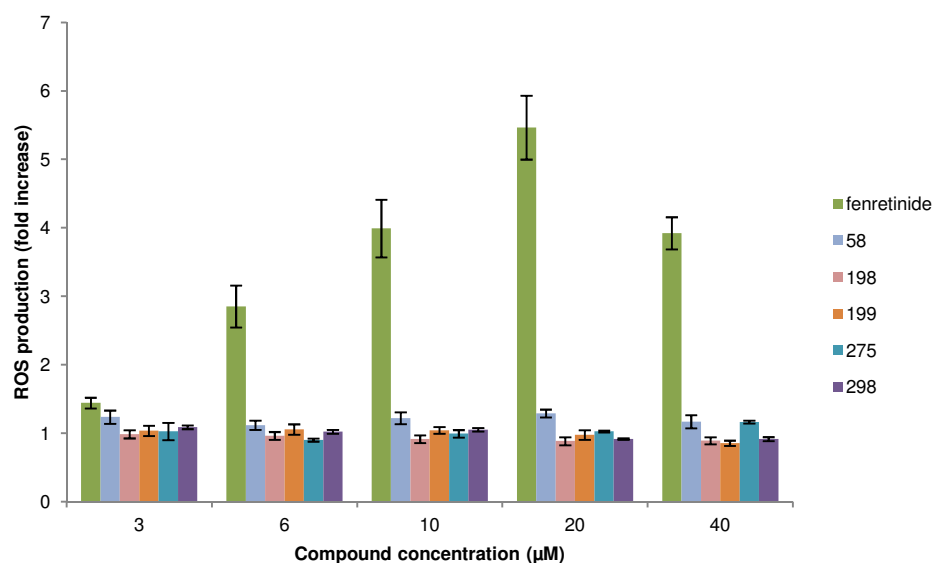


Chart 4.8 A graph to show ROS accumulation in TC32 cells after 30 min treatment with fenretinide, three retinoids (**58**, **198** and **199**) and two non-retinoids (**275** and **298**) ($n = 9$).

4.4 ADME properties

To investigate whether any of the compounds have physicochemical and pharmacokinetic properties consistent with a good hit compound, three hits (**58**, **198** and **275**) plus fenretinide (**1**) and 4-oxo-fenretinide (**3**) as controls were selected for ADME testing, carried out by Cyprotex.¹⁷⁴ The potential for improved aqueous solubility, metabolic stability and intestinal permeability was quantified (Table 4.2). All of the retinoid-based structures (**1**, **3**, **58** and **198**) demonstrate quite poor aqueous solubility under the conditions tested ($\leq 6 \mu\text{M}$), as would be predicted based on the high hydrophobicity for these compounds. In contrast, the aqueous solubility for the non-retinoid compound was high ($80 \mu\text{M}$), presumably owing to the reduced hydrophobicity of this compound. The metabolic stability for both retinoids and non-retinoids in mouse and human liver microsomes is relatively high, indicating that the compounds are quite stable to phase 1 metabolism. Passive diffusion of the compounds was tested using the Caco-2 cell monolayer simulated intestinal permeability assay. The apparent

permeability coefficient (P_{app}) for the retinoids was 0 (*i.e.* none of the compound diffused across the cell monolayer from the donor well to receiver well). For fenretinide and the 4-amiophenyl (**58**), 69 % and 42 % of the compound was recovered from the donor well, respectively, indicating that these lipophilic compounds accumulate in the lipid bilayer of the Caco-2 cells. This correlates with the poor permeability of fenretinide in Caco-2 cells observed by others⁴⁴ and supports our hypothesis that entry of fenretinide into the cancer cells is facilitated by a cell surface receptor (*e.g.* STRA6, currently under investigation within our group). In contrast, the non-retinoid compound (**275**) is more permeable (P_{app} 0.81×10^{-6} cm s^{-1}). In all, the data suggests that the generation of non-retinoid mimetics might offer a more attractive scaffold for the generation of drug candidates, owing to a significantly improved solubility and permeability, whilst maintaining the robust metabolic stability of the compounds.

Compound	Estimated precipitation (μM)	t1/2 (min) (mouse/human)	Mean Papp (10^{-6} cm s^{-1}) \pm SD	Mean Recovery from donor well (%)
1 (fenretinide)	3.75	62/49	0	69
3 (4-oxo-fenretinide)	<5	ND/5	ND	ND
58	2	78/68	0	42
198	6	69/ND	0	ND
275	80	120/ND	0.81 ± 0.20	ND

Table 4.2 ADME data quantified for 3 selected hit compounds (**58**, **198** and **275**), alongside fenretinide (**1**) and 4-oxo-fenretinide (**3**) controls. (ND = not determined.)

4.5 Conclusion

The *ortho*-amino substituted analogue (**198**) demonstrated very interesting activity in the concentration response studies. Not only did this compound induce similar levels of activity to fenretinide in all of the ESFT and neuroblastoma cell lines, activity was significantly increased compared to fenretinide at the lowest concentration (3 μM) in three out of the five cell lines (TC32, TTC466 and SHEP-1).

The 4-pyridyl analogue (**199**) demonstrated dose-dependent activity across all cell lines tested. However, this was often reduced compared to fenretinide, particularly in the SHEP-1 and TTC466 cell lines. Activity of this compound was comparable or approaching that of fenretinide in TC32, SK-N-MC and SK-N-SH cell lines, particularly at the lower concentrations.

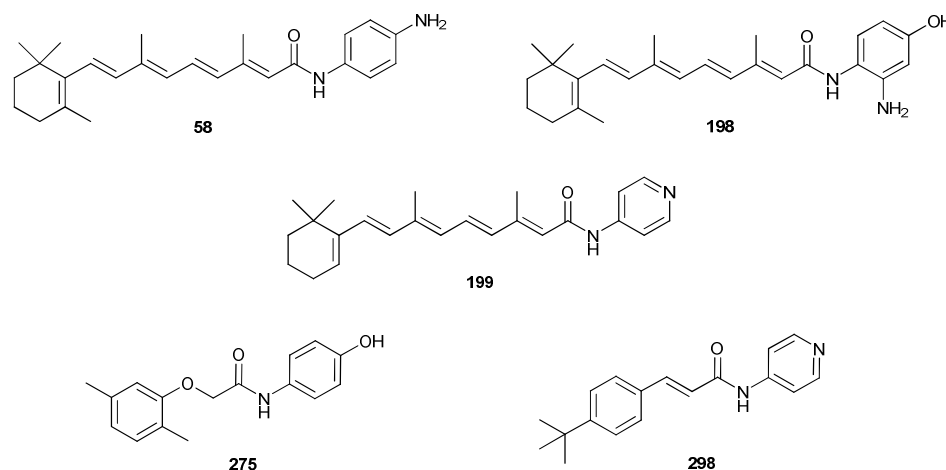
The *para*-amino analogue (**58**) demonstrated significant dose-dependent activity in all cell lines tested. Activity in ESFT cells was comparable to fenretinide at higher concentrations and approaching that of fenretinide at lower concentrations. Likewise, good activity was observed against neuroblastoma cell lines at higher concentrations and activity was comparable to fenretinide in SK-N-SH cells. Although this compound consistently showed reduced activity to fenretinide across the concentration range in SHEP-1 cells, very good activity was still observed at the higher concentrations.

Of the non-retinoid compounds tested, the 4-pyridyl compound (**298**) demonstrated activity comparable to or approaching that of fenretinide in the TC32 and SK-N-SH cell lines across the concentration range, and in the TTC466, SK-N-MC and SHEP-1 cell lines at concentrations $\geq 10 \mu\text{M}$. The 4-hydroxyphenyl non-retinoid compound (**275**) also demonstrated activity comparable to or approaching that of fenretinide in TC32 and SK-N-SH cell lines across the concentration range. However, the compound was dramatically less active in the other four cell lines tested. At $10 \mu\text{M}$ in SHEP-1 cells, activity was comparable to fenretinide but a reduction in activity was observed at higher concentrations (possibly due to precipitation of the compound). Activity in TTC466 cells was markedly reduced compared to fenretinide and the compound did not induce cytotoxicity across the concentration range in SK-N-MC cells. Since SK-N-MC and TTC466 cell lines differ from the others by deletion and missense mutation of p53 respectively, this could indicate that this compound acts *via* a p53-dependent mechanism.

Consistent with published studies, fenretinide increased ROS and induced cleavage of caspase-3 in ESFT cells that correlated with a decrease in viable cell number.

Due to lack of ROS production (for all synthetic compounds) and caspase-3 activation (for the 4-pyridyl retinoid (**199**) and non-retinoid analogues (**275** and **298**), it is possible that these compounds induce cell death *via* an alternative mechanism to fenretinide (*Table 4.3*). Alternatively, this could indicate that ROS production and/or caspase-3 activation is not essential for activation of the cell death pathway. However, caspase-3 cleavage would be

expected if the compound induces programmed cell death. It could be that the time course of caspase-3 cleavage varies between the different compounds. Alternatively, compounds could be acting through nonphysiological pathways to kill the cell. *e.g.* necrosis. Similarly, ROS may be elevated at different time courses; however, this is less likely to be the case as there are many opportunities to initiate programmed cell death through ROS independent pathways. The cell death pathway could be activated *via* multiple mechanisms, for example, mitochondrial membrane depolarisation,¹⁷⁵ increase in intracellular calcium concentration¹⁷⁶ or *via* the caspase-independent apoptosis inducing factor which is a flavoprotein that initiates apoptosis by inducing DNA fragmentation and chromatin condensation.¹⁷⁷



Compound	ROS elevation	Caspase-3 cleavage
1 (fenretinide)	+	+
58	-	+
198	-	+
199	-	-
275	-	-
298	-	-

Table 4.3 A summary table of observed ROS elevation and caspase-3 cleavage.

The physicochemical and *in vitro* pharmacokinetic properties of the non-retinoid analogue (**275**) demonstrated a markedly improved simulated intestinal permeability and solubility as well as low phase 1 metabolism liability. This suggests that the generation of non-retinoid mimetics might offer a more attractive scaffold for new chemotherapeutic agents, with improved pharmaceutical properties compared to retinoids.

5. Target identification by affinity chromatography

Isolation of binding-proteins using affinity chromatography is an attractive method for discerning the protein binding partners of ligands (as discussed in Chapter 1, Section 1.1). The technique relies on specific binding interactions between a known inhibitor, which is covalently immobilised on a solid resin (*e.g.* Sepharose), and the target protein within cell lysates.

This chapter describes the design and synthesis of suitable ligands and negative controls, their immobilisation onto a solid supported medium, and their application in a pull-down assay to identify binding partners to fenretinide.

5.1 Design of Sepharose-supported ligands for affinity chromatography

For affinity chromatography, the biologically active ligand is covalently immobilised on a solid resin through a linker. The siting of the linker on the active ligand is a crucial concern such that the biological activity of the ligand is maintained, *i.e.* so that incorporation of the linker does not adversely affect the biological activity of the ligand. Identification of an appropriate attachment point for a linker moiety on to the ligand is often the primary limitation of affinity chromatography, requiring extensive SAR studies. Synthetically, there are two amenable sites of attachment of a linker on the fenretinide structure, one at each of the two termini of the ligand; the phenyl and cyclohexyl rings (*Figure 5.1*). The SAR studies in Chapter 2 showed that substitution of the phenyl ring invariably results in loss or reduction of activity of the ligand.

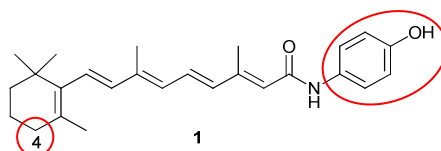


Figure 5.1 Synthetically accessible sites for attachment of a linker on the fenretinide structure for affinity chromatography studies.

Hence, this would suggest that this region of the molecule may interact directly with a macromolecular target responsible for the observed biological activity and therefore may not be a suitable site for incorporation of a linker for affinity chromatography studies. In contrast, substitution at the 4-position, of the cyclohexene ring is tolerated, at least for certain oximes (See Chapter 2). Therefore it is possible that the 4-position of the cyclohexyl ring could be a suitable site for incorporation of a linker, as substitution at this site may not adversely compromise the binding activity of the ligand. As such, the affinity chromatography ligands proposed for synthesis were planned with linkers extending from the 4-position of the cyclohexyl ring. Two ligands which were expected to be inactive *in vitro* were also synthesised as negative controls which, in addition to uncoupled Sepharose beads, were used to eliminate any proteins which bound non specifically to the column or a column plus linker that had no activity.

5.2 Synthesis and biological affirmation of solid supported ligands for affinity chromatography

This section describes the design and synthesis of two solid supported ligands for affinity chromatography. The section also describes the biological affirmation of the ligands prior to incorporation of the affinity support (to act as a control validating the biological activity of the affinity supported ligand).

5.2.1 Design of solid supported ligands

Two solid-supported ligands predicted to have *in vitro* activity based on SAR studies were designed, utilising two different linker groups, one based on an amino oxime (**352**), the other on an amino acylhydrazone (**353**) (*Figure 5.2*). These ligands were chosen for synthesis to satisfy that, a) they should be readily synthesisable from a common intermediate, 4-oxo-fenretinide (**3**), based on a simple condensation chemistry, and b) the location of the linker or affinity support accommodated at this position should not interfere with binding to the biological target based on historical SAR for substitution at this site (Chapter 2). Two structurally distinct linkers were chosen for synthesis in an attempt to negate any non-specific binding due to the presence of groups within the linker moiety.

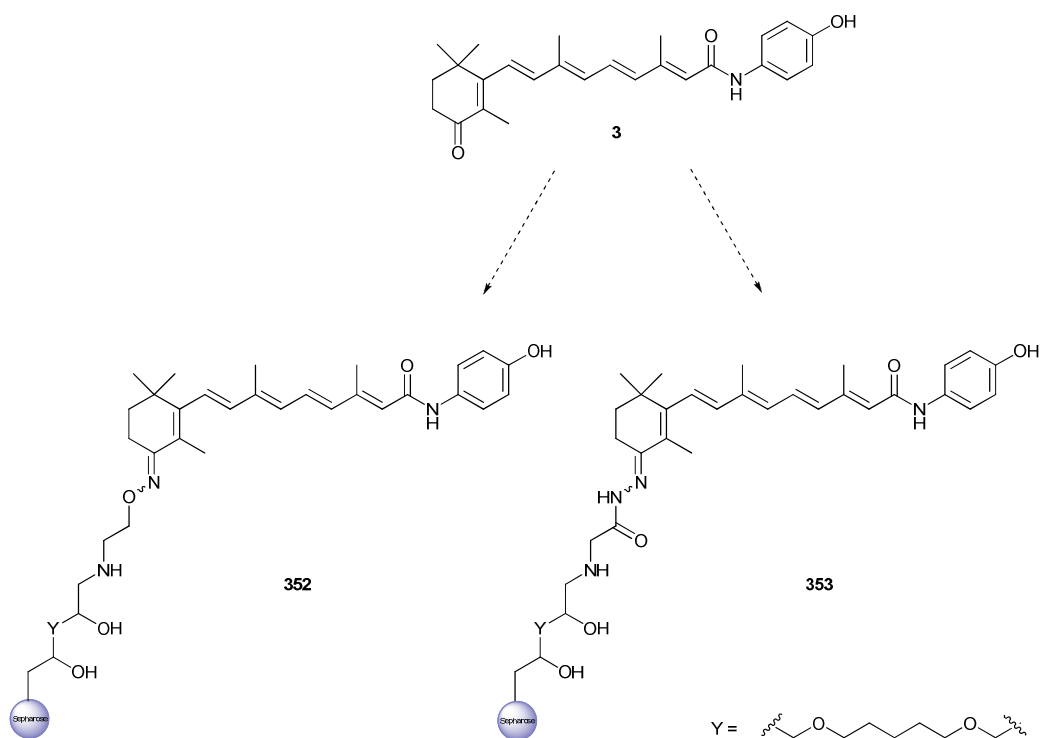
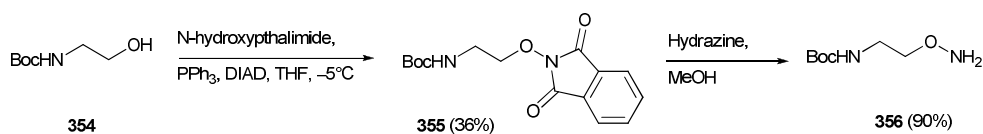


Figure 5.2 Two solid-supported ligands for affinity chromatography proposed for synthesis from 4-oxo-fenretinide.

5.2.2 Synthesis of the oxime linked solid supported ligand (352)

The key intermediate, hydroxylamine (**356**), was synthesised in a two step process from N-Boc-ethanolamine (**354**) (*Scheme 5.1*). The pthalimide (**355**) was generated from the alcohol (**354**) using a Mitsunobu reaction from *N*-hydroxyphthalimide, PPh₃ and DIAD in moderate yield. Deprotection of the pthalimide (**355**) with hydrazine then generated the amine (**356**) in excellent yield following purification by silica column chromatography and recrystallisation (*Scheme 5.1*).

Coupling of the hydroxylamine (**356**) to 4-oxo-fenretinide (**3**) (previously synthesised in Chapter 2, Scheme 2.28) was firstly attempted by adaptation



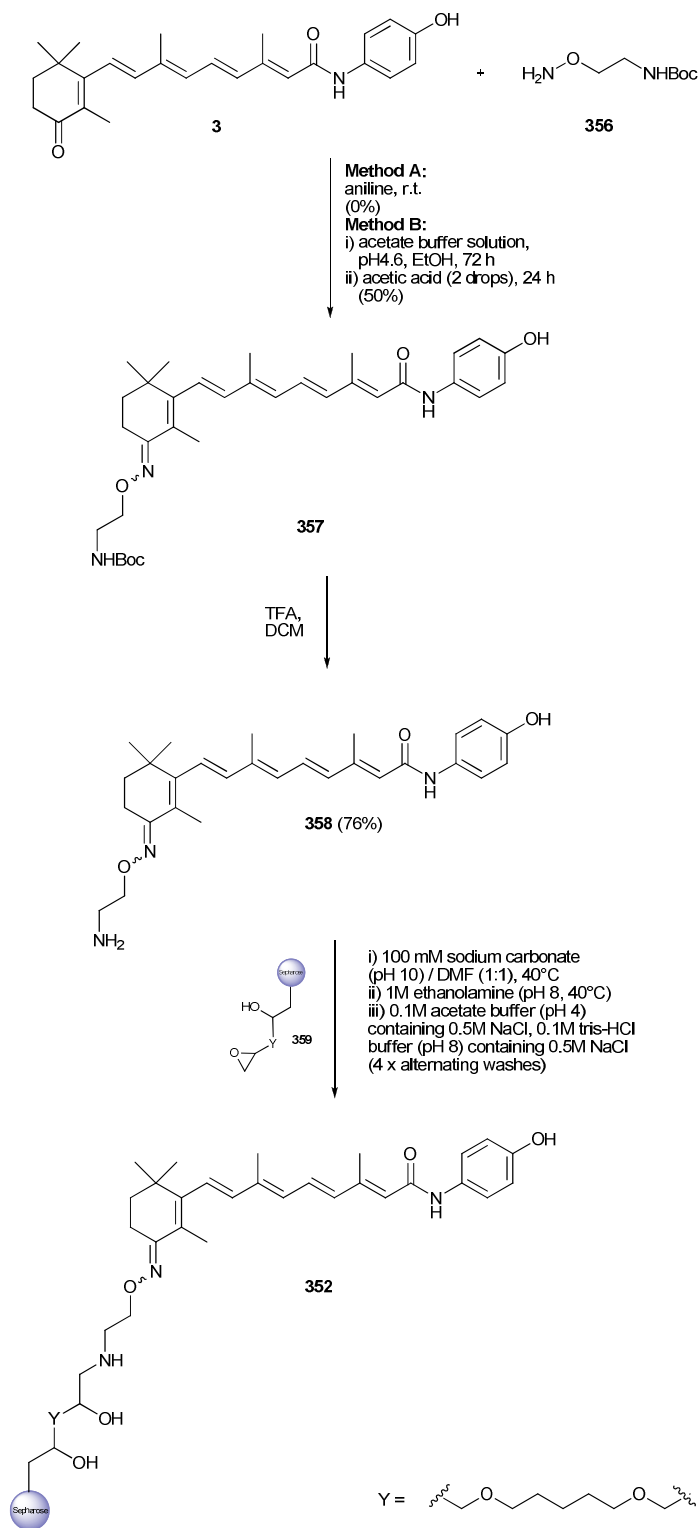
Scheme 5.1 Synthesis of the hydroxylamine linker as a precursor for the affinity chromatography ligand (**352**).

of a method for the synthesis of oximes under non acidic conditions reported by Dirksen *et al.* (*Scheme 5.2, Method A*).¹⁷⁸ The synthesis of oximes by condensation of a hydroxylamine and a carbonyl group under non-acidic conditions is known to be quite slow.¹⁷⁹ However, Dirksen *et al.* showed that aniline can act as an effective nucleophilic transamination catalyst which forces the equilibrium towards oxime formation.¹⁷⁸ Upon application of these conditions to our reaction, this generated only trace quantities of the desired oxime (**357**) together with a large quantity of unreacted starting material observed by LCMS after 48 h at room temperature.

No attempt was made to force this reaction to completion. Instead, an alternative method for formation of the desired oxime was attempted by use of weak acid catalysis (*Scheme 5.2, Method B*).¹⁸⁰ Here, an acetate buffer solution of pH 4.6 was prepared and added to a mixture of compounds **3** and **356** at room temperature. This generated a 2:1 mixture of the desired product (**357**) plus remaining starting material (**3**) after 72 h. Addition of a further quantity of acetic acid and stirring for a further 24 h forced the reaction to completion giving the oxime (**357**), with no evidence of deprotection of the Boc group, in reasonable yield (50 %) after purification. The product exists as a single isomer; however, nOe experiments to identify this were inconclusive.

Compound **357** was then deprotected using TFA and the resulting free amine (**358**) obtained in good yield (76 %) after trituration with Et₂O. Notably, it appeared that deprotection of protected amine (**357**) had resulted in isomerisation of the hydrazone to yield an approximately 1:1 *E:Z* ratio by ¹H NMR. *E,Z* isomerisation of oximes by acid catalysis has previously been described by others.¹⁸¹

Compound **358** was then coupled to epoxy-activated Sepharose beads (**359**) under weakly basic conditions. Epoxy-activated Sepharose is a pre-activated medium for immobilization of a range of ligand types bearing hydroxyl, amino or thiol groups which can be readily coupled to the epoxide. This medium has a long hydrophilic spacer arm, making it particularly suitable for immobilization of small molecules.¹⁸² Following incubation overnight, any remaining active epoxy groups were blocked using ethanolamine and the



Scheme 5.2 Synthesis of an oxime-linked solid supported affinity chromatography ligand.

resin was washed with alternating pH cycles (pH 4 and 8) to remove any unbound molecules. In order to confirm that the ligand had been successfully immobilised on to the support, LCMS was used to compare the relative

extinction coefficient for the non-immobilised ligand (**358**) on the loading and eluted solution, respectively, with reference to an internal standard (an uncharacterisable minor impurity of mass 476.3, RT *ca.*2.30 min remaining in the sample following deprotection, which was not detected by ^1H NMR) (*Figure 5.3*). It was noted that the absorbance for the ligand (**358**) (RT *ca.*1.65 min) was reduced by 1 order of magnitude relative to the internal standard (RT *ca.*2.30 min). Thus, it was reasoned that a considerable amount of the ligand was successfully immobilised on the resin. Analysis of the condensed elution fraction by ^1H NMR also confirmed the presence of little or no recovered ligand, supporting the conclusion that a significant quantity of the ligand had been bound to the solid support.

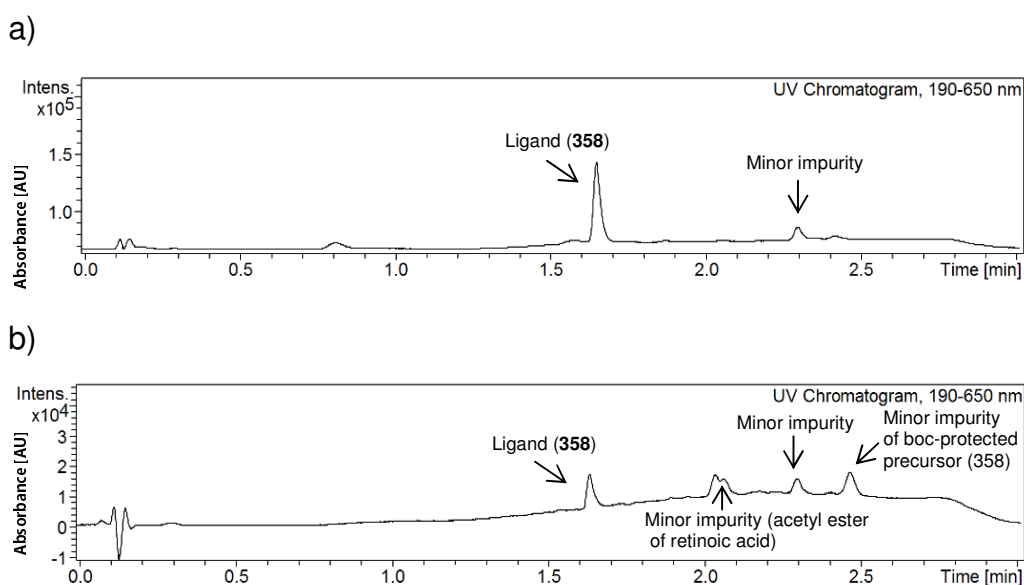


Figure 5.3 LCMS analysis of affinity chromatography ligand present in **a)** loading solution and **b)** eluted solution.

5.2.3 Affirming biological activity of the oxime linked ligand

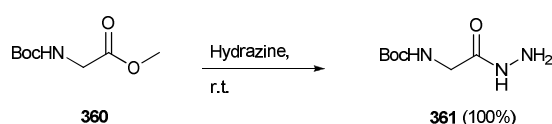
To confirm the biological activity of the oxime-linked ligand (**358**), the compound was screened at 10 μM over 24 h in the TC32 cell viability assay, as described previously (see page 51). Encouragingly, compound **358** displayed statistically significant activity (72 ± 2 % cell viability), although the activity was reduced in comparison to the fenretinide control (38 ± 2 % cell viability) in this experiment. The observed reduction in activity may be due to the presence of the polar NH_2 moiety which will reduce the concentration of

compound available to permeate the cell membrane. To support the affirmation of the biological activity of the oxime ligand, the Boc-protected precursor (**357**) was also screened. This compound displayed a similar level of activity (78 ± 2 % cell viability) as for the deprotected compound. Although the activity for both the protected and non-protected compounds was reduced in comparison to fenretinide, the demonstration of a statistically significant cell death response for the compounds suggests that incorporation of a narrow, extended polar linker at the 4-position of the cyclohexyl ring is tolerated and does not appreciably eliminate binding.

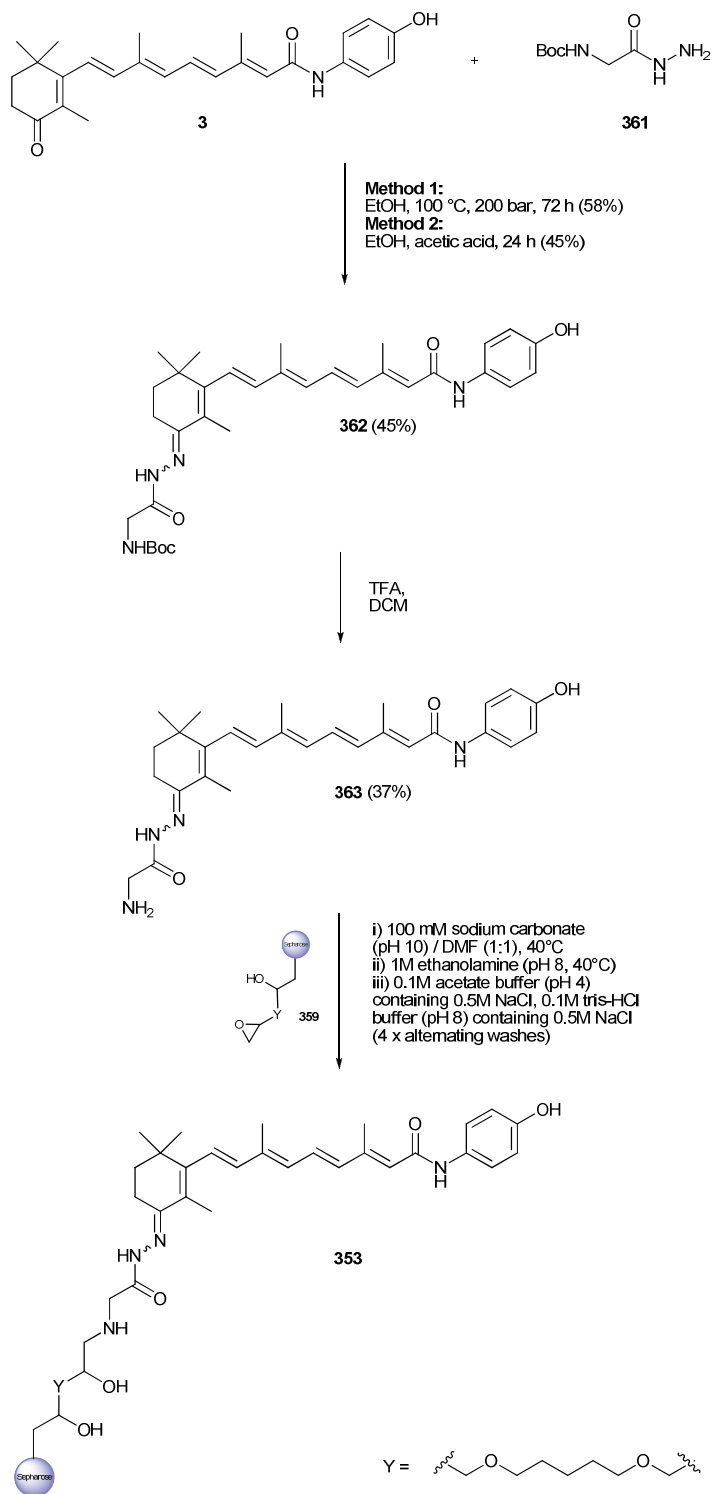
5.2.4 Synthesis of the acyl-hydrazone linkered solid supported ligand

The acyl-hydrazone linked solid supported ligand (**353**) was synthesised in four steps from 4-oxo-fenretinide (**3**) and the methyl ester, **361**. The acylhydrazine (**361**) was synthesised in quantitative yield by substitution of the methyl ester (**360**) with hydrazine at room temperature (*Scheme 5.3*). Condensation of acylhydrazine (**361**) with 4-oxo-fenretinide (**3**) under microwave conditions (100 °C at 200 bar) (*Method 1*) yielded the acylhydrazone (**362**) in moderate yield as a single isomer. This reaction was very slow, requiring 72 h heating in order for the reaction to go to completion. No nOe studies were carried out to confirm the stereochemistry of the single isomer.

In an attempt to improve the efficiency of the reaction, the hydrazone (**362**) was also synthesised using the acid catalysed method deployed for the oxime formation (*Method 2, Scheme 5.4*). Using this method the hydrazone (**362**) was generated in a lower yield than for the microwave approach (45 % vs 58 %) but the reaction was complete in a much shorter period of time (24 h vs 72 h).



Scheme 5.3 Synthesis of the acylhydrazine linker moiety.



Scheme 5.4 Synthesis of an acyl-hydrazone linked solid supported ligand.

The Boc-group of compound **362** was then removed using TFA and the resulting free amine (**363**) was obtained in modest yield (37 %) after

purification by HPLC. Interestingly, unlike compound 4 which was obtained as a single isomer, compound **363** was generated as an inseparable mixture of two isomers (assumed to be the *E/Z* isomers) as observed by ¹H NMR. Owing to the complexity of the NMR (also evidence for amide rotation/rotamers) no attempt was made to confirm the ratio of *E*- and *Z*-isomer present in the sample.

Compound **363** was then coupled to epoxy activated Sepharose beads (**359**) using the method described previously (see page 137) (*Scheme 5.4*).

5.2.5 Affirming biological activity of the acyl-hydrazone linked solid supported ligand 353

Both the Boc-protected amine (**362**) and the amine (**363**) were assessed for their ability to induce cell death in the TC32 cell viability assay using the method as previously described, (see page 51). Encouragingly, the Boc-protected amine (**362**) showed a similar level of activity (40 ± 2 % cell viability) to fenretinide (38 ± 2 % cell viability) *in vitro*. However, the deprotected amine (**363**) was inactive (109 ± 6 % cell viability). The apparent inactivity of compound **363** may be attributed to the presence of the polar primary amine group, which might limit the amount of compound able to permeate through the cell membrane and reach the intracellular target.

5.3 Negative controls

A negative control is required for the affinity chromatography experiment to eliminate non-specific binding to the column. Two Sepharose supported ligands were designed for this purpose. The SAR work in Chapter 1 suggested that the biological activity of variants at the phenyl ring-side of fenretinide is quite sensitive to synthetic modification. Hence, it seemed sensible to base the negative control ligands from within the pool of 'inactive' ligands identified during the SAR section of the project, which principally focussed on modifications to this portion of the molecule. Of the inactive ligands identified, the methoxy (**24**) and benzylamine (**184**) analogues were selected as ligands from which to base the negative controls as they showed no statistically significant activity in the cell viability assay (93 ± 2 % and 99 ± 10 % cell viability, respectively). Furthermore, the methoxy analogue (**24**)

has previously been found to be incapable of inducing RAR-dependent activity in F9 murine embryonal carcinoma cells (discussed in Section 1.10.1). Equally, these ligands would allow for synthetic accessibility to the proposed affinity supported ligand. Using the methoxy (**24**) and benzylamine (**184**) analogues as starting points, affinity chromatography supported ligands were designed such that the linker to the solid support extended from the fenretinide structure from one of two termini of the molecule, *i.e.* to generate one solid supported ligand from the phenyl, and one supported ligand from cyclohexyl ring side of the molecule (*Figure 5.4*). Specifically, the benzylamine affinity ligand (**364**) was designed with the linker extending from the amine (so from the phenyl ring side of the molecule). In contrast, the methoxy variant (**366**) was planned to extend with a linker from the cyclohexyl ring. The methoxy variant (**366**) should behave as a direct negative control of the oxime-linked ligand (**352**) as the substitution of the *para*-hydroxy group with *para*-methoxy has previously been confirmed to be detrimental to activity for fenretinide (Chapter 2, Section 2.2.3). If the lack of

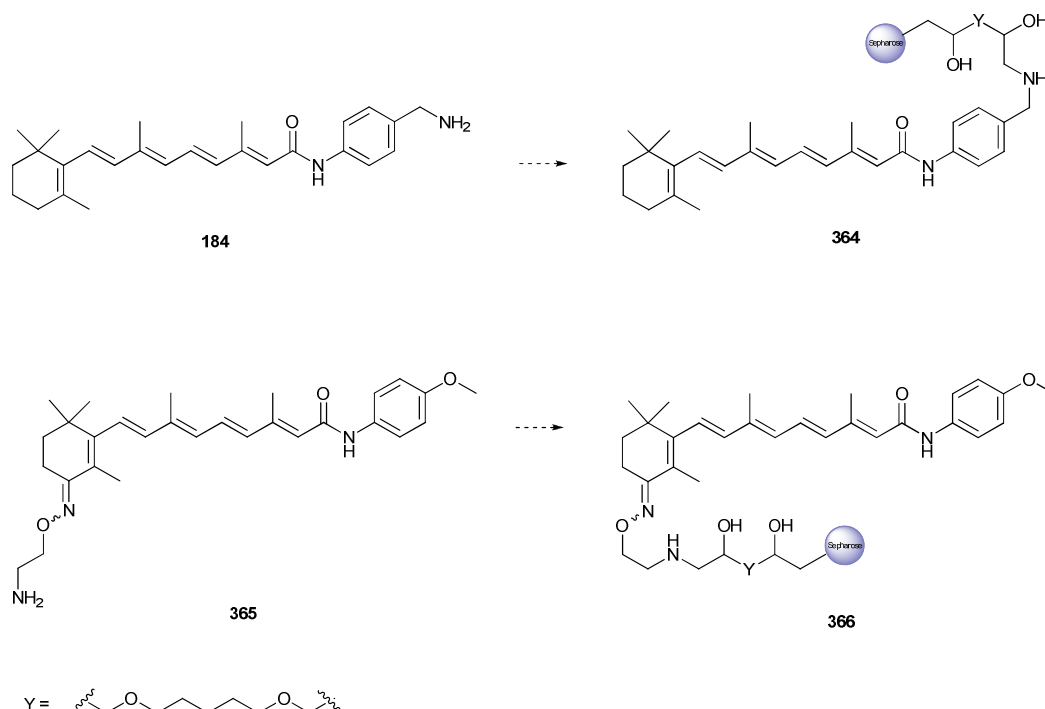


Figure 5.4 Structures of proposed negative control ligands for affinity chromatography.

activity for methoxy substitution is a result of disruption of binding to the target protein(s) through which cell death is initiated, the proposed OMe affinity supported ligand should not identify these proteins. However, the possibility that the reduction of activity for this compound reflects disruption of a downstream pathway involved in the execution of fenretinide-induced cell death rather than its initiation cannot be excluded.

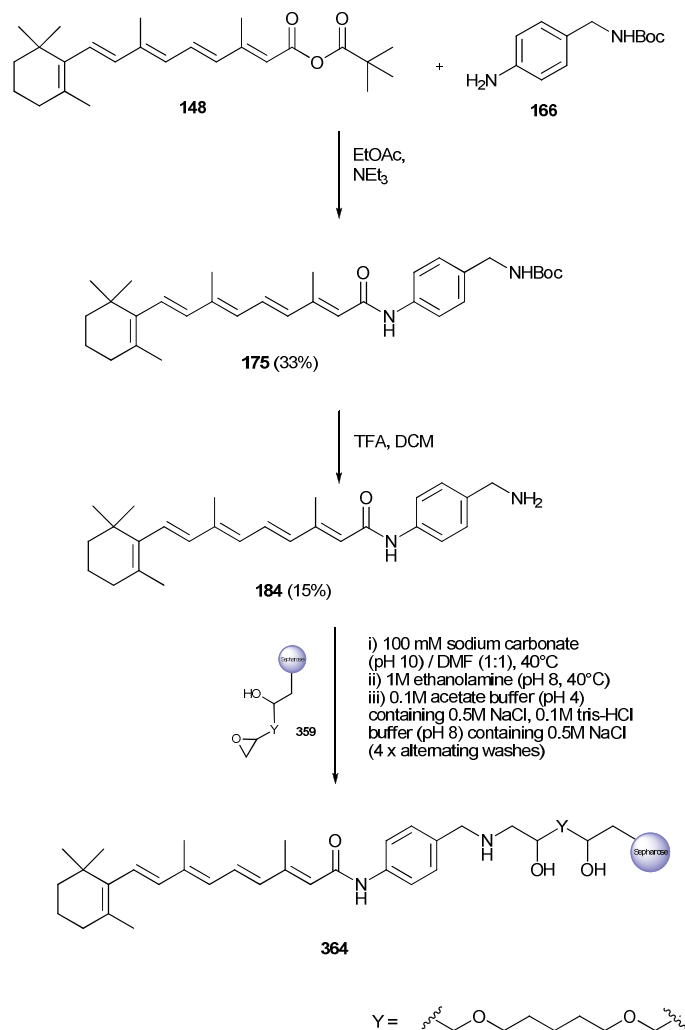
5.3.1 Synthesis of the benzylamine linkered solid supported ligand (364)

The pre-solid supported ligand for affinity ligand **364** – amine **184** – was synthesised by coupling of the Boc-protected aniline (**166**) to the mixed anhydride (**148**) in modest yield after purification (*Scheme 5.5*). The Boc-group of compound **175** was removed using TFA and the resulting free amine (**184**) was obtained in excellent yield without need for further purification.

Amine **184** was then coupled to epoxy-activated Sepharose beads (**359**) to generate the benzylamine supported ligand (**364**) using the method as described previously (see page 137).

5.3.2 Affirmation of absence of biological activity of the benzylamine solid supported ligand

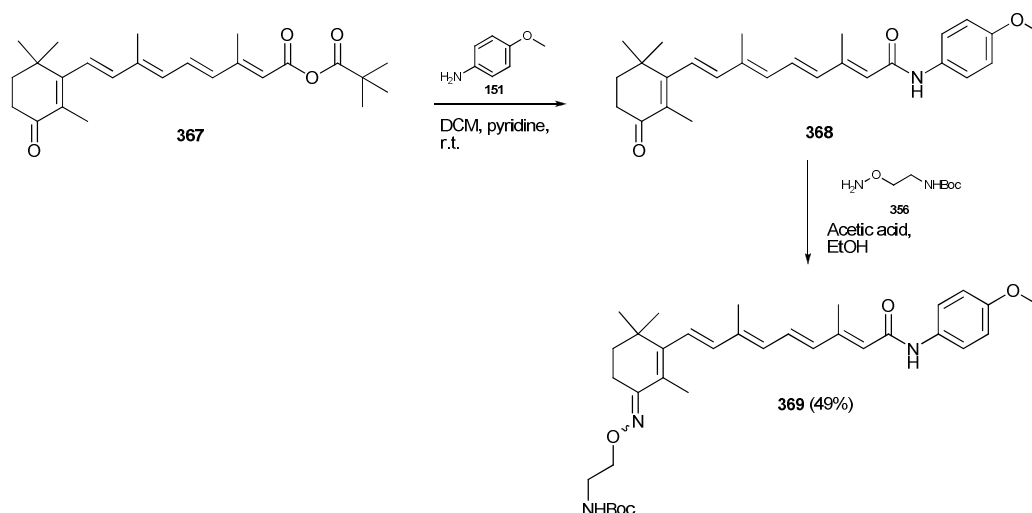
The biological inactivity of the pre-supported ligand, amine **184**, has been previously described (99 ± 10 % cell viability vs fenretinide 43 ± 2 % for fenretinide, see Section 2.2.6). As confirmation to validate the biological relevance of extending from the amine, *in vitro* screening of the Boc-protected compound (**175**) also showed absence of any activity (106 ± 6 % cell viability vs 43 ± 2 % for fenretinide). Hence, the SAR shows that the incorporation of the aminomethyl group as well as a lipophilic extension to the aminomethyl group at the *para*-position of the phenyl ring were both detrimental to activity; thus validating the approach for use of the benzylamine-derived solid supported ligand (**364**) as a negative control to distinguish between potential targets and non-specific binders.



Scheme 5.5 Synthesis of a benzyl amide 'negative control' affinity chromatography ligand.

5.3.3 Synthesis of the *para*-methoxy oxime solid supported ligand

The pre-Sepharose supported ligand (**369**) was synthesised *via* an acid-catalysed condensation of the hydroxylamine linker (**356**) (synthesised previously, see page 136) to the methylated 4-oxo-fenretinide (**368**) (itself synthesised by coupling of *para*-methoxyaniline (**150**) to the mixed anhydride of 4-oxo-retinoic acid (**367**) which was synthesised previously in Chapter 2) at room temperature in reasonable yield (*Scheme 5.6*). A single isomer was observed; however, nOe studies to identify this were inconclusive.



Scheme 5.6 Synthesis of the methylated negative control affinity chromatography ligand.

5.3.4 Affirmation of absence of biological activity of the *para*-methoxy oxime solid supported ligand

In order to confirm that the pre-Sepharose loaded *para*-methoxy oxime ligand showed no biological activity, the Boc-protected compound (**369**) was tested in the same cell viability assay. Unexpectedly, compound **369** decreased viable cell number (59 ± 4 % cell viability) in the assay, demonstrating activity which was approaching that of fenretinide (43 ± 2 % cell viability). This result was contradictory to the historical SAR developed for fenretinide activity (Chapter 2) in which the importance of the OH group on the phenyl ring was established. Hence, this ligand cannot be used as negative control in the affinity chromatography experiment. Interestingly, the *para*-methoxy-4-oxo-fenretinide precursor (**368**) also demonstrated significant activity (66 ± 4 % cell viability). The ability of this compound to induce cell death has never before been described, despite the fact that fenretinide is known to metabolise to both the 4-oxo- and methoxy-variants (see Chapter 1). It is possible that the positive biological data observed for compounds **369** and **368** may be the result of the compounds acting *via* an alternative mechanism to fenretinide, yet producing the same phenotype in this assay. The deprotected precursor (**365**) was not screened owing to the likelihood of poor cell permeability for this compound (as has been proposed

for other ligands with protonatable primary amines). This ligand was therefore not taken forward for binding to the epoxy activated Sepharose.

No further negative controls were proposed for synthesis, although Sepharose itself was also used as a negative control in the experiment.

5.4 Affinity chromatography

This section describes the processes used in order to carry out the affinity chromatography pull down assay using the selected ligands discussed above. Fragments bound to the linker with activity (but not the negative control or Sepharose column alone) were subsequently identified and isolated using SDS-PAGE and identified using mass spectrometry. A literature review was carried out on any fragments which were found to bind specifically to those ligands which demonstrated activity *in vitro*, without non-specific binding to the negative controls.

5.4.1 Isolation of membrane proteins binding to fenretinide

The affinity chromatography studies were carried out by Dr Paul O'Regan (LICAP, University of Leeds).

Precleared membrane enriched biotinylated cell lysate from SKES1 ESFT cells was incubated with each of the covalently immobilised molecules (**352**, **353** and **364**) bound to the Sepharose resin or Sepharose resin alone overnight at 4 °C. The resin was then poured into a column under gravity and the flow through (fraction containing unbound proteins) was collected. The column was then washed in wash buffer (10 mM, HEPES (pH 7.1), 100 mM KCl, 2 mM MgCl₂, 1 mM EDTA) to remove any unbound proteins. Bound proteins were subsequently eluted in 50 mM glycine pH 2.3, 10 % sucrose buffer.

The purified proteins were analysed by 1D gradient SDS-PAGE (4-20 % acrylamide) and silver staining (Proteosilver Plus, Sigma). In total 12 bands were identified that were eluted from the specific affinity columns but were absent in the non-specific negative control column (*Figure 5.6*).

Each protein band was analysed by mass spectrometry for identification using an Agilent 1100 Series nano-LC System (Agilent Technologies)

coupled online with a QSTAR XL quadrupole TOF hybrid mass spectrometer (Applied Biosystems) as previously described.¹⁸³ Data was analysed using a local Mascot database search engine (Matrix Science) and the UniProt protein sequence database (restricted to human; 88214 sequences). Peptides with scores over the identity threshold ($p < 0.05$) were considered as identified, proteins required at least one significant bold red peptide (that is, the highest scoring match to a particular query listed under the highest scoring protein containing that match).

The expression of proteins that appeared to be specifically binding to the fenretinide molecule was confirmed by western and immunoprecipitation blot of ESFT cellular extracts (results not shown). No hits were identified for two bands, one at *ca.*100 kDa and one at *ca.*30 kDa. In the remaining bands many ribosomal proteins were identified, along with tubulin and nucleolin (an exhaustive list of which can be found in the Appendix C). Five proteins were identified to bind to one or both of affinity chromatography ligands **352** or **353**, with weak or no non-specific binding to the negative control ligand (**364**) or Sepharose (discussed below).

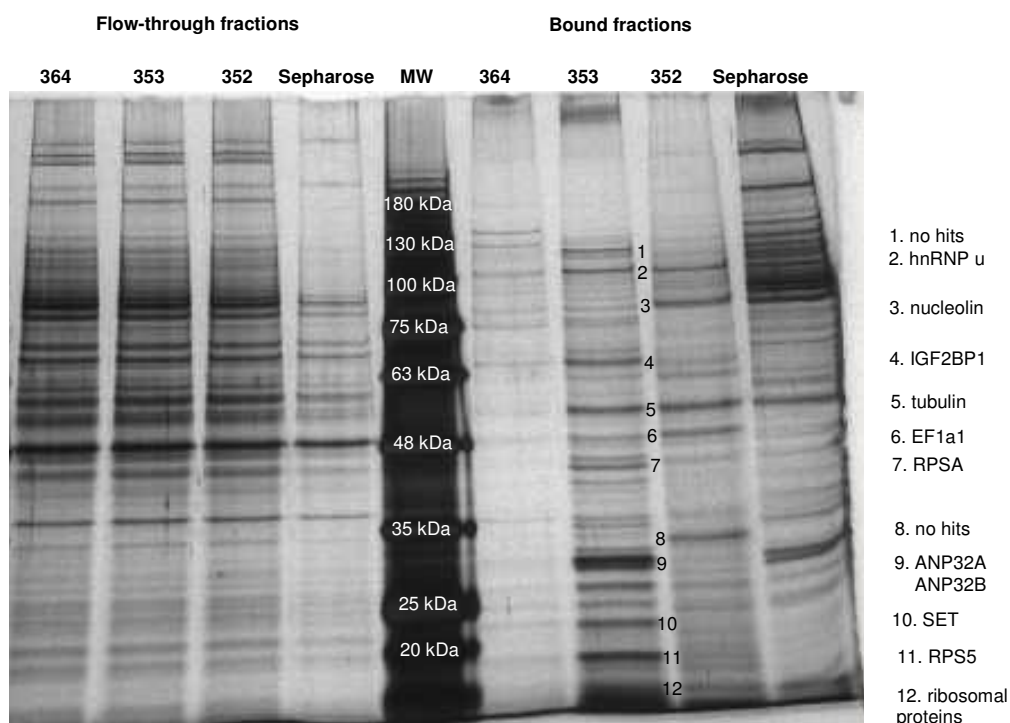


Figure 5.6 SDS-PAGE of silver-stained proteins from SKES1 cells in the flow-through and isolated by binding to the ligands **364** (negative control), **352**, **353** and Sepharose (negative control). The size of isolated proteins was identified by comparing to the molecular weight markers (MW).

5.4.2 Literature review of binding fragments

Q00839 - Heterogeneous nuclear riboprotein U (HNRPU)

Strong binding of HNRPU to both ligands **352** and **353** was observed. However, the protein was also seen to bind to the Sepharose and the negative control ligand (**364**), albeit much more weakly, meaning binding may not be specific to the ligand under investigation. HNRPU is predominantly localised in the nucleus, cytoplasm and cell surface. The protein has multiple functions; firstly, binding to RNA has been observed and the protein is a component of HNRNP complexes, important in RNA processing (splicing, polyA addition, cytoplasmic shuttling).¹⁸⁴ HNRPU inhibits transcript elongation by RNA polymerase II.¹⁸⁵ Additionally, scaffold attachment regions of HNRPU bind DNA to tether chromatin loops to nuclear matrix.¹⁸⁶ More relevantly, the protein is cleaved in the DNA-binding domain during apoptosis and released from the nuclear matrix, which may contribute to apoptotic nuclear breakdown.¹⁸⁷ Interactions with the Wilms tumour suppressor gene 1 (WT1) have been reported¹⁸⁸ and binding to EWS protein was observed by Pahlich *et al.*¹⁸⁹ However, in the pull-down assay of Pahlich *et al.*, it was noted that the interaction could be a non-specific interaction with the Agarose pull-down resin. HNRPU is a substrate for and is phosphorylated by DNA-PK in response to DNA double strand breaks.¹⁹⁰ Together with IGF2BP1, also identified as a bound fragment in the pull-down assay, HNRPU forms part of a complex that protects c-Myc mRNA (a template for the Myc protein, which is associated with rapid proliferation of cancer cells and is upregulated in ESFT cells) from degradation.¹⁹¹

Q9NZ18 Insulin-like growth factor 2 mRNA-binding protein 1 (IGF2BP1)

IGF2BP1 was identified as a binding protein for both affinity chromatography ligands (**352** and **353**), although stronger binding to ligand **353** was observed. No apparent binding to Sepharose was observed and very weak binding to the negative control ligand (**364**). IGF2BP1 is localised in cytoplasmic mRNP particles containing untranslated mRNAs. It functions as a binding partner to mRNAs of certain genes (*e.g.* IGF2, beta actin) and regulates their translation and is a component of the coding region instability determinant (CRD)-mediated complex that promotes Myc mRNA stabilisation. IGF2BP1 is

a target of the Wnt signalling pathway and knockdown of the CRD-binding protein induces apoptosis.¹⁹² Wnt signalling is reported to be upregulated in metastatic compared to localised Ewing sarcoma and several lines of evidence suggest that another component of the IGF pathway, IGF1R signalling, is critical to the biology of ESFT.¹⁹³ Additionally, increased expression of IGF2BP1 is associated with advanced clinical stage and poor prognosis in ovarian cancer.¹⁹⁴

P68104 Elongation factor 1-alpha 1 (EF1a1)

EF1a1 was found to bind to both ligands (**352** and **353**), binding to **352** with greater affinity. No apparent binding to the Sepharose and the negative control ligand (**364**) was observed. However, the protein was abundant in all flow-through fractions. This could be due to very high levels of the protein present in the sample, therefore the column becomes saturated. The protein is an isoform of the α -subunit of the elongation factor-1 complex and is highly abundant in cytoplasm. The protein is responsible for enzymatic transfer of aminoacyl tRNAs to the ribosome. It is known to have GTP-binding and hydrolysis activity,¹⁹⁵ which implies that the enzyme may be druggable *via* small molecule inhibition. EF1a1 binds to and activates Sphingosine Kinase 1, a cell proliferation regulator which converts the proapoptotic lipid sphingosine into the antiapoptotic lipid sphingosine-1-phosphate.¹⁹⁶ Increased expression of EF1a1 correlates with poor prognosis in prostate cancer.¹⁹⁷

P08865 40S ribosomal protein SA (RPSA)

RPSA was identified bound to the hydrazone ligand (**353**). No apparent binding to the oxime ligand (**352**) was observed, nor the Sepharose or negative control ligand (**364**); however, the protein was abundant in all flow-through fractions. RPSA is found in the cell membrane (as 67kDa dimer), cytoplasm and nucleus and is involved in the maturation of ribosomal subunit proteins. It also functions as a cell surface receptor for laminin, implicated in cell adhesion to the basement membrane, differentiation, migration, signalling transduction pathways, neurite outgrowth and metastasis. Expression of RPSA is induced by hypoxia and it is over expressed in many types of cancer, as well as being an important factor in tumour cell migration, invasion and angiogenesis.¹⁹⁸ The target is potentially druggable and there are currently 14

known active peptide mimetics identified.¹⁹⁹ Virtual screening has also identified a small molecule inhibitor, NSC47924 (**370**) (Figure 5.7).²⁰⁰ In future experiments it would be interesting to investigate the effect of this small molecule inhibitor in ESFT cells.

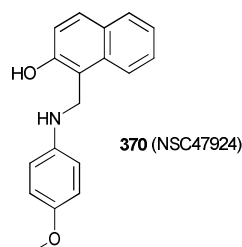


Figure 5.7 A small molecule inhibitor of RPSA identified by virtual screening.

Q01105 Phosphatase 2A inhibitor I2PP2A (aka SET)

Strong binding of I2PP2A to the hydrazone ligand (**353**) was observed. There was no apparent binding to the oxime ligand (**352**) nor the negative controls, ligand **364** and Sepharose. I2PP2A is a multifunctional protein expressed in proliferating cells. It is predominantly nuclear but relocates to cytoplasm under genotoxic stress, which in turn induces cytotoxicity.²⁰¹ SET was found to relocate to the plasma membrane as part of Rac1-mediated cell migration, responsible for cell adhesion and motility.²⁰² It has histone chaperone activity and along with ANP32A, is a subunit of the inhibitor of acetyltransferases complex. SET is a negative regulator of neuronal development²⁰³ and is associated with a neuronal apoptotic pathway in Alzheimer's disease.²⁰⁴ PP2A activity is inhibited by SET (as well as ANP32A), which targets proteins of oncogenic signalling cascades.²⁰⁵ SET is a target of chromosomal translocation in leukaemia²⁰⁵ and is overexpressed in primary chronic lymphocytic leukemia cells, where increased expression levels correlate with severity and progression of disease.²⁰⁶ A peptide antagonist COG449 was developed against SET by Christensen *et al.* and successfully inhibited growth of NHL tumour xenografts in mice.²⁰⁶ SET binds ceramides, which decreases association with PP2A, leading to c-Myc degradation.²⁰⁷ With ANP32A, SET has function in Granzyme-A induced apoptosis.²⁰⁸ Overexpression of SET is known to activate MAPK and prevent Fas-mediated apoptosis.²⁰⁹

Non-specific binders

Many ribosomal proteins were identified, along with tubulin and nucleolin. These proteins frequently bind to Sepharose, and therefore may not be specifically associated with binding to the fenretinide molecule.²¹⁰ Three proteins bound to both the solid-supported ligand **353** and the Sepharose and ligand **364** negative controls; P19338 nucleolin and both Q6PKH8 Acidic nuclear phosphoprotein 32 members A and B (ANP32A and ANP32B). There was no apparent binding of these proteins to solid supported ligand **352**.

5.5 Conclusion

Very little is known about the mechanism through which fenretinide initiates cell death. The identification of a biological target or targets responsible for activation of the cell death cascade following exposure of ESFT cells to fenretinide may aid in the design of future therapeutic agents. The target may also be useful as a biomarker to identify which cancers are likely to respond to fenretinide, allowing for selection of patients for so called personalised medicine.

Several proteins were identified that bound to affinity chromatography ligands **352** and **353**, where binding to the **364** negative control was not observed (*Table 5.1*). However, non-specific binding to Sepharose was observed for 4/8 of the proteins isolated. Previous studies have identified non-specific binding of hnRNP and nucleolin proteins to Sepharose resin, with nucleolin proteins extracted in 73 % of all pull-down experiments using Sepharose beads.²¹⁰ RPSA and SET were found to bind specifically to ligand **353**, both of which have significant associations to a range of cancer types and are potentially druggable, with peptide inhibitors of both and a small molecule inhibitor of

Protein	Binding to	Localisation*	Druggable?
hnRNP U	353, 354, Sepharose	nuc / cyt	
Nucleolin	353, Sepharose	nuc / cyt / memb	+ (peptide)
IGF2BP1	353, 354	cyt	
EF1a1	352, 353	cyt	++ (GTP binding)
RSSA	353	nuc / cyt / memb	++ (peptide, small molecule)
ANP32A	353, Sepharose	nuc / cyt	
ANP32B	353, Sepharose	nuc / cyt	
I2PP2A (SET)	353	nuc / cyt / memb	+ (peptide)

*nuc = nucleus; cyt = cytoplasm; memb = membrane.

Table 5.1 Summary of affinity chromatography binding proteins.

RPSA already identified. IGF2BP1 bound strongly to ligand **353** and weakly to **352** and the negative control ligand (**364**). Binding of this protein is perhaps most relevant, as reports by Elcheva *et al.* suggest this is a target of the Wnt signalling pathway, upregulated in metastatic ESFT.¹⁹² Additionally, Ho *et al.* have suggested that that IGF1R signalling is critical to the biology of ESFT.¹⁹³ Although current literature suggests that EF1a1 is likely to be the least relevant potential target isolated, this protein is known to have GTP-binding and hydrolysis activity implying that it may be druggable *via* small molecule inhibition.

6. Discussion and future work

Through extensive design and synthesis for biological evaluation studies, a series of compounds which demonstrate fenretinide-like activity in ESFT cells have been identified. Compounds containing both retinoid and non-retinoid structural features have been investigated. The studies have allowed the development of a preliminary SAR for retinoid and non-retinoid molecules for fenretinide-like activity in ESFT cells. Much of the SAR developed within the project to-date can be summarised as described in *Figure 6.1*.

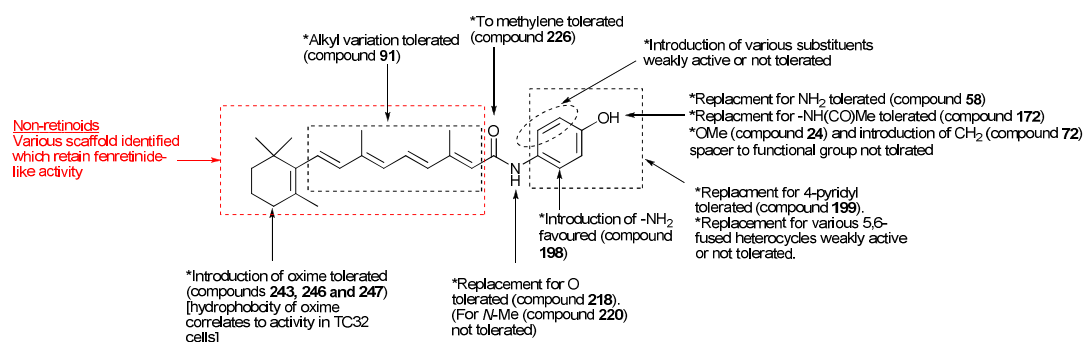


Figure 6.1 SAR for retinoids and non-retinoids demonstrating fenretinide-like activity in TC32 cells.

Perhaps the most significant observation is the requirement for the presence of a NH or OH group at the 4-position of the phenyl ring which would appear to be important for induction of cell death in ESFT TC32 cells. Additionally, incorporation of a NH_2 group at the *ortho*-position of the fenretinide structure was well tolerated, as was replacement of the 4-hydroxyphenyl group with a 4-pyridyl structure. Although the 4-pyridyl structure does not contain a hydroxy group at the position corresponding to that of fenretinide, it does contain a polar atom at this site which may, in part, be responsible for the activity observed. Many of the other variants investigated at the phenyl ring of fenretinide, including replacement of the phenyl group for a range of heterocycles, as well as incorporation of variable substituents, and

substituent patterns, were either less active or not tolerated in TC32 cells. As for substitution at the phenyl ring, variation at the amide group suggested that this site was relatively sensitive to synthetic modification, with only the ester variant showing positive biological activity. The SAR at the central repeating isoprenoid scaffold and the cyclohexyl ring regions of fenretinide is complicated by the lack of compound numbers synthesised and tested based on variation at these sites, however there does seem to be some tolerance to substitution (with an oxime or hydrazone, at least) at the 4-position of the cyclohexyl ring. Future work could look at incorporation of alternative cyclohexyl moieties, including heterocycles, which may reduce the lipophilicity at this site. Few variations of the isoprenoid scaffold were investigated. However, principally through investigative SAR work carried out for the non-retinoid compounds, it would appear that a number of different structural variations at this site are tolerated and as such further synthetic variation at the central scaffold would appear warranted by, for instance, incorporation of heterocycles or polar atoms to improve both the physicochemical profile of the compounds as well as the activity.

Mechanistic studies on hit compounds from the retinoid and non-retinoid series demonstrated interesting mechanisms of action, possibly distinct from fenretinide. For the retinoids, the phenyl-containing retinoid mimetics - the *para*-amino (**58**) and the direct *ortho*-amino substituted analogue of fenretinide (**198**) - induced caspase-3 cleavage, indicating that these compounds initiate programmed cell death through a mechanism that may be similar to fenretinide. However, the 4-pyridyl containing retinoid (**199**) did not induce caspase-3 cleavage, suggesting a novel mechanism of decreasing viable cell number. None of the three retinoids were found to induce ROS in TC32 cells, which is reported to be important for fenretinide-induced activity in a range of cancer types.^{40,46,49,53,66,67} This observation suggests that elevated ROS levels are not essential for the activity of these compounds and programmed cell death (and caspase-3 activation in the case of **58** and **198**) is initiated *via* an alternative mechanism. It is currently unclear as to whether ROS generation is an important factor in fenretinide-induced apoptosis or whether it is generated as a consequence of cell

death.⁷¹ There are conflicting reports that fenretinide can act through different mechanisms in different cell types; ROS-independent mechanisms such as endoplasmic reticulum stress⁷⁰, and ceramide production⁷¹ as well as *via* ROS-dependent mechanisms such as modulation of p38^{MAPK} activity and mitochondrial membrane depolarisation.⁶⁷ Future work may look at more detailed studies on the mechanism through which the compounds are killing the cancer cells, including possible alternative mechanisms such as mitochondrial membrane depolarisation¹⁷⁵, intracellular calcium concentration¹⁷⁶ or apoptosis inducing factor studies.¹⁷⁷ Alternatively, compounds could be acting through nonphysiological pathways to kill the cell (*e.g.* necrosis) therefore it is important to carry out further toxicity studies (*i.e.* *in vivo*).

In dose response studies across multiple cell lines, the three retinoids, in particular the *ortho*-amino substituted analogue (**198**), demonstrated very interesting activity in the concentration response studies. Not only did this compound induce similar levels of activity to fenretinide in all of the ESFT and neuroblastoma cell lines, activity was significantly increased compared to fenretinide at the lowest concentration (3 μ M) in three out of the five cell lines (TC32, TTC466 and SHEP-1). The 4-pyridyl and *para*-amino analogues (**199** and **58**) also demonstrated dose-dependent activity across all cell lines which was comparable to or approaching that of fenretinide.

Through ligand-based studies directed towards generation of non-retinoid mimetics of fenretinide, we have discovered that it is relatively straightforward to identify fenretinide-like activity using a variety of mainly hydrophobic scaffolds as retinoid mimetics. The activity and therapeutic ratio of the hit non-retinoid compounds identified through these studies, suggest they are not as active or safe (*i.e.* potential therapeutic ratio) as the retinoids, although there is considerable scope for optimisation of these compounds given the encouraging data achieved to-date and the relative ease with which it should be possible to synthesise libraries of variants for future testing.

The mechanism-based studies for the non-retinoids suggest that the compounds may induce activity *via* alternative processes to fenretinide. The two non-retinoids selected for investigation (compounds **275** and **298**) did not

induce elevation of ROS levels or activation of caspase-3 (which would be expected if programmed cell death was induced). It is therefore possible that these compounds are inducing cytotoxicity by necrosis or an alternative mechanism. Concentration-response studies against multiple cell lines highlighted that the phenyl ether (**275**) may induce activity *via* a p53-dependent mechanism due to inactivity/reduced activity in those cell lines which do not express p53. This is in contrast to fenretinide which is known to induce activity *via* a p53-independent mechanism.¹⁶⁷ Future work should further investigate the possible alternative mechanisms (described above) to identify whether these compounds are suitable lead compounds for further optimisation. It would also be of interest to further rationalise the mechanism of action of these compounds and to determine whether there was any mechanistic commonality between different (non-retinoid) scaffold types.

Future work should aim to identify additional non-retinoids with a good activity and increased fold-differential toxicity over normal cells to demonstrate a more complete SAR for one or more of the non-retinoid scaffold types. The data generated to-date for the non-retinoids has been rather sporadic based on the acquisition of biological data for a number of different scaffold types. It would be beneficial to focus the collection of biological data on one (or possibly two) scaffold types for optimisation. Non-retinoids are particularly interesting as they offer the potential to instil favourable pharmaceutical properties, including improved metabolic stability, solubility and reduced lipophilicity, which consequently may improve the bioavailability (and possibly efficacy) achieved in comparison to fenretinide. A focus of future work may be to generate additional hybrid molecules containing features of the positive pharmacokinetic profile of the non-retinoids with the more favourable activity, therapeutic ratio and mechanism of action of the retinoids.

The best of the compounds characterised to date from both the retinoid and non-retinoid optimisation studies have the potential to progress for additional biological evaluation in a range of cancer cell line types (*e.g.* the NCI60 panel), *in vivo* preclinical studies with pharmacokinetic assessment and combination therapy studies (for compounds which may indicate that their activity is induced by opposing mechanisms, therefore may act

synergistically). Although the compounds demonstrate a robust metabolic stability profile, additional metabolism studies (hepatocyte stability, for instance) would be useful to identify whether the compounds are less liable to oxidative metabolism than fenretinide. It would also be of value to understand whether the metabolites of the compound were themselves cytotoxic. The metabolites of fenretinide behave in this way; 4-oxo-fenretinide and the glucuronidation product of the phenol are known to be active in cancer cells and positively reinforce the cytotoxic effect *in vivo*.^{47,80,102} All of the hit compounds generated within this project contain a polar head group which could potentially undergo glucuronidation, therefore future work may include synthesis of the glucuronate product to test for their activity. In the case of the retinoid-containing lead compound(s), this could also include oxidation at the 4-position of the cyclohexyl ring.

By screening against MSCs it has been helpful to identify compounds with minimal toxicity in normal cells. However, it was unclear as to what level of toxicity should be considered acceptable (there is currently no literature precedence for this). An acceptable therapeutic index is important to ensure safe concentrations of the drug can be administered to achieve the desired therapeutic effect. Unfortunately, due to the slow-growing nature of MSCs, it was not possible to obtain enough cells to carry out concentration response studies to identify optimum concentrations whereby toxicity in the cancer cells is significantly higher than the normal cells. The majority of compounds tested demonstrated activity statistically comparable to or less than that of fenretinide. The accuracy of the predictive value of this screening could be tested by comparing the outcome from MSC screen with a classical toxicity study in mice. It would certainly provide a cheaper, more convenient method for initial toxicity predictions than the classic *in vivo* preclinical screens if this proved to be the case.

In an effort to support the understanding of the mechanism of action of fenretinide, a protein-capture technique (affinity chromatography) was utilised in an attempt to identify the macromolecule(s) within the cancer cell through which fenretinide might interact with to initiate cell death. To optimise the likelihood of binding of ligands to proteins that are involved in initiation of cell

death, affinity chromatography was carried out on membrane enriched protein extracts. Fenretinide is known to efficiently bind RBP4, however, this was not pulled out by affinity chromatography as this is not a membrane protein. This implies that the strategy to enrich membrane proteins was somewhat successful. However, proteins predominantly located in the nucleus and cytoplasm as well as the cell surface were isolated, therefore further optimisation of this technique may allow for identification of less abundant proteins in the cell membrane which have greater significance. Several proteins were identified to bind to a fenretinide-like ligand in affinity chromatography studies. Four proteins were identified to have selectivity to the ligand compared to the negative controls. 3 of these (IGF2BP1, RPSA and SET) have significant associations to a range of cancer types, with IGF2BP1 reported to have implications in the biology of ESFT.^{189,192,193,195,198} Furthermore, RPSA and SET are potentially druggable with peptide inhibitors and a small molecule inhibitor for RPSA already identified.¹⁹⁹ Crystal structures of both IGF2BP1 (PDB ID: 3KRM) and SET (PDB ID: 2E50) are available, therefore it would be interesting to identify, by structure-based design, potential small molecule inhibitors of these proteins which could be synthesised/purchased and screened against ESFT cells. Activity of these inhibitors or elimination of fenretinide activity upon co-treatment with the inhibitors may help to confirm or eliminate the potential role of this protein as a target for fenretinide-induced cell death. Also isolated in the pull-down assay was EF1a1. Although literature suggests that this protein is perhaps least relevant potential target isolated, this protein is known to have GTP-binding and hydrolysis activity, implying that it may be druggable *via* small molecule inhibition.¹⁹⁵ There are some limitations to the affinity chromatography approach, for example, fenretinide might bind to proteins through which it does not induce cell death. Furthermore, this approach will preferentially identify abundant proteins to which fenretinide binds, although these may not be the most important factors through which fenretinide initiates cell death. For example, STRA6 was not identified, but this has been shown to regulate fenretinide induced cell death.⁸⁶

7. Experimental

7.1 Materials

All chemicals and solvents that were purchased were used without further purification. Anhydrous solvents were passed through activated alumina in a solid state still (SPS PureSolve MD6).

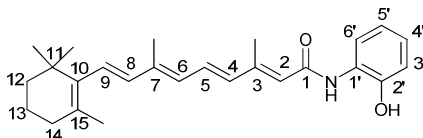
7.2 Methods

¹H Nuclear Magnetic Resonance spectra were recorded at 500 MHz using a Bruker DRX 500 instrument or at 300 MHz using a Bruker DPX 300. ¹H spectra are referenced based on the residual proton in the solvent (*e.g.* the CHCl₃, 0.01 % in 99.99 % CDCl₃). Coupling constants (*J*) are reported to the nearest 0.1 Hz. ¹³C NMR spectra were recorded at 75 MHz on 300 MHz spectrometers or at 125 MHz on 500 MHz spectrometers. Infrared spectra were recorded on a Perkin-Elmer Spectrum 1 or Bruker Alpha Platinum ATR FTIR spectrometer and samples analysed in the solid phase. LCMS was performed on a Bruker Daltonics instrument running a gradient of increasing acetonitrile (5 to 95 %) in water both containing 0.1 % formic acid at 1 ml/min, on a short path C18 reverse phase column (Luna 5 μ C18(2) 100A, 50 \times 2.00 mm), detecting compounds with both a diode array detector and a Bruker HCT Ultra analyser. High resolution mass spectra were recorded on a Waters Micromass GCT Premier for electron impact (EI) spectra. Electrospray (ESI) spectra were recorded on a Bruker Daltonics micrOTOF or Bruker MaXis Impact spectrometer. Melting points were measured on a Stuart SMP30. Biotage silica column chromatography was carried out using an Isolera Four EXP with Spektra. HPLC was performed on an Agilent 1290 Infinity Series instruments equipped with a UV detector and Hyperprep C₁₈ reverse phase column, running a gradient of increasing acetonitrile (5 to 95 %) in water containing 0.1 % formic acid at 0.5 ml/min over an eight minute period.

7.3 Synthesis

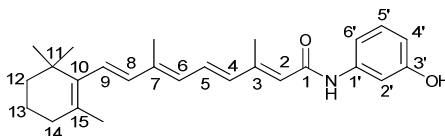
7.3.1 Phenyl analogues

(2E,4E,6E,8E)-N-(2-hydroxyphenyl)-3,7-dimethyl-9-(2,6,6-trimethylcyclohex-1-enyl)nona-2,4,6,8-tetraenamide (19)



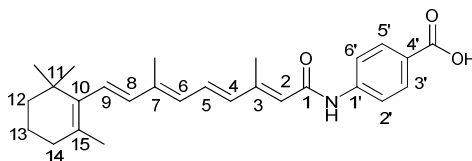
The mixed anhydride (**148**) (49.9 mg, 1 eq) was dissolved in DCM (3 ml) and pyridine (200 μ l) at room temperature and 2-aminophenol (**151**) (18.5mg, 1.3 eq) was added. The solution was allowed to stir overnight at room temperature. Once complete, the reaction was diluted with EtOAc (50 ml) and washed with saturated sodium bicarbonate solution (2 \times 50 ml) and brine (2 \times 50 ml). The organic layer was dried over sodium sulphate and concentrated *in vacuo*. The residue purified using silica column chromatography, eluted with 0-100 % EtOAc in hexane, to yield the product as a yellow solid (31 mg, 61 %). **LCMS (M+H)⁺** found 392.2, requires 392.2, RT 2.68 min; **HRMS ESI (M+H)⁺** found 392.2588, C₂₆H₃₄NO₂ requires 392.2584; **δ_{H} (500 MHz, CDCl₃)** 1.02 (6H, s, C11(CH₃)₂), 1.38 (2H, m, C12H₂), 1.56 (2H, m, C13H₂), 1.65 (3H, s, C3CH₃), 1.96 (2H, m, C14H₂), 1.94 (3H, s, C7CH₃), 2.36 (3H, s, C15CH₃), 5.81 (1H, s, C2H), 6.26 (5H, m, C5-, C4-, C6-, C8-, C9-H), 6.96 (4H, m, C3', C4', C5', C6'-H), 9.26 (1H, br s, OH); **δ_{C} (125 MHz; CDCl₃)** 12.89 (C3CH₃), 13.95 (C7CH₃), 20.33 (C13), 21.96 (C15CH₃), 29.43 (C11(CH₃)₂), 34.00 (C14), 35.27 (C11), 40.79 (C12), 117.70 (C3'), 120.77 (C2), 122.24 (C6'), 123.35 (C5'), 126.63 (C4'), 127.67 (C1'), 129.31 (C5), 130.63 (C15), 131.08 (C9), 131.51 (C6), 136.98 (C4), 139.02 (C8), 139.10 (C7), 140.05 (C10), 149.60 (C3), 149.60 (C2'), 151.77 (C1); **IR (cm⁻¹)** 3288, 2922, 2854, 1605, 1520, 1469, 1453, 1313, 1173, 966, 749, 634; **MP** 138-140 °C.

(2E,4E,6E,8E)-N-(3-hydroxyphenyl)-3,7-dimethyl-9-(2,6,6-trimethylcyclohex-1-enyl)nona-2,4,6,8-tetraenamide (20)



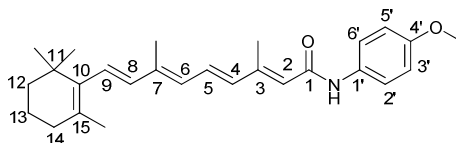
The mixed anhydride (**148**) (50.1 mg, 1 eq) was dissolved in DCM (3 ml) and pyridine (200 μ l) at room temperature and 3-aminophenol (**152**) (18 mg, 1.3 eq) was added. The solution was allowed to stir overnight at room temperature. Once complete, the reaction was diluted with EtOAc (50 ml) and washed with saturated sodium bicarbonate solution (2 \times 50 ml) and brine (2 \times 50 ml). The organic layer was dried over sodium sulphate and concentrated *in vacuo*. The residue was purified using silica column chromatography, eluted with 0-100 % EtOAc in hexane, to yield the product as a yellow solid (25 mg, 50 %). **LCMS (M+H)⁺** found 392.2 requires 392.2, RT 2.53 min; **HRMS ESI (M+H)⁺** found 392.2595, C₂₆H₃₄NO₂ requires 392.2584; **δ_{H} (500 MHz, CDCl₃)** 1.07 (6H, s, C11(CH₃)₂), 1.50 (2H, m, C12H₂), 1.67 (2H, m, C13H₂), 1.75 (3H, s, C3CH₃), 2.10 (3H, s, C7CH₃), 2.10 (2H, m, C14H₂), 2.40 (3H, s, C15CH₃), 5.84 (1H, s, C2H), 6.20 (1H, s, C2'H), 6.26 (4H, m, C4-, C6-, C8-, C9-H), 6.54 (1H, d, *J* = 8.1 Hz, C6'H), 6.76 (1H, d, *J* = 8.1 Hz, C4'H), 7.00 (1H, m, C5H), 7.05 (1H, t, *J* = 8.1 Hz, C5'H), 7.49 (1H, br s, OH); **δ_{C} (125 MHz, CDCl₃)** 12.99 (C3CH₃), 14.02 (C7CH₃), 20.37 (C13), 22.06 (C15CH₃), 29.51 (C11(CH₃)₂), 34.04 (C14), 35.29 (C11), 40.80 (C12), 108.25 (C2'), 112.04 (C6'), 112.35 (C4'), 123.18 (C2), 129.23 (C5'), 130.50 (C5), 131.12 (C9), 131.19 (C6), 131.78 (C15), 137.07 (C4), 139.01 (C7), 139.08 (C8), 139.84 (C1'), 141.31 (C10), 150.98 (C3), 158.87 (C3'), 167.77 (C1); **IR (cm⁻¹)** 3311, 2924, 1598, 1415, 964, 773, 686; **MP** 101-104 °C.

4-((2E,4E,6E,8E)-3,7-dimethyl-9-(2,6,6-trimethylcyclohex-1-enyl)nona-2,4,6,8-tetraenamido)benzoic acid (23)



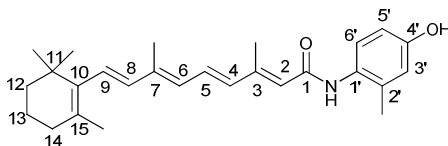
The mixed anhydride (**148**) (200 mg, 1 eq) was dissolved in DCM (5 ml) and pyridine (200 μ L) at room temperature and 4-aminobenzoic acid (**167**) (90 mg, 1.2 eq) was added. The solution was allowed to stir overnight at room temperature. Once complete by TLC, the reaction was diluted with EtOAc (50 ml) and washed with saturated sodium bicarbonate solution (2 \times 50 ml) and brine (2 \times 50 ml). The organic layer was dried over sodium sulphate and concentrated *in vacuo*. The residue was purified using silica column chromatography, eluted with 0-100 % EtOAc in hexane, to yield the product as a yellow solid (49 mg, 22 %). **LCMS (M+H)⁺** found 420.2, requires 420.3, RT 2.53 min; **HRMS ESI (M+H)⁺** found 420.2542, C₂₇H₃₄NO₃ requires 420.2533; δ_{H} (**300 MHz, CDCl₃**) 1.05 (6H, s, C11(CH₃)₂), 1.60 (2H, m, C12H₂), 1.65 (2H, m, C13H₂), 1.73 (3H, s, C3CH₃), 2.03 (3H, s, C7CH₃), 2.04 (2H, t, *J* = 6 Hz, C14H₂), 2.42 (3H, s, C15CH₃), 6.04 (1H, s, C2H), 6.19 (4H, m, C4-, C6-, C8-, C9-H), 7.11 (1H, m, C5-H), 7.73 (2H, d, *J* = 8.7 Hz, C3'-, C5'-H), 7.87 (2H, d, *J* = 8.7 Hz, C2'-, C6'-H), 10.00 (1H, s, NH); δ_{C} (**125 MHz; CDCl₃**) 12.93 (C3), 14.05 (C7), 20.38 (C13), 21.98 (C15CH₃), 29.47 (C11(CH₃)₂), 34.06 (C14), 35.32 (C11), 40.85 (C12), 119.98 (C2', C6'), 122.58 (C2), 126.64 (C4'), 129.49 (C5), 131.07 (C9), 131.78 (C6), 131.85 (C3', C5'), 136.91 (C4), 139.05 (C8), 140.30 (C10), 144.93 (C1'), 152.28 (C3), 167.96 (C1), 169.66 (C4'CO); **IR (cm⁻¹)** 3333, 2919, 2861, 1682, 1308, 854, 768; **MP** 174-178 °C.

(2E,4E,6E,8E)-N-(4-methoxyphenyl)-3,7-dimethyl-9-(2,6,6-trimethylcyclohex-1-enyl)nona-2,4,6,8-tetraenamide (24)



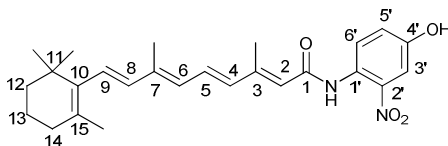
The mixed anhydride (**148**) (100 mg, 1 eq) was dissolved in DCM (3 ml) and pyridine (200 μ L) at room temperature and *para*-methoxyaniline (**150**) (39 mg, 1.2 eq) was added. The solution was allowed to stir overnight at room temperature. Once complete by TLC, the reaction was diluted with EtOAc (50 ml) and washed with saturated sodium bicarbonate solution (2 \times 50 ml) and brine (2 \times 50 ml). The organic layer was dried over sodium sulphate and concentrated *in vacuo*. The residue was purified using Biotage silica column chromatography, eluted with 0-100 % EtOAc in hexane, to yield the product as a yellow solid (37 mg, 35 %). The product was not ionised by LCMS. **HRMS ESI (M+H)⁺** found 406.2724, C₂₇H₃₆NO₂ requires 406.2741; **δ_{H} (300 MHz, CDCl₃)** 0.98 (6H, s, C11(CH₃)₂), 1.46 (2H, m, C12H₂), 1.53 (2H, m, C13H₂), 1.83 (3H, s, C3CH₃), 1.95 (2H, m, C14H₂), 2.34 (3H, s, C7CH₃), 3.71 (3H, s, OCH₃), 5.74 (1H, s, C2H), 6.10 (4H, m, C4-, C6-, C8-, C9-H), 6.78 (2H, d, *J* = 9 Hz, C3'-, C5'-H), 6.90 (1H, m, C5-H), 7.42 (1H, s, NH).), 7.53 (2H, d, *J* = 9 Hz, C2'-, C6'-H); **δ_{C} (125 MHz; CDCl₃)** 12.91 (C3CH₃), 13.65 (C7CH₃), 19.23 (C13), 21.78 (C15CH₃), 28.97(C11(CH₃)₂), 33.11 (C14), 34.27 (C11), 39.58 (C12), 55.47 (OCH₃), 114.09 (C3', C5'), 114.93 (C2), 121.52 (C2', C6'), 128.41 (C5), 129.59 (C9), 129.91 (C1'), 130.17 (C6), 131.47 (C15), 135.47 (C4), 137.32 (C8), 137.73 (C7), 139.10 (C10), 150.11 (C3), 156.19 (C4'), 165.11 (C1); **IR (cm⁻¹)** 3301, 2933, 1653, 1506, 1241, 1172, 1035, 828; **MP** 124-127 °C.

(2E,4E,6E,8E)-N-(4-hydroxy-2-methylphenyl)-3,7-dimethyl-9-(2,6,6-trimethylcyclohex-1-enyl)nona-2,4,6,8-tetraenamide (25)



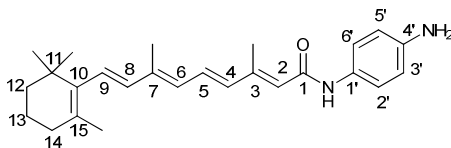
The mixed anhydride (**148**) (100 mg, 1 eq) was dissolved in DCM (3 ml) and pyridine (200 μ L) at room temperature and 2-methyl-4-aminophenol (**189**) (39 mg, 1.2 eq) was added. The solution was allowed to stir overnight at room temperature. Once complete by TLC, the reaction was diluted with EtOAc (50 ml) and washed with saturated sodium bicarbonate solution (2 \times 50 ml) and brine (2 \times 50 ml). The organic layer was dried over sodium sulphate and concentrated *in vacuo*. The residue was purified using Biotage silica column chromatography eluted, eluted with 0-100 % EtOAc in hexane, to yield the product as a yellow solid (31 mg, 29 %). **LCMS (2M+Na)⁺** found 833.4, requires 833.5, RT 2.54 min; **HRMS ESI (M+H)⁺** found 406.2746, C₂₇H₃₆NO₂ requires 406.2741; δ_{H} (**300 MHz, CDCl₃**) 0.96 (6H, s, C11(CH₃)₂), 1.39 (2H, m, C12H₂), 1.55 (2H, m, C13H₂), 1.59 (3H, s, C15CH₃), 1.94 (3H, s, C3H₃), 1.96 (2H, m, C14H₂), 2.11 (3H, s, C2'CH₃), 2.35 (3H, s, C7CH₃), 5.78 (1H, s, C2H), 6.18 (4H, m, C4-, C6-, C8-, C9-H), 6.62 (1H, d, *J* = 8 Hz, C5'H), 6.78 (1H, s, C3'H), 6.89 (1H, m, C5H), 7.28 (1H, d, *J* = 8 Hz, C6'H); δ_{C} (**125 MHz; CDCl₃**) 12.88 (C3CH₃), 13.92 (C7CH₃), 18.36 (C2'CH₃), 20.34 (C13), 21.98 (C15), 29.44 (C11(CH₃)₂), 34.00 (C14), 35.27 (C11), 40.76 (C12), 113.94 (C6'), 116.11 (C5'), 117.87 (C3'), 122.71 (C2), 128.57 (C5), 128.71 (C1'), 129.12 (C9), 130.55 (C15), 131.06 (C6), 131.13 (C4), 136.29 (C2'), 137.08 (C7), 139.09 (C8), 139.70 (C15), 150.54 (C3), 156.92 (C4'), 168.66 (C1); **IR (cm⁻¹)** 3298, 2927, 2417, 1637, 1608, 1586, 1501, 1437, 1381, 965; **MP** 170-173 °C.

(2E,4E,6E,8E)-N-(4-hydroxy-2-nitrophenyl)-3,7-dimethyl-9-(2,6,6-trimethylcyclohex-1-enyl)nona-2,4,6,8-tetraenamide (41)



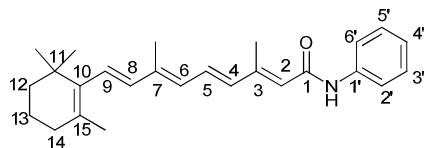
The mixed anhydride (**148**) (200 mg, 1 eq) was dissolved in DCM (4 ml) and pyridine (200 μ L) at room temperature and 4-amino-3-nitrophenol (**187**) (96 mg, 1.2 eq) was added. The solution was allowed to stir overnight at room temperature. Once complete by TLC, the reaction was diluted with EtOAc (50 ml) and washed with saturated sodium bicarbonate solution (2 \times 50 ml) and brine (2 \times 50 ml). The organic layer was dried over sodium sulphate and concentrated *in vacuo*. The residue was purified using Biotage silica column chromatography, eluted with 0-100 % EtOAc in hexane, to yield the product as a yellow solid (130 mg, 57 %). **LCMS (M+H)⁺** found 437.3, requires 437.2; **HRMS ESI (M+H)⁺** 437.2436 C₂₆H₃₃N₂O₄ requires 437.2435; **δ_{H} (500 MHz, CDCl₃)** 1.07 (6H, s, C11(CH₃)₂), 1.51 (2H, m, C12H₂), 1.65 (2H, m, C13H₂), 1.77 (3H, s, C3CH₃), 2.06 (3H, s, C7CH₃), 2.07 (2H, m, C14H₂), 2.43 (3H, s, C15CH₃), 5.99 (1H, s, C2H), 6.102 (1H, s, OH), 6.21 (2H, m, C4-, C6-H), 6.38 (2H, m, C8-, C9-H), 6.83 (1H, d, *J* = 9 Hz, C5'-H), 7.13 (1H, m, C5-H), 7.21 (1H, d, *J* = 9 Hz, C6'-H), 7.91 (1H, s, C3'-H); **δ_{C} (75 MHz; CDCl₃)** 12.98 (12.98), 14.17 (14.17), 19.22 (19.22), 21.75 (15C_H3), 28.97 (C11(CH₃)₂), 33.15 (C14), 34.45 (C11), 39.64 (C12), 116.37 (C3'), 118.46 (C2), 119.16 (C5'), 129.31 (C6'), 129.35 (C5), 130.65 (C9), 131.56 (C15), 132.39 (C6), 134.54 (C4), 137.14 (8), 137.68 (C1'), 137.71 (C7), 140.75 (C10), 142.42 (C2'), 142.46 (C3), 156.36 (C4'), 165.48 (C1); **IR (cm⁻¹)** 3478, 3354, 1704, 1572, 1513, 1125, 974; **MP** 150-153 °C.

(2E,4E,6E,8E)-N-(4-aminophenyl)-3,7-dimethyl-9-(2,6,6-trimethylcyclohex-1-enyl)nona-2,4,6,8-tetraenamide (58)



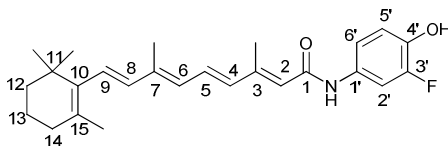
The mixed anhydride (**148**) (100 mg, 1 eq) was dissolved in DCM (3 ml) and pyridine (250 μ L) at room temperature and *para*-phenylenediamine (**153**) (34 mg, 1.2 eq) was added. The solution was allowed to stir overnight at room temperature. Once complete by TLC, the reaction was diluted with EtOAc (50 ml) and washed with saturated sodium bicarbonate solution (2 \times 50 ml) and brine (2 \times 50 ml). The organic layer was dried over sodium sulphate and concentrated *in vacuo*. The residue was purified using silica column chromatography, eluted with 0-100 % EtOAc in hexane, to yield the product as a red gum (43 mg, 42 %). **LCMS (M+H)⁺** found 391.2, requires 391.3, RT 2.19 min; **HRMS EI (M)⁺** found 390.2680, C₂₆H₃₄N₂O requires 390.2671; **δ_{H} (300 MHz, CDCl₃)** 1.05 (6H, s, C11(CH₃)₂), 1.50 (2H, m, C12H₂), 1.63 (2H, m, C13H₂), 1.74 (3H, s, C3CH₃), 2.02 (3H, s, C7CH₃), 2.04 (2H, t, *J* = 6 Hz, C14H₂), 2.43 (3H, s, C15CH₃), 3.65 (2H, br s, NH₂), 5.79 (1H, s, C2H), 6.18 (4H, m, C4-, C6-, C8-, C9-H), 6.67 (2H, d, *J* = 8.7 Hz, C3'-, C5'-H), 6.98 (1H, m, C5-H), 7.03 (1H, s, NH), 7.35 (2H, d, *J* = 8.7 Hz, C2'-, C6'-H); **δ_{C} (125 MHz; CDCl₃)** 12.92 (C3CH₃), 13.64 (C7CH₃), 19.25 (C13), 21.81 (C15CH₃), 28.99 (C11(CH₃)₂), 33.12 (C14), 34.28 (C11), 39.60 (C12), 115.44 (C3', C5'), 121.84 (C2), 121.91 (C2', C6'), 128.27 (C5), 129.69 (C9), 129.77 (C1'), 129.86 (C15), 129.88 (C6), 135.69 (C4), 137.36 (C8), 137.75 (C7), 138.87 (C10), 143.09 (C4'), 149.54 (C3), 165.17 (C1); **IR (cm⁻¹)** 3429, 3320, 2939, 1626, 1510, 969, 839, 515.

(2E,4E,6E,8E)-3,7-dimethyl-N-phenyl-9-(2,6,6-trimethylcyclohex-1-enyl)nona-2,4,6,8-tetraenamide (61)



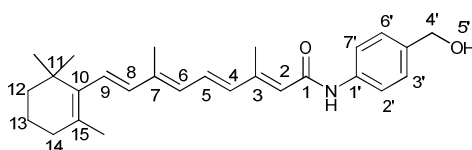
The mixed anhydride (**148**) (17.8 mg, 1 eq) was dissolved in DCM (3 ml) and pyridine (200 μ l) at room temperature and aniline (**149**) (1 ml, 4.2 eq) was added. The solution was allowed to stir overnight at room temperature. Once complete by TLC, the reaction was diluted with EtOAc (50 ml) and washed with saturated sodium bicarbonate solution (2 \times 50 ml) and brine (2 \times 50 ml). The organic layer was dried over sodium sulphate and concentrated *in vacuo*. The residue was purified using silica column chromatography, eluted with 0-100 % EtOAc in hexane, to yield the product as a yellow solid (5.2 mg, 30 %). **LCMS (2M+Na)⁺** found 774.0 requires 773.5, RT 2.45 min; **HRMS ESI (M+H)⁺** found 376.2648, C₂₆H₃₄NO requires 376.2635; **δ_{H} (500 MHz, CDCl₃)** 1.04 (6H, C11(CH₃)₂), 1.46 (2H, m, C12H₂), 1.57 (2H, m, C13H₂), 1.65 (3H, s, C15CH₃), 1.85 (3H, s, C3CH₃), 2.95 (2H, m, C14H₂), 2.34 (3H, s, C7CH₃), 5.74 (1H, s, C2H), 6.23 (4H, m, C4-, C6-, C8-, C9-H), 6.90 (1H, m, C5H), 7.00 (1H, t, *J* = 7.5 Hz, C4'H), 7.23 (2H, t, *J* = 7.5 Hz, C3'-, C5'-H), 7.48 (2H, d, *J* = 7.5 Hz, C2'-, C6'-H). **δ_{C} (125 MHz, CDCl₃)** 12.91 (C₃CH₃), 13.73 (C7CH₃), 19.24 (C13), 21.76 (C15CH₃), 28.97 (C11(CH₃)₂), 33.12 (C14), 34.28 (C11), 39.63 (C12), 119.79 (C2), 121.35 (C5), 124.07 (C9), 128.51 (C4'), 128.96(C2', C6'), 129.55 (C3', C5'), 129.93 (C15), 130.40 (C6), 135.34 (C4), 137.30 (C8), 137.75 (C7), 138.32 (C10), 139.25 (C1'), 150.58 (C3), 165.35 (C1); **IR (cm⁻¹)** 3306, 2822, 1649, 1596, 1511, 1436, 1154, 965, 749, 690; **MP** 120-122 °C.

(2E,4E,6E,8E)-N-(2-fluoro-4-hydroxyphenyl)-3,7-dimethyl-9-(2,6,6-trimethylcyclohex-1-enyl)nona-2,4,6,8-tetraenamide (70)



The mixed anhydride (**148**) (100 mg, 1 eq) was dissolved in DCM (2 ml) and pyridine (200 μ L) at room temperature and 4-amino-2-fluorophenol (**185**) (40 mg, 1.2 eq) was added. The solution was allowed to stir overnight at room temperature. Once complete by TLC, the reaction was diluted with EtOAc (50 ml) and washed with saturated sodium bicarbonate solution (3 \times 50 ml) and brine (3 \times 50 ml). The organic layer was dried over sodium sulphate and concentrated *in vacuo*. The residue was purified using Biotage silica column chromatography, eluted with 0-100 % EtOAc in hexane, to yield the product as a yellow solid (43 mg, 40 %). **LCMS (2M+Na)⁺** found 841.6, requires 841.5, RT 2.63 min; **HRMS ESI (M+H)⁺** found 410.2494, C₂₆H₃₃FNO₂ requires 410.2490; δ_{H} (500 MHz, CDCl₃) 0.96 (6H, s, C11(CH₃)₂), 1.39 (2H, m, C12H₂), 1.55 (2H, m, C13H₂), 1.64 (3H, s, C3CH₃), 1.92 (3H, s, C7CH₃), 1.95 (2H, m, C14H₂), 2.32 (3H, s, C15CH₃), 5.69 (1H, s, C2H), 5.91 (1H, s, OH), 6.14 (5H, m, C4-, C5-, C6-, C8-, C9-H), 6.85 (3H, m, C2'-, C5', C6'-H), 7.47 (1H, s, NH); δ_{C} (75 MHz; CDCl₃) 12.94 (C3CH₃), 13.77 (C7CH₃), 19.23 (C13), 21.80 (C15CH₃), 28.98 (C11(CH₃)₂), 33.13 (C14), 34.27 (C11), 39.59 (C12), 108.94 (C2'), 109.24 (C5'), 116.67 (C6'), 117.34 (C2), 120.88 (C1'), 128.59 (C5), 129.54 (C9), 130.00 (C15), 130.64 (C6), 137.22 (C4), 137.29 (C8), 137.71 (C7), 139.45 (C10), 149.13 (C4'), 150.97 (C3), 152.28 (C3'), 165.58 (C1); **IR (cm⁻¹)** 3313, 2924, 1608, 1511, 1187, 963; **MP** 118-120 °C.

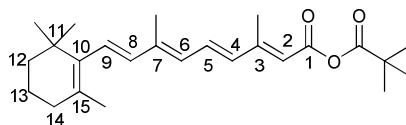
(2E,4E,6E,8E)-N-(4-(hydroxymethyl)phenyl)-3,7-dimethyl-9-(2,6,6-trimethylcyclohex-1-enyl)nona-2,4,6,8-tetraenamide (72)



The mixed anhydride (**148**) (50.2 mg, 1 eq) was dissolved in DCM (3 ml) and pyridine (200 μ l) at room temperature and 4-aminobenzylalcohol (**163**) (20.3

mg, 1.3 eq) was added. The solution was allowed to stir overnight at room temperature. Once complete, the reaction was diluted with EtOAc (50 ml) and washed with saturated sodium bicarbonate solution (2 × 50 ml) and brine (2 × 50 ml). The organic layer was dried over sodium sulphate and concentrated *in vacuo*. The residue was purified using Biotage silica column chromatography, eluted with 0-100 % EtOAc in hexane, to yield the product as a yellow solid (28 mg, 53 %). **LCMS (2M+Na)⁺** found 833.5, requires 833.5, RT 2.52 min; **HRMS ESI (M+H)⁺** found 406.2741, C₂₇H₃₆NO₂ requires 406.2741; **δ_H (500 MHz, CDCl₃)** 1.02 (6H, s, C11(CH₃)₂), 1.45 (2H, m, C12H₂), 1.56 (2H, m, C13H₂), 1.69 (3H, s, C15CH₃), 1.98 (3H, m, C3CH₃), 2.05 (2H, m, C14H₂), 2.36 (3H, m, C7CH₃), 4.44 (2H, d, *J* = 5.4 Hz, C4'CH₂), 5.08 (1H, t, *J* = 5.4 Hz, OH), 6.04 (1H, s, C2H), 6.29 (4H, m, C4-, C6-, C8-, C9-H), 6.99 (1H, m, C5-H), 7.24 (2H, d, *J* = 8.4 Hz, C3'-, C6'-H), 7.61 (2H, d, *J* = 8.4 Hz, C2'-, C7'-H), 9.95 (1H, s, NH); **δ_C (125 MHz, CDCl₃)** 12.54 (C3), 13.22 (C7), 18.71 (C13), 21.46 (C15CH₃), 28.75(C11(CH₃)₂), 32.57 (C14), 33.81 (C11), 39.21 (C12), 62.65 (C4'CH₂), 118.61 (C2), 122.71 (C5), 126.86 (C2', C6'), 127.43 (C9), 129.29 (C15), 129.67 (C3', C5'), 130.06 (C6), 135.97 (C4), 136.96 (C8), 137.09 (C1'), 137.15 (C4'), 137.23 (C7), 138.13 (C10), 148.17 (C3), 164.62 (C1); **IR (cm⁻¹)** 3300, 2920, 2854, 1649, 1598, 1522, 1159, 965, 824; **MP** 163-166 °C.

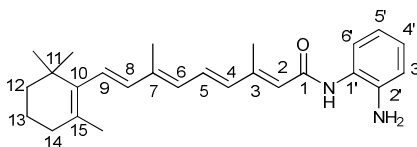
(2E,4E,6E,8E)-3,7-dimethyl-9-(2,6,6-trimethylcyclohex-1-enyl)nona-2,4,6,8-tetraenoic pivalic anhydride (148)



This compound was synthesised as previously described by Cabaj *et al.*²¹¹ Retinoic acid (**6**) (500 mg, 1 eq) and triethylamine (280 μl, 2.3 eq) were dissolved in ethyl acetate (10 ml) at -5 °C. Trimethyl acetyl chloride (**147**) (250 μl, 1.2 eq) was slowly added and the mixture was allowed to warm to room temperature and stirred for 1 hour. The reaction was monitored by LCMS and when complete, diluted with EtOAc (50 ml), washed with 20 % HCl (2 × 50 ml) and saturated sodium bicarbonate solution (2 × 50 ml). The organic layer was dried over sodium sulphate and concentrated *in vacuo*.

The mixture was purified using a silica flash column chromatography plug with 20 % ethyl acetate and hexane. The pure compound was obtained as a yellow oil (640 mg, 100 %). The compound was not ionised by LCMS; δ_{H} (500 MHz, CDCl_3) 1.05 (6H, s, $\text{C11}(\text{CH}_3)_2$), 1.28 (9H, s, $\text{C}(\text{CH}_3)_3$), 1.49 (2H, m, C12H_2), 1.64 (2H, m, C13H_2), 1.73 (3H, s, C15CH_3), 2.04 (3H, s, C3CH_3), 2.05 (2H, m, C14H_2), 2.42 (3H, s, C7CH_3), 5.75 (1H, s, C2H), 6.15 (2H, m, $\text{C8-}, \text{C9-H}$), 6.34 (2H, m, $\text{C4-}, \text{C6-H}$), 7.14 (1H, m, C5H); δ_{C} (125 MHz, CDCl_3) 13.01 (C3CH_3), 14.43 (C7CH_3), 19.21 (C13), 21.76 (C15CH_3), 26.64 ($\text{C}(\text{CH}_3)_3$), 28.97 ($\text{C11}(\text{CH}_3)_2$), 33.15 (C14), 34.28 (C11), 39.62 ($\text{C}(\text{CH}_3)_3$), 39.72 (C12), 116.32 (C2), 129.26 (C5), 129.70 (C9), 130.43 (C6), 133.31 (C15), 134.24 (C4), 137.09 (C7), 137.66 (C8), 141.39 (C10), 158.51 (C3), 162.37 (C1), 174.75 (OCO).

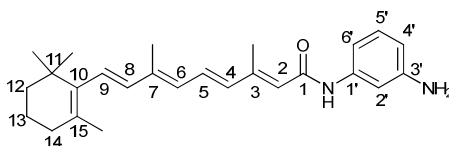
(2E,4E,6E,8E)-N-(2-aminophenyl)-3,7-dimethyl-9-(2,6,6-trimethylcyclohex-1-enyl)nona-2,4,6,8-tetraenamide (156)



The mixed anhydride (**148**) (100 mg, 1 eq) was dissolved in DCM (2 ml) and pyridine (200 μL) at room temperature and *ortho*-phenylenediamine (**154**) (34 mg, 1.2 eq) was added. The solution was allowed to stir overnight at room temperature. Once complete by TLC, the reaction was diluted with EtOAc (50 ml) and washed with saturated sodium bicarbonate solution (2 \times 50 ml) and brine (2 \times 50 ml). The organic layer was dried over sodium sulphate and concentrated *in vacuo*. The residue was purified using Biotage silica column chromatography, eluted with 0-100 % EtOAc in hexane, to yield the product as a yellow solid (30 mg, 28 %). LCMS ($2\text{M}+\text{Na}$)⁺ found 803.6, requires 803.5, RT 2.57 min; HRMS ESI ($\text{M}+\text{H}$)⁺ found 391.2750, $\text{C}_{26}\text{H}_{35}\text{N}_2\text{O}$ requires 391.2744; δ_{H} (500 MHz, CDCl_3) 1.96 (6H, s, $\text{C11}(\text{CH}_3)_2$), 1.40 (2H, m, C12H_2), 1.49 (2H, m, C13H_2), 1.65 (3H, s, C3CH_3), 1.93 (3H, s, C7CH_3), 1.95 (2H, m, C14H_2), 2.33 (3H, s, C15CH_3), 3.66 (2H, br s, NH_2), 5.78 (1H, s, C2H), 6.17 (4H, m, $\text{C4-}, \text{C6-}, \text{C8-}, \text{C9-H}$), 6.72 (2H, m, $\text{C3'-}, \text{C5'-H}$), 6.90 (1H, m, C5-H), 6.97 (1H, m, C6'-H), 7.13 (1H, m, C4'-H), 7.35 (1H, s, NH); δ_{C} (75 MHz; CDCl_3) 12.92 (C3CH_3), 13.73 (C7CH_3), 19.23 (C13), 21.79 (C15CH_3),

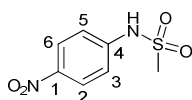
28.98 (C11(CH₃)₂), 33.12 (C14), 34.28 (C11), 39.59 (C12), 119.10 (C2'), 120.54 (C4'), 121.04 (C6'), 125.28 (C2), 125.71 (C15), 126.92 (C5), 128.52 (C9), 129.59 (C5'), 129.96 (C1'), 130.54 (C6), 135.41 (C4), 137.33 (C8), 137.72 (C7), 138.15 (C10), 139.30 (C3'), 150.96 (C3), 165.90 (C1); **IR (cm⁻¹)** 2915, 1655, 1580, 1509, 1449, 1157, 966, 746; **MP** 131-133 °C.

(2E,4E,6E,8E)-N-(3-aminophenyl)-3,7-dimethyl-9-(2,6,6-trimethylcyclohex-1-enyl)nona-2,4,6,8-tetraenamide (157)



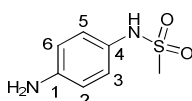
The mixed anhydride (**148**) (100 mg, 1 eq) was dissolved in DCM (2 ml) and pyridine (200 μ L) at room temperature and *meta*-phenylenediamine (**155**) (34 mg, 1.2 eq) was added. The solution was allowed to stir overnight at room temperature. Once complete by TLC, the reaction was diluted with EtOAc (50 ml) and washed with saturated sodium bicarbonate solution (2 \times 50 ml) and brine (2 \times 50 ml). The organic layer was dried over sodium sulphate and concentrated *in vacuo*. The residue was purified using Biotage silica column chromatography, eluted with 0-100 % EtOAc in hexane, to yield the product as a yellow solid (36 mg, 35 %). **LCMS (M+H)⁺** found 391.3, requires 391.3, RT 2.49 min; **HRMS ESI (M+H)⁺** found 391.2753, C₂₆H₃₄N₂O requires 391.2744; **δ _H (500 MHz, CDCl₃)** 0.96 (6H, s, C11(CH₃)₂), 1.41 (2H, m, C12H₂), 1.55 (2H, m, C13H₂), 1.64 (3H, s, C3CH₃), 1.92(3H, s, C7CH₃), 1.95 (2H, m, C14H₂), 2.33 (3H, s, C15CH₃), 5.71 (1H, s, C2H), 6.17 (4H, m, C4-, C6-, C8-, C9-H), 6.33 (1H, d, *J* = 7.8 Hz, C6'-H), 6.62 (1H, d, *J* = 7.8 Hz, C4'-H), 6.88 (1H, m, C5-H), 6.98 (1H, t, *J* = 7.8 Hz, C5'-H), 7.16 (1H, br s, NH), 7.25 (1H, s, C2'-H); **δ _C (75 MHz; CDCl₃)** 12.93 (C3CH₃), 13.70 (C7CH₃), 19.24 (C13), 21.80 (C15CH₃), 28.99 (C11(CH₃)₂), 33.12 (C14), 34.28 (C11), 39.60 (C12), 106.45 (C2'), 109.70 (C4'), 110.89 (C6'), 121.57 (C2), 128.47 (C5), 129.59 (C9), 129.66 (C5'), 129.94 (C15), 130.34 (C6), 135.40 (C4), 137.32 (C8), 137.73 (C7), 139.21 (C1'), 139.36 (C10), 147.21 (C3'), 150.42 (C3), 165.28 (C1); **IR (cm⁻¹)** 3313, 2923, 1604, 1538, 1437, 1155, 964, 686; **MP** 106-108 °C.

***N*-(4-nitrophenyl)methanesulfonamide (159)**



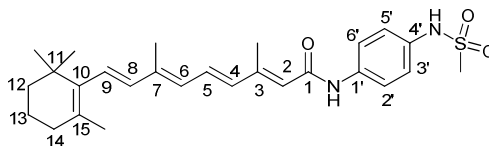
This compound was synthesised as previously described by Lee *et al.*²¹² MsCl (1.6 g, 1 eq) was dissolved in 1:1 pyridine:DCM (15 ml) and the solution was cooled to 0 °C. *para*-nitroaniline (**158**) (1.6 g, 1.2 eq) was added and the reaction was allowed to warm to room temperature and stirred for 3 hours. Solvents were removed under reduced pressure. The residue was re-dissolved in EtOAc (50 ml) and washed with deionised water (3 × 50 ml), saturated sodium bicarbonate solution (3 × 50 ml), CuSO₄ solution (3 × 50 ml) and brine (2 × 50 ml). The organic layer was dried over sodium sulphate and concentrated *in vacuo* to yield the product as a white powder (1.8 g, 72 %). The product was not ionised by LCMS. δ_{H} (500 MHz, CDCl₃) 3.17 (3H, s, CH₃), 7.32 (2H, d, *J* = 9 Hz, C2-, C6-H), 8.27 (2H, d, *J* = 9 Hz, C3-, C5-H).

***N*-(4-aminophenyl)methanesulfonamide (160)**



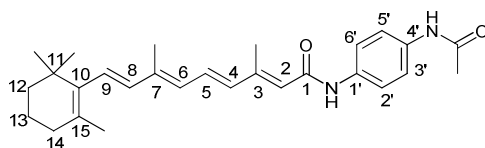
This compound was synthesised as previously described by Lee *et al.*²¹² Compound (**159**) (1.8 g) was dissolved in MeOH (50 ml) to which Pd/C (500 mg) was added. The reaction was allowed to stir under H₂ overnight. The Pd/C was filtered through Celite and the filtrate was concentrated *in vacuo* to yield the product as a white solid (1.6 g, 100 %). LCMS (M-CH₂)⁺ found 173.0, requires 173.0, RT 0.27 min; δ_{H} (500 MHz, CDCl₃) 2.89 (1H, s, CH₃), 4.88 (2H, br s, NH₂), 6.77 (2H, d, *J* = 8.4 Hz, C2-, C6-H), 7.08 (2H, d, *J* = 8.4 Hz, C3-, C5-H).

(2E,4E,6E,8E)-3,7-dimethyl-N-(4-(methylsulfonyl)phenyl)-9-(2,6,6-trimethylcyclohex-1-enyl)nona-2,4,6,8-tetraenamide (171)



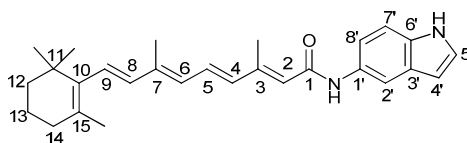
The mixed anhydride (**148**) (100 mg, 1 eq) was dissolved in DCM (2 ml) and pyridine (200 μ L) at room temperature and compound **160** (59 mg, 1.2 eq) was added. The solution was allowed to stir overnight at room temperature. Once complete by TLC, the reaction was diluted with EtOAc (50 ml) and washed with saturated sodium bicarbonate solution (2 \times 50 ml) and brine (2 \times 50 ml). The organic layer was dried over sodium sulphate and concentrated *in vacuo*. The residue was purified using Biotage silica column chromatography eluted with 0-100 % EtOAc in hexane and recrystallised in MeOH to yield the product as a yellow solid (19 mg, 16 %). **LCMS (2M+Na)⁺** found 959.5, requires 959.5, RT 2.58 min; **HRMS ESI (M+H)⁺** found 469.2522, C₂₇H₃₇N₂O₃S requires 469.2519; **δ_{H} (500 MHz, CDCl₃)** 0.95 (6H, s, C11(CH₃)₂), 1.52 (2H, m, C12H₂), 1.67 (2H, m, C13H₂), 1.73 (3H, s, C3CH₃), 2.03 (3H, s, C7CH₃), 2.03 (2H, m, C14H₂), 2.40 (3H, s, C15CH₃), 2.94 (3H, s, SO₂C-H), 6.01 (1H, s, C2H), 6.23 (4H, m, C4-, C6-, C8-, C9-H), 7.08 (1H, m, C5-H), 7.23 (2H, d, *J* = 8.7 Hz, C3'-, C5'-H), 7.59 (2H, d, *J* = 8.7 Hz, C4'-, C6'-H); **δ_{C} (125 MHz; MeOD)** 12.58 (C3CH₃), 13.27 (C7CH₃), 18.71 (C13), 21.49 (C15CH₃), 33.85 (C11(CH₃)₂), 33.85 (C11), 38.90 (C12), 39.61 (SO₂CH₃), 119.85 (C3', C5'), 121.34 (C2', C6'), 122.54 (C2), 127.49 (C5), 129.37 (C1'), 129.81 (C9), 130.07 (C6), 133.15 (C15), 135.94 (C4), 136.17 (C4'), 136.95 (C8), 137.26 (C7), 138.25 (C10), 148.32 (C3), 164.59 (C1); **IR (cm⁻¹)** 3213, 2922, 1571, 1511, 1269, 1123, 961, 729; **MP** 154-156 °C.

(2E,4E,6E,8E)-N-(4-acetamidophenyl)-3,7-dimethyl-9-(2,6,6-trimethylcyclohex-1-enyl)nona-2,4,6,8-tetraenamide (172)



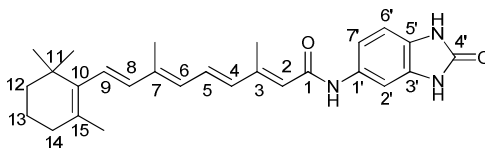
The mixed anhydride (**148**) (200 mg, 1 eq) was dissolved in DCM (3 ml) and pyridine (200 μ L) at room temperature and 4-aminoacetanilide (**162**) (94 mg, 1.2 eq) was added. The solution was allowed to stir overnight at room temperature. Once complete by TLC, the reaction was diluted with EtOAc (50 ml) and washed with saturated sodium bicarbonate solution (2 \times 50 ml) and brine (2 \times 50 ml). The organic layer was dried over sodium sulphate and concentrated *in vacuo*. The residue was purified using Biotage silica column chromatography, eluted with 0-100 % EtOAc in hexane, to yield the product as a yellow solid (93 mg, 41 %). **LCMS (2M+Na)⁺** found 887.8, requires 887.5, RT 2.53 min; **HRMS ESI (M+H)⁺** found 433.2858, C₂₈H₃₇N₂O₂ requires 433.2850; δ_{H} (**500 MHz, CDCl₃**) 1.02 (6H, s, C11(CH₃)₂), 1.45 (2H, m, C12H₂), 1.57 (2H, m, C13H₂), 1.69 (3H, s, C3CH₃), 1.98 (3H, s, C7-H), 2.00 (2H, m, C14H₂), 2.01 (3H, s, COCH₃), 1.34 (3H, s, C7CH₃), 6.01 (3H, s, C15CH₃), 6.29 (4H, m, C4-, C6-, C8-, C9-H), 6.98 (1H, m, C5-H), 7.48 (2H, d, *J* = 8.7 Hz, C3'-, C5'-H), 7.55 (2H, d, *J* = 8.7 Hz, C2'-, C6'-H), 9.85 (1H, s, C4'-NH), 9.93 (1H, s, C1-NH); δ_{C} (**75 MHz; DMSO-d₆**) 12.55 (C3CH₃), 13.21 (C7CH₃), 18.69 (C13), 21.48 (C15CH₃), 23.83 (COCH₃), 28.77 (C11(CH₃)₂), 32.58 (C14), 33.82 (C11), 40.31 (C12), 119.30 (C2', C3', C5', C6'), 122.69 (C2), 127.42 (C5), 129.33 (C15), 129.66 (C9), 130.08 (C6), 134.63 (C1'), 134.75 (C4'), 145.99 (C4), 136.95 (C8), 137.24 (C7), 138.14 (C10), 148.03 (C3), 164.44(C1), 167.68 (CO); **IR (cm⁻¹)** 3299, 2919, 2859, 1661, 1518, 963; **MP** 235-238 °C.

(2E,4E,6E,8E)-N-(1H-indol-5-yl)-3,7-dimethyl-9-(2,6,6-trimethylcyclohex-1-enyl)nona-2,4,6,8-tetraenamide (173)



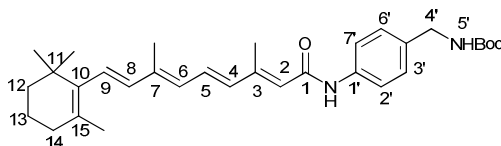
The mixed anhydride (**148**) (100 mg, 1 eq) was dissolved in DCM (3 ml) and pyridine (200 μ L) at room temperature and 5-aminoindole (**164**) (41 mg, 1.2 eq) was added. The solution was allowed to stir overnight at room temperature. Once complete by TLC, the reaction was diluted with EtOAc (50 ml) and washed with saturated sodium bicarbonate solution (2 \times 50 ml) and brine (2 \times 50 ml). The organic layer was dried over sodium sulphate and concentrated *in vacuo*. The residue was purified using Biotage silica column chromatography, eluted with 0-100 % EtOAc in hexane, to yield the product as a yellow solid (8 mg, 7 %) **LCMS (2M+Na)⁺** found 851.4, requires 851.5, RT 2.66 min; **HRMS ESI (M+H)⁺** found 415.2752, C₂₈H₃₅N₂O requires 415.2744; δ_{H} (**500 MHz, CDCl₃**) 1.09 (6H, s, C11(CH₃)₂), 1.51 (2H, m, C12H₂), 1.58 (2H, m, C13H₂), 1.81 (3H, s, C3CH₃), 2.02 (3H, s, C7CH₃), 2.06 (2H, m, C14H₂), 2.46 (3H, s, C15CH₃), 5.87 (1H, s, C2H), 6.17 (4H, m, C4-, C6-, C8-, C9-H), 6.32 (1H, s, C2'-H), 6.98 (1H, m, C5-H), 7.16 (1H, s, C4'-H), 7.44 (1H, s, C5'-H), 7.91 (1H, s, C7'-H), 8.41 (1H, s, C8'-H); δ_{C} (**125 MHz; CDCl₃**) 12.86 (C3CH₃), 13.65 (C7CH₃), 19.22 (C13), 21.72 (C15CH₃), 28.94 (C11(CH₃)₂), 33.09 (C14), 34.25 (C11), 39.60 (C12), 102.48 (C4'), 102.55 (C2'), 111.14 (C8'), 112.31 (C7'), 116.12 (C5'), 121.94 (C2), 125.18 (C1'), 127.98 (C5), 128.26 (C9), 129.54 (C3'), 129.63 (C9), 129.82 (C6'), 129.89 (C6), 130.57 (C15), 135.62 (C4), 137.34 (C8), 137.75 (C7), 138.86 (C10), 149.51 (C3), 165.48 (C31); **IR (cm⁻¹)** 3401, 3268, 2925, 1645, 1539, 1471, 968; **MP** 155-157 °C.

(2E,4E,6E,8E)-3,7-dimethyl-N-(2-oxo-2,3-dihydro-1H-benzo[d]imidazol-5-yl)-9-(2,6,6-trimethylcyclohex-1-enyl)nona-2,4,6,8-tetraenamide (174)



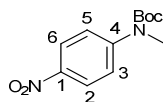
The mixed anhydride (**148**) (53 mg, 1 eq) was dissolved in DCM (3 ml) and pyridine (200 μ L) at room temperature and 5-aminobenzimidazolinone (**165**) (25 mg, 1.2 eq) was added. The solution was allowed to stir overnight at room temperature. Once complete by TLC, the reaction was diluted with EtOAc (50 ml) and washed with saturated sodium bicarbonate solution (2 \times 50 ml) and brine (2 \times 50 ml). The organic layer was dried over sodium sulphate and concentrated *in vacuo*. The residue was purified using silica column chromatography, eluted with 0-40 % EtOAc in hexane, to yield the product as a yellow solid (7 mg, 11 %). **LCMS (M+H)⁺** found 432.2, requires 432.3, RT 2.39 min; **HRMS ESI (M-H)⁺** found 430.2491, C₂₇H₃₂N₃O₂ requires 430.2489; δ_{H} (**500 MHz, CDCl₃**) 0.98 (6H, s, C11(CH₃)₂), 1.41 (2H, m, C12H₂), 1.52 (2H, m, C13H₂), 1.62 (3H, s, C3CH₃), 1.91 (3H, s, C7CH₃), 1.95 (2H, m, C14H₂), 2.29 (3H, s, C15CH₃), 5.90 (1H, s, C2H), 6.22 (4H, m, C4-, C6-, C8-, C9-H), 6.87 (1H, d, *J* = 8.4 Hz, C6'-H), 9.96 (1H, m, C5-H), 6.98 (1H, d, *J* = 8.4 Hz, C7'-H), 7.49 (1H, s, C2'-H).); δ_{C} (**125 MHz; CDCl₃**) 12.93 (C3CH₃), 13.99 (C7CH₃), 20.39 (C13), 22.00 (C15CH₃), 29.49 (C11(CH₃)₂), 34.06 (C14), 35.32 (C11), 40.85 (C12), 103.52 (C6'), 110.25 (C2'), 115.10 (C7'), 123.13 (C2), 127.44 (C15), 129.27 (C5), 130.65 (C3'), 131.02 (C1'), 131.13 (C9), 131.18 (C6), 134.66 (C5'), 137.11 (C4), 139.09 (C8), 139.17 (C7), 139.88 (C10), 150.85 (C3), 158.38 (C4'), 167.77 (C1); **IR (cm⁻¹)** 2934, 1736, 1505, 1363, 1193, 966, 714; **MP** 223-226 °C.

***tert*-butyl 4-((2*E*,4*E*,6*E*,8*E*)-3,7-dimethyl-9-(2,6,6-trimethylcyclohex-1-enyl)nona-2,4,6,8-tetraenamido)benzylcarbamate (175)**



The mixed anhydride (**148**) (50.2 mg, 1 eq) was dissolved in DCM (3 ml) and pyridine (200 μ l) at room temperature and 4-[(N-Boc)aminomethyl]aniline (**166**) (35 mg, 1.2 eq) was added. The solution was allowed to stir overnight at room temperature. Once complete, the reaction was diluted with EtOAc (50 ml) and washed with saturated sodium bicarbonate solution (2 \times 50 ml) and brine (2 \times 50 ml). The organic layer was dried over sodium sulphate and concentrated *in vacuo*. The residue was purified using silica column chromatography, eluted with 0-100 % EtOAc in hexane, to yield the product as a yellow solid (22 mg, 33 %). **LCMS (M+H)⁺** found 505.5, requires 505.3, RT 2.51 min; **HRMS ESI (M+H)⁺** found 505.3426, C₃₂H₄₅N₂O₃ requires 505.3430; δ_{H} (500 MHz, CDCl₃): 1.04 (6H, s, C11CH₃), 1.39 (9H, s, (CH₃)₃), 1.42 (2H, m, C12H₂), 1.55 (2H, m, C13H₂), 1.68 (3H, s, C15CH₃), 1.89 (3H, s, C3CH₃), 1.93 (2H, m, C14H₂), 2.35 (3H, s, C7CH₃), 4.19 (2H, d, *J* = 5.4 Hz, C4'H₂), 4.76 (1H, s, OH), 5.73 (1H, s, C2H), 6.09 (4H, m, C4-, C5-, C8-, C9-H), 6.92 (1H, m, C6-H), 7.12 (2H, d, *J* = 7.5 Hz, C3'-, C6'-H), 7.43 (2H, d, *J* = 7.5 Hz, C2'-, 7'-H); **IR (cm⁻¹)** 3320, 3124, 2927, 1696, 1652, 1601, 1391, 1361, 1254, 1167, 1027, 966, 827, 729, 509; **MP** 69-71 °C.

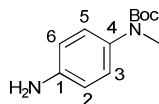
***tert*-butyl methyl(4-nitrophenyl)carbamate (181)**



N-methyl-4-nitroaniline (**180**) (500 mg, 1 eq) was dissolved in anhydrous THF (20 ml) and Boc anhydride (860 mg, 1.2 eq) was added slowly, followed by DMAP (482 mg, 1.2 eq). The mixture was stirred for 4 h at room temperature until the reaction was seen to be complete by TLC. The volatiles were removed *in vacuo* and the residue was washed with 20 % HCl (2 \times 50 ml) and saturated sodium bicarbonate solution (2 \times 50 ml) in EtOAc (50 ml). The organic layer was dried over sodium sulphate and concentrated *in vacuo*

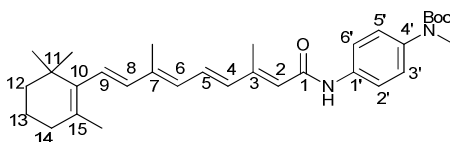
to yield the product as a light brown solid (667 mg, 80 %). The product was not ionised by LCMS. δ_{H} (500 MHz, CDCl_3) 1.48 (9H, s, $\text{C}(\text{CH}_3)_3$), 3.32 (3H, s, CH_3), 7.44 (2H, d, $J = 9.2$ Hz, C3-, 5-H), 6.15 (2H, d, $J = 9.2$ Hz, C2-, 6-H).

***tert*-butyl 4-aminophenyl(methyl)carbamate (182)**



This compound was synthesised as previously described by Martini *et. al.*²¹³ Compound (**181**) (755 mg) and Pd/C (100 mg) were dissolved in MeOH (10 ml). The reaction was allowed to stir under H_2 overnight. The Pd/C was filtered through Celite and the filtrate was concentrated *in vacuo* to yield the product as a light brown solid (667 mg, 100 %) LCMS ($2\text{M}+\text{Na}$)⁺ found 467.2, requires 467.3, RT 1.57 min; δ_{H} (500 MHz, CDCl_3) 1.36 (9H, s, $\text{C}(\text{CH}_3)_3$), 3.09 (3H, s, CH_3), 4.52 (2H, br s, NH_2), 6.58 (2H, d, $J = 5.4$ Hz, C2-, 6-H), 6.88 (2H, d, $J = 5.4$ Hz, C3-, 5-H).

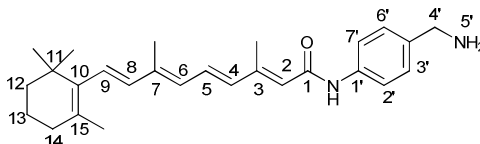
***tert*-butyl 4-((2*E*,4*E*,6*E*,8*E*)-3,7-dimethyl-9-(2,6,6-trimethylcyclohex-1-enyl)nona-2,4,6,8-tetraenamido)phenyl(methyl)carbamate (183)**



The mixed anhydride (**148**) (200 mg, 1 eq) was dissolved in DCM (3 ml) and pyridine (200 μL) at room temperature and compound **182** (139 mg, 1.2 eq) was added. The solution was allowed to stir overnight at room temperature. Once complete by TLC, the reaction was diluted with EtOAc (50 ml) and washed with saturated sodium bicarbonate solution (2 \times 50 ml) and brine (2 \times 50 ml). The organic layer was dried over sodium sulphate and concentrated *in vacuo*. The residue was purified using silica column chromatography, eluted with 0-100 % EtOAc in hexane, to yield the product as a yellow solid (136 mg, 52 %). The compound was not ionised by LCMS. δ_{H} (300 MHz, CDCl_3) 0.96 (9H, s, $\text{C}(\text{CH}_3)_3$), 1.38 (6H, s, $\text{C11}(\text{CH}_3)_2$), 1.41 (2H, m, C12H_2), 1.54 (2H, m, C13H_2), 1.64 (3H, s, C3CH_3), 1.92 (3H, s, C7CH_3), 1.95 (2H, t, $J = 6$ Hz, C14H_2), 2.33 (3H, s, C15CH_3), 3.13 (3H, s,

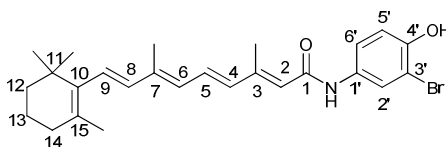
NCH₃), 5.75 (1H, s, C2H), 6.11 (4H, m, C4-, C6-, C8-, C9-H), 6.89 (1H, m, C5-H), 7.04 (2H, d, *J* = 8.7 Hz, C3'-, C5'-H), 7.40 (2H, d, *J* = 8.7 Hz, C2'-, C6'-H), 7.80 (1H, s, NH).

(2E,4E,6E,8E)-N-(4-(aminomethyl)phenyl)-3,7-dimethyl-9-(2,6,6-trimethylcyclohex-1-enyl)nona-2,4,6,8-tetraenamide (184)



TFA (1 ml) was added to a stirred solution of Boc-protected retinoic 4-aminobenzylamide (**175**) (56.6 mg, 1.1 mmol) in DCM (5 ml) for 1 h. The progress of the reaction was monitored by LCMS and once complete the DCM was removed *in vacuo* to afford the pure product as a yellow oil (44.8 mg, 98.9 %). **LCMS (M+H)⁺** found 405.3, requires 405.3; δ_{H} (500 MHz, CDCl₃) 1.17 (6H, s, C11CH₃), 1.50 (2H, m, C12H₂), 1.61 (2H, m, C13H₂), 1.72 (2H, m, C14H₂), 2.52 (3H, s, C15CH₃), 3.35 (3H, s, C3CH₃), 4.30 (2H, m, C4'H₂), 5.77 (1H, s, C2H), 6.05 (5H, m, C4-, C5-, C6-, C8-, C9-H), 7.29 (4H, m, C2'-, C3'-, C6', C7'-H), 8.14 (2H, s, NH₂), 10.21 (1H, s, NH); IR (cm⁻¹) 3392, 2928, 1650, 1439, 1289, 1140, 1019, 952, 707, 616.

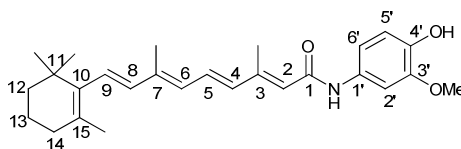
(2E,4E,6E,8E)-N-(3-bromo-4-hydroxyphenyl)-3,7-dimethyl-9-(2,6,6-trimethylcyclohex-1-enyl)nona-2,4,6,8-tetraenamide (191)



The mixed anhydride (**148**) (100 mg, 1 eq) was dissolved in DCM (3 ml) and pyridine (200 μ L) at room temperature and 4-amino 2-bromophenol (**186**) (59 mg, 1.2 eq) was added. The solution was allowed to stir overnight at room temperature. Once complete by TLC, the reaction was diluted with EtOAc (50 ml) and washed with saturated sodium bicarbonate solution (2 \times 50 ml) and brine (2 \times 50 ml). The organic layer was dried over sodium sulphate and concentrated *in vacuo*. The residue was purified using Biotage silica column chromatography, eluted with 0-100 % EtOAc in hexane, to yield the product as a yellow solid (33 mg, 27 %). The compound was not ionised by LCMS.

HRMS ESI (M+H)⁺ found 470.1699, C₂₆H₃₃BrNO₂ requires 470.1689; **δ_H (500 MHz, CDCl₃)** 1.07 (6H, s, C11(CH₃)₂), 1.50 (2H, m, C12H₂), 1.58 (2H, m, C13H₂), 1.70 (3H, s, C15CH₃), 2.01 (3H, s, C3H₃), 2.04 (2H, m, C14H₂), 2.46 (3H, s, C7CH₃), 5.78 (1H, s, C2H), 6.17 (2H, m, C4-, C6-H), 6.31 (2H, m, C8-, C9-H), 6.99 (1H, d, *J* = 9 Hz, C5'H), 7.04 (1H, m, C5H), 7.08 (1H, s, C2'H), 7.25 (1H, d, *J* = 9 Hz, C6'H), 7.97 (1H, s, NH); **δ_C (75 MHz; CDCl₃)** 12.94 (C3CH₃), 13.95 (C7CH₃), 20.34 (C13), 22.02 (C15CH₃), 29.47 (C11(CH₃)₂), 34.01 (C14), 35.28 (C11), 40.76 (C12), 110.44 (C3'), 116.99 (C5'), 121.74 (C2), 122.78 (C6'), 125.96 (C2'), 129.24 (C5), 130.61 (C15), 131.09 (C9), 131.27 (C6), 133.19 (C1'), 137.00 (C4), 139.06 (C8), 139.10 (C7), 139.91 (C10), 151.07 (C3), 151.95 (C4'), 167.57 (C1); **IR (cm⁻¹)** 2924, 2498, 2346, 1625, 1492, 1380, 1282, 958, 814; **MP** 193-196 °C.

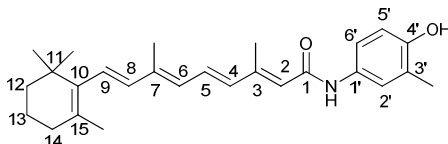
(2E,4E,6E,8E)-N-(4-hydroxy-3-methoxyphenyl)-3,7-dimethyl-9-(2,6,6-trimethylcyclohex-1-enyl)nona-2,4,6,8-tetraenamide (192)



The mixed anhydride (**148**) (200 mg, 1 eq) was dissolved in DCM (4 ml) and pyridine (200 μL) at room temperature and compound (**188**) (78 mg, 1.2 eq) was added. The solution was allowed to stir overnight at room temperature. Once complete by TLC, the reaction was diluted with EtOAc (50 ml) and washed with saturated sodium bicarbonate solution (2 × 50 ml) and brine (2 × 50 ml). The organic layer was dried over sodium sulphate and concentrated *in vacuo*. The residue was purified using Biotage silica column chromatography, eluted with 0-100 % EtOAc in hexane, to yield the product as a yellow solid (52 mg, 24 %). **LCMS (2M+Na)⁺** found 865.6, requires 865.5, RT 2.60 min; **HRMS ESI (M)⁺** found 422.2692, C₂₇H₃₆NO₃ requires 422.2689; **δ_H (500 MHz, CDCl₃)** 0.96 (6H, s, C11(CH₃)₂), 1.39 (2H, m, C12H₂), 1.54 (2H, m, C13H₂), 1.64 (3H, s, C3CH₃), 1.92 (3H, s, C7CH₃), 1.95 (2H, m, C14H₂), 2.34 (3H, s, C15CH₃), 3.78 (3H, s, OCH₃), 5.51 (1H, br s, OH), 5.72 (1H, s, C2H), 6.14 (4H, m, C4-, C6-, C8-, C9-H), 6.62 (1H, d, *J* = 8.4 Hz, C5'-H), 6.72 (1H, d, *J* = 8.4 Hz, C6'-H), 6.89 (1H, m, C5-H), 7.39 (1H, s, C2'-H), 7.51 (1H, s, NH); **δ_C (75 MHz; CDCl₃)** 12.89 (C3CH₃), 13.68

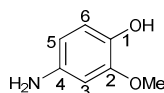
(C7CH₃), 19.23 (C13), 21.74 (C15CH₃), 29.05 (C11(CH₃)₂), 33.11 (C14), 34.27 (C11), 39.61 (C12), 104.61 (OCH₃), 112.42 (C2'), 121.47 (C6'), 128.46 (C5'), 129.54 (C2), 129.90 (C5), 130.25 (C9), 131.33 (C15), 135.38 (C4), 137.29 (C8), 137.73 (1'), 139.16 (C10), 142.26 (C4'), 146.43 (C3), 150.18 (C3'), 165.16 (C1); **IR (cm⁻¹)** 3303, 2923, 1510, 1150, 963; **MP** 119-121 °C.

(2E,4E,6E,8E)-N-(4-hydroxy-3-methylphenyl)-3,7-dimethyl-9-(2,6,6-trimethylcyclohex-1-enyl)nona-2,4,6,8-tetraenamide (193)



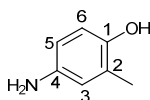
The mixed anhydride (**148**) (195 mg, 1 eq) was dissolved in DCM (5 ml) and pyridine (200 μL) at room temperature and 2-methyl 4-aminophenol (**190**) (77, 1.2 eq) was added. The solution was allowed to stir overnight at room temperature. Once complete, the reaction was diluted with EtOAc (50 ml) and washed with saturated sodium bicarbonate solution (2 × 50 ml) and brine (2 × 50 ml). The organic layer was dried over sodium sulphate and concentrated *in vacuo*. The residue was purified using silica column chromatography eluted with 0-100 % EtOAc in hexane and recrystallised in MeOH to yield the product as a yellow solid (68 mg, 33 %). **LCMS (2M+Na)⁺** found 833.9, requires 833.5, RT 2.62 min; **HRMS ESI (M+Na)⁺** found 428.2557, C₂₇H₃₅NNaO₂ requires 428.2560; **δ_H (500 MHz, CDCl₃)** 0.96 (6H, s, C11(CH₃)₂), 1.41 (2H, m, C12H₂), 1.55 (2H, m, C13H₂), 1.65 (3H, s, C15CH₃), 1.87 (3H, s, C3H₃), 1.96 (2H, m, C14H₂), 2.09 (3H, s, C3'CH₃), 2.34 (3H, s, C7CH₃), 5.71 (1H, s, C2H), 6.14 (4H, m, C4-, C6-, C8-, C9-H), 6.62 (1H, d, *J* = 7.5 Hz, C5'H), 6.90 (1H, app t, *J* = 13 Hz, C5H), 7.06 (1H, s, C2'H), 7.20 (1H, d, *J* = 7.5 Hz, C6'H); **δ_C (125 MHz; CDCl₃)** 12.93 (C3CH₃), 13.74 (C7CH₃), 15.95 (C3'CH₃), 19.23 (C13), 21.79 (C15CH₃), 28.97 (C11(CH₃)₂), 33.12 (C14), 34.27 (C11), 39.59 (C12), 115.24 (C5'), 119.67 (C6'), 121.22 (C2), 123.69 (C2'), 124.58 (C3'), 128.51 (C5), 129.54 (C9), 129.96 (C15), 130.38 (C6), 130.56 (C1'), 135.31 (C4), 137.30 (C8), 137.73 (C7), 139.29 (10), 150.40 (C3), 151.06 (C4'), 165.46 (C1); **IR (cm⁻¹)** 3347, 2921, 1645, 1549, 1416, 1199, 958, 807; **MP** 165-167 °C.

4-amino-2-methoxyphenol (**196**)



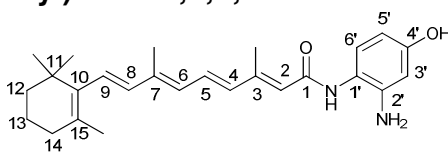
This compound was synthesised as described by Mégnard *et. al.*²¹⁴ 4-nitroguaiacol (**194**) (505 mg) and Pd/C (100 mg) were dissolved in MeOH (10 ml). The reaction was allowed to stir under H₂ overnight. The Pd/C was filtered through Celite and the filtrate was concentrated *in vacuo* to yield the product as a black/brown solid (233 mg, 57 %) **LCMS (M+H)⁺** found 140.0, requires 140.1, RT 0.15 min; **δ_{H} (500 MHz, CDCl₃)** 3.51 (2H, br s, NH₂), 3.62 (3H, s, CH₃), 5.10 (1H, br s, OH), 6.24 (1H, d, *J* = 8.1 Hz, C6-H), 6.32 (1H, s, C2-H), 6.75 (1H, d, *J* = 8.1 Hz, C6-H); **δ_{C} (75 MHz; CDCl₃)** 55.22 (OMe), 100.15 (C3), 105.95 (C5), 116.01 (C6), 137.13 (C1), 141.31 (C4), 147.96 (C2).

4-amino-2-methylphenol (**197**)



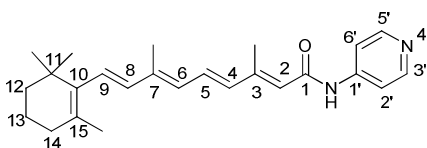
This compound was synthesised as previously described by Mégnard, *et. al.*²¹⁴ 2-Methyl 4-nitrophenol (**195**) (1g) was dissolved in MeOH (10 ml) and Pd/C (50mg) was added as a solution in MeOH. The reaction was stirred under H₂ overnight at room temperature. The Pd/C was filtered and the residue was concentrated *in vacuo* to yield the product as a black/brown solid (837mg, 100 %) **LCMS (M+H)⁺** found 124.0, requires 124.0, RT 0.16 min; **δ_{H} (500 MHz, CDCl₃)** 2.34 (3H, s, CH₃), 6.56 (1H, brs, ArOH), 6.85 (2H, d, *J* = 9 Hz, C2-, C6-H), 8.02 (1H, d, *J* = 9 Hz, C5-H), 8.09 (1H, s, C3-H); **δ_{C} (125 MHz; CDCl₃)** 16.38 (CH₃), 115.39 (C5), 120.43 (C6), 126.30 (C3), 127.10 (C2), 139.93 (C4), 149.57 (C1); **IR (cm⁻¹)** 3355, 3287, 1585, 1468, 1211; **MP** 99-102 °C.

(2E,4E,6E,8E)-N-(2-amino-4-hydroxyphenyl)-3,7-dimethyl-9-(2,6,6-trimethylcyclohex-1-enyl)nona-2,4,6,8-tetraenamide (198)



Compound (**148**) (45 mg) was dissolved in acetic acid (3 ml) and zinc powder (68 mg, 10 eq) was added. The reaction was allowed to stir for 1 h at room temperature and monitored by LCMS. Once complete, zinc was removed by filtration through Celite. The filtrate was diluted with EtOAc (50 ml) and washed with 10 % NaOH solution (3 × 50 ml), saturated sodium bicarbonate solution (3 × 50 ml) and brine (3 × 50 ml). The organic layer was dried over sodium sulphate and concentrated *in vacuo*. The residue was purified using Biotage silica column chromatography, eluted with 0-100 % EtOAc in hexane, to yield the product as a yellow solid (17 mg, 41 %). **LCMS (M+H)⁺** found 407.2, requires 407.3, RT 2.43 min; **HRMS EI (M)⁺** found 407.2693, C₂₆H₃₅N₂O₂ requires 407.2693; **δ_H (500 MHz, CDCl₃)** 1.06 (6H, s, C11(CH₃)₂), 1.49 (2H, m, C12H₂), 1.66 (2H, m, C13H₂), 1.74 (3H, s, C3CH₃), 2.04 (3H, s, C7CH₃), 2.04 (2H, m, C14H₂), 2.13 (3H, s, C15CH₃), 3.41 (2H, br s, NH₂), 5.98 (1H, s, C2H), 6.18 (2H, m, C4-, C6-H), 6.48 (3H, m, C8-, C9-, C5'-H), 6.69 (1H, d, *J* = 8.1 Hz, C6'-H), 7.08 (1H, m, C5-H); **δ_C (125 MHz; CDCl₃)** 12.95 (C3), 14.03 (C7), 19.23 (C13), 21.75 (C15CH₃), 28.97 (C11(CH₃)₂), 33.14 (C14), 34.28 (C11), 39.64 (C12), 109.98 (C3'), 112.61 (C5'), 117.10 (C2), 117.62 (C6'), 128.98 (C9), 129.44 (C6), 130.15 (C1'), 131.65 (C5), 131.93 (C15), 134.94 (C4), 135.84 (7), 137.23 (C8), 137.71 (C10), 140.14 (C2'), 144.44 (C3), 154.86 (C4'), 166.06 (C1); **IR (cm⁻¹)** 3396, 3369, 3207, 2925, 1699, 1515, 1354, 1205, 1025, 878; **MP** 169-173 °C.

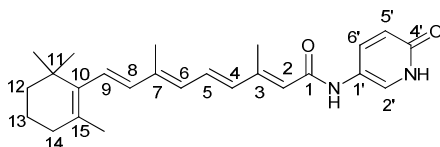
(2E,4E,6E,8E)-3,7-dimethyl-N-(pyridin-4-yl)-9-(2,6,6-trimethylcyclohex-1-enyl)nona-2,4,6,8-tetraenamide (199)



The mixed anhydride (**148**) (200 mg, 1 eq) was dissolved in DCM (4 ml) and pyridine (400 μL) at room temperature and 4-aminopyridine (61 mg, 1.2 eq)

was added. The solution was allowed to stir overnight at room temperature. Once complete by TLC, the reaction was diluted with EtOAc (50 ml) and washed with saturated sodium bicarbonate solution (2 × 50 ml) and brine (2 × 50 ml). The organic layer was dried over sodium sulphate and concentrated *in vacuo*. The residue was purified using Biotage silica column chromatography, eluted with 0-100 % EtOAc in hexane, to yield the product as a yellow solid (72 mg, 37 %). **LCMS (M+H)⁺** found 377.2, requires 377.3, RT 2.35 min; **HRMS ESI (M+H)⁺** found 377.2596, C₂₅H₃₃N₂O requires 377.2587; **δ_H (500 MHz, CDCl₃)** 1.05 (6H, s, C11(CH₃)₂), 1.50 (2H, m, C12H₂), 1.64 (2H, m, C13H₂), 1.73 (3H, s, C3CH₃), 2.02 (3H, s, C7CH₃), 2.06 (2H, m, C14H₂), 2.45 (3H, s, C15CH₃), 5.86 (1H, s, C2H), 6.24 (4H, m, C4-, C6-, C8-, C9-H), 7.05 (1H, m, C5-H), 7.57 (2H, d, *J* = 6 Hz, C2'-, C6'-H), 8.37 (1H, s, NH), 8.48 (2H, d, *J* = 6 Hz, C3'-, C5'-H); **δ_C (75 MHz; CDCl₃)** 13.09 (C3), 14.18 (C7), 20.38 (C13), 22.15 (C15CH₃), 29.57 (C11(CH₃)₂), 34.08 (C14), 35.29 (C11), 40.81 (C12), 114.84 (C2', C6'), 122.40 (C2), 129.62 (C5), 130.80 (C15), 131.02 (C9), 132.20 (C6), 136.70 (C4), 138.89 (C8), 139.03 (C7), 140.57 (C10), 148.59 (C3), 150.60 (C3', C5'), 153.31 (C1'), 168.01 (C1); **IR (cm⁻¹)** 2929, 1588, 1560, 1140, 828; **MP** 111-115 °C.

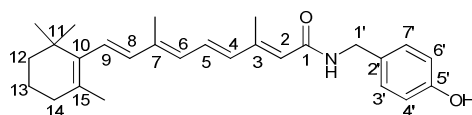
(2E,4E,6E,8E)-N-(6-hydroxypyridin-3-yl)-3,7-dimethyl-9-(2,6,6-trimethylcyclohex-1-enyl)nona-2,4,6,8-tetraenamide (200)



The mixed anhydride (**148**) (200 mg, 1 eq) was dissolved in DCM (4 ml) and pyridine (400 μL) at room temperature and 5-amino 2-hydroxypyridine (70 mg, 1.2 eq) was added. The solution was allowed to stir overnight at room temperature. Once complete by TLC, the reaction was diluted with EtOAc (50 ml) and washed with saturated sodium bicarbonate solution (2 × 50 ml) and brine (2 × 50 ml). The organic layer was dried over sodium sulphate and concentrated *in vacuo*. The residue was purified using Biotage silica column chromatography, eluted with 0-100 % EtOAc in hexane, to yield the product as a yellow solid (97 mg, 48 %). **LCMS (M+H)⁺** found 393.2, requires 393.3, RT 2.37 min; **HRMS ESI (M+H)⁺** found 393.2541, C₂₅H₃₃N₂O₂ requires

393.2537; δ_{H} (500 MHz, CDCl_3) 0.95 (6H, s, $\text{C11}(\text{CH}_3)_2$), 1.40 (2H, m, C12H_2), 1.48 (2H, m, C13H_2), 1.63 (3H, s, C15CH_3), 1.94 (3H, s, C3H_3), 1.88 (2H, m, C14H_2), 2.28 (3H, s, C7CH_3), 5.79 (1H, s, C2H), 6.14 (4H, m, C4-, C6-, C8-, C9-H), 6.31 (1H, d, $J = 7.5$ Hz, C5'H), 6.83 (1H, m, C5H), 7.48 (1H, d, $J = 7.5$ Hz, C6'H), 7.65 (1H, s, C2'H), 8.89 (1H, s, NH); δ_{C} (75 MHz; CDCl_3) 12.93 (C3CH_3), 13.94 (C7CH_3), 20.34 (C13), 22.00 (C15CH_3), 29.46 ($\text{C11}(\text{CH}_3)_2$), 34.01 (C14), 35.27 (C11), 40.79 (C12), 120.73 (C5'), 121.90 (C6'), 123.24 (C15), 126.60 (C2), 129.38 (C2'), 130.67 (C7), 131.02 (C5), 131.59 (C9), 136.81 (C6), 138.93 (C4), 138.97 (C8), 139.08 (C10), 140.14 (C1'), 151.64 (C3), 163.73 (C4'), 167.57 (C1); IR (cm^{-1}) 3271, 2926, 1664, 1607, 1564, 967, 833; MP 95-98 °C.

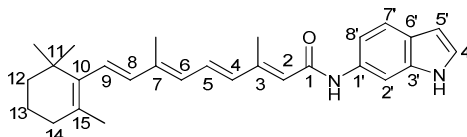
(2E,4E,6E,8E)-N-(4-hydroxybenzyl)-3,7-dimethyl-9-(2,6,6-trimethylcyclohex-1-enyl)nona-2,4,6,8-tetraenamide (201)



The mixed anhydride (**148**) (100 mg, 1 eq) was dissolved in DCM (3 ml) and pyridine (200 μL) at room temperature and 4-hydroxybenzylamine monohydrate (45 mg, 1.2 eq) was added. The solution was allowed to stir overnight at room temperature. Once complete by TLC, the reaction was diluted with EtOAc (50 ml) and washed with saturated sodium bicarbonate solution (2 \times 50 ml) and brine (2 \times 50 ml). The organic layer was dried over sodium sulphate and concentrated *in vacuo*. The residue was purified using Biotage silica column chromatography, eluted with 0-35 % EtOAc in hexane, to yield the product as a yellow solid (13 mg, 12 %) LCMS ($2\text{M}+\text{Na}$)⁺ found 833.4, requires 833.5, RT 2.50 min; HRMS EI (M)⁺ found 405.2688, $\text{C}_{27}\text{H}_{35}\text{NO}_2$ requires 405.2668; δ_{H} (300 MHz, CDCl_3) 0.98 (6H, s, $\text{C11}(\text{CH}_3)_2$), 1.41 (2H, m, C12H_2), 1.57 (2H, m, C13H_2), 1.67 (3H, s, C3CH_3), 1.90 (3H, s, C7CH_3), 1.95 (2H, m, C14H_2), 2.33 (2H, d, $J = 5.7$ Hz, C1'H), (3H, s, C15CH_3), 5.62 (1H, s, C2H), 5.70 (1H, t, $J = 5.4$ Hz, NH), 6.06 (4H, m, C4-, C6-, C8-, C9-H), 6.73 (2H, d, $J = 8.4$ Hz, C4' -, C6' -H), 6.86 (1H, m, C5-H), 7.13 (2H, d, $J = 8.4$ Hz, C3' -, C7' -H); δ_{C} (125 MHz; CDCl_3) 12.88 (C3CH_3), 13.78 (C7CH_3), 19.24 (C13), 21.74 (C15CH_3), 28.97 ($\text{C11}(\text{CH}_3)_2$), 33.11

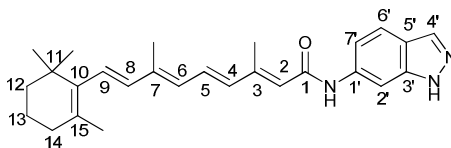
(C14), 34.27 (C11), 39.63 (C12), 43.18 (C1'), 115.72 (C4', C6'), 121.01 (C2), 128.35 (C5), 129.21 (C3', C7'), 129.50 (C15), 129.56 (C9), 129.86 (C2'), 130.06 (C6), 135.40 (C4), 137.31 (C8), 137.74 (C7), 138.95 (C10), 149.24 (C3), 155.88 (C5'), 167.38 (C1); **IR** (cm^{-1}) 3332, 2925, 1645, 1515, 1446, 1361, 1229; **MP** 78-80 °C.

(2E,4E,6E,8E)-N-(1H-indol-6-yl)-3,7-dimethyl-9-(2,6,6-trimethylcyclohex-1-enyl)nona-2,4,6,8-tetraenamide (202)



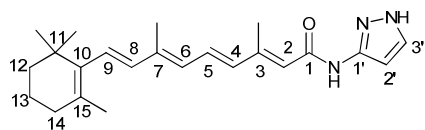
The mixed anhydride (**148**) (100 mg, 1 eq) was dissolved in DCM (3 ml) and pyridine (200 μL) at room temperature and 6-aminoindole (42 mg, 1.2 eq) was added. The solution was allowed to stir overnight at room temperature. Once complete by TLC, the reaction was diluted with EtOAc (50 ml) and washed with saturated sodium bicarbonate solution (2 \times 50 ml) and brine (2 \times 50 ml). The organic layer was dried over sodium sulphate and concentrated *in vacuo*. The residue was purified using Biotage silica column chromatography, eluted with 0-100 % EtOAc in hexane, to yield the product as a yellow solid (47 mg, 44 %). **LCMS (M+H)⁺** found 415.2, requires 415.3, RT 2.65 min; **HRMS ESI (M+H)⁺** found 415.2763, $\text{C}_{28}\text{H}_{35}\text{N}_2\text{O}$ requires 415.2744; δ_{H} (**500 MHz, CDCl_3**) 1.08 (6H, s, C11(CH_3)₂), 1.52 (2H, m, C12 H_2), 1.66 (2H, m, C13 H_2), 1.76 (3H, s, C3 CH_3), 2.04 (3H, s, C7 CH_3), 2.07 (2H, m, C14 H_2), 2.48 (3H, s, C15 CH_3), 5.87 (1H, s, C2 H), 6.30 (4H, m, C4-, C6-, C8-, C9- H), 6.52 (1H, s, C2'- H), 7.00 (1H, m, C5- H), 7.19 (1H, s, C4'- H), 7.39 (1H, s, C5'- H), 7.94 (1H, s, C7'- H), 8.36 (1H, s, C8'- H); δ_{C} (**125 MHz; CDCl_3**) 12.93 (C3 CH_3), 13.97 (C7 CH_3), 20.36 (C13), 22.02 (C15 CH_3), 29.48 (C11(CH_3)₂), 34.02 (C14), 35.28 (C11), 40.79 (C12), 102.56 (C5'), 112.11 (C2'), 113.47 (C8'), 117.03 (C7'), 123.59 (C2), 126.49 (C5), 129.07 (C4'), 129.43 (C6'), 130.56 (C1'), 130.80 (C9), 131.17 (C6), 131.75 (C15), 135.08 (C3'), 137.25 (C4), 139.06 (C8), 139.10 (C7), 139.57 (C10), 150.07 (C3), 167.82 (C1); **IR** (cm^{-1}) 3306, 2923, 1538, 1474, 1360, 1186, 966, 727; **MP** 157-160 °C.

(2E,4E,6E,8E)-N-(1H-indazol-6-yl)-3,7-dimethyl-9-(2,6,6-trimethylcyclohex-1-enyl)nona-2,4,6,8-tetraenamide (203)



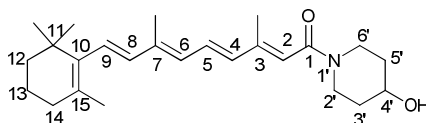
The mixed anhydride (**148**) (200 mg, 1 eq) was dissolved in DCM (3 ml) and pyridine (200 μ L) at room temperature and 6-aminoindazole (83 mg, 1.2 eq) was added. The solution was allowed to stir overnight at room temperature. Once complete by TLC, the reaction was diluted with EtOAc (50 ml) and washed with saturated sodium bicarbonate solution (2 \times 50 ml) and brine (2 \times 50 ml). The organic layer was dried over sodium sulphate and concentrated *in vacuo*. The residue was purified using Biotage silica column chromatography, eluted with 0-100 % EtOAc in hexane, to yield the product as a yellow solid (65 mg, 31 %). **LCMS (M+H)⁺** found 416.3, requires 416.3, RT 2.52 min; **HRMS ESI (M+H)⁺** found 416.2704, C₂₇H₃₄N₃O requires 416.2696; **δ_{H} (500 MHz, CDCl₃)** 1.07 (6H, s, C11(CH₃)₂), 1.52 (2H, m, C12H₂), 1.66 (2H, m, C13H₂), 1.73 (3H, s, C3CH₃), 2.02 (3H, s, C7CH₃), 2.05 (2H, m, C14H₂), 2.42 (3H, s, C15CH₃), 6.05 (1H, s, C2H), 6.33 (4H, m, C4-, C6-, C8-, C9-H), 6.52 (1H, s, C2'-H), 7.08 (1H, m, C5-H), 7.09 (1H, d, *J* = 8.7 Hz, C7'-H), 7.68 (1H, d, *J* = 8.7 Hz, C6'-H), 7.95 (1H, s, C2'-H), 8.23 (1H, s, C4'-H); **δ_{C} (75 MHz; CDCl₃)** 12.94 (C3), 14.02 (C7), 20.34 (C13), 22.00 (C15CH₃), 29.46 (C11(CH₃)₂), 34.02 (C14), 35.28 (C11), 40.79 (C12), 100.96 (C2'), 116.27 (C7'), 120.93 (C5'), 121.97 (C6'), 122.94 (C2), 129.31 (C5), 130.63 (C15), 131.06 (C9), 131.38 (C6), 134.66 (C4), 136.99 (C4'), 139.01 (C8), 139.10 (C1'), 139.25 (C7), 139.99 (C10), 142.19 (C3'), 151.38 (C3), 168.03 (C1); **IR (cm⁻¹)** 3179, 2923, 1567, 1356, 1152, 943, 839; **MP** 227-229 °C.

(2E,4E,6E,8E)-3,7-dimethyl-N-(1H-pyrazol-3-yl)-9-(2,6,6-trimethylcyclohex-1-enyl)nona-2,4,6,8-tetraenamide (204)



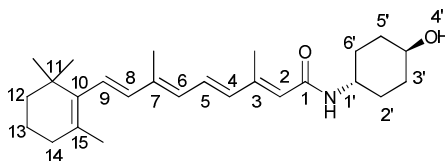
The mixed anhydride (**148**) (150 mg, 1 eq) was dissolved in DCM (3 ml) and pyridine (200 μ L) at room temperature and 3-amino-1H-pyrazole (39 mg, 1.2 eq) was added. The solution was allowed to stir overnight at room temperature. Once complete by TLC, the reaction was diluted with EtOAc (50 ml) and washed with saturated sodium bicarbonate solution (2 \times 50 ml) and brine (2 \times 50 ml). The organic layer was dried over sodium sulphate and concentrated *in vacuo*. The residue was purified using silica column chromatography eluted with a hexane / EtOAc gradient (1:0 to 0:1) to yield the product as a yellow solid (37mg, 26 %). The product was obtained as a mixture of isomers (major isomer (> 70 % by ^1H NMR) reported). **LCMS (2M+Na) $^+$** found 753.8, requires 753.5, RT 2.59 min; **HRMS ESI (M+Na) $^+$** found 388.2363, $\text{C}_{23}\text{H}_{32}\text{N}_3\text{O}$ requires 388.2359; **δ_{H} (300 MHz, CDCl_3) (major isomer)** 0.96 (6H, s, $\text{C}(\text{CH}_3)_2$), 1.39 (2H, m, $\text{C}12\text{H}_2$), 1.55 (2H, m, $\text{C}13\text{H}_2$), 1.64 (3H, s, $\text{C}3\text{CH}_3$), 1.94 (3H, s, $\text{C}7\text{CH}_3$), 1.95 (2H, m, $\text{C}14\text{H}_2$), 2.29 (3H, s, $\text{C}15\text{CH}_3$), 5.73 (1H, s, $\text{C}2\text{H}$), 5.81 (1H, d, $J = 3$ Hz, $\text{C}2'\text{-H}$), 6.16 (4H, m, $\text{C}4\text{-}, \text{C}6\text{-}, \text{C}8\text{-}, \text{C}9\text{-H}$), 6.93 (1H, s, NH), 6.97 (1H, m, $\text{C}5\text{-H}$), 8.03 (1H, d, $J = 3$ Hz, $\text{C}3'\text{H}$); **δ_{C} (125 MHz; CDCl_3) (major isomer)** 12.93 (C3), 14.05 (C7), 19.22 (C13), 21.74 ($\text{C}15\text{CH}_3$), 28.96 ($\text{C}11(\text{CH}_3)_2$), 33.12 (C14), 34.27 (C11), 39.61 (C12), 100.17 ($\text{C}2'$), 117.75 (C2), 128.99 (C5), 129.41 (C9), 130.14 (C15), 131.77 (C6), 132.17 ($\text{C}3'$), 134.93 (C4), 135.72 ($\text{C}1'$), 137.21 (C8), 137.67 (C7), 140.19 (C10), 155.11 (C3), 172.14 (C1); **IR (cm^{-1})** 3350, 2926, 1683, 1572, 1159, 963; **MP** 127-130 $^{\circ}\text{C}$.

(2E,4E,6E,8E)-1-(4-hydroxypiperidin-1-yl)-3,7-dimethyl-9-(2,6,6-trimethylcyclohex-1-enyl)nona-2,4,6,8-tetraen-1-one (205)



The mixed anhydride (**148**) (100 mg, 1 eq) was dissolved in DCM (3 ml) and pyridine (100 μ l) at room temperature and 4-hydroxypiperidine (32 mg, 1.2 eq) was added. The solution was allowed to stir overnight at room temperature. Once complete, the reaction was diluted with EtOAc (50 ml) and washed with saturated sodium bicarbonate solution (2 \times 50 ml) and brine (2 \times 50 ml). The organic layer was dried over sodium sulphate and concentrated *in vacuo*. The residue was purified using Biotage silica column chromatography, eluted with 0-100 % EtOAc in hexane, to yield the product as a yellow oil (95 mg, 95 %). **LCMS (M+H)⁺** found 384.4, requires 384.3, RT 2.39 min; **HRMS ESI (M+H)⁺** found 384.2912, C₂₅H₃₈NO₂ requires 384.2897; **δ_{H} (500 MHz, CDCl₃)** 0.93 (6H, s, C11CH₃), 1.37 (2H, m, C3'a-, C5'a-H), 1.40 (2H, m, C12-H), 1.52 (2H, m, C3'b-, C5'b-H), 1.60 (3H, s, C15CH₃), 1.74 (2H, m, C13H₂), 1.88 (3H, s, C3CH₃), 1.92 (3H, s, C7CH₃), 1.92 (2H, m, C14-H), 3.20 (2H, m, C2'-a, C6'-a-H), 3.74 (2H, m, C2'b-, C6'b-H), 3.99 (1H, m, C4'H), 6.12 (5H, m, C2-, C4-, C6-, C8, C9-H), 6.77 (1H, m, C5H); **δ_{C} (125 MHz, CDCl₃)** 15.47 (C₃(CH₃), 17.26 (C7(C₇H₃)), 22.91 (C13), 24.59 (C15(C₁₅H₃)), 32.05 (C11(C₁₁H₃)₂), 36.55 (C14), 37.38 (C11), 37.82 (C3', C5'), 38.17 (C3', C5'), 42.65 (C12), 43.33 (C2', C6'), 47.67 (C2', C6'), 70.27 (C4'), 125.33 (C2), 131.30 (C5), 132.34 (C9), 132.96 (C15), 133.64 (C6), 138.63 (C4), 141.52 (C7), 141.60 (C8), 141.64 (C10), 148.14 (C3), 171.69 (C1); **IR (cm⁻¹)** 3386, 2925, 1602, 1447, 1266, 1199, 1077, 966.

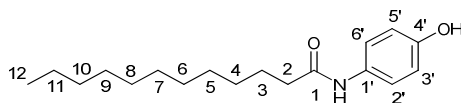
(2E,4E,6E,8E)-N-((1r,4r)-4-hydroxycyclohexyl)-3,7-dimethyl-9-(2,6,6-trimethylcyclohex-1-enyl)nona-2,4,6,8-tetraenamide (206)



The mixed anhydride (**148**) (50.0 mg, 1 eq) was dissolved in DCM (3 ml) and pyridine (200 μ l) at room temperature and *trans*-4-aminocyclohexanol (18.2 mg, 1.2 eq) was added. The solution was allowed to stir overnight at room temperature. Once complete, the reaction was diluted with EtOAc (50 ml) and washed with saturated sodium bicarbonate solution (2 \times 50 ml) and brine (2 \times 50 ml). The organic layer was dried over sodium sulphate and concentrated *in vacuo*. The residue was purified using Biotage silica column chromatography, eluted with 0-100 % EtOAc in hexane, to yield the product as a yellow solid (18.1 mg, 36 %). **LCMS (2M+Na)⁺** found 817.6, requires 817.6, RT 2.38 min; **HRMS EI (M)⁺** found 397.2986, C₂₆H₃₉NO₂ requires 397.2981; **δ_{H} (500 MHz, CDCl₃)** 1.00 (6H, s, C11CH₃), 1.25 (2H, m C3'a-, C5'a-H), 1.39 (2H, m, C3'b-, C5'b-H), 1.47 (2H, m, C12H₂), 1.63 (2H, m, C13H₂), 1.72 (3H, s, C15CH₃), 2.00 (3H, s, C3CH₃), 2.03 (6H, m, C2', C6', C14-H₂), 2.36 (3H, s, C7CH₃), 3.60 (1H, m, C4'H), 3.81 (1H, m, C1'H), 5.32 (1H, d, *J* = 8.1 Hz, OH), 5.63 (1H, s, C2H), 6.20 (4H, m, C4-, C6-, C8, C9-H), 6.93 (1H, m, C5H), 7.3 (1H, s, NH); **δ_{C} (125 MHz, CDCl₃)** 12.86 (C3CH₃), 13.55 (C7CH₃), 19.24 (C13), 21.72 (C15CH₃), 28.95 (C11(CH₃)₂), 31.00 (C2', C6'), 33.10 (C14), 34.05 (C3', C5'), 34.27 (C11), 39.63 (C12), 47.43 (C1'), 69.91 (C4'), 121.51 (C2), 128.23 (C5), 129.56 (C9), 129.70 (C6), 129.79 (C15), 135.49 (C4), 137.32 (C8), 137.76 (C7), 138.71 (C10), 148.48 (C3), 166.43 (C1); **IR (cm⁻¹)** 3400, 2936, 1655, 1542, 1437, 1364, 1293, 1140, 1019, 952, 901, 707; **MP** 88-91 °C.

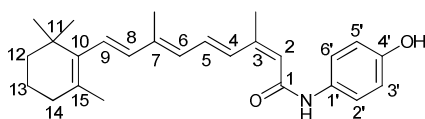
7.3.2 Central scaffold analogues

N-(4-hydroxyphenyl)dodecanamide (91)



Lauroyl chloride (**241**) (0.4 ml, 1 eq), 4-aminophenol (**225**) (208.0 mg, 1.1 eq) and pyridine (0.2 ml, 1.5 eq) were dissolved in THF and stirred overnight. The solution was washed with saturated sodium bicarbonate solution (2 × 50 ml) in ethyl acetate (50 ml). The organic layer was dried over sodium sulphate and concentrated *in vacuo*. The residue was purified by silica column chromatography eluted with a 0-100 % EtOAc in hexane. The pure compound was obtained as a white solid (50 mg, 90 %). **LCMS (2M+Na)⁺** found 605.5 requires 605.4, RT 2.20 min; **HRMS ESI (M+H)⁺** found 292.2279, C₁₈H₃₀NO₂ requires 292.2271; **δ_{H} (500 MHz, CDCl₃)** 0.93 (3H, t, *J* = 6.4 Hz, C12H₃), 1.32 (16H, m, C4-C11H₂), 1.61 (2H, m, C3H₂), 2.33 (2H, m, CH₂), 4.88 (1H, s, OH), 6.75 (2H, d, *J* = 8.8 Hz, C3', C5'-H), 6.95 (1H, s, NH), 7.33 (2H, d, *J* = 8.8 Hz, C2', C6'-H); **δ_{C} (125 MHz, CDCl₃)** 14.51 (C12), 23.78 (C11), 27.15 (C3), 30.40 (C5), 30.52 (C9, C8), 30.68 (C4), 30.77 (C7, C6), 33.12 (C10), 37.89 (C2), 116.25 (C3', C5'), 123.48 (C2', C6'), 131.79 (C1'), 155.41 (C4'), 174.52 (C1) ; **IR (cm⁻¹)** 3311, 2916, 2850, 1651, 1545, 1515, 1245, 831, 534; **MP** 128-130 °C.

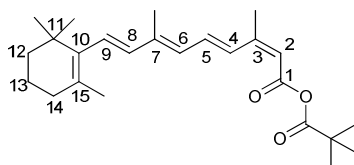
(2*Z*,4*E*,6*E*,8*E*)-*N*-(4-hydroxyphenyl)-3,7-dimethyl-9-(2,6,6-trimethylcyclohex-1-enyl)nona-2,4,6,8-tetraenamide (238)



4-aminophenol (**225**) (22.5 mg, 1.3 eq) was added to a stirred solution of mixed anhydride (**240**) (60 mg, 1 eq) in DCM (3 ml) and pyridine (200 μ l). The solution was stirred overnight at room temperature. Once complete, as observed by LCMS, ethyl acetate (5 ml) was added and the solution was washed with saturated sodium bicarbonate solution (2 × 50 ml) and brine (2 × 50 ml). The organic layer was dried over sodium sulphate and

concentrated *in vacuo*. The mixture was purified by Biotage column chromatography, eluted with 0-100 % EtOAc in hexane, to afford the pure compound was as a yellow oil (36 mg, 58 %). **LCMS (2M+Na)⁺** found 805.6 requires 805.5, RT 2.50 min; **HRMS ESI (M+H)⁺** found 392.2596, C₂₆H₃₄NO₂ requires 392.2584; **δ_{H} (500 MHz, CDCl₃)** 1.06 (6H, C11CH₃), 1.40 (2H, m, C12H₂), 1.58 (2H, m, C13H₂), 1.64 (2H, C15CH₃), 1.81 (3H, m, C3CH₃), 1.99 (2H, m, C14H₂), 2.23 (3H, m, C7CH₃), 5.70 (1H, s, C2H), 6.10 (4H, m, C4-, C6-, C8-, C9-H), 6.60 (2H, d, *J* = 8.7 Hz, C3'-, C5'-H), 6.90 (1H, dd, *J*₁ = 15.3, *J*₂ = 11.4, C5H), 7.27 (2H, d, *J* = 8.7 Hz, C2'-, C6'-H), 7.78 (1H, d, *J* = 15.3 Hz, C4H); **δ_{C} (125 MHz; CDCl₃)** 12.89 (C7CH₃), 20.39 (C13), 21.17 (C3CH₃), 21.98 (C15CH₃), 29.47 (C11(CH₃)₂), 34.05 (C14), 35.32 (C11), 40.85 (C12), 116.30 (C3', C5'), 121,16 (C2), 123.25 (C1', C6'), 129.18 (C5), 130.66 (C15), 131.26 (C9), 131.81 (C6), 132.06 (C7), 132.10 (C4), 139.15 (C8), 140.03(C10), 148.97 (C3), 155.35 (C4'), 167.17 (C1); **IR (cm⁻¹)** 3302, 2924, 1608, 1509, 1442, 1316, 1237, 968, 837, 519; **MP** 85-87 °C.

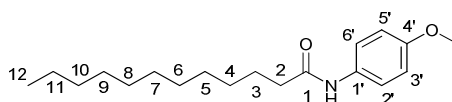
(2Z,4E,6E,8E)-3,7-dimethyl-9-(2,6,6-trimethylcyclohex-1-enyl)nona-2,4,6,8-tetraenoic pivalic anhydride (240)



13-*cis*-Retinoic acid (**239**) (49.5 mg, 1 eq) and trimethyl acetyl chloride (**147**) (30 μ l, 1.5 eq) were dissolved in ethyl acetate (5 ml) at -5°C. Triethylamine (10 μ l, 0.5 eq) was added and the mixture was stirred for 2 hours. The reaction was monitored by LCMS and when complete, washed with 20 % HCl (2 \times 50 ml) and saturated sodium bicarbonate solution (2 \times 50 ml). The organic layer was dried over sodium sulphate and concentrated *in vacuo*. The mixture was purified using a silica flash column chromatography plug with 20 % ethyl acetate and hexane. The pure compound was obtained as a yellow oil (60 mg, 95 %). The compound was not ionised by LCMS. **δ_{H} (500 MHz, CDCl₃)** 0.95 (6H, s, C11(CH₃)₂), 1.19 (9H, s, pivaloyl(CH₃)₃), 1.38 (2H, m, C12H₂), 1.52 (2H, m, C13H₂), 1.64 (3H, s, C15CH₃), 1.94 (3H, s, C3CH₃), 1.96 (2H, m, C14H₂), 2.02 (3H, s, C7CH₃), 5.62 (1H, s, C2CH), 6.09 (1H, d, *J*

= 16 Hz, C9H), 6.18 (1H, d, $J = 11.5$ Hz, C4H), 6.25 (1H, d, $J = 16$ Hz, C9H), 7.04 (1H, dd, $J_1 = 11.5$, $J_2 = 15.5$, C5H), 7.67 (1H, d, $J = 15.5$ Hz, C6H); δ_c (125 MHz, CDCl₃) 13.0, 14.3, 14.4, 19.2, 21.8, 26.5, 26.6, 29.0, 33.2, 34.3, 39.6, 39.7, 116.3, 129.3, 129.7, 130.4, 133.3, 134.2, 137.1, 137.7, 141.4, 158.5, 162.4, 174.8.

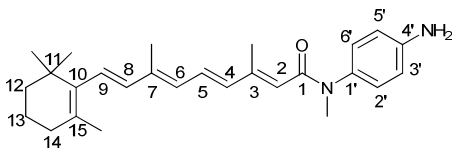
***N*-(4-methoxyphenyl)dodecanamide (242)**



Lauroyl chloride (**241**) (200 μ l, 1 eq), *para*-methoxyaniline (**150**) (128 mg, 1.1 eq) and pyridine (130 μ l, 1 eq) were dissolved in DCM (3 ml) and stirred overnight. The solution was washed with saturated sodium bicarbonate solution (2 \times 50 ml) and brine (2 \times 50 ml) in ethyl acetate (50 ml), dried over sodium sulphate, and concentrated *in vacuo*. The residue was recrystallised from MeOH to yield the pure compound as a white solid (25 mg, 9 %). **LCMS (2M+Na)⁺** found 633.4 requires 633.5, RT 2.52 min; **HRMS ESI (M+H)⁺** found 306.2439, C₁₉H₃₃NO₂ requires 306.2428; δ_H (500 MHz, CDCl₃) 0.81 (3H, t, $J = 6.3$ Hz, C12H₃), 1.12 (16H, m, C4-C11H₂), 1.64 (2H, m, C3H₂), 2.24 (2H, m, C2H₂), 3.71 (3H, s, CH₃), 6.77 (2H, d, $J = 9$ Hz, C3'-, C5'-H), 7.19 (1H, s, NH), 7.33 (2H, d, $J = 9$ Hz, C2'-, C6'-H); δ_c (125 MHz, CDCl₃) 14.15 (C12), 22.71 (C11), 25.76 (C3), 29.33 (C4), 29.36 (C5), 29.43 (C9), 29.52 (C8), 29.63 (C7), 31.93 (C6), 37.65 (C2), 55.47 (OMe), 114.07 (C3', C5'), 121.77 (C2', C6'), 131.11 (C1'), 156.28 (C4'), 171.43 (C1); **IR (cm⁻¹)** 3302, 2916, 2848, 1651, 1513, 1247, 1030, 826; **MP** 102-104 °C.

7.3.3 Amide isosteres

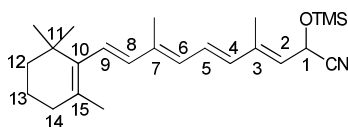
(2*E*,4*E*,6*E*,8*E*)-*N*-(4-aminophenyl)-*N*,3,7-trimethyl-9-(2,6,6-trimethylcyclohex-1-enyl)nona-2,4,6,8-tetraenamide (179)



The mixed anhydride (**148**) (200 mg, 1 eq) was dissolved in DCM (1 ml) and pyridine (200 μ L) at room temperature and *N*-methyl-1,4-phenylenediamine

dihydrochloride (**170**) (79 mg, 1.2 eq) was added. The solution was allowed to stir overnight at room temperature. Once complete by TLC, the reaction was diluted with EtOAc (50 ml) and washed with saturated sodium bicarbonate solution (2 × 50 ml) and brine (2 × 50 ml). The organic layer was dried over sodium sulphate and concentrated *in vacuo*. The residue was purified using silica column chromatography, eluted with a 0-100 % EtOAc in hexane, to yield the product as a yellow solid (43 mg, 20 %). **LCMS (M+H)⁺** found 405.3, requires 405.3, RT 2.52 min; **HRMS ESI (M+H)⁺** found 405.2912, C₂₇H₃₇N₂O requires 405.2900; **δ_H (300 MHz, CDCl₃)** 0.93 (6H, s, C11(CH₃)₂), 1.38 (2H, m, C12H₂), 1.53 (2H, m, C13H₂), 1.61 (3H, s, C3CH₃), 1.87 (3H, s, C7CH₃), 1.93 (2H, m, C14H₂), 2.23 (3H, s, C15CH₃), 3.19 (3H, s, NCH₃), 5.55 (1H, s, C2H), 6.01 (4H, m, C4-, C6-, C8-, C9-H), 6.57 (2H, d, *J* = 8.4 Hz, C3'-, C5'H), 6.73 (1H, m, C5-H), 6.84 (2H, d, *J* = 8.4 Hz, C2'-, C3'-H); **δ_C (125 MHz; CDCl₃)** 12.79 (C3CH₃), 13.79 (C7CH₃), 19.22 (C13), 21.69 (C15CH₃), 28.93 (C11(CH₃)₂), 33.06 (C14), 34.23 (C11), 39.58 (C12), 115.47 (C3', C5'), 121.61 (C2), 127.78 (C5), 127.99 (C9), 128.71 (C6), 129.61 (C15), 129.71 (C2', C6'), 134.94 (C1'), 136.24 (C4), 137.44 (C8), 137.77 (C7), 138.08 (C10), 145.60 (C4'), 147.02 (C3), 167.72 (C1); **IR (cm⁻¹)** 3347, 2923, 1621, 1514, 1360, 1278, 1120, 964, 829, 555; **MP** 93-96 °C.

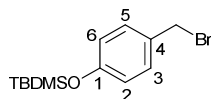
(3E,5E,7E,9E)-4,8-dimethyl-10-(2,6,6-trimethylcyclohex-1-enyl)-2-(trimethylsilyloxy)deca-3,5,7,9-tetraenenitrile (211)



This compound was synthesised as previously described by Weiss *et al.*¹²¹ TMSCN (250 µl, 2 eq) was added to retinal (**210**) (52 mg, 1 eq) at room temperature. Triethylamine (1 drop) was added and the solution was allowed to stir for 2 h. The excess TMSCN and triethylamine were removed under reduced pressure to yield the product as a yellow solid (69 mg, 98 %). The product was not ionised by LCMS. **δ_H (500 MHz, CDCl₃)** 0.25 (9H, s, Si(CH₃)₃), 1.08 (6H, s, C11(CH₃)₂), 1.50 (2H, m, C12H₂), 1.66 (2H, m, C13H₂), 1.75 (3H, s, C3CH₃), 1.95 (3H, s, C7CH₃), 2.02 (3H, s, C15CH₃),

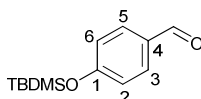
2.08 (2H, m, C14H₂), 5.28 (1H, d, $J = 8.5$ Hz, C1H), 5.59 (1H, d, $J = 8.5$ Hz, C2H), 6.20 (4H, m, C4-, C6-, C8-, C9-H), 6.76 (1H, m, C5H).

(4-(bromomethyl)phenoxy)(*tert*-butyl)dimethylsilane (212)



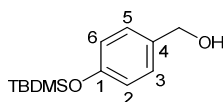
This compound was synthesised as previously described by Weiss *et al.*¹²¹ Compound (**216**) (228 mg, 1 eq) was dissolved in dry THF (4 ml). TFAA (3 ml, 2.2 eq) was added at room temperature and allowed to stir for 1 h, then LiBr (88 mg, 0.8 eq) was added. The mixture was allowed to stir for 1 h and once complete by TLC the residue was purified by filtration through a bed of silica eluting with DCM (100 ml) to yield the product as a colourless oil (164 mg, 57 %). **LCMS (M-Br)⁺** found 221.1 requires 221.1, RT 2.47 min; **δ_{H} (500 MHz, CDCl₃)** 0.19 (6H, s, SiCH₃), 1.01 (9H, s, SiC(CH₃)₃), 4.45 (2H, s, CH₂Br), 6.79 (2H, d, $J = 6.5$ Hz, C2-,C6-H), 7.15 (2H, d, $J = 6.5$ Hz, C3-,C5-H); **δ_{C} (125 MHz, CDCl₃)** 18.21 (C(CH₃)₃), 25.70 (C(CH₃)₃), 64.96 (CH₂Br), 120.13 (C2, C6), 128.55 (C3, C5), 133.76 (C4), 155.25 (C1).

4-(*tert*-butyldimethylsilyloxy)benzaldehyde (215)



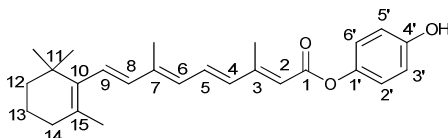
The synthesis of this compound was adapted from that previously detailed by Weiss *et al.*¹²¹ 4-hydroxybenzaldehyde (**214**) (200.1 mg, 1 eq) was dissolved in dry DCM (5 ml) at room temperature. Triethylamine (370 μ l, 1.5 eq) was added, followed by TBDMSCl (321 mg, 1.2 eq). The reaction mixture was stirred for 2 h and monitored by TLC. The solution was diluted with DCM (50 ml) and washed with saturated sodium bicarbonate solution (3 \times 50 ml). The organic layer was dried over sodium sulphate and concentrated *in vacuo*. The residue was purified by silica plug, eluting with DCM, to yield the product as a viscous yellow oil (304 mg, 72 %). **LCMS (M+H)⁺** found 237.1 requires 237.1, RT 2.33 min; **δ_{H} (500 MHz, CDCl₃)** 0.00 (6H, s, SiCH₃), 0.744 (9H, s, SiC(CH₃)₃), 6.70 (2H, d, $J = 3.5$ Hz, C2-,C6-H), 7.55 (2H, d, $J = 3.5$ Hz, C3-,C5-H), 9.60 (1H, s, CHO).

(4-(*tert*-butyldimethylsilyloxy)phenyl)methanol (**216**)



This compound was synthesised as previously described by Weiss *et al.*¹²¹ Compound (**215**) (304 mg, 1 eq) was dissolved in EtOH (3 ml) at room temperature and NaBH₄ (244 mg, 5 eq) was added. The solution was allowed to stir for 1 h and monitored by TLC. Once complete, the reaction was quenched with water (20 ml), washed with saturated sodium bicarbonate solution (3 × 50 ml) in DCM (50 ml) and dried over sodium sulphate. The solvents were removed under reduced pressure to yield the pure residue as a colourless oil (228 mg, 75 %). **LCMS (M-OH)⁺** found 221.1 requires 221.1, RT 2.14 min; **δ_{H} (500 MHz, CDCl₃)** 0.00 (6H, s, SiCH₃), 0.80 (9H, s, SiC(CH₃)₃), 4.40 (1H, s, CH₂OH), 6.63 (2H, d, *J* = 3.5 Hz, C2-,C6-H), 7.46 (2H, d, *J* = 3.5 Hz, C3-,C5-H).

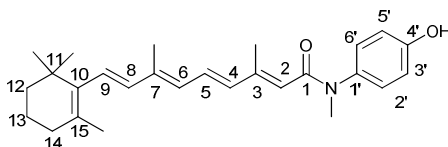
(*2E,4E,6E,8E*)-4-hydroxyphenyl 3,7-dimethyl-9-(2,6,6-trimethylcyclohex-1-enyl)nona-2,4,6,8-tetraenoate (**218**)



The mixed anhydride (**148**) (50.3 mg, 1 eq) was dissolved in pyridine (3 ml) at room temperature and the hydroquinone (**217**) (18.2 mg, 1.3 eq) was added. The solution was allowed to stir overnight. Once complete, the reaction was diluted with EtOAc (50 ml) and washed with saturated sodium bicarbonate solution (2 × 50 ml) and brine (2 × 50 ml). The organic layer was dried over sodium sulphate and concentrated *in vacuo*. The residue was purified using silica column chromatography, eluted with 0-100 % EtOAc in hexane, to yield the product as a yellow solid (31 mg, 61 %). **LCMS (M+H)⁺** found 393.2 requires 393.2, RT 2.78 min; **HRMS ESI (M+H)⁺** found 393.2426, requires 393.2424; **δ_{H} (500 MHz, CDCl₃)** 1.08 (6H, s, C11(CH₃)₂), 1.50 (2H, m, C12H₂), 1.71 (2H, m, C13H₂), 1.74 (3H, s, C3CH₃), 2.10 (2H, m, C14H₂), 2.20 (3H, s, C7CH₃), 2.45 (3H, s, C15CH₃), 5.54 (1H, br s, C4'OH), 6.02 (1H, s, C2H), 6.79 (4H, m, C4-, C6-, C8-, C9-H), 6.78 (2H, d, *J* = 8.5 Hz,

C3'-, C5'-H), 6.95 (2H, d, $J = 8.5$ Hz, C2'-, C6'-H), 7.13 (1H, m, C5H); δ_c (125 MHz, CDCl₃) 12.64 (C3CH₃), 13.72 (C7CH₃), 18.70 (C13), 21.49 (C15CH), 28.77 (C11(CH₃)₂), 32.61 (C14), 33.84 (C11), 40.02 (C12), 115.47 (C3', C5'), 117.10 (C2), 122.47 (C2', C6'), 128.31 (C5), 129.65 (C15), 129.75 (C9), 132.18 (C6), 134.83 (C4), 136.86 (C8), 137.22 (C7), 139.94 (C10), 142.52 (C1'), 154.82 (C3), 165.11 (C1); IR (cm⁻¹) 3447, 2923, 2853, 1704, 1602, 1579, 1580, 1448, 1376, 1348, 1238, 1185, 1143, 966, 873, 841, 777, 721, 595, 524, 461; MP 180-182 °C.

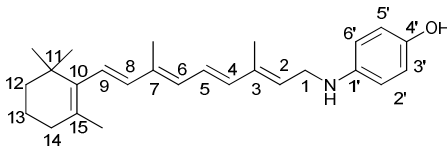
(2E,4E,6E,8E)-N-(4-hydroxyphenyl)-N,3,7-trimethyl-9-(2,6,6-trimethylcyclohex-1-enyl)nona-2,4,6,8-tetraenamide (220)



The mixed anhydride (**148**) (115 mg, 1 eq) was dissolved in DMF (1 ml) and pyridine (200 μ L) at room temperature and 4-methylaminophenol sulphate (**219**) (126 mg, 1.2 eq) was added. The solution was allowed to stir overnight at room temperature. Once complete by TLC, the reaction was diluted with EtOAc (50 ml) and washed with saturated sodium bicarbonate solution (2 \times 50 ml) and brine (2 \times 50 ml). The organic layer was dried over sodium sulphate and concentrated *in vacuo*. The residue was purified using silica column chromatography, eluted with a 0-100 % EtOAc in hexane, to yield the product as a brown oil (22 mg, 18 %) LCMS (2M+Na)⁺ found 833.9, requires 833.5, RT 2.53 min; HRMS ESI (M+Na)⁺ found 428.2565, C₂₇H₃₅NNaO₂ requires 428.2560; δ_H (300 MHz, CDCl₃) 0.95 (6H, s, C11(CH₃)₂), 1.40 (2H, m, C12H₂), 1.50 (2H, m, C13H₂), 1.63 (3H, s, C3CH₃), 1.88 (3H, s, C7CH₃), 1.93 (2H, t, $J = 6$ Hz, C14H₂), 2.24 (3H, s, C15CH₃), 3.24 (3H, s, NCH₃) 5.54 (1H, s, C2H), 6.02 (4H, m, C4-, C6-, C8-, C9-H), 6.71 (1H, m, C5-H), 6.76 (2H, d, $J = 8.7$ Hz, C3'-, C5'H), 6.95 (2H, d, $J = 8.7$ Hz, C2'-, C3'-H); δ_c (125 MHz; CDCl₃) 12.83 (C3CH₃), 14.27 (C7CH₃), 20.38 (C13), 21.96 (C15CH₃), 29.45 (C11(CH₃)₂), 34.62 (C14), 35.29 (C11), 37.71 (NCH₃), 40.84 (C12), 117.21 (C3', C5'), 122.64 (C2), 124.59 (C15), 128.96 (C2', C6'), 129.33 (C5), 130.53 (C9), 131.13 (C6), 136.77 (C7), 136.88 (C4), 139.10 (C8), 139.16

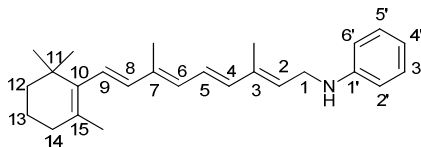
(C1'), 139.41 (C10), 148.44 (C3), 158.36 (C4'), 170.01 (C1); **IR (cm⁻¹)** 2951, 1558, 1516, 1373, 1275, 1126, 974, 841.

4-((2E,4E,6E,8E)-3,7-dimethyl-9-(2,6,6-trimethylcyclohex-1-enyl)nona-2,4,6,8-tetraenylamino)phenol (226)



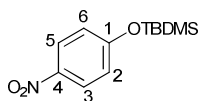
Compound (**232**) (348 mg, 1 eq) was dissolved in THF and TBAF (200 μ l, 1.1 eq) was added. The reaction was allowed to stir at room temperature for 40 minutes. Once seen to be complete by TLC, the reaction was diluted with EtOAc (50ml) and washed with saturated sodium bicarbonate solution (3 \times 50 ml) and brine (3 \times 50 ml). The organic layer was dried over sodium sulphate and concentrated *in vacuo*. The residue was purified using Biotage silica column chromatography, eluted with 0-35 % EtOAc in hexane, to yield the product as a brown oil (67.2 mg, 25 %); **LCMS (M-H)⁺** found 376.2, requires 376.3, RT 2.15 min; **HRMS ESI (M-H)⁺** found 376.2661, C₂₆H₃₄NO requires 376.2635; * **δ_{H} (500 MHz, CDCl₃)** 1.04 (6H, s, C11(CH₃)₂) 1.48 (2H, m, C12H₂), 1.62 (2H, m, C13H₂), 1.72 (3H, s, C15CH₃), 1.90 (3H, s, C3H₃), , 1.97 (3H, s, C7CH₃), 2.03 (2H, m, C14H₂), 3.84 (2H, d, *J* = 7 Hz, C1H₂), 5.64 (1H, t, *J* = 7 Hz, C2H), 6.16 (4H, m, C4-, C6-, C8-, C9-H), 6.56 (2H, d, *J* = 8.5 Hz, C3', C5'-H), 6.62 (1H, m, C5-H), 6.62 (2H, d, *J* = 8.5 Hz, C2', C6'-H); **δ_{C} (125 MHz; CDCl₃)** 12.76 (C3CH₃), 12.83 (C7CH₃), 19.28 (C13), 21.79 (C15CH₃), 28.98 (C11(CH₃)₂), 33.07 (C14), 34.27 (C11), 39.60 (C12), 43.55 (C1), 115.02 (C2', C6'), 116.28 (C3', C5'), 124.51 (C2), 126.60 (C5), 129.12 (C9), 129.28 (C15), 130.17 (C6), 135.95 (C3), 136.40 (C4), 136.71 (C7), 137.71 (C8), 137.84 (C10), 141.86 (C1'), 148.42 (C4'); **IR (cm⁻¹)** 3003, 1708, 1588, 1505, 1372, 1233, 964, 828, 728; **MP** 68-70 °C.

***N*-((2*E*,4*E*,6*E*,8*E*)-3,7-dimethyl-9-(2,6,6-trimethylcyclohex-1-enyl)nona-2,4,6,8-tetraenyl)aniline (**228**)**



Retinal (**210**) (49.1 mg, 1 eq) and aniline (**149**) (20 μ l, 1.3 eq) were dissolved in methanol (3 ml) and the reaction mixture was allowed to stir at room temperature overnight. Sodium borohydride (74.2 mg, 1.96 eq) was added and allowed to stir for a further 6 h. Once complete, as observed by LCMS, ethyl acetate (50 ml) was added and the solution was washed with saturated sodium bicarbonate solution (2 \times 50 ml). The organic layer was dried over sodium sulphate and concentrated *in vacuo*. The mixture was purified by Biotage column chromatography eluted with 0-100 % EtOAc in hexane. The pure compound was obtained as a brown oil (28 mg, 44 %). The compound was not ionised by LCMS; **HRMS ESI (M-H)⁺** found 360.2701, C₂₆H₃₄N requires 360.2686; δ_{H} (**500 MHz, CDCl₃**) 1.37 (6H, C11CH₃), 1.48 (2H, m, C12H₂), 1.50 (2H, m, C13H₂), 1.54 (2H, C15CH₃), 1.61 (3H, m, C7CH₃), 1.88 (3H, m, C3CH₃), 1.89 (2H, m, C14H₂), 3.59 (1H, br s, NH), 3.81 (2H, d, *J* = 6.6 Hz, C1H₂), 5.43 (2H, t, *J* = 6.6 Hz, C2H₂), 6.05 (4H, m, C4-, C6-, C8-, C9-H), 6.58 (2H, m, C2'-, C6'-H), 6.64 (1H, t, *J* = 7.5 Hz, C4'-H), 7.11 (2H, app t, *J* = 7.5 Hz, C5-H); **IR (cm⁻¹)** 3404, 2927, 2864, 1601, 1504, 967, 748, 692, 510.

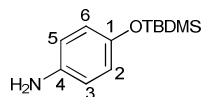
***tert*-butyldimethyl(4-nitrophenoxy)silane (**230**)**



This compound was synthesised as previously described by Bridgeman *et al.*²¹⁵ *para*-nitrophenol (**229**) (601 mg, 1 eq) and TBDMSCl (724 mg, 1.1 eq) were dissolved in DCM and NEt₃ (500 μ l) and allowed to stir for 2 h at room temperature. Once seen to be complete by TLC, the reaction was diluted with EtOAc (50ml) and washed with saturated sodium bicarbonate solution (3 \times 50 ml) and brine (3 \times 50 ml). The organic layer was dried over sodium sulphate and concentrated *in vacuo* to yield the product as a colourless

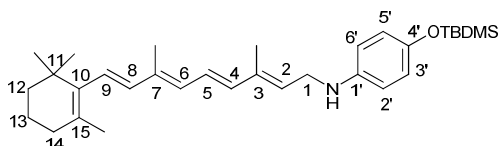
viscose oil (994 mg, 90 %). The product was not ionised by LCMS. δ_{H} (500 MHz, CDCl_3) 0.23 (6H, s, $\text{Si}(\text{CH}_3)_2$), 0.96 (9H, s, $\text{C}(\text{CH}_3)_3$), 6.86 (2H, d, $J = 9$ Hz, C2-, C6-H), 8.10 (2H, d, $J = 9$ Hz, C3-, C5-H).

4-(*tert*-butyldimethylsilyloxy)aniline (**231**)



This compound was synthesised as previously described by Bridgeman *et al.*²¹⁵ *Tert*-butyldimethyl(4-nitrophenoxy)silane (**230**) (994 mg, 1 eq) was dissolved in MeOH (10 ml) and Pd/C (50mg) was added as a solution in MeOH. The reaction was stirred under H_2 overnight at room temperature. The Pd/C was filtered and the residue was concentrated *in vacuo* to yield the product as a dark brown viscose oil (790 mg, 90 %). LCMS ($\text{M}+\text{H}$)⁺ found 224.1, requires 224.1, RT 1.62 min; δ_{H} (300 MHz, CDCl_3) 0.00 (6H, s, $\text{Si}(\text{CH}_3)_2$), 0.82 (9H, s, $\text{C}(\text{CH}_3)_3$), 6.38 (2H, d, $J = 8.7$ Hz, C2-, C6-H), 6.49 (2H, d, $J = 8.7$ Hz, C3-, C5-H).

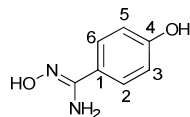
4-(*tert*-butyldimethylsilyloxy)-*N*-((2*E*,4*E*,6*E*,8*E*)-3,7-dimethyl-9-(2,6,6-trimethylcyclohex-1-enyl)nona-2,4,6,8-tetraenyl)aniline (**232**)



Retinal (**210**) (203 mg, 1 eq) and 4-(*tert*-butyldimethylsilyloxy)aniline (**231**) (183 mg, 1.1 eq) were dissolved in MeOH (5 ml) and NaBH_4 (275 mg, 10 eq) was added. The reaction was allowed to stir at room temperature for 2 h. The reaction was monitored by TLC and once complete, diluted with EtOAc (50ml) and washed with saturated sodium bicarbonate solution (3 \times 50 ml) and brine (3 \times 50 ml). The organic layer was dried over sodium sulphate and concentrated *in vacuo* to yield the product as a yellow oil (348 mg, 98 %). The product was not ionised by LCMS. δ_{H} (500 MHz, CDCl_3) 0.61 (6H, s, $\text{Si}(\text{CH}_3)_2$), 0.82 (9H, s, $\text{C}(\text{CH}_3)_2$), 0.88 (6H, s, C11(CH_3)₂), 1.33 (2H, m, C12H₂), 1.46 (2H, m, C13H₂), 1.56 (3H, s, C15CH₃), 1.76 (3H, s, C3H₃), 1.85 (2H, m, C14H₂), 1.95 (3H, s, C7CH₃), 3.53 (1H, br s, NH), 3.6 (2H, d, $J = 6$

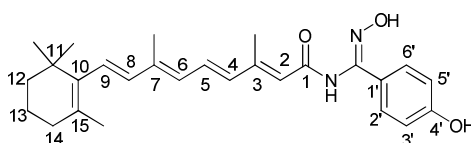
Hz, C1H₂), 5.45 (1H, t, *J* = 6 Hz, C2H), 6.01 (4H, m, C4-, C6-, C8-, C9-H), 6.50 (5H, m, C5, C2'-, C3', C5', C6'-H).

(Z)-N',4-dihydroxybenzimidamide (235)



This compound was synthesised as previously described by Porwal *et al.*²¹⁶ Hydroxylamine hydrochloride (3.51 g, 42.1 mmol) was added to a solution of hydroxybenzotrile (**234**) (5.02 g, 51.7 mmol) and sodium bicarbonate (7.06 g, 84.0 mmol) in methanol (4 ml/mmol of nitrile) at room temperature. The solution was heated to reflux at 80 °C overnight. The mixture was analysed by LCMS and, upon completion, the methanol was removed and the residue triturated with deionised water, filtered and concentrated *in vacuo* to afford the pure amidoxime as a white solid (1.48 g, 23 %). **LCMS (M+H)⁺** found 153.0, requires 153.1, RT 0.50 min; **δ_H (300 MHz, DMSO)** 3.32 (1H, s, NOH), 5.61 (1H, s, ArOH), 6.74 (2H, d, *J* = 8.6 Hz, C2-, C6-H), 7.49 (2H, d, *J* = 8.6 Hz, C3-, C5-H), 9.32 (1H, s, NH), 9.57 (1H, s, NH); **δ_C (300 MHz, MeOH)** 116.15 (C3, C5), 125.16 (C1), 128.75 (C2, C6), 155.90 (C4), 160.29 (CN); **IR (cm⁻¹)** 3440, 3315, 2431, 1645, 1505, 1392, 1285, 1185, 1119, 1005, 835, 731, 667, 637, 609, 520; **mp** 149 °C.

(2E,4E,6E,8E)-N-((E)-(hydroxyimino)(4-hydroxyphenyl)methyl)-3,7-dimethyl-9-(2,6,6-trimethylcyclohex-1-enyl)nona-2,4,6,8-tetraenamide (236)

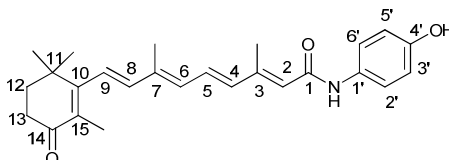


The mixed anhydride (**148**) (50.1 mg, 1 eq) was dissolved in pyridine (3 ml) at room temperature and 4-hydroxyphenylimidoxime (**235**) (24 mg, 1.2 eq) was added. The solution was allowed to stir overnight. Once complete, the reaction was diluted with EtOAc (50 ml) and washed with saturated sodium bicarbonate solution (2 × 50 ml) and brine (2 × 50 ml). The organic layer was dried over sodium sulphate and concentrated *in vacuo*. The residue was

purified using silica column chromatography, eluted with a 0-100 % EtOAc in hexane, to yield the product as a yellow solid (31 mg, 55 %). **LCMS (M+H)⁺** found 435.4 requires 435.2, RT 2.48 min; **HRMS ESI (M+H)⁺** found 435.2647, C₂₇H₃₅N₂O₃ requires 435.2642; **δ_H (500 MHz, CDCl₃)** 1.07 (6H, s, C11(CH₃)₂), 1.51 (2H, m, C12H₂), 1.65 (2H, m, C13H₂), 1.75 (3H, s, C3CH₃), 2.02 (3H, s, C7CH₃), 2.09 (2H, m, C14H₂), 2.44 (3H, s, C15CH₃), 2.90 (1H, m, NH), 5.86 (1H, s, C2H), 6.32 (4H, m, C4-, C6-, C8-, C9-H), 6.86 (2H, d, *J* = 8.2 Hz, C3'-, C5'-H), 7.12 (1H, m, C5H), 7.48 (2H, d, *J* = 8.2 Hz, C2'-, C6'-H), 7.96 (1H, d, *J* = 8.7 Hz, oxime-NH), 8.67 (1H, br s, OH); **δ_C (125 MHz, CDCl₃)** 12.91 (C3CH₃), 13.98 (C7CH₃), 20.38 (C13), 21.96 (C15CH₃), 29.46 (C11(CH₃)₂), 34.05 (C14), 35.31 (C11), 40.84 (C12), 117.44 (C2), 119.92 (C3', C5'), 120.62 (C5), , 130.75 (C1'), 131.00 (C9), 132.25 (C6), 132.62 (C15), 135.30 (C2', C6'), 136.59 (C4), 139.02 (C8), 139.08 (C7), 139.14 (C10), 140.50 (C3), 154.30 (C4'), 164.02 (CN), 170.63 (C1); **IR (cm⁻¹)** 3351, 2922, 1710, 1608, 1133, 839; **MP** 101-104 °C.

7.3.4 Cyclohexyl analogues

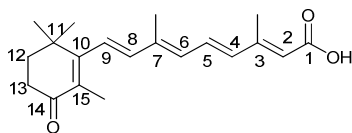
(2E,4E,6E,8E)-N-(4-hydroxyphenyl)-3,7-dimethyl-9-(2,6,6-trimethyl-3-oxocyclohex-1-enyl)nona-2,4,6,8-tetraenamide (3)



Compound (**376**) (196 mg, 1 eq) and 4-aminophenol (**225**) (65 mg, 1.2 eq) were dissolved in DCM (5 ml) and pyridine (400 μl) was added. The reaction was allowed to stir overnight at room temperature. Once complete, the reaction was diluted with EtOAc (50 ml) and washed with saturated sodium bicarbonate solution (2 × 50 ml) and brine (2 × 50 ml). The organic layer was dried over sodium sulphate and concentrated *in vacuo*. The residue was purified using silica column chromatography, eluted with a 0-100 % EtOAc in hexane, and recrystallised in MeOH to yield the product as a yellow solid (81 mg, 41 %). **LCMS (M+H)⁺** found 406.2, requires 406.2, RT 2.09 min; **HRMS ESI (M+H)⁺** found 406.2392, C₂₆H₃₂NO₃ requires 406.2377; **δ_H (300 MHz, CDCl₃)** 1.12 (6H, s, C11(CH₃)₂), 1.79 (3H, s, C3CH₃), 1.79 (2H, m, C12H₂),

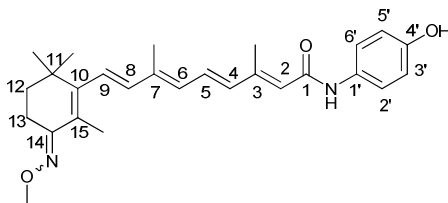
1.96 (3H, s, C7CH₃), 2.35 (3H, s, C15CH₃), 2.45 (2H, m, C13H₂), 5.23 (1H, br s, OH), 5.77 (1H, s, C2H), 6.25 (4H, m, C4-, C6-, C8-, C9-H), 6.71 (2H, d, *J* = 4.8 Hz, C3'-, C5'-H), 6.90 (1H, m, C5-H), 7.31 (2H, d, *J* = 4.8 Hz, C2'-, C6'-H); δ_c (125 MHz; DMSO) 12.43 (C3), 13.16 (C7), 13.47 (C15CH₃), 27.32 (C11(CH₃)₂), 33.80 (C13), 36.89 (C12), 39.03 (C11), 115.02 (C3', C5'), 122.70 (C2', C6'), 123.91(C2), 125.48 (C9), 125.79 (C15), 129.05 (C5), 131.14 (C1'), 133.24 (C6), 137.19 (C7), 137.84 (C4), 140.36 (C8), 147.14 (C7), 153.22 (C3), 160.48 (C4'), 164.04 (C10), 164.04 (C1), 197.80 (C14); IR (cm⁻¹) 3330, 2916, 1644, 1510, 1250, 1175, 968, 826; MP 233-235 °C.

(2E,4E,6E,8E)-3,7-dimethyl-9-(2,6,6-trimethyl-3-oxocyclohex-1-enyl)nona-2,4,6,8-tetraenoic acid (7)



Compound (**245**) was dissolved in 1:1 MeOH:THF solution (5 ml) and 10 % NaOH solution was added. The reaction was allowed to stir at room temperature overnight. 20 % HCl (2 ml) solution was added and the product formed a yellow precipitate. The product was purified using Biotage silica column chromatography, eluted with a 0-100 % EtOAc in hexane, to yield the product as a yellow solid (15 mg, 17 %) **LCMS (M+H)⁺** found 315.2, requires 315.2, RT 2.06 min; δ_H (300 MHz, CDCl₃) 1.21 (6H, s, C11(CH₃)₂), 1.78 (3H, s, C3CH₃), 1.78 (2H, m, C13H₂), 1.97 (3H, s, C7CH₃), 2.30 (3H, s, C15CH₃), 2.45 (2H, m, C14H₂), 5.77 (1H, s, C2H), 6.27 (4H, m, C4-, C6-, C8-, C9-H), 6.94 (1H, m, C5-H).

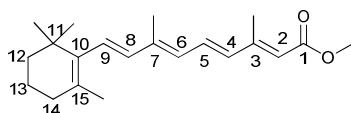
(2E,4E,6E,8E)-N-(4-hydroxyphenyl)-9-((E)-3-(methoxyimino)-2,6,6-trimethylcyclohex-1-enyl)-3,7-dimethylnona-2,4,6,8-tetraenamide (243)



4-Oxo-fenretinide (**3**) (50 mg, 1 eq) and methoxylamine hydrochloride (12 mg, 1.1 eq) were dissolved in EtOH (3 ml) and the reaction was stirred at

room temperature. After 72 h the reaction was seen to be complete by LCMS. The residue was concentrated *in vacuo* to yield the product as a yellow solid (27 mg, 50 %). **LCMS (M+H)⁺** found 435.4, requires 435.3, RT 2.41 min; **HRMS ESI (M+H)⁺** found 435.2652, C₂₇H₃₅N₂O₃ requires 435.2642; **δ_{H} (300 MHz, CDCl₃)** 1.10 (6H, s, C11(CH₃)₂), 1.59 (2H, t, *J* = 6.6 Hz, C12H₂), 1.92 (3H, s, C3CH₃), 2.04 (3H, s, C7CH₃), 2.39 (3H, s, C15CH₃), 2.60 (2H, t, *J* = 6.6 Hz, C13H₂), 5.86 (1H, s, OH), 6.00 (1H, s, C2H), 6.30 (4H, m, C4-, C6-, C8-, C9-H), 6.75 (2H, d, *J* = 8.7 Hz, C2'-, C6'-H), 7.04 (1H, m, C5-H), 7.39 (2H, d, *J* = 8.7 Hz, C3'-, C5'-H), 7.94 (1H, br d, *J* = 15.3 Hz, NH); **δ_{C} (125 MHz; CDCl₃)** 12.82 (C15), 13.91 (C3), 15.29 (C7), 23.03 (C13), 28.12 (C11(CH₃)₂), 35.80 (C11), 37.40 (O12), 62.03 (OCH₃), 116.26 (C3', C5'), 123.17 (C2', C6'), 123.72 (C2), 126.39 (C15), 127.74 (C9), 130.69 (C5), 132.05 (C1'), 132.75 (C6), 138.08 (C4), 139.06 (C7), 140.48 (C8), 150.09 (C3), 150.23 (C4'), 155.27 (C4), 157.74 (C10), 167.48 (C1); **IR (cm⁻¹)** 3291, 2929, 1607, 1511, 1050, 832; **MP** 108-111 °C.

(2E,4E,6E,8E)-methyl 3,7-dimethyl-9-(2,6,6-trimethylcyclohex-1-enyl)nona-2,4,6,8-tetraenoate (244)



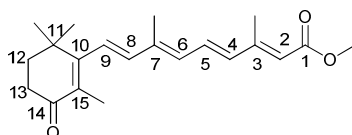
Synthesis of this compound was adapted from that previously described by Patel, *et. al.*¹⁰⁰ Retinoic acid (**6**) (500 mg, 1 eq) was dissolved in MeOH (10 ml) and TMSCH₂N₂ (2 M in hexanes) (1 ml) was added. The reaction was allowed to stir at room temperature overnight. The reaction was seen to have not proceeded to completion by TLC, therefore additional TMSCH₂N₂ (2 M in hexanes) (2 ml) was added and the reaction was allowed to stir for a further 2 h. The reaction was seen to be complete by TLC and the volatiles were removed under reduced pressure to yield the product as a yellow oil (523 mg, 100 %).

OR

Retinoic acid (**6**) (2 g, 1 eq) and K₂CO₃ (2 g, 2 eq) were dissolved in DMF (20 ml) and iodomethane (11 ml, 11.6 eq) was added under N₂. The reaction was allowed to stir overnight at room temperature. The reaction was seen to

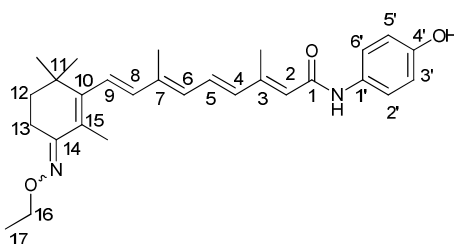
be complete by TLC and was diluted with EtOAc (50 ml), washed with deionised water (2 × 50 ml) and brine (2 × 50 ml). The organic layer was dried over sodium sulphate and concentrated *in vacuo* to yield the product as a yellow oil (2.1 g, 100 %). Product did not ionise by LCMS. δ_{H} (300 MHz, CDCl_3) 1.04 (6H, s, C11(CH₃)₂), 1.48 (2H, m, C12H₂), 1.63 (2H, m, C13H₂), 1.72 (3H, s, C3CH₃), 2.01 (3H, s, C7CH₃), 2.03 (2H, m, C14H₂), 2.37 (3H, s, C15CH₃), 3.72 (3H, s, OCH₃), 5.79 (1H, s, C2H), 6.17 (4H, m, C4-, C6-, C8-, C9-H), 7.01 (1H, m, C5-H).

(2E,4E,6E,8E)-methyl 3,7-dimethyl-9-(2,6,6-trimethyl-3-oxocyclohex-1-enyl)nona-2,4,6,8-tetraenoate (245)



This compound was synthesised as previously described by Patel, *et. al.*¹⁰⁰ Compound (**244**) (2.1 g, 1 eq) was dissolved in DCM (200 ml) and MnO₂ (30 g, 50 eq) was added. The reaction was allowed to stir at room temperature for 72 h. The reaction was seen to be complete by TLC and the MnO₂ was removed by filtration through Celite. The filtrate was concentrated *in vacuo* to yield the product as a yellow oil (1.4 g, 64 %). The product was not ionised by LCMS. δ_{H} (300 MHz, CDCl_3) 1.12 (6H, s, C11(CH₃)₂), 1.78 (3H, s, C3CH₃), 1.78 (2H, m, C13H₂), 1.96 (3H, s, C7CH₃), 2.29 (3H, s, C15CH₃), 2.44 (2H, m, C14H₂), 3.65 (3H, s, OCH₃), 5.75 (1H, s, C2H), 6.32 (4H, m, C4-, C6-, C8-, C9-H), 6.92 (1H, m, C5-H).

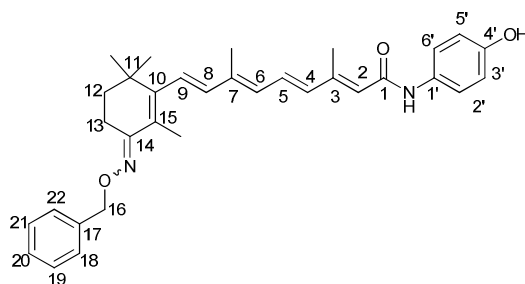
(2E,4E,6E,8E)-9-((E)-3-(ethoxyimino)-2,6,6-trimethylcyclohex-1-enyl)-N-(4-hydroxyphenyl)-3,7-dimethylnona-2,4,6,8-tetraenamide (246)



4-Oxo-fenretinide (**3**) (40 mg, 1 eq) and *O*-ethylhydroxylamine (11 mg, 1.1 eq) were dissolved in EtOH (3 ml) and the reaction was allowed to stir

overnight at room temperature. The reaction was seen to be complete by LCMS. The residue was concentrated *in vacuo* and purified by Biotage silica column chromatography, eluted with a 0-100 % EtOAc in hexane, to yield the product as a brown oil (35 mg, 79 %). **LCMS (M+H)⁺** found 449.3, requires 449.3, RT 2.51 min; **HRMS ESI (M+H)⁺** found 449.2811, C₂₈H₃₇N₂O₃ requires 449.2799; **δ_{H} (500 MHz, CDCl₃)** 1.07 (6H, s, C11(CH₃)₂), 1.22 (3H, t, *J* = 6.9 Hz, C17-H), 1.51 (2H, t, *J* = 6.9 Hz, C12H₂), 1.86 (3H, s, C3CH₃), 1.94 (3H, s, C7CH₃), 2.33 (3H, s, C15CH₃), 2.55 (2H, t, *J* = 6.9 Hz, C14H₂), 4.09 (2H, q, *J* = 6.9 Hz, C16-H), 5.08 (2H, s, C16-H), 5.75 (1H, s, C2H), 6.18 (4H, m, C4-, C6-, C8-, C9-H), 6.67 (2H, d, *J* = 8.7 Hz, C3'-, C5'-H), 6.17 (1H, m, C5-H), 7.23 (2H, d, *J* = 6.9 Hz, C2'-, C6'-H); **δ_{C} (75 MHz; CDCl₃)** 12.81 (C15CH₃), 13.76 (C3CH₃), 14.74 (CH₂CH₃), 14.95 (C7CH₃), 20.12 (C13), 27.69 (C11(CH₃)₂), 34.78 (C11), 36.29 (C12), 69.41 (OCH₂), 115.85 (C3', C5'), 121.93(C2'), 122.75 (C2', C6'), 125.63 (C15), 127.01 (C9), 129.93 (C5), 130.22 (C1'), 131.25 (C6), 136.44 (C4), 138.32 (C7), 138.87 (C8), 148.34 (C3), 150.02 (C4'), 153.39 (C14), 156.61 (C10), 165.76 (C1); **IR (cm⁻¹)** 3280, 2923, 1510, 1161, 1050, 961, 831.

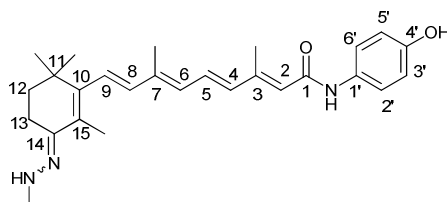
(2E,4E,6E,8E)-9-((E)-3-(benzyloxyimino)-2,6,6-trimethylcyclohex-1-enyl)-N-(4-hydroxyphenyl)-3,7-dimethylnona-2,4,6,8-tetraenamide (247)



4-Oxo-fenretinide (**3**) (49 mg, 1 eq) and *O*-benzylhydroxylamine hydrochloride (21 mg, 1.1 eq) were dissolved in EtOH (3 ml) and the reaction was allowed to stir overnight at room temperature. The reaction was seen to be complete by LCMS. The residue was concentrated *in vacuo* and purified by Biotage silica column chromatography eluted, with a 0-100 % EtOAc in hexane, to yield the product as a yellow solid (47 mg, 76 %). **LCMS (M+H)⁺** found 511.3, requires 511.3, RT 2.57 min; **HRMS ESI (M+H)⁺** found 511.2968, C₃₃H₃₉N₂O₃ requires 511.2955; **δ_{H} (500 MHz, CDCl₃)** 0.99 (6H, s,

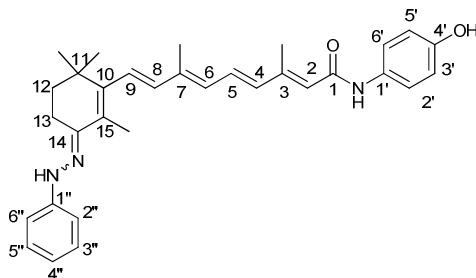
C11(CH₃)₂, 1.49 (2H, t, *J* = 6.6 Hz, C12H₂), 1.83 (3H, s, C3CH₃), 1.89 (3H, s, C7CH₃), 2.30 (3H, s, C15CH₃), 2.58 (2H, t, *J* = 6.6 Hz, C13H₂), 5.08 (2H, s, C16H), 5.75 (1H, s, C2H), 6.14 (4H, m, C4-, C6-, C8-, C9-H), 6.65 (2H, d, *J* = 8.4 Hz, C3'-, C5'-H), 6.85 (1H, m, C5-H), 7.26 (7H, m, C18-22-, C2'-, C6'-H), 7.52 (1H, s, OH); δ_c (75 MHz; CDCl₃) 12.83, 13.77, 14.98, 20.29, 27.69, 34.81, 36.20, 76.05, 115.86, 121.91, 122.76, 125.51, 126.94, 127.68, 128.20, 128.29, 129.95, 130.24, 131.32, 136.47, 138.22, 138.31, 138.96, 148.79, 150.06, 153.38, 157.25, 165.74; IR (cm⁻¹) 3479, 3357, 2924479, 3357, 2924, 1707, 1573, 1514, 1246, 1195, 1116, 964; MP 101-103 °C.

(2E,4E,6E,8E)-N-(4-hydroxyphenyl)-3,7-dimethyl-9-((Z)-2,6,6-trimethyl-3-(2-methylhydrazono)cyclohex-1-enyl)nona-2,4,6,8-tetraenamide (248)



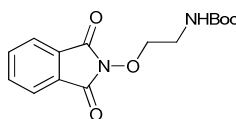
4-Oxo-fenretinide (**3**) (50 mg, 1 eq) and methylhydrazine (7.5 μ l, 1.1 eq) were dissolved in EtOH (3 ml). Acetic acid (3 drops) was added and the reaction was stirred at room temperature for a 72 h when it was seen to be complete by LCMS. The residue was concentrated *in vacuo* to yield the product as a yellow solid (23 mg, 46 %). LCMS (M+H)⁺ found 434.4, requires 434.3, RT 1.86 min; HRMS ESI (M+H)⁺ found 434.2797, C₃₂H₃₈N₃O₂ requires 434.2802; δ_H (300 MHz, CDCl₃) 0.99 (6H, s, C11(CH₃)₂), 1.76 (2H, m, C12H₂), 1.82 (3H, s, C3CH₃), 1.92 (3H, s, C7CH₃), 2.27 (3H, s, C15CH₃), 2.80 (2H, m, C14H₂), 2.80 (3H, s, NHCH₃), 6.00 (1H, s, C2H), 3.21 (1H, m, NH), 5.88 (1H, s, C2-H), 6.21 (4H, m, C4-, C6-, C8-, C9-H), 6.64 (2H, d, *J* = 8.7 Hz, C17-H), 6.93 (1H, m, C5-H), 7.28 (2H, d, *J* = 8.7 Hz, C3'-, C5'-H); δ_c (125 MHz; CDCl₃) 12.71 (C15CH₃), 13.90 (C3CH₃), 14.00 (C7CH₃), 24.47 (C13), 27.95 (C11(CH₃)₂), 35.18 (C11), 36.93 (NHCH₃), 38.41 (C12), 116.31 (C3', C5'), 123.16 (C2', C6'), 123.65 (C2), 124.31 (C9), 126.58 (C5), 130.48 (C6), 130.76 (C15), 132.07 (C1'), 134.60 (C4), 138.63 (C7), 139.18 (C8), 142.43 (C14), 150.06 (C3), 155.38 (C10), 164.17 (C4'), 167.47 (C1); IR (cm⁻¹) 3287, 2920, 2851, 1640, 1440, 1225, 1165, 966, 831; MP 79-82 °C.

(2E,4E,6E,8E)-N-(4-hydroxyphenyl)-3,7-dimethyl-9-((Z)-2,6,6-trimethyl-3-(2-phenylhydrazono)cyclohex-1-enyl)nona-2,4,6,8-tetraenamide (249)



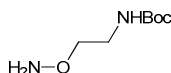
4-Oxo-fenretinide (**3**) (20 mg, 1 eq) and phenylhydrazine (9 mg, 1.1 eq) were dissolved in EtOH (3 ml) and the reaction was stirred at room temperature. The reaction was seen to be partially complete by LCMS after 48h. Acetic acid (3 drops) was added and the reaction was stirred for a further 72 h when it was seen to be complete by LCMS. The residue was concentrated *in vacuo* to yield the product as a yellow solid (4 mg, 16 %). **LCMS (M+H)⁺** found 496.4, requires 496.3, RT 2.42 min; **HRMS ESI (M+H)⁺** found 496.2960, C₃₂H₃₈N₃O₂ requires 496.2959; **δ_{H} (300 MHz, CDCl₃)** 1.16 (6H, s, C11(CH₃)₂), 1.74 (2H, t, *J* = 6.6 Hz, C12H₂), 2.07 (3H, s, C3CH₃), 2.09 (3H, s, C7CH₃), 2.39 (3H, s, C15CH₃), 2.57 (2H, t, *J* = 6.6 Hz, C13H₂), 6.00 (1H, s, C2H), 6.34 (4H, m, C4-, C6-, C8-, C9-H), 6.76 (2H, d, *J* = 8.8 Hz, C3', 5'-H), 7.07 (1H, m, C5-H), 7.12 (4H, m, C2''-, C3''-, C5''-, C6''-H), 7.39 (2H, d, *J* = 8.8 Hz, C2'-, C6'-H), 7.40 (1H, m, C4''H), 7.78 (1H, br s, NH); **δ_{C} (125 MHz; CDCl₃)** 12.85 (C15CH₃), 13.94 (C3CH₃), 15.61 (C7CH₃), 21.89 (C13), 28.33 (C11(CH₃)₂), 35.49 (C11), 37.96 (C12), 114.07 (C2'', 6''), 117.31 (C3', C5'), 120.19 (C2), 123.17 (C2', C6'), 123.26 (C4''), 123.48 (C5), 128.68 (C9), 129.93 (C3'', C5''), 130.15 (C1'), 130.24 (C7), 130.94 (C15), 132.20 (C6), 137.68 (C4), 139.57 (C8), 145.63 (C1''), 145.92 (C4), 147.81 (C3), 150.43 (C10), 155.32 (C4'), 167.65 (C1); **IR (cm⁻¹)** 3316, 2922, 1510, 1306, 1162, 831; **MP** 174-178 °C.

***tert*-butyl 2-(1,3-dioxoisindolin-2-yloxy)ethylcarbamate (355)**



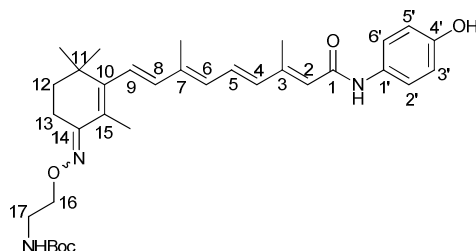
This compound was synthesised as previously described by Takeda Pharmaceutical company Ltd.²¹⁷ N-Boc-ethanol amine (**354**) (1.4 g, 1 eq), N-hydroxyphthalimide (1.6 g, 1.1 eq) and PPh₃ (2.5 g, 1.1 eq) were dissolved in dry THF (50 ml) under N₂ and cooled to –5 °C. DIAD (2.35 ml, 1.3 eq) was dissolved in dry THF (15 ml) and slowly added to the reaction. The reaction was stirred at –5 °C for 10 minutes and subsequently allowed to warm to room temperature to stir overnight. The residue was concentrated *in vacuo* and purified using Biotage silica column chromatography eluted with a hexane / EtOAc gradient (1:0 to 0:1) and recrystallised in Et₂O to yield the product as colourless crystals (902 mg, 36 %). **LCMS (M+H)⁺** found 207.0, requires 207.1, RT 1.87 min; **δ_H (300 MHz, CDCl₃)** 1.36 (9H, s, C(CH₃)₃), 3.35 (2H, t, *J* = 4.2 Hz, NHCH₂), 4.15 (2H, t, *J* = 4.2 Hz, OCH₂), 5.62 (1H, s, NH), 7.71 (4H, m, ArCH); **δ_C (125 MHz; CDCl₃)** 28.78 (C(CH₃)₃), 39.89 (NHCH₂), 76.10 (OCH₂), 80.32 (C(CH₃)₃), 124.46 (C2', C5'), 129.56 (C1, C6), 131.34 (C3, C4), 131.54 (C1/C6-CO), 133.47 (CO).

***tert*-butyl 2-(aminoxy)ethylcarbamate (356)**



Synthesis of this compound was adapted from that previously described by Takeda Pharmaceutical company Ltd.²¹⁷ Compound (**355**) (450 mg, 1 eq) was dissolved in MeOH (10 ml) and hydrazine monohydrate (1 ml, 2 eq) was added. The reaction was allowed to stir at room temperature overnight and once seen to be complete, the product was isolated by removal of solvents and excess hydrazine under reduced pressure (246 mg, 90 %). The product did not ionise by LCMS. **δ_H (300 MHz, CDCl₃)** 1.26 (C(CH₃)₃), 3.15 (2H, q, *J* = 5.1 Hz, NHCH₂), 3.51 (2H, t, *J* = 5.1 Hz, OCH₂), 5.33 (1H, br s, NH).

***tert*-butyl 2-((*Z*)-3-((1*E*,3*E*,5*E*,7*E*)-9-(4-hydroxyphenylamino)-3,7-dimethyl-9-oxonona-1,3,5,7-tetraenyl)-2,4,4-trimethylcyclohex-2-enylideneaminoxy)ethylcarbamate (**357**)**



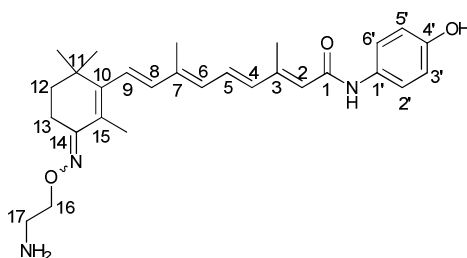
4-oxo-fenretinide (**3**) (51 mg, 1 eq) and compound **356** (25 mg, 1.1 eq) were dissolved in EtOH (5 ml). Acetic acid (2 drops) was added and the reaction was stirred at room temperature for a 72 h when it was seen to be complete by LCMS. The reaction was diluted with EtOAc (20 ml) and washed with saturated sodium bicarbonate solution (3 × 20 ml) and brine (3 × 20 ml). The organic layer was dried over sodium sulphate and concentrated *in vacuo*. The residue was purified by Biotage silica column chromatography, eluted with a 0-100 % EtOAc in hexane, to yield the product as a yellow solid (30 mg, 42 %).

OR

4-Oxo-fenretinide (**3**) (70 mg, 1 eq) and compound **356** (11 mg, 1.1 eq) were dissolved in EtOH (3 ml) and the reaction was heated to 100 °C at 200 bar by microwave radiation. After 72 h the reaction was seen to be complete by LCMS. The product was concentrated *in vacuo* to yield the product as a yellow solid (45 mg, 45 %). **LCMS (M+H)⁺** found 564.5, requires 564.4, RT 2.40 min; **HRMS ESI (M+H)⁺** found 564.3448, C₃₃H₄₆N₃O₂ requires 564.3432; **δ_H (500 MHz, CDCl₃)** 1.09 (6H, s, C11(CH₃)₂), 1.47 (9H, s, C(CH₃)₃), 1.60 (2H, t, *J* = 6.0 Hz, C12H₂), 1.91 (3H, s, C3CH₃), 2.02 (3H, s, C7CH₃), 2.41 (3H, s, C15CH₃), 2.62 (2H, t, *J* = 6.0 Hz, C13H₂), 3.45 (2H, br m, C16-H), 4.15 (1H, m, C15-H), 5.15 (1H, br s, OH), 5.85 (1H, s, C2H), 6.26 (4H, m, C4-, C6-, C8-, C9-H), 6.78 (2H, d, *J* = 8.7 Hz, C3'-, C5'-H), 6.94 (1H, m, C5-H), 7.34 (2H, d, *J* = 8.7 Hz, C2'-, C6'-H), 7.53 (1H, s, C17NH) 7.93 (1H, app d, *J* = 15 Hz, C1NH); **δ_C (125 MHz; CDCl₃)** 12.82 (C15C₃), 13.72 (C3), 14.90 (C7), 20.06 (C13), 27.66 (C11(CH₃)₂), 28.44 (C(CH₃)₃), 34.84

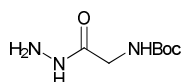
(C11), 36.12 (NHCH₂), 40.98 (C12), 72.62 (OCH₂), 79.39 (C(CH₃)₃), 115.80 (C3', C5'), 122.15 (C2), 122.38 (C2', C6'), 125.21 (C15), 126.75 (C9), 129.77 (C5), 130.43 (C1'), 131.43 (C6), 136.61 (C4), 138.14 (C7), 139.10 (C8), 149.25 (C4), 149.79 (C4'), 153.41 (OCO), 156.17 (C14), 157.46 (C15), 165.48 (C1); **IR (cm⁻¹)** 3306, 2925, 1724, 1673, 1510, 1267, 1122; **MP** 122-125 °C.

(2E,4E,6E,8E)-9-((E)-3-(2-aminoethoxyimino)-2,6,6-trimethylcyclohex-1-enyl)-N-(4-hydroxyphenyl)-3,7-dimethylnona-2,4,6,8-tetraenamide (358)



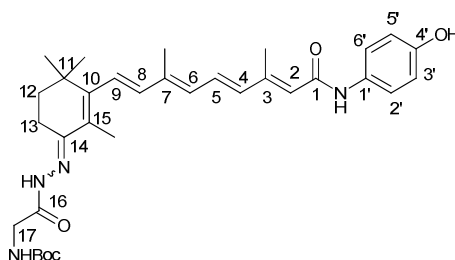
Compound **357** (56 mg) was dissolved in DCM (3 ml) and TFA (1 ml) was added. The reaction was allowed to stir at room temperature for 1 h, when it was seen to be complete by LCMS. The reaction was diluted with EtOAc (50 ml) and washed with saturated sodium bicarbonate solution (3 × 50 ml). The organic layer was dried over sodium sulphate and concentrated *in vacuo*. Trituration with EtOAc yielded the clean product as a yellow solid (35 mg, 76 %). **LCMS (M+H)⁺** found 464.3, requires 464.3, RT 1.71 min; **HRMS ESI (M+H)⁺** found 464.2917, C₂₈H₃₈N₃O₃ requires 464.2908; **δ_H (500 MHz, CDCl₃)** 0.98 (6H, s, C11(CH₃)₂), 1.47 (2H, m, C12H₂), 1.81 (3H, s, C3CH₃), 1.92 (3H, s, C7CH₃), 2.23 (3H, s, C15CH₃), 2.53 (2H, m, C13H₂), 3.20 (2H, m, C16-H), 4.02 (1H, m, C15-H), 4.21 (2H, m NH₂), 5.90 (1H, s, C2H), 6.21 (4H, m, C4-, C6-, C8-, C9-H), 6.64 (2H, d, *J* = 8.1 Hz, C3'-, C5'-H), 6.81 (1H, m, C5-H), 7.28 (2H, d, *J* = 8.1 Hz, C2'-, C6'-H); **δ_C (125 MHz; CDCl₃)** 12.93 (C15CH₃), 14.03 (C3CH₃), 15.57 (C7CH₃), 21.21 (C13), 28.28 (C11(CH₃)₂), 36.02 (C11), 37.51 (NH₂CH₂), 40.74 (C12), 74.25 (OCH₂), 116.38 (C3', C5'), 123.22 (C2', C6'), 123.91 (C2), 123.96 (C15), 127.85 (C9), 130.77 (C5), 132.16 (C1'), 132.96 (C6), 138.38 (C4), 139.09 (C7), 140.68 (C8), 150.35 (C3), 155.40 (C4'), 158.37 (C14), 159.81 (C15), 167.59 (C1) ; **IR (cm⁻¹)** 3650, 3305, 2923, 1509, 1447, 1363, 1167, 1065, 969, 833; **MP** 119-122 °C.

tert-butyl 2-hydrazinyl-2-oxoethylcarbamate (361)



N-Boc-glycine methylester (**360**) (500 mg, 1 eq) was dissolved in MeOH (10 ml) and hydrazine monohydrate (1 ml, 12 eq) was added. The reaction was allowed to stir at room temperature overnight and once seen to be complete, the product was isolated by removal of solvents and excess hydrazine under reduced pressure (503 mg, 100 %). **LCMS (M+Na)⁺** found 212.0, requires 212.1, RT 0.62 min; **δ_{H} (500 MHz, CDCl₃)** 1.37 (9H, s, C(CH₃)₃), 3.74 (2H, d, *J* = 6.3 Hz, CH₂), 4.02 (2H, br s, NH₂), 5.94 (1H, br s, NHNH₂), 7.28 (1H, br s, CH₂NH); **δ_{C} (75 MHz; CDCl₃)** 28.71 (C(CH₃)₃), 43.39 (CH₂), 80.74 (C(CH₃)₃), 158.39 (OCO), 171.81 (CH₂CO); **MP** 94-98 °C.

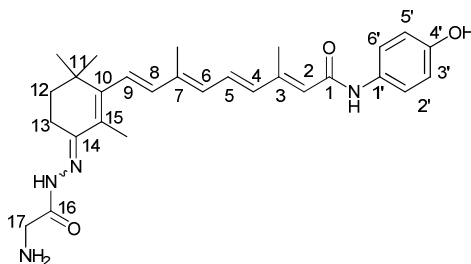
tert-butyl 2-((E)-2-(3-((1E,3E,5E,7E)-9-(4-hydroxyphenylamino)-3,7-dimethyl-9-oxonona-1,3,5,7-tetraenyl)-2,4,4-trimethylcyclohex-2-enylidene)hydrazinyl)-2-oxoethylcarbamate (362)



4-Oxo-fenretinide (**3**) (70 mg, 1 eq) and compound **361** (33 mg, 1 eq) were dissolved in EtOH (3 ml) the reaction was heated by microwave radiation (100 °C, 200 bar) for 24 h. A further quantity of compound **361** (60 mg, 1.8 eq) was added and the reaction was heated for a further 48 h until seen to be complete by LCMS. The residue was purified by Biotage, eluted with a 0-100 % EtOAc in hexane, to yield the product as a yellow solid (45 mg, 45 %). **LCMS (M+H)⁺** found 577.4, requires 577.3, RT 2.43 min; **HRMS ESI (M+H)⁺** found 577.3402, C₃₃H₄₄N₄O₅ requires 577.3384; **δ_{H} (500 MHz, CDCl₃)** 1.10 (6H, s, C11(CH₃)₂), 1.48 (9H, s, C(CH₃)₃), 1.69 (2H, m, C12H₂), 1.91 (3H, s, C3CH₃), 2.02 (3H, s, C7CH₃), 2.35 (2H, m, C13H₂), 2.40 (3H, s, C15CH₃), 3.91 (1H, br s, OH), 4.35 (2H, d, *J* = 4.2 Hz, NHCH₂), 5.44 (1H, s, NNH), 5.86 (1H, s, C2H), 6.26 (4H, m, C4-, C6-, C8-, C9-H), 6.78 (2H, d, *J* = 8.7 Hz,

C3'-, C5'-H), 6.94 (1H, m, C5-H), 7.37 (2H, d, $J = 8.7$ Hz, C2'-, C6'-H), 7.68 (1H, s, C17NH), 8.74 (1H, s, C1NH); δ_c (125 MHz; CDCl₃) 12.81 (C15), 13.69 (C3), 15.04 (C7), 20.58 (C13), 27.58 (C11(CH₃)₂), 28.31 (C(CH₃)₃), 34.68 (C11), 35.85 (C12), 42.50 (C17), 79.86 (C(CH₃)₃), 115.77 (C3', C5'), 122.21 (C2', C6'), 126.50 (C2), 126.75 (C9), 127.59 (C15), 129.70 (C5), 130.67 (C1'), 131.81 (C6), 136.84 (C4), 138.02 (C7), 139.42 (C8), 149.72 (C14), 150.45 (C3), 150.98 (C10), 153.20 (C4'), 156.18 (OCO), 165.30 (C1), 171.38 (NHCO) ; IR (cm⁻¹) 3306, 2958, 2925, 2857, 1724, 1510, 1267, 1122; MP 122-125 °C.

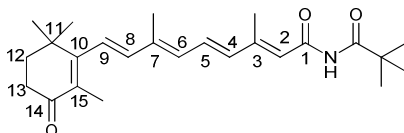
(2E,4E,6E,8E)-9-((E)-3-(2-(2-aminoacetyl)hydrazono)-2,6,6-trimethylcyclohex-1-enyl)-N-(4-hydroxyphenyl)-3,7-dimethylnona-2,4,6,8-tetraenamide (363)



Compound **362** (34 mg) was dissolved in DCM (10 ml) and TFA (5 ml) was added. The reaction was allowed to stir for 1 h at room temperature. The solvents were removed under reduced pressure, the residue was dissolved in EtOAc (20 ml) and washed with saturated sodium bicarbonate solution (3 × 20 ml). The organic layer was dried over sodium sulphate and concentrated *in vacuo*. The residue was purified by HPLC to yield the product as a yellow solid consisting of 4 isomers (10 mg, 37 %); **LCMS (M+H)⁺** found 477.3, requires 477.3; δ_H (500 MHz, MeOD) (Major isomer) 1.03 (6H, s, C11(CH₃)₂), 1.61 (2H, m, C12H₂), 1.86 (3H, s, C3CH₃), 1.95 (3H, s, C7CH₃), 2.28 (3H, s, C15CH₃), 2.40 (2H, m, C13H₂), 4.04 (2H, d, $J = 4.2$ Hz, NHCH₂), 5.90 (1H, s, C2H), 6.30 (4H, m, C4-, C6-, C8-, C9-H), 6.64 (2H, d, $J = 8.7$ Hz, C3'-, C5'-H), 6.95 (1H, m, C5-H), 7.27 (2H, d, $J = 8.7$ Hz, C2'-, C6'-H); δ_c (125 MHz; MeOD) (Major isomer) 13.13 (C15CH₃), 14.26 (C3CH₃), 15.87 (C7CH₃), 22.96 (C13), 28.33 C11(CH₃)₂, 36.16 (C11), 37.66 (C12), 41.89 (C17), 116.64 (C3', C5'), 123.50 (C2', C6'), 124.21 (C15),

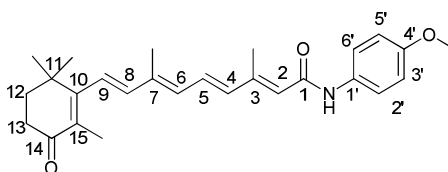
128.00 (C2), 131.00 (C9), 132.39 (C5), 133.47 (C6), 138.66 (C1'), 139.35 (C7), 141.15 (C8), 150.50 (C14), 152.84 (C3), 154.50 (C14), 155.70 (C1'), 167.87 (C10), 169.84 (CO).

(2E,4E,6E,8E)-3,7-dimethyl-9-(2,6,6-trimethyl-3-oxocyclohex-1-enyl)nona-2,4,6,8-tetraenoic pivalic anhydride (367)



Compound (**7**) (240 mg, 1 eq) and triethylamine (150 μ l) were dissolved in EtOAc (5 ml). Trimethyl acetyl chloride (**147**) (150 μ l, 1.7 eq) was added and the mixture was allowed stir for 2 h. The reaction was seen to be complete by TLC after 30 minutes. The reaction was diluted with EtOAc (50 ml) and was washed with 20 % HCl (2 \times 50 ml) and saturated sodium bicarbonate solution (2 \times 50 ml). The organic layer was dried over sodium sulphate and concentrated *in vacuo* to yield the pure compound as a yellow oil (93 mg, 31 %). The compound was not ionised by LCMS; δ_{H} (**300 MHz**, CDCl_3) 1.05 (6H, s, C11(CH₃)₂), 1.26 (9H, s, C(CH₃)₃), 1.85 (3H, s, C3CH₃), 1.85 (2H, m, C12H₂), 2.05 (3H, s, C7CH₃), 2.40 (3H, s, C15CH₃), 2.51 (2H, m, C13H₂), 5.78 (1H, s, C2H), 6.34 (4H, m, C4-, C6-, C8-, C9-H), 7.01 (1H, m, C5-H).

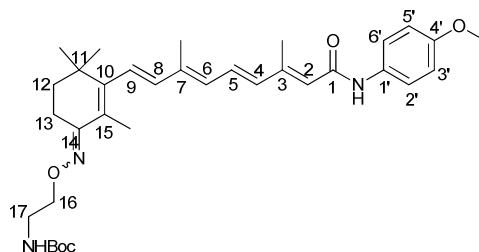
(2E,4E,6E,8E)-N-(4-methoxyphenyl)-3,7-dimethyl-9-(2,6,6-trimethyl-3-oxocyclohex-1-enyl)nona-2,4,6,8-tetraenamide (368)



Compound (**367**) (194 mg, 1 eq) and *para*-methoxyaniline (**150**) (137 mg, 1.2 eq) were dissolved in DCM (10 ml) and pyridine (1 μ l) was added. The reaction was allowed to stir overnight at room temperature. Once complete, the reaction was diluted with EtOAc (50 ml) and washed with saturated sodium bicarbonate solution (2 \times 50 ml) and brine (2 \times 50 ml). The organic layer was dried over sodium sulphate and concentrated *in vacuo*. The residue was purified using Biotage silica column chromatography, eluted with

a 0-30 % EtOAc in hexane, as a yellow solid (59 mg, 23 %). **LCMS (M+H)⁺** found 420.5, requires 420.3, RT 2.28 min; **HRMS ESI (M+H)⁺** found 420.2545, C₂₇H₃₄NO₃ requires 420.2533; **δ_H (300 MHz, CDCl₃)** 1.20 (6H, s, C11(CH₃)₂), 1.26 (2H, m, C12H₂), 1.88 (3H, s, C3CH₃), 2.03 (3H, s, C7CH₃), 2.41 (3H, s, C15CH₃), 2.52 (2H, d, *J* = 6.3 Hz, C13H₂), 3.77 (3H, s, OCH₃), 5.91 (1H, s, C2H), 6.29 (4H, m, C4-, C6-, C8-, C9-H), 6.84 (2H, d, *J* = 8.7 Hz, C3'-, C5'-H), 6.93 (1H, m, C5-H), 7.50 (2H, d, *J* = 4.8 Hz, C2'-, C6'-H), 7.98 (1H, s, NH); **δ_C (75 MHz; CDCl₃)** 12.72 (C3CH₃), 13.59 (C7CH₃), 13.85 (C15CH₃), 27.61 (C11(CH₃)₂), 34.28 (C13), 35.75 (C11), 37.30 (C12), 55.44 (OCH₃), 114.08 (C3', C5'), 121.54 (C2', C6'), 123.07 (C2), 125.50 (C9), 129.19 (C5), 129.92 (C5), 131.61 (C15), 133.10 (C6), 137.31 (C7), 137.78 (C4), 140.77 (C8), 149.20 (C3), 156.20 (C4'), 161.32 (C10), 165.00 (C1), 195.50 (C14); **IR (cm⁻¹)** 3331, 2923, 1641, 1438, 1110, 965, 832; **MP** 153-156 °C.

***tert*-butyl 2-((*Z*)-3-((1*E*,3*E*,5*E*,7*E*)-9-(4-methoxyphenylamino)-3,7-dimethyl-9-oxonona-1,3,5,7-tetraenyl)-2,4,4-trimethylcyclohex-2-enylideneaminoxy)ethylcarbamate (369)**

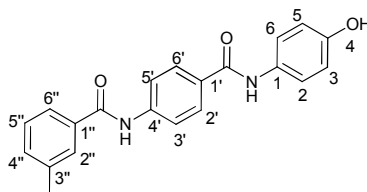


Compound **368** (25 mg, 1 eq) and compound **356** (13 mg, 1.1 eq) were dissolved in EtOH (2 ml). Acetic acid (2 drops) was added and the reaction was stirred at room temperature for a 72 h when it was seen to be complete by LCMS. The reaction was diluted with EtOAc (20 ml) and washed with saturated sodium bicarbonate solution (3 × 20 ml) and brine (3 × 20 ml). The organic layer was dried over sodium sulphate and the residue was concentrated *in vacuo* to yield the product as a yellow solid (17 mg, 49 %). **LCMS (M+H)⁺** found 578.6, requires 578.4, RT 2.58 min; **HRMS ESI (M+H)⁺** found 578.3602, C₃₄H₄₈N₃O₅ requires 578.3588; **δ_H (500 MHz, CDCl₃)** 0.98 (6H, s, C11(CH₃)₂), 1.47 (9H, s, C(CH₃)₃), 1.60 (2H, t, *J* = 6.6 Hz, C12H₂), 1.92 (3H, s, C3CH₃), 2.04 (3H, s, C7CH₃), 2.43 (3H, s, C15CH₃), 2.63 (2H, t,

$J = 6.6$ Hz, C13H₂), 3.46 (2H, br m, C17-H₂), 3.80 (3H, s, OCH₃), 4.18 (1H, t, $J = 4.8$ Hz, C16-H₂), 5.1 (1H, br s, C1NH), 5.84 (1H, s, C2H), 6.26 (4H, m, C4-, C6-, C8-, C9-H), 6.87 (2H, d, $J = 8.7$ Hz, C3'-, C5'-H), 6.97 (1H, m, C5-H), 7.36 (1H, s, C17NH), 7.49 (2H, d, $J = 8.7$ Hz, C2'-, C6'-H); δ_c (125 MHz; CDCl₃) 12.83 (C15C_H3), 13.65 (C3C_H3), 14.87 (C7C_H3), 20.05 (C13), 27.67 (C11(CH₃)₂), 28.44 (C(C_H3)₃), 34.85 (C11), 36.15 (NHCH₂), 40.98 (C12), 55.49 (OCH₃), 72.72 (OCH₂), 79.17 (C(CH₃)₃), 114.16 (C3', C5'), 121.54 (C2', C6'), 122.13 (C2), 125.26 (C15), 126.81 (C9), 129.74 (C5), 131.36 (C6), 131.46 (C11), 136.56 (C4), 138.16 (C7), 139.05 (C8), 149.14 (C3), 149.79 (C10), 155.99 (OCO), 156.30 (C14), 157.35 (C4'), 164.92 (C1); IR (cm⁻¹) 3309, 2930, 1710, 1642, 1510, 1242, 1167, 953, 798; MP 168-170 °C.

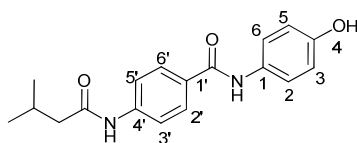
7.3.5 Non-retinoid analogues

N-(4-(4-hydroxyphenylcarbamoyl)phenyl)-3-methylbenzamide (251)



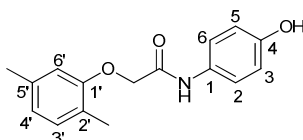
Compound **339** (33 mg) was dissolved in THF (3 ml) and TBAF (1 ml) was added. The reaction was allowed to stir for 30 min at room temperature and, once complete by TLC, reaction was diluted with EtOAc (50 ml) and washed with saturated sodium bicarbonate solution (3 × 50 ml). The organic layer was dried over sodium sulphate and the residue was concentrated *in vacuo* to yield the product as a white solid (22 mg, 89 %). The product did not ionise by LCMS; HRMS ESI (M+H)⁺ found 347.1397, C₂₁H₁₉N₂O₃ requires 347.1390; δ_H (300 MHz, (CD₃)₂SO) 2.23 (3H, s, CH₃), 6.58 (2H, d, $J = 9$ Hz, C3-, C5-H), 7.21 (2H, m, C5''-, C4''-H), 7.24 (2H, d, $J = 9$ Hz, C2-, C6-H), 7.52 (2H, m, C2''-, C6''-H), 7.66 (2H, d, $J = 9$ Hz, C2'-, C6'-H) 7.73 (2H, d, $J = 9$ Hz, C3'-, C5'-H); δ_c (75 MHz; CDCl₃) 20.94 (CH₃), 114.93 (C3, C5), 119.36 (C3', C5'), 122.23 (C2, C6), 124.90 (C6''), 129.18 (C5''), 128.21 (C2', C6'), 128.32 (C2''), 129.80 (C1'), 130.77 (C1), 132.33 (C4''), 134.68 (C1''), 137.74 (C3''), 141.94 (C4'), 153.60 (C4), 164.31 (C1''CO), 165.90 (C1'CO); IR (cm⁻¹) 3310, 2919, 1638, 1433, 1272, 1251, 807, 656; MP 260-262 °C.

***N*-(4-hydroxyphenyl)-4-(3-methylbutanamido)benzamide (263)**



Compound **340** (114 mg) was dissolved in THF (3 ml) and TBAF (1 ml) was added. The reaction was allowed to stir for 30 min at room temperature and, once complete by TLC, reaction was diluted with EtOAc (50 ml) and washed with saturated sodium bicarbonate solution (3 × 50 ml). The organic layer was dried over sodium sulphate and the residue was concentrated *in vacuo* to yield the product as a white solid (83 mg, 100 %). **LCMS (M+H)⁺** found 313.2, requires 313.2, RT 1.67 min; **HRMS ESI (M+H)⁺** found 313.1555, C₁₈H₂₁N₂O₃ requires 313.1547; **δ_H (300 MHz, (CD₃)₂SO)** 1.03 (6H, d, *J* = 6.3 Hz, C(CH₃)₂), 2.19 (1H, m, CH), 2.29 (2H, d, *J* = 6.9 Hz, CH₂), 6.80 (2H, d, *J* = 9 Hz, C3-, C5-H), 7.45 (2H, m, C2-, C6-H), 7.24 (2H, d, *J* = 9 Hz, C2-, C6-H), 7.73 (2H, d, *J* = 8.7 Hz, C2'-, C6'-H), 7.91 (2H, d, *J* = 8.7 Hz, C3'-, C5'-H); **δ_C (75 MHz; CDCl₃)** 22.79 (CH(CH₃)₂), 27.57 (CH), 116.31 (C3, C5), 120.46 (C3', C5'), 124.54 (C2, C6), 129.50 (C2', C6'), 131.32 (C1'), 131.69 (C1), 143.26 (C4'), 155.81 (C4), 168.12 (C1'CO), 174.37 (CHCO); **IR (cm⁻¹)** 3303, 2955, 1637, 1512, 1248, 1103, 826; **MP** 277-279 °C.

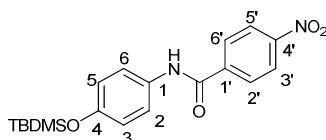
2-(2,5-dimethylphenoxy)-*N*-(4-hydroxyphenyl)acetamide (275)



2,5-dimethylphenoxyacetic acid (**341**) (500 mg, 1 eq) was dissolved in DMF (10 ml), HOBT (450 mg, 1.2 eq) was added and the reaction was allowed to stir for 5 min. EDC·HCl (638 mg, 1.2 eq) was added and the reaction was allowed to stir for 20 min. Triethylamine (386 μl, 1.1 eq) and 4-aminophenol (**226**) (333 mg, 1.1 eq) were added and the reaction was allowed to stir overnight at room temperature. The reaction was seen to be complete by LCMS. Water was added until the product precipitated out of solution and was subsequently filtered. The residue was purified by recrystallisation in MeOH to afford the product as a white solid (132 mg, 18 %). **LCMS (M+H)⁺**

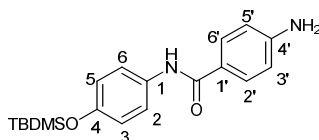
found 272.0, requires 272.1; **HRMS ESI (M+H)⁺** found, 272.1283 C₁₆H₁₈NO₃ requires 272.1281; **δ_{H} (300 MHz, (CD₃)₂SO)** 2.20 (3H, s, C2'CH₃), 2.25 (3H, s, C5'CH₃), 4.62 (2H, s, CH₂), 6.70 (4H, m, C3-, C5-, C4'-, C6'-H), 7.03 (1H, d, *J* = 7.5 Hz, C3'H), 7.40 (2H, d, *J* = 8.4 Hz, C2-, C6-H), 9.23 (1H, s, NH/OH), 9.70 (1H, s, NH/OH); **δ_{C} (75 MHz; CDCl₃)** 15.72 (C2'CH₃), 20.99 (C5'CH₃), 67.48 (CH₂), 112.40 (C6'), 115.04 (C3, C5), 121.35 (C4'), 121.49 (C2, C6), 122.96 (C2'), 129.91 (C3'), 130.28 (C1), 136.01 (C5'), 153.65 (C4), 155.91 (C1'), 165.98 (CO); **IR (cm⁻¹)** 3360, 2909, 1670, 1555, 1510, 832, 807; **MP** 196-198 °C.

***N*-(4-(*tert*-butyldimethylsilyloxy)phenyl)-4-nitrobenzamide (337)**



Compound **231** (1 g, 1.2 eq) was dissolved in DCM (5 ml) and NEt₃ (400 μ l) and *para*-nitrobenzoyl chloride (**336**) (1 g, 1 eq) was added. The reaction was allowed to stir at room temperature overnight. Once seen to be complete by LCMS, the reaction was diluted with DCM (50 ml) and washed with 10 % HCl solution (2 \times 50 ml), saturated sodium bicarbonate solution (2 \times 50 ml) and brine (2 \times 50 ml). The organic layer was dried over sodium sulphate and concentrated *in vacuo*. The residue was purified by Biotage silica column chromatography, eluted with a 0-100 % EtOAc in hexane, to yield the product as a white solid (676 mg, 40 %). The product was not ionised by LCMS. **δ_{H} (300 MHz, CDCl₃)** 0.00 (6H, s, Si(CH₃)₂), 0.80 (9H, s, C(CH₃)₃), 6.59 (2H, d, *J* = 8.7 Hz, C3-, C5-H), 7.27 (2H, d, *J* = 8.7 Hz, C2-, C6-H), 7.74 (2H, d, *J* = 8.7 Hz, C2'-, C6'-H), 7.94 (2H, d, *J* = 8.7 Hz, C3'-, C5'-H), 8.57 (1H, br s, NH).

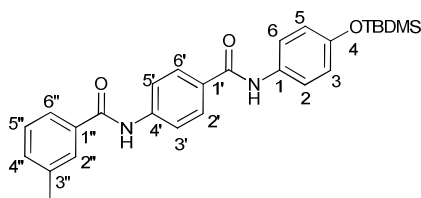
4-amino-*N*-(4-(*tert*-butyldimethylsilyloxy)phenyl)benzamide (338)



Compound (**337**) (676 mg) was dissolved in MeOH (20 ml). Pd/C (50mg) was added as a suspension in MeOH. The reaction was stirred under H₂ overnight at room temperature. The Pd/C was filtered through celite and the

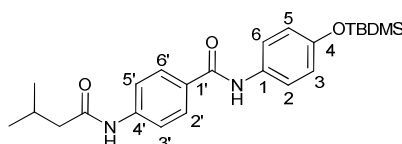
residue was concentrated *in vacuo* to yield the product as a white solid (574 mg, 92 %). The product was not ionised by LCMS. δ_{H} (300 MHz, CDCl_3) 0.00 (6H, s, $\text{Si}(\text{CH}_3)_2$), 0.81 (9H, s, $\text{C}(\text{CH}_3)_3$), 4.28 (2H, br s, NH_2), 6.36 (2H, d, $J = 8.4$ Hz, C3'-, C5'-H), 6.58 (2H, d, $J = 8.7$ Hz, C3-, C5-H), 7.30 (2H, d, $J = 8.7$ Hz, C2-, C6-H), 7.41 (2H, d, $J = 8.4$ Hz, C2'-, C6'-H), 8.43 (1H, br s, NH); δ_{C} (125 MHz; DMSO) -4.55 ($\text{Si}(\text{CH}_3)_2$), 17.92 ($\text{Si}(\text{C}(\text{CH}_3)_3$), 25.58 ($\text{Si}(\text{C}(\text{CH}_3)_3$), 113.15 (C3', C5'), 119.52 (C3, C5), 121.71 (C2, C6), 122.05 (C1'), 129.16 (C2', C6'), 133.53 (C1), 150.61 (C4'), 150.91 (C4), 164.89 (CO); IR (cm^{-1}) 3336, 2929, 2856, 1601, 1569, 1471, 1254, 909, 833, 778; MP 64-66 °C.

***N*-4-(4-hydroxyphenylcarbamoyl)phenyl)-3-methylbenzamide (339)**



Compound (**338**) (100 mg, 1 eq) was dissolved in DCM (5 ml) and NEt_3 (100 μl) and *meta*-toluoyl chloride (42 μl , 1 eq) was slowly added. The reaction was allowed to stir overnight at room temperature. The residue was concentrated *in vacuo* and triturated with MeOH to yield the product as a white solid (33 mg, 25 %). LCMS ($\text{M}+\text{H}$)⁺ found 461.2, requires 461.2, RT 2.47 min; δ_{H} (300 MHz, $(\text{CD}_3)_2\text{SO}$) 0.00 (6H, s, $\text{Si}(\text{CH}_3)_2$), 0.79 (9H, s, $\text{C}(\text{CH}_3)_3$), 2.20 (3H, s, CH_3), 6.62 (2H, d, $J = 8.7$ Hz, C3-, C5-H), 7.14 (2H, m, C5''-, C4''-H), 7.30 (2H, d, $J = 8.7$ Hz, C2-, C6-H), 7.50 (2H, m, C2''-, C6''-H), 7.51 (2H, d, $J = 8.7$ Hz, C3'-, C5'-H), 7.62 (2H, d, $J = 8.7$ Hz, C2'-, C6'-H) 7.86 (NH), 8.11 (1H, s, NH).

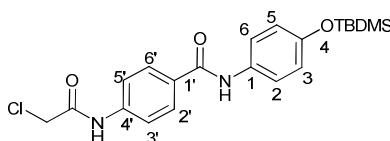
***N*-4-(*tert*-butyldimethylsilyloxy)phenyl)-4-(3-methylbutanamido)benzamide (340)**



Compound (**338**) (100 mg, 1 eq) was dissolved in DCM (5 ml) and NEt_3 (100 μl) and isovaleryl chloride (**347**) (36 μl , 1 eq) was slowly added. The reaction was allowed to stir overnight at room temperature. The residue was

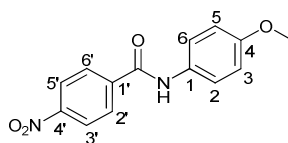
concentrated *in vacuo* and triturated with MeOH to yield the product as a white solid (114 mg, 91 %). **LCMS (M+H)⁺** found 427.3, requires 427.2, RT 2.39 min; **δ_{H} (300 MHz, (CD₃)₂SO)** 0.00 (6H, s, Si(CH₃)₂), 0.77 (6H, app s, (CH₃)₂), 0.80 (9H, s, C(CH₃)₃), 1.99 (1H, m, CH), 2.03 (2H, app s, CH₂), 6.62 (2H, d, *J* = 8.7 Hz, C3-, C5-H), 7.32 (2H, d, *J* = 8.7 Hz, C2-, C6-H), 7.36 (2H, m, C2'-, C6'-H), 7.56 (2H, d, *J* = 8.7 Hz, C3'-, C5'-H), 7.92 (1H, s, NH), 8.03 (1H, s, NH).

***N*-(4-(*tert*-butyldimethylsilyloxy)phenyl)-4-(2-chloroacetamido)benzamide (342)**



Compound (**338**) (315 mg, 1 eq) was dissolved in DCM (5 ml) and NEt₃ (100 μ l) and chloroacetyl chloride (75 μ l, 1 eq) was slowly added. The reaction was allowed to stir overnight at room temperature. The residue was concentrated *in vacuo* and triturated with MeOH to yield the product as a white solid (137 mg, 36 %). The product did not ionise by LCMS; **δ_{H} (300 MHz, CDCl₃)** 0.00 (6H, s, Si(CH₃)₂), 0.79 (9H, s, C(CH₃)₃), 4.03 (2H, s, CH₂), 6.65 (2H, d, *J* = 8.7 Hz, C3-, C5-H), 7.28 (2H, d, *J* = 8.7 Hz, C2-, C6-H), 7.50 (2H, m, C2'-, C6'-H), 7.68 (2H, d, *J* = 8.7 Hz, C3'-, C5'-H), 8.19 (1H, s, NH).

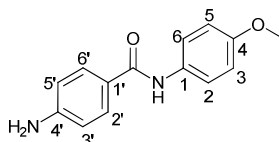
***N*-(4-methoxyphenyl)-4-(3-methylbutanamido)benzamide (345)**



Synthesis of this compound was adapted from that previously described by Martins *et al.*²¹⁸ *para*-Methoxyaniline (**150**) (507 mg, 1.2 eq) was dissolved in DCM (10 ml) and NEt₃ (305 μ l) and *para*-nitrobenzoyl chloride (**336**) (637, 1 eq) was added slowly. The reaction was allowed to stir overnight at room temperature when it was seen to be complete by TLC. The reaction was diluted with EtOAc (50 ml) and washed with saturated sodium bicarbonate solution (3 \times 50 ml) and brine (3 \times 50 ml). The organic layer was dried over sodium sulphate and concentrated *in vacuo*. The residue was recrystallised from MeOH to yield the pure product as a white solid (460 mg, 50 %). The

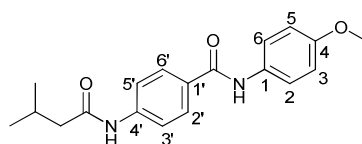
product did not ionise by LCMS. δ_{H} (300 MHz, $(\text{CD}_3)_2\text{SO}$) 3.76 (3H, s, CH_3), 6.95 (2H, d, $J = 9$ Hz, C3-, C5- $\underline{\text{H}}$), 6.91 (2H, d, $J = 9$ Hz, C2-, C6- $\underline{\text{H}}$), 8.17 (2H, d, $J = 9$ Hz, C2'-, C6'- $\underline{\text{H}}$), 8.36 (2H, d, $J = 9$ Hz, C3'-, C5'- $\underline{\text{H}}$), 7.64 (1H, br s, NH).

4-amino-*N*-(4-methoxyphenyl)benzamide (346)



This compound has been previously synthesised by Zhichkin *et al.*²¹⁹ Compound (345) (460 mg) was dissolved in MeOH (20 ml) and Pd/C (50 mg) was added as a solution in MeOH. The reaction was stirred under H_2 overnight at room temperature. The Pd/C was filtered through celite and the residue was concentrated *in vacuo* to yield the product as a white solid (407 mg, 100 %). **LCMS (M+H)⁺** found 243.0, requires 243.1, RT 1.52 min; δ_{H} (300 MHz, CDCl_3) 3.82 (3H, s, CH_3), 4.04 (2H, br s, NH_2), 6.71 (2H, d, $J = 9$ Hz, C3'-, C5'- $\underline{\text{H}}$), 6.91 (2H, d, $J = 9$ Hz, C2-, C6- $\underline{\text{H}}$), 7.53 (2H, d, $J = 9$ Hz, C2'-, C6'- $\underline{\text{H}}$), 7.64 (1H, br s, NH), 7.71 (2H, d, $J = 9$ Hz, C2'-, C6'- $\underline{\text{H}}$); δ_{C} (75 MHz; CDCl_3) 55.10 (OCH₃), 112.51 (C3', C5'), 113.57 (C3, C5), 121.25 (C1'), 121.69 (C2, C6), 129.13 (C2', C6'), 132.82 (C1), 151.88 (C4'), 155.02 (C4), 164.89 (CO).

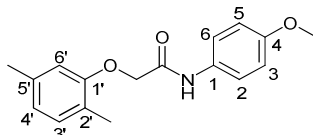
N-(4-methoxyphenyl)-4-(3-methylbutanamido)benzamide (348)



Compound (346) (100 mg, 1 eq) was dissolved in DCM (20 ml) and NEt_3 (100 μl) and isovaleryl chloride (347) (50 μl , 1 eq) was slowly added. The reaction was allowed to stir overnight at room temperature. The residue was concentrated *in vacuo* and triturated with MeOH to yield the product as a white solid (68 mg, 51 %). **LCMS (2M+Na)⁺** found 675.3, requires 675.3; **HRMS ESI (M+H)⁺** found 327.1714, $\text{C}_{19}\text{H}_{22}\text{N}_2\text{O}_3$ requires 327.1703; δ_{H} (300 MHz, $(\text{CD}_3)_2\text{SO}$) 0.95 (6H, d, $J = 6.6$ Hz, C(CH_3)₂), 2.10 (1H, m, CH), 2.23 (2H, d, $J = 7.1$ Hz, CH_2), 3.74 (3H, s, OCH₃), 6.92 (2H, d, $J = 8.7$ Hz, C3-,

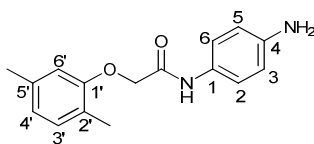
C5-H), 7.66 (2H, d, $J = 8.7$ Hz, C2-, C6-H), 7.72 (2H, d, $J = 8.7$ Hz, C2', C6'-H), 7.91 (2H, d, $J = 8.7$ Hz, C3', C5'-H), 9.97 (1H, s, NH), 10.11 (1H, s, NH); δ_c (75 MHz; CDCl_3) 22.25 ($\text{CH}(\underline{\text{C}}\text{H}_3)_2$), 25.51 (CH), 45.61 (CH_2), 55.11 (OCH_3), 113.64 (C3, C5), 118.13 (C3', C5'), 121.88 (C2, C6), 128.40 (C2', C6'), 129.02 (C1'), 132.27 (C1), 142.03 (C4'), 155.36 (C4), 164.41 (C1), 171.06 ($\text{CH}\underline{\text{C}}\text{O}$); IR (cm^{-1}) 3297, 2995, 1507, 818; MP 271-273 °C.

2-(2,5-dimethylphenoxy)-*N*-(4-methoxyphenyl)acetamide (349)



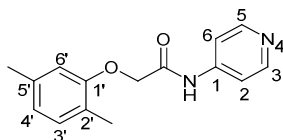
2,5-dimethylphenoxyacetic acid (**341**) (250 mg, 1 eq) was dissolved in DMF (5 ml), HOBt (225 mg, 1.2 eq) were added and the reaction was allowed to stir for 5 min. EDC·HCl (320 mg, 1.2 eq) was added and the reaction was allowed to stir for a further 5 min. Triethylamine (170 μl , 1.2 eq) was added and allowed to stir for 20 min, followed by *para*-methoxy aniline (**150**) (188 mg, 1.1 eq) and the reaction was allowed to stir for 24 h at room temperature. The reaction was seen to be complete by LCMS. Water was added and the precipitate was washed with excess water. The residue was recrystallised in Et_2O to afford the product as a brown crystalline solid (20 mg, 21 %). LCMS ($\text{M}+\text{H}$)⁺ found 286.1, requires 286.1; HRMS ESI ($2\text{M}+\text{Na}$)⁺ found 593.2645, $\text{C}_{34}\text{H}_{38}\text{N}_2\text{NaO}_6$ requires 257.1285; δ_H (500 MHz, CDCl_3) 2.24 (3H, s, C2' $\underline{\text{C}}\text{H}_3$), 2.26 (3H, s, C5' $\underline{\text{C}}\text{H}_3$), 3.74 (3H, s, OCH_3), 4.52 (2H, s, $\underline{\text{C}}\text{H}_2$), 6.59 (1H, s, C6' $\underline{\text{H}}$), 6.71 (2H, d, $J = 7.5$ Hz, C4' $\underline{\text{H}}$), 6.83 (2H, d, $J = 9$ Hz, C3-, C5'- $\underline{\text{H}}$), 7.01 (1H, d, $J = 7.5$ Hz, C3' $\underline{\text{H}}$), 7.42 (2H, d, $J = 9$ Hz, C2-, C6-H), 8.17 (1H, s, NH); δ_c (75 MHz; CDCl_3) 15.97 (C2' $\underline{\text{C}}\text{H}_3$), 21.33 (C5' $\underline{\text{C}}\text{H}_3$), 55.52 (OCH_3), 67.82 (CH_2), 112.94 (C6'), 114.30 (C3, C5), 121.78 (C2, C6), 122.74 (C4'), 123.31 (C2'), 130.03 (C1), 130.92 (C3'), 137.33 (C5'), 155.21 (C1'), 157.82 (C4), 166.34 (CO).

***N*-(4-aminophenyl)-2-(2,5-dimethylphenoxy)acetamide (350)**



2,5-dimethylphenoxyacetic acid (**341**) (250 mg, 1 eq) was dissolved in DCM (10 ml), DMAP (203 mg, 1.2 eq) and DCC (343, 1.2 eq) were added and the reaction was allowed to stir for 10 min. *para*-phenylenediamine (**153**) (150 mg, 1 eq) was added and the reaction was allowed to stir for 2 h at room temperature. The reaction was seen to be complete by LCMS. The reaction was diluted with EtOAc (20 ml) and washed with saturated sodium bicarbonate solution (3 × 20 ml) and brine (3 × 20 ml). The organic layer was dried over sodium sulphate and concentrated *in vacuo*. The residue was purified by Biotage silica column chromatography, eluted with a 0-100 % EtOAc in hexane, and recrystallised in acetonitrile to afford the product as a pale brown solid (46 mg, 12 %). **LCMS (M+H)⁺** found 271.1, requires 271.1; **HRMS ESI (M+H)⁺** found 271.1452, C₁₆H₁₉N₂O₂ requires 271.1441; **δ_H (500 MHz, CDCl₃)** 2.23 (3H, s, C2'CH₃), 2.25 (3H, s, C5'CH₃), 3.56 (2H, s, NH2), 4.50 (2H, s, CH2), 6.61 (3H, m, C3-, C5-, C6'-H), 6.70 (1H, d, *J* = 7.5 Hz, C4'H), 7.01 (1H, d, *J* = 7.5 Hz, C3'H), 7.27 (2H, m, C2'-, C6'-H), 8.09 (1H, s, NH); **δ_C (75 MHz; CDCl₃)** 15.97 (C2'CH₃), 21.33 (C5'CH₃), 67.81 (CH2), 112.91 (C6'), 115.46 (C3, C5), 121.96 (C2, C6), 122.66 (C4'), 123.31 (C2'), 128.28 (C1), 130.89 (C3'), 137.30 (C5'), 143.74 (C4), 155.25 (C1'), 165.20 (CO).

2-(2,5-dimethylphenoxy)-*N*-(pyridin-4-yl)acetamide (351)



2,5-dimethylphenoxyacetic acid (**341**) (350 mg, 1 eq) was dissolved in DMF (10 ml), HOBt (446 mg, 1.2 eq) was added and the reaction was allowed to stir for 5 min. EDC·HCl (446 mg, 1.2 eq) was added and the reaction was allowed to stir for 20 min. Triethylamine (236 μl, 1.2 eq) and 4-aminopyridine (201 mg, 1.1 eq) were added and the reaction was allowed to stir for 3 h at room temperature. The reaction was seen to be complete by LCMS. Water

was added and the product extracted with EtOAc. The organic layer was dried over sodium sulphate and concentrated *in vacuo*. The residue was purified by Biotage silica column chromatography, eluted with a 0-100 % EtOAc in hexane, to afford the product as a white solid (72 mg, 14 %). **LCMS (M+H)⁺** found 257.1, requires 257.1; **HRMS ESI (M+H)⁺** found 257.1308, C₁₅H₁₇N₂O₂ requires 257.1285; **δ_{H} (300 MHz, CDCl₃)** 2.21 (3H, s, C2'CH₃), 2.23 (3H, s, C5'CH₃), 4.49 (2H, s, CH₂), 6.54 (1H, s, C6'H), 6.70 (1H, d, *J* = 7.5 Hz, C4'H), 6.99 (1H, d, *J* = 7.5 Hz, C3'H), 7.45 (2H, m, C2-, C6-H), 8.44 (2H, m, C3-, C5-H) 8.53 (1H, s, NH); **δ_{C} (75 MHz; CDCl₃)** 15.94 (C2'CH₃), 21.30 (C5'CH₃), 67.84 (CH₂), 112.99 (C6'), 113.71 (C2, C6), 123.07 (C4'), 123.28 (C2'), 131.03 (C3'), 137.38 (C5'), 143.90 (C1), 150.87 (C3, C5), 154.94 (C1'), 167.42 (CO).

7.4 ROCS ligand-based database search

The structure of fenretinide was drawn using Maestro (Schrödinger)²²⁰ and energy minimised in an aqueous environment using Maestro Macromodel. The ChemBridge database search was carried out by comparison of the database structures with the fenretinide structure (based on structural and pharmacophoric patterns), using ROCS (Rapid Overlay of Chemical Structures, OpenEye Scientific Software) software script. The overlay of the structures and the calculated scores could be viewed using the 3D modelling software, VIDA (Visualization and Communication of Modelling Results, OpenEye Scientific Software). The results were ranked in order of their likeness of shape and chemical features to fenretinide.

7.5 Biological evaluation

7.5.1 Cell lines and tissue culture

The human TC32, SK-N-MC and TTC466 ESFT, SHEP-1 and SK-N-SH neuroblastoma and MSC (immortalised with hTERT) cell lines were used to test the effect of compounds on viable cell number. All cell lines were substrate adherent, growing as a single monolayer, and were mycoplasma free. Cells were used at 70 % confluency for experimental procedures, seeded and treated in a sterile environment using aseptic techniques in a

Envair class II microbiological safety cabinet. After washing with 5 ml of 1 × Phosphate Buffered Saline (PBS; w/v; Oxoid Ltd, Hampshire, UK), cells were harvested by treating for 2 minutes with ethylenediaminetetraacetate (EDTA; 0.1 % in PBS, w/v; Invitrogen Life Technologies, Paisley, Scotland), followed by a 2 minute incubation with 5 ml of 1x trypsin (0.25 % in PBS, w/v; Sigma Aldrich Company Ltd, Dorset, UK). Cells were maintained at 37 °C in a saturated humid atmosphere of 5 % CO₂ in air (v/v) in a Sanyo Gallenkemp CO₂ incubator (MCO-20AIC, Sanyo Gallenkamp PLC, Leicestershire, UK). Cells were maintained in cell line specific tissue culture media supplemented with 10 % fetal calf serum (FCS) (v/v) and 2 mM glutamine (w/v). ESFT cell lines, TC32 and TTC466 were maintained in RPMI 1640 (TTC466 media was supplemented with 10 % conditioned media (v/v)) and SK-N-MC cells were maintained in DMEM F12. Neuroblasoma cell lines SK-N-SH and SHEP-1 were maintained in 1:1 mixture of Dulbecco's Minimum Essential Medium (DMEM) and Eagle's Minimum Essential Medium (EMEM). MSC cells were maintained in NH expansion media.

7.5.2 Preparation of stock solutions

All synthetic retinoids and ChemBridge compounds plus fenretinide were dissolved in DMSO to give 10 mM stock solutions. Samples were aliquoted into 20 µl single use aliquots and stored at –20 °C until required.

7.5.3 Seeding of cells

Cells were harvested for experiments at *ca.*70 % confluency. The media and PBS were warmed to 37 °C in a water bath prior to use. The cells were washed with PBS (5 ml) to remove any floating cells and debris. For cancer cell lines, EDTA (0.1 %, 5 ml) was added and left on the cells for 2 minutes before removing by aspiration. Trypsin (0.1 %, 5ml) was added and the flask was tapped gently to remove the cells from the surface of the flask. For the MSC cell line, cells were removed from the flask by incubation (5 min) with trypsin-EDTA (0.25 % trypsin, 1 mM EDTA, 5 ml) solution. Trypsin was neutralised by adding media containing serum (5ml) and the contents of the flask were transferred to a sterile Falcon centrifuge tube and centrifuged at 500g for 5 minutes. The supernatant was removed by aspiration and discarded; the cell pellet was resuspended in 30 ml of fresh media using a

pastette to ensure a single cell suspension. The number of viable cells was counted using the trypan blue exclusion assay and a Neubauer haemocytometer, visualised by light microscopy on a Nikon ECLIPSE TS100. Cells were seeded in Primedia™ 6-well (2×10^5) or 24-well (2.5×10^4) plates.

7.5.4 Effect of compounds on viable cell number

Cells were treated with 10µM of a compound in an initial TC32 and MSC screen for activity, or with a concentration range (3, 6, 10, 20 and 40 µM) in dose response studies. Cells were also treated with DMSO (vehicle control) and fenretinide (positive control) at the maximum volume/concentration used in the assay. After 24 hours the media was collected and the wells were each washed with PBS (1 ml). For cancer cell lines, this was followed by EDTA (0.1 %, 1 ml). The media, PBS and EDTA from each well were collected and pooled into a centrifuge tube. Trypsin (0.1 %, 1 ml) was added to the well and the plate tapped gently to remove the cells from the surface. For MSC cells, the cells were incubated with trypsin-EDTA (0.25 % trypsin, 1 mM EDTA, 1 ml) solution for 5 minutes and the plate tapped gently to remove the cells from the surface. Media (1 ml) was added to neutralise the trypsin and the cells and media then collected and also pooled in the centrifuge tube. The tubes were centrifuged at 500g for 5 minutes, the supernatant aspirated from the cell pellet, and the cell pellet resuspended in 0.5 ml of fresh media. A cell viability analyser (Vi-Cell XR 2.03) was used to count the number of viable cells using the trypan blue exclusion assay. Each compound was analysed by in 3 technical repeats in each experiment and each independent experiment was repeated a minimum of three times. The mean viable cell number \pm standard error is presented as a percentage of the vehicle (DMSO) treated control.

7.5.5 Statistical analysis of data

Statistical analysis was carried out using GraphPad InStat 3. The effects of compounds on viable TC32 cell number were compared using a 1-way ANOVA with Dunnett's post hoc test to identify any significant effects on viable cell number, where $p < 0.05$ was considered significant. Compounds were deemed significantly active when they displayed a significant decrease

in viable cell number compared to the DMSO control and comparable to fenretinide when activity was statistically comparable to fenretinide, evaluated by ANOVA with Dunnetts post hoc tests.

7.6 ROS studies

TC32 cells were seeded into 6 well plates and allowed to adhere to the plate surface overnight. Cells were treated with the compounds at 10 μ M of the solution and incubated for 30 min. Cells were harvested by trypsination (as described in Section 7.5.4) and centrifuged at 500g for 5 min. DCFDA (Molecular Probes, 50 μ g) was dissolved in DMSO (87 μ l). The DCFDA/DMSO solution was diluted to (2.5 μ l/ml) in PBS and was made up in sufficient volume to resuspend each cell pellet in 1 ml of solution. The cell pellet was resuspended in 1 ml of PBS containing DCFDA solution and the suspension was incubated in the dark at 37 °C for 15 min. The cells were centrifuged at 500g for 5 min, the supernatant removed and the cell pellet resuspended in PBS (500 μ l). An aliquot of untreated cells were treated with H₂O₂ (50 μ l) 10 minutes prior to analysis to use as a positive control. Fluorescence was detected immediately by FACS (Attune Acoustic Focusing Cytometer with Attune Cytometric Software), where 10,000 events were recorded per sample. Each compound was analysed in 3 technical repeats in each experiment and a minimum of three independent experiments were carried out.

7.7 Caspase-3 activation

7.7.1 Protein extraction

TC-32 cells were seeded into 10 cm plates (as described in Section 7.5.3) and allowed to adhere to the plate surface overnight. Cells were treated with the compounds at 10 μ M for 24 h. Cells were washed with PBS (5 ml) and scraped from the plate surface into PBS (3 ml) using a silicone rubber cell scraper. Jurkat control cells were treated with etoposide (25 μ M, 4 h). The cell suspensions were centrifuged (500 g, 5 min), the supernatant was discarded following aspiration and the cell pellet resuspended in RIPA lysis buffer (PBS containing 1 % nonidet P-40, 0.5 % sodium deoxycholate, 0.1 %

w/v SDS and the protease inhibitors phenylmethylsulfonyl fluoride (PMSF, 1 mM), sodium orthovanadate (1 mM), leupeptin (10 µg/ml) and aprotinin (2 µg/ml). The cell lysate was incubated on ice for 30 min and vortexed twice within this time. The cell suspension was centrifuged at 12,500g for 10 minutes at 4 °C and the supernatant was collected and incubated on ice. 5 µl of the supernatant was added to deionised H₂O (45 µl) for protein analysis. The remaining supernatant was mixed with an equal volume of 2 × SDS-loading buffer (100 mM Tris-HCl (pH 6.8), 20 % w/v glycerol, 4 % w/v SDS, 200 mM dithiothreitol (DTT) and 0.2 % w/v bromophenol blue) and stored at -20 °C. Extracts were heated to 95 °C for 5 min immediately prior to use.

7.7.2 Protein assay

An estimation of the protein content of the supernatant was made using the Bio-rad DC Protein Assay. The chemical composition of buffer solutions used in the assay is company proprietary. A standard curve using bovine serum albumin (BSA) diluted in lysis buffer at six concentrations ranging from 0.1 µg/µL – 1.5 µg/µL was prepared. Protein samples and standards (5 µl) were pipette in triplicate into a 96-well standard microplate. Reagent SA (20 µl, 1:50 dilution of reagent S:A) was added to each well, followed by Reagent B (200 µl) and the plate was shaken for 10 sec. The plate was incubated at room temperature for 15 min. The absorbance was measured at 690 nm using a plate reader (Titertek Multiscan Plus MK II) and the protein concentration of test samples was calculated from the BSA standard curve.

7.7.3 SDS-Polyacrylamide Gel Electrophoresis (SDS-PAGE)

Protein samples (100 µg) were loaded onto precast Mini-PROTEAN TGX Gels (4-15 %, 15 well comb, 15 µl, Bio-Rad) alongside LI-COR molecular weight markers (5 µl). The gel was run at 150 volts in SDS electrophoresis buffer (250mM glycine, 25 mM Tris-HCl (pH 8.3), 0.1 % w/v SDS) in a Mini-PROTEAN Tetra Cell (Bio-Rad) until adequate protein separation was observed, as determined by movement of the bromophenol blue dye front and molecular weight marker separation.

7.7.4 Western blot

The SDS-PAGE gel was washed by shaking on a rotating platform for 5 min in transfer buffer (192 mM glycine, 25 mM Tris base, 20 % v/v methanol). The gel was then placed on a Hybond-C nitrocellulose membrane and sandwiched between two pieces of 3 mm filter paper and two foam pads. The gel was locked into the blotting apparatus and proteins were transferred on to the nitrocellulose membrane at 300 mA for 90 min with constant stirring in a Mini-PROTEAN Tetra Cell (Bio-Rad) cooled with an ice block.

After transfer the membrane was removed from the blotting apparatus and placed in LI-COR blocking buffer (5 ml) on a rotating platform for 30 min at room temperature; this blocking step was important to minimise non-specific binding of antibodies. The membrane was then incubated in the dark overnight at 4 °C with caspase-3 rabbit Ab (1:1000 dilution, Cell Signalling) and α -tubulin B-7 mouse monoclonal IgG_{2a} (1:5000, Santa Cruz Biotechnology) primary antibodies diluted in a 1:1 solution of PBS and blocking buffer with 0.1 % Tween-20. The membrane was then washed three times by shaking in PBS containing 0.1 % Tween (5 ml) for 5 min. The membrane was shaken for 1 h in the dark at room temperature in goat Alexa Fluor 680 goat anti-rabbit IgG (H+L) and Alexa Fluor 680 rabbit anti-mouse IgG (H+L) secondary antibodies (1:5000, Molecular Probes) diluted in a 1:1 solution of PBS and blocking buffer with 0.1 % Tween-20. The membrane was washed three times by shaking in PBS containing 0.1 % Tween (5 ml) for 5 min followed by two washes for 5 min each in PBS. Membranes were visualised using a LI-COR Odyssey CLx Infrared Imaging System.

7.8 Affinity chromatography

7.8.1 Preparation of Sepharose affinity chromatography resin

Epoxy activated Sepharose 6B was purchased from GE Healthcare as a freeze-dried solid in the presence of additives. In order to wash away the additives, the Sepharose (300 mg) was suspended in distilled water (5 ml) and washed with distilled water (100 ml) on a sintered filter. The ligand (*ca.*30 mg) was dissolved in a 1:1 solution of 100 mM sodium carbonate

(coupling buffer) at pH10 and DMF (5 ml) and added to the Sepharose 6B slurry. The mixture was shaken in an incubator at 40 °C overnight. The suspension was filtered on a sintered disc and excess ligand was washed off using coupling buffer. To block any remaining active groups, the medium was suspended in 1 M ethanolamine at pH8 and shaken overnight at 40 °C. The suspension was filtered on a sintered disc and washed with four cycles of alternating pH to remove any unbound fragments, consisting of a wash with 0.1 M acetate buffer pH4 containing 0.5 M NaCl followed by a wash with 0.1 M Tris-HCL buffer pH 8 containing 0.5 M NaCl.

The resin was stored in a 20 % EtOH/ 0.1M Tris-HCL buffer pH 8 at 4 °C.

7.8.2 Enrichment of cellular protein extracts for membrane proteins

ESFT SKES1 (5×10^6) cells were suspended in 2.5 ml of PBS to which was added EZ link Sulfo-NHS-SS-Biotin (0.5 mg/ml). Cells were incubated with rotation for 30 minutes at room temperature. After biotinylation the reaction was stopped by adding an equal volume of 50 mM Tris-HCl (pH 7.4). Cells were collected by centrifugation (1500 g, 5 minutes), washed twice with ice-cold PBS and then homogenised in 500 μ l of RIPA buffer using a glass-glass homogeniser. The protein concentration in a 5 μ l aliquot of the lysate was analysed using the modified Bradford assay. Nuclei and unbroken cell debris were removed from the remaining lysate by centrifugation at 1000 g for 10 min at 4 °C and the supernatant retained. Biotin-labelled proteins were extracted from the supernatant by incubation with rotation for 2 h at 4 °C with streptavidin-sepharose beads (20 μ l beads/ 10^6 cells). The beads were collected by centrifugation (10,000 g, 1 min), the supernatant removed and the beads washed in RIPA buffer, followed by a wash in RIPA buffer containing 1 M KCl and then in RIPA buffer containing 0.1 M NaHCO₃. Bound membrane proteins were solubilised in PBS + 1 % NP40 (non-ionic detergent). This method was optimised to obtain the greatest protein yield whilst maintaining the native protein state. Cellular extracts were subsequently precleared by incubating extracts with sepharose beads and removing these by centrifugating prior to application to the columns. An

aliquot of the solubilised membrane proteins was retained for SDS-PAGE (unbound proteins).

7.8.3 Pull down assay

The precleared membrane enriched biotinylated cell lysate was incubated with the covalently immobilised molecules (**352**, **353** and **364**) bound to the sepharose resin or sepharose resin alone overnight at 4 °C. The resin was then poured into a column under gravity, and the Flow through (fraction containing unbound proteins) collected. The column was then washed in 50ml of wash buffer (10 mM, HEPES (pH 7.1), 100 mM KCl, 2 mM MgCl₂, 1 mM EDTA) and bound proteins eluted in 50 mM glycine pH2.3, 10 % sucrose buffer.

The purified proteins, bound and unbound, were analysed by 1D gradient SDS-PAGE (4-20 % acrylamide) and silver staining (Proteosilver Plus, Sigma). In total 12 bands were identified that were eluted from the specific affinity columns but were absent in the non-specific negative control column. The bands were excised from the gels, each one placed into a separate eppendorf tube and digested with trypsin for identification.

7.8.4 Identification of proteins

Each protein band was analysed by mass spectrometry using an Agilent 1100 Series nano-LC System (Agilent Technologies) coupled online with a QSTAR XL quadrupole TOF hybrid mass spectrometer (Applied Biosystems) as previously described.¹⁸³ Data was analysed using a local Mascot database search engine (Matrix Science) and the UniProt protein sequence database (restricted to human; 88214 sequences) with the following search parameters: Fixed modification: Carbamidomethyl (C), Variable modification: Oxidation (M), Peptide Mass Tolerance: 0.15 Da, Fragment Mass Tolerance: 0.1 Da, Missed Cleavages: 1. Peptides with scores over the identity threshold ($p < 0.05$) were considered as identified, proteins required at least one significant bold red peptide (that is, the highest scoring match to a particular query listed under the highest scoring protein containing that match).

The expression of proteins that appeared to be specifically binding to the fenretinide molecule was confirmed by western and immunoprecipitation blot of ESFT cellular extracts (results not shown). No hits were identified for two bands, one at *ca.*100 kDa and one at *ca.*30 kDa. In the remaining bands many ribosomal proteins were identified, along with tubulin and nucleolin. 4 proteins demonstrated specificity towards affinity chromatography ligands **352** and **353**.

References

- (1) Patrick, G. L. *An Introduction to Medicinal Chemistry (Fourth Edition)*; 2009; pp. 519–528.
- (2) Futreal, P. A.; Coin, L.; Marshall, M.; Down, T.; Hubbard, T.; Wooster, R.; Rahman, N.; Stratton, M. R. *Nat. Rev. Cancer* **2004**, *4*, 177–183.
- (3) Hanahan, D.; Weinberg, R. A.; Francisco, S. *Cell* **2000**, *100*, 57–70.
- (4) Hanahan, D.; Weinberg, R. a. *Cell* **2011**, *144*, 646–674.
- (5) Anand, P.; Kunnumakkara, A. B.; Kunnumakara, A. B.; Sundaram, C.; Harikumar, K. B.; Tharakan, S. T.; Lai, O. S.; Sung, B.; Aggarwal, B. B. *Pharm. Res.* **2008**, *25*, 2097–2116.
- (6) World Health Organization, *Press Release No.224*, **2014**.
- (7) Siegel, R.; Naishadham, D.; Jemal, A. *A Cancer J. Clin.* **2013**, *63*, 11–30.
- (8) Ramani, P.; Shipley, J. *Br. Med. Bull.* **1996**, *52*, 724–741.
- (9) Giovannini, M.; Biegel, J. A.; Serra, M.; Wang, J.; Wei, Y. H.; Nycum, L.; Emanuel, B. S.; Evans, G. A. 489–496.
- (10) Ewing, J. *Proc. New York Pathological Soc.* **1921**, *21*, 17–24.
- (11) Riggi, N.; Suva, M.; Stamenkovic, I. *Expert Rev. Anticancer Ther.* **2009**, *9*, 1025–1030.
- (12) Grannowetter, L. *Curr. Opin. Oncol.* **1992**, *4*, 696–703.
- (13) Eyre, R.; Feltbower, R. G.; Mubwandarikwa, E.; Eden, T. O. B.; Obst, M. D.; Mcnally, R. J. Q. *Pediatr. Blood Cancer* **2009**, 941–952.
- (14) Batra, S.; Reynolds, C. P.; Maurer, B. J. *Cancer Res.* **2004**, *64*, 5415–5424.
- (15) Seth, T. *Indian J. Med. Paediatr. Oncol.* **2004**, *25*, 51–53.
- (16) Marchetti, S.; Schellens, J. H. M. *Br. J. Cancer* **2007**, *97*, 577–581.
- (17) Kola, I.; Landis, J. *Nat. Rev. Drug Discov.* **2004**, *3*, 1–5.
- (18) Hay, M.; Thomas, D. W.; Craighead, J. L.; Economides, C.; Rosenthal, J. *Nat. Biotechnol.* **2014**, *32*, 40–51.

- (19) Sausville, E. *Eur. J. Cancer* **2004**, *40*, 783–784.
- (20) Caponigro, G.; Sellers, W. R. *Nat. Rev. Drug Discov.* **2011**, *10*, 179–187.
- (21) Burchill, S. A. *Futur. Oncol.* **2006**, *2*, 201–211.
- (22) Li, A.; Walling, J.; Kotliarov, Y.; Center, A.; Steed, M. E.; Ahn, S. J.; Rosenblum, M.; Mikkelsen, T.; Zenklusen, J. C.; Fine, H. A. *Mol. Cancer Res.* **2008**, *6*, 21–30.
- (23) Phillips, R. M.; Bibby, M. C.; Double, J. A. *J. Natl. Cancer Inst.* **1990**, *82*, 1457–1468.
- (24) Shoemaker, R. H. *Nat. Rev. Cancer* **2006**, *6*, 813–823.
- (25) Holbeck, S. L. *Eur. J. Cancer* **2004**, *40*, 785–793.
- (26) <http://pubchem.ncbi.nlm.nih.gov/> (Accessed 06.09.14)
- (27) Bais, R.; Paulls, K. D.; Herald, C. L.; Malspeis, L.; Pettit, G. R.; Hamel, E. *J. Biol. Chem.* **1991**, *266*, 15882–15889.
- (28) De Jong, M.; Maina, T. *J. Nucl. Med.* **2010**, *51*, 501–504.
- (29) Johnson, J. I.; Decker, S.; Zaharevitz, D.; Rubinstein, L. V.; Venditti, J. M.; Schepartz, S.; Kalyandrug, S.; Christian, M.; Arbutnot, S.; Hollingshead, M.; Sausville, E. A. *Br. J. Cancer* **2001**, *84*, 1424–1431.
- (30) Fiebig, H. H.; Maier, A.; Burger, A. M. *Eur. J. Cancer* **2004**, *40*, 802–820.
- (31) Lin, J. H. *Drug Metab. Dispos.* **1998**, *26*, 1202–1212.
- (32) Artursson, P. *J. Pharm. Sci.* **1990**, *79*, 476–482.
- (33) Howe, P. R.; Wolbach, S. B. *J. Exp. Med.* **1925**, *42*, 753–780.
- (34) Gander, R.; Gurney, J. Retinoic acid derivatives. US4190594, 1980.
- (35) Gander, R. Method of treating carcinogenesis. US4323581, 1982.
- (36) Moon, R. C.; Thompson, H. J.; Becci, P. J.; Grubbs, C. J.; Gander, R. J.; Dianne, L.; Smith, J. M.; Phillips, S. L.; Henderson, W. R.; Mullen, L. T.; Brown, C. C.; Sporn, M. B. *Cancer Res.* **1979**, *39*, 1339–1346.
- (37) Villani, M. G.; Appierto, V.; Cavadini, E.; Bettiga, A.; Prinetti, A.; Clagett-Dame, M.; Curley, R. W.; Formelli, F. *Cancer Res.* **2006**, *66*, 3238–3247.

- (38) Sabichi, A. L.; Xu, H.; Fischer, S.; Zou, C.; Yang, X.; Steele, V. E.; Kelloff, G. J.; Lotan, R.; Clifford, J. L. *Clin. Cancer Res.* **2003**, *9*, 4606–4613.
- (39) Lotan, R. *Curr. Cancer Drug Targets* **2004**, *4*, 285–298.
- (40) Sun, S.; Li, W.; Yue, P. *Cancer Res.* **1999**, *59*, 2493–2498.
- (41) De Palo, G.; Veronesi, U.; Marubini, E.; Camerini, T.; Chiesa, F.; Nava, M.; Formelli, F.; Del Vecchio, M.; Costa, a; Boracchi, P. *J. Cell. Biochem. Suppl.* **1995**, *22*, 11–17.
- (42) <https://clinicaltrials.gov/ct2/results?term=fenretinide+cancer&pg=1>
(Accessed 06.09.14)
- (43) Reynolds, C. *Cancer Lett.* **2003**, *197*, 185–192.
- (44) Kokate, A.; Li, X.; Jasti, B. *Invest. New Drugs* **2007**, *25*, 197–203.
- (45) Malone, W.; Perloff, M.; Crowell, J.; Sigman, C.; Higley, H. *Expert Opin. Investig. Drugs* **2003**, *12*, 1829–1842.
- (46) Sun, S.; Yue, P.; Lotan, R. *Mol. Pharmacol.* **1999**, *410*, 403–410.
- (47) Formelli, F.; Cavadini, E.; Luksch, R.; Garaventa, A.; Villani, M. G.; Appierto, V.; Persiani, S. *Cancer Chemother. Pharmacol.* **2008**, *62*, 655–665.
- (48) Fanjul, A. N.; Delia, D.; Pierotti, M. A.; Rideout, D.; Yu, J. Q.; Pfahl, M.; Qiu, J. *J. Biol. Chem.* **1996**, *271*, 22441–22446.
- (49) Fontana, J. A.; Rishi, A. K. *Leukemia* **2002**, *16*, 463–472.
- (50) Um, S.; Kwon, Y.; Han, H.; Park, S.; Park, M.; Rho, Y.; Sin, H. *Chem. Pharm. Bull. (Tokyo)*. **2004**, *52*, 501–506.
- (51) Asumendi, A.; Morales, M. C.; Alvarez, A.; Aréchaga, J.; Pérez-Yarza, G. *Br. J. Cancer* **2002**, *86*, 1951–1956.
- (52) Donnell, P. H. O.; Guo, W.; Reynolds, C. P.; Maurer, B. J. *Leukemia* **2002**, *16*, 902–910.
- (53) Clifford, J. L.; Menter, D. G.; Wang, M.; Lotan, R.; Lippman, S. M. *Cancer Res.* **1999**, *59*, 14–18.
- (54) Halliwell, B.; Gutteridge, J. M. C. *J. Biochem.* **1984**, *219*, 1–14.
- (55) Muller, F. *J. Am. Aging Assoc.* **2000**, *23*, 227–253.

- (56) Andreyev, A. Y.; Kushnareva, Y. E.; Starkov, A. A. *Biochem. Biokhimiya* **2005**, *70*, 200–214.
- (57) Wong, J. M. S. *J. Biol. Chem.* **1996**, *271*, 15703–15707.
- (58) Lee, R. L.; Westendorf, J.; Gold, M. R. *J. Cell Commun. Signal.* **2007**, *1*, 33–43.
- (59) Irani, K. *Science* **1997**, *275*, 1649–1652.
- (60) Jackson, A. L.; Loeb, L. A. *Mutat. Res.* **2001**, *477*, 7–21.
- (61) Hail, N.; Lotan, R. *Cancer, Epidemiology, Biomarkers Prev.* **2000**, *9*, 1293–1301.
- (62) Dipietrantonio, A. M.; Hsieh, T.; Juan, G.; Traganos, F.; Darzynkiewicz, Z.; Wu, J. M. *Cancer Res.* **2000**, *60*, 4331–4335.
- (63) Lovat, P. E.; Corazzari, M.; Di Sano, F.; Piacentini, M.; Redfern, C. P. F. *Cancer Lett.* **2005**, *228*, 105–110.
- (64) Hail, N.; Kim, H. J.; Lotan, R. *Apoptosis* **2006**, *11*, 1677–1694.
- (65) Lovat, P. E.; Corazzari, M.; Goranov, B.; Piacentini, M.; Redfern, C. P. F. *Ann. N. Y. Acad. Sci.* **2004**, *1028*, 81–89.
- (66) Cuperus, R.; Leen, R.; Tytgat, G. a M.; Caron, H. N.; van Kuilenburg, A. B. P. *Cell. Mol. Life Sci.* **2010**, *67*, 807–816.
- (67) Myatt, S. S.; Redfern, C. P. F.; Burchill, S. A. *Clin. Cancer Res.* **2005**, *11*, 3136–3148.
- (68) Liu, Y. *Circ. Res.* **2002**, *90*, 1259–1266.
- (69) Hattori, K.; Naguro, I.; Runchel, C.; Ichijo, H. *Cell Commun. Signal.* **2009**, *7*.
- (70) Armstrong, J. L.; Flockhart, R.; Veal, G. J.; Lovat, P. E.; Redfern, C. P. F. *J. Biol. Chem.* **2010**, *285*, 6091–6100.
- (71) Reed, J. C. *J. Natl. Cancer Inst.* **1999**, *91*, 1099–1100.
- (72) Lavrik, I. N.; Golks, A.; Krammer, P. H. *J. Clin. Invest.* **2005**, *115*, 2665–2672.
- (73) Salvesen, G. S. *Cell Death Differ.* **2002**, *9*, 3–5.
- (74) Appierto, V.; Tiberio, P.; Villani, M. G.; Cavadini, E.; Formelli, F. *Carcinogenesis* **2009**, *30*, 824–831.

- (75) Delia, D.; Aiello, A.; Meroni, L.; Nicolini, M.; Reed, J. C.; Pierotti, M. A. *Carcinogenesis* **1997**, *18*, 943–948.
- (76) Oridate, N.; Suzuki, S.; Higuchi, M.; Mitchell, M. F.; Hong, W. K.; Lotan, R. *J. Natl. Cancer Inst.* **1997**, *89*, 1191–1198.
- (77) White, D. E.; Burchill, S. A. *Br. J. Cancer* **2010**, *103*, 1380–1390.
- (78) Ulukaya, E.; Sarimahmut, M.; Cevatemre, B.; Ari, F.; Yerlikaya, A.; Dimas, K. *Biomed. Pharmacother.* **2014**, *68*, 477–482.
- (79) Cooper, J. P.; Hwang, K.; Singh, H.; Wang, D.; Reynolds, C. P.; Curley, R. W.; Williams, S. C.; Maurer, B. J.; Kang, M. H. *Br. J. Pharmacol.* **2011**, *163*, 1263–1275.
- (80) Villani, M. G.; Appierto, V.; Cavadini, E.; Valsecchi, M.; Sonnino, S.; Curley, R. W.; Formelli, F. *Clin. Cancer Res.* **2004**, *10*, 6265–6275.
- (81) Mehta, R. G.; Hultin, T. a; Moon, R. C. *Biochem. J.* **1988**, *256*, 579–584.
- (82) Villablanca, J. G.; Krailo, M. D.; Ames, M. M.; Reid, J. M.; Reaman, G. H.; Reynolds, C. P.; Reynolds, P. C. *J. Clin. Oncol.* **2006**, *24*, 3423–3430.
- (83) Das, B. C.; Smith, M. E.; Kalpana, G. V. *Bioorg. Med. Chem. Lett.* **2008**, *18*, 4177–4180.
- (84) Sani, B. P.; Shealy, Y. F.; Hill, D. L. *Carcinogenesis* **1995**, *16*, 2531–2534.
- (85) Campos-Sandoval, J. A.; Redondo, C.; Kinsella, G. K.; Pal, A.; Jones, G.; Eyre, G. S.; Hirst, S. C.; Findlay, J. B. C. *J. Med. Chem.* **2011**, *54*, 4378–4387.
- (86) Burchill, S. A., personal communication.
- (87) Blaner, W. S. *Cell Metab.* **2007**, *5*, 164–166.
- (88) Roberts, B.; Nichols, D.; Newton, D. L.; Sporn, B. *J. Biol. Chem.* **1979**, *254*, 6296–6302.
- (89) Barnard, J. H.; Collings, J. C.; Whiting, A.; Przyborski, S. a; Marder, T. B. *Chemistry (Easton)*. **2009**, *15*, 11430–11442.
- (90) Illingworth, N. A.; Boddy, A. V; Daly, A. K.; J, V. G. *Br. J. Cancer* **2011**, *162*, 989–999.
- (91) Van Wauwe, J. P.; Coene, M. C.; Goossens, J.; Cools, W.; Monbaliu, J. *J. Pharmacol. Exp. Ther.* **1990**, *252*, 365–369.

- (92) Maurer, B. J.; Reynolds, C. P. WO2009045345A1, 2009.
- (93) Barrier Therapeutics Inc. *Press Release* **2003**.
- (94) Van heusden, J.; Wouters, W.; Ramaekers, F. C.; Krekels, M. D.; Dillen, L.; Borgers, M.; Smets, G. *Br. J. Cancer* **1998**, *77*, 1229–1235.
- (95) Krekels, M. D.; Zimmerman, J.; Janssens, B.; Van Ginckel, R.; Cools, W.; Van Hove, C.; Coene, M. C.; Wouters, W. *Prostate* **1996**, *29*, 36–41.
- (96) Bossche, H. Vanden. *J. Steroid Biochem. Mol. Biol.* **1992**, *43*, 1003–1021.
- (97) Bruynseels, J.; De Coster, R.; Van Rooy, P.; Wouters, W.; Coene, M. C.; Snoeck, E.; Raeymaekers, a; Freyne, E.; Sanz, G.; Vanden Bussche, G. *Prostate* **1990**, *16*, 345–357.
- (98) Stoppie, P.; Borgers, M.; Borghgraef, P.; Dillen, L.; Goossens, J. A. N.; Sanz, G.; Szel, H.; Hove, C. V. A. N.; Nyen, G. V. A. N.; Nobels, G.; Bossche, H. Vanden; Venet, M.; Willemsens, G.; Wauwe, J. V. A. N. *J. Pharmacol. Exp. Ther.* **2000**, *293*, 304–312.
- (99) Van, J.; Ginckel, R. Van; Bruwiere, H.; Moelans, P.; Janssen, B.; Floren, W.; Leede, B. J. Van Der. *Br. J. Cancer* **2002**, *86*, 605–611.
- (100) Patel, J. B.; Huynh, C. K.; Handratta, V. D.; Gediya, L. K.; Brodie, A. M. H.; Goloubeva, O. G.; Clement, O. O.; Nanne, I. P.; Soprano, D. R.; Njar, V. C. O. *J. Med. Chem.* **2004**, *47*, 6716–6729.
- (101) Dawson, M. I.; Hobbs, P. D. *Carbohydr. Res.* **1980**, *85*, 121–129.
- (102) Swanson, B. N.; Newton, L.; Roller, P.; Sporn, B. *J. Pharmacol. Exp. Ther.* **1981**, *219*, 632–637.
- (103) Dawson, M.I.; Fontana, J. A. *Mini Rev. Med. Chem.* **2010**, *10*, 455–491.
- (104) Abou-Issa, H.; Curley, R. W.; Panigot, M. J.; Wilcox, K. A.; Webb, T. E. *Anticancer Res.* **1993**, *13*, 1431–1436.
- (105) Abou-Issa, H. M.; Alshafie, G. A.; Curley, R. W., J.; Wong, M. F.; Clagett-Dame, M.; Repa, J. J.; Sikri, V. *Anticancer Res.* **1999**, *19*, 999–1004.
- (106) Garaventa, A.; Luksch, R.; Serena, M.; Piccolo, L.; Cavadini, E.; Montaldo, P. G.; Pizzitola, M. R.; Boni, L.; Ponzoni, M.; Decensi, A.; Bernardi, B. De; Bellani, F. F. *Clin. Cancer Res.* **2003**, *9*, 2032–2039.

- (107) Puduvalli, V. K.; Yung, W. K. A.; Hess, K. R.; Kuhn, J. G.; Groves, M. D.; Levin, V. a; Zwiebel, J.; Chang, S. M.; Cloughesy, T. F.; Junck, L.; Wen, P.; Lieberman, F.; Conrad, C. a; Gilbert, M. R.; Meyers, C. a; Liu, V.; Mehta, M. P.; Nicholas, M. K.; Prados, M. *J. Clin. Oncol.* **2004**, *22*, 4282–4289.
- (108) Schneider, B. J.; Worden, F. P.; Gadgeel, S. M.; Parchment, R. E.; Hodges, C. M.; Zwiebel, J.; Dunn, R. L.; Wozniak, A. J.; Kraut, M. J.; Kalemkerian, G. P. *Invest. New Drugs* **2009**, *27*, 571–578.
- (109) Sabichi, A. L.; Lerner, S. P.; Atkinson, E. N.; Grossman, H. B.; Caraway, N. P.; Dinney, C. P.; Penson, D. F.; Matin, S.; Kamat, A.; Pisters, L. L.; Lin, D. W.; Katz, R. L.; Brenner, D. E.; Hemstreet, G. P.; Wargo, M.; Bleyer, A.; Sanders, W. H.; Clifford, J. L.; Parnes, H. L.; Lippman, S. M. *Clin. Cancer Res.* **2008**, *14*, 224–229.
- (110) Maurer, B. J.; Kalous, O.; Yesair, D. W.; Wu, X.; Janeba, J.; Maldonado, V.; Khankaldyyan, V.; Frgala, T.; Sun, B.-C.; McKee, R. T.; Burgess, S. W.; Shaw, W. a; Reynolds, C. P. *Clin. Cancer Res.* **2007**, *13*, 3079–3086.
- (111) <https://clinicaltrials.gov/ct2/results?term=fenretinide+cancer&pg=2>
(Accessed 06.09.14)
- (112) Moglia, D.; Formelli, F.; Balivab, G.; Bonoa, A.; Accetturib, M.; Navac, M.; Palo, G. De. *Cancer Lett.* **1996**, *110*, 87–91.
- (113) Berni, R.; Formelli, F. *FEBS Lett.* **1992**, *308*, 43–45.
- (114) Anding, A. L.; Chapman, J. S.; Barnett, D. W.; Curley, R. W.; Clagett-Dame, M. *Cancer Res.* **2007**, *67*, 6270–6277.
- (115) Law, W. C.; Rando, R. R. *Biochem. Biophys. Res. Commun.* **1989**, *161*, 825–829.
- (116) Mershon, S. M.; Anding, A. L.; Chapman, J. S.; Clagett-Dame, M.; Stonerock, L. a; Curley, R. W. *Bioorg. Med. Chem. Lett.* **2007**, *17*, 836–840.
- (117) Das, B. C.; Smith, M. E.; Kalpana, G. V. *Bioorg. Med. Chem. Lett.* **2008**, *18*, 3805–3808.
- (118) Sadikoglou, E.; Magoulas, G.; Theodoropoulou, C.; Athanassopoulos, C. M.; Giannopoulou, E.; Theodorakopoulou, O.; Drainas, D.; Papaioannou, D.; Papadimitriou, E. *Eur. J. Med. Chem.* **2009**, *44*, 3175–3187.
- (119) Coward, P.; Conn, M.; Tang, J.; Xiong, F.; Menjares, A.; Reagan, J. D. *Anal. Biochem.* **2009**, *384*, 312–320.

- (120) Zanottiso, G.; Marcello, M.; Malpelinll, G.; Follil, C.; Sartori, G. *J. Biol. Chem.* **1994**, *26*, 29613–29620.
- (121) Weiss, K. L.; Alshafie, G.; Chapman, J. S.; Mershon, S. M.; Abou-issa, H.; Clagett-dame, M.; Curley, R. W. *Bioorg. Med. Chem. Lett.* **2001**, *11*, 1583–1586.
- (122) Suzui, M.; Sunagawa, N.; Chiba, I.; Moriwaki, H.; Yoshimi, N. *Int. J. Oncol.* **2006**, *28*, 1193–1199.
- (123) Wada, A.; Wang, F.; Suhara, Y.; Yamano, Y.; Okitsu, T.; Nakagawa, K.; Okano, T. *Bioorg. Med. Chem.* **2010**, *18*, 5795–5806.
- (124) Takahashi, N.; Ohba, T.; Yamauchi, T.; Higashiyama, K. *Bioorg. Med. Chem.* **2006**, *14*, 6089–6096.
- (125) Takahashi, N.; Watanabe, Y.; Maitani, Y.; Yamauchi, T.; Higashiyama, K.; Ohba, T. *Int. J. Cancer* **2008**, *122*, 689–698.
- (126) Benbrook, D. M.; Madler, M. M.; Spruce, L. W.; Birckbichler, P. J.; Nelson, E. C.; Subramanian, S.; Weerasekare, G. M.; Gale, J. B.; Patterson, M. K.; Wang, B.; Wang, W.; Lu, S.; Rowland, T. C.; DiSivestro, P.; Lindamood, C.; Hill, D. L.; Berlin, K. D. *J. Med. Chem.* **1997**, *40*, 3567–3583.
- (127) Simoni, D.; Invidiata, F. P.; Rondanin, R.; Grimaudo, S.; Cannizzo, G.; Barbusca, E.; Porretto, F.; D'Alessandro, N.; Tolomeo, M. *J. Med. Chem.* **1999**, *42*, 4961–4969.
- (128) Baraldil, P. G.; Guarneril, M.; Manfredinil, S.; Simonil, D.; Tabrizil, M. A.; Barbieriz, R.; Nastruzziq, R. G. C. *Eur. J. Med. Chem.* **1990**, *25*, 279–284.
- (129) Zacheis, D.; Dhar, A.; Lu, S.; Madler, M. M.; Klucik, J.; Brown, C. W.; Liu, S.; Clement, F.; Subramanian, S.; Weerasekare, G. M.; Berlin, K. D.; Gold, M. a; Houck, J. R.; Fountain, K. R.; Benbrook, D. M. *J. Med. Chem.* **1999**, *42*, 4434–4445.
- (130) Liu, T.; Hannafon, B.; Gill, L.; Kelly, W.; Benbrook, D. *Mol. Cancer Ther.* **2007**, *6*, 1814–1822.
- (131) Liu, S.; Brown, C. W.; Berlin, K. D.; Dhar, A.; Guruswamy, S.; Brown, D.; Gardner, G. J.; Birrer, M. J.; Benbrook, D. M. *J. Med. Chem.* **2004**, *47*, 999–1007.
- (132) Chun, K.; Benbrook, D. M.; Berlin, K. D.; Hong, W. K.; Lotan, R. *Cancer Res.* **2003**, *63*, 3826–3832.
- (133) Benbrook, Doris M.; Kamelle, Scott A.; Guruswamy, Suresh B.; Lightfoot, Stan A.; Rutledge, Teresa L.; Gould, Natalie S.; Hannafon,

- Bethany N.; Dunn, S. Terence; Berlin, K. D. *Invest. New Drugs* **2005**, *23*, 417–428.
- (134) Wada, A.; Fukunaga, K.; Ito, M.; Mizuguchi, Y. *Bioorg. Med. Chem.* **2004**, *12*, 3931–3942.
- (135) Das, B. C.; Mahalingam, S. M.; Panda, L.; Wang, B.; Campbell, P. D.; Evans, T. *Tetrahedron Lett.* **2010**, *51*, 1462–1466.
- (136) Schneider, G.; Fechner, U. *Nat. Rev. Drug Discov.* **2005**, *4*, 649–663.
- (137) Kumar, V.; Krishna, S.; Siddiqi, M. I. *Methods* **2014**, In Press.
- (138) Ou-Yang, S.-S.; Lu, J.-Y.; Kong, X.-Q.; Liang, Z.-J.; Luo, C.; Jiang, H. *Acta Pharmacol. Sin.* **2012**, *33*, 1131–1140.
- (139) <http://www.eyesopen.com/rocs> (Accessed 10.08.14)
- (140) <http://www.schrodinger.com/Phase> (Accessed 05.08.14)
- (141) Lomenick, B.; Olsen, R. W.; Huang, J. *ACS Chem. Biol.* **2010**, *6*, 34–46.
- (142) Chapman, J. M.; Curley, R. W. *J. Biochem. Biophys. Methods* **1989**, *19*, 287–300.
- (143) Wilchek, M.; Miron, T. *React. Funct. Polym.* **1999**, *41*, 263–268.
- (144) Cuatrecasas, P. *Biochemistry* **1968**, *61*, 636–643.
- (145) Carra, P. O.; Barry, S.; Griffin, T. *FEBS Lett.* **1974**, *43*, 169–175.
- (146) Fex, G and Hansson, B. *Biochim. Biophys. Acta.* **1978**, *537*, 358–365.
- (147) Schrenk, D.; Orzechowski, A.; Schwarz, L. R.; Snyder, R.; Burchell, B.; Ingelman-Sundberg, M.; Bock, K. W. *Environ. Health Perspect.* **1996**, *104*, 1183–1188.
- (148) Strober, W. *Curr. Protoc. Immunol.* **2001**, Appendix 3.
- (149) <http://www.graphpad.com/scientific-software/instat/> (Accessed 05.08.14)
- (150) <http://www.chembridge.com/index.php> (Accessed 05.08.14)
- (151) <http://www.organic-chemistry.org/prog/peo/> (Accessed 05.08.14)
- (152) Pierens, G. K.; Venkatachalam, T. K.; Reutens, D. *Magn. Reson. Chem.* **2014**, *52*, 453–459.

- (153) Wassvik, C. M.; Holmén, A. G.; Draheim, R.; Artursson, P.; Bergström, C. a S. *J. Med. Chem.* **2008**, *51*, 3035–3039.
- (154) Y, M. In *Application of Bioisosteres in Drug Design*, 2012.
- (155) A Novel Cyanopyrimidine Derivative. WO2010090299, 2010.
- (156) Gilli, P.; Pretto, L.; Bertolasi, V.; Gilli, G. *Acc. Chem. Res.* **2009**, *42*, 33–44.
- (157) Mati, I. K.; Adam, C.; Cockroft, S. L. *Chem. Sci.* **2013**, *4*, 3965–3972.
- (158) Dorgan, R. *J. Chem. Res.* **1979**, *6*, 198.
- (159) Kobayasi, S.; Tsuchiya, Y.; Mukaiyama, T. *Chem. Lett.* **1991**, *20*, 537–540.
- (160) Baeza, A.; Nájera, C.; Sansano, J. M. *Arkivoc* **2005**, *2005*, 353–363.
- (161) Olszewski, J. D.; Marshalla, M.; Sabat, M.; Sundberg, R. J. *J. Org. Chem.* **1994**, *59*, 4285–4296.
- (162) Fernando, C. R.; Calder, I. C.; Ham, K. N. *J. Med. Chem.* **1980**, *23*, 1–6.
- (163) Armstrong, J. L.; Redfern, C. P. F.; Veal, G. J. *Biochem. Pharmacol.* **2005**, *69*, 1299–1306.
- (164) Shealy, Y. F. *J. Med. Chem.* **1988**, *31*, 190–196.
- (165) Moon, R. C.; Becd, P. J. *Carcinogenesis* **1982**, *3*, 1469–1472.
- (166) <http://www.eyesopen.com/vida> (Accessed 10.08.14)
- (167) Corazzari, M.; Lovat, P. E.; Oliverio, S.; Di Sano, F.; Donnorso, R. P.; Redfern, C. P. F.; Piacentini, M. *Biochem. Biophys. Res. Commun.* **2005**, *331*, 810–815.
- (168) Mendgen, T.; Steuer, C.; Klein, C. D. *J. Med. Chem.* **2012**, *55*, 743–753.
- (169) www.emolecules.com (Accessed 11.09.14)
- (170) Jiang, L.; Pan, X.; Chen, Y.; Wang, K.; Du, Y.; Zhang, J. *Biochem. Biophys. Res. Commun.* **2011**, *405*, 314–318.
- (171) Zhang, H.; Mi, J.-Q.; Fang, H.; Wang, Z.; Wang, C.; Wu, L.; Zhang, B.; Minden, M.; Yang, W.-T.; Wang, H.-W.; Li, J.-M.; Xi, X.-D.; Chen, S.-J.; Zhang, J.; Chen, Z.; Wang, K.-K. *Proc. Natl. Acad. Sci. U. S. A.* **2013**, *110*, 5606–5611.

- (172) Gianni, M.; Ponzanelli, I.; Mologni, L.; Reichert, U.; Rambaldi, A.; Terao, M.; Garattini, E. *Cell Death Differ.* **2000**, *7*, 447–460.
- (173) Gumireddy, K.; Sutton, L. N.; Phillips, P. C.; Reddy, C. D. *Clin. Cancer Res.* **2003**, *9*, 4052–4059.
- (174) www.cyprotex.com (Accessed 25.09.14)
- (175) Dubmann, H. *J. Cell Sci.* **2002**, *116*, 525–536.
- (176) Pinton, P.; Giorgi, C.; Siviero, R.; Zecchini, E.; Rizzuto, R. *Oncogene* **2010**, *27*, 6407–6418.
- (177) Susin, S. a; Lorenzo, H. K.; Zamzami, N.; Marzo, I.; Snow, B. E.; Brothers, G. M.; Mangion, J.; Jacotot, E.; Costantini, P.; Loeffler, M.; Larochette, N.; Goodlett, D. R.; Aebersold, R.; Siderovski, D. P.; Penninger, J. M.; Kroemer, G. *Nature* **1999**, *397*, 441–446.
- (178) Dawson, A. D. and P. E. *Bioconjug. Chem.* **2009**, *19*, 2543–2548.
- (179) Rashidian, M.; Song, J. M.; Pricer, R. E.; Distefano, M. D. *J. Am. Chem. Soc.* **2012**, *134*, 8455–8467.
- (180) Horiguchi, Y.; Hiroshi, I.; Wolf, M. A. 6-Azaindole Compound. WO2005097129, 2005.
- (181) Dugave, C.; Demange, L. *Chem. Rev.* **2003**, *103*, 2475–2535.
- (182) GE Healthcare. *Epoxy-activated Sepharose™ 6B, Instructions 71-7087-00 AG*; 2010; pp. 1–12.
- (183) Aggelis, V.; Craven, R. A.; Peng, J.; Harnden, P.; Cairns, D. A.; Maher, E. R.; Tonge, R.; Selby, P. J.; Banks, R. E. *Proteomics* **2009**, *9*, 2118–2130.
- (184) Dreyfuss, G.; Matunis, M. J.; Piñol-Roma, S.; Burd, C. G. *Annu. Rev. Biochem.* **1993**, *62*, 289–321.
- (185) Kim, M. K.; Nikodem, V. M. *Mol. Cell. Biol.* **1999**, *19*, 6833–6844.
- (186) Fackelmayer, F. O.; Richter, A. *Biochim. Biophys. Acta.* **1994**, *1217*, 232–234.
- (187) Bortul, R.; Zweyer, M.; Billi, a M.; Tabellini, G.; Ochs, R. L.; Bareggi, R.; Cocco, L.; Martelli, a M. *J. Cell. Biochem. Suppl.* **2001**, *36*, 19–31.
- (188) Spraggon, L.; Dudnakova, T.; Slight, J.; Lustig-Yariv, O.; Cotterell, J.; Hastie, N.; Miles, C. *Oncogene* **2007**, *26*, 1484–1491.

- (189) Pahlich, S.; Quero, L.; Roschitzki, B.; Leemann-zakaryan, R. P.; Gehring, H. *J. Proteome Res.* **2009**, *8*, 4455–4465.
- (190) Berglund, F. M.; Clarke, P. R. *Biochem. Biophys. Res. Commun.* **2009**, *381*, 59–64.
- (191) Weidensdorfer, D.; Stöhr, N.; Baude, A.; Lederer, M.; Köhn, M.; Schierhorn, A.; Buchmeier, S.; Wahle, E.; Hüttelmaier, S. *RNA* **2009**, *15*, 104–115.
- (192) Elcheva, I.; Tarapore, R. S.; Bhatia, N.; Spiegelman, V. S. *Oncogene* **2008**, *27*, 5069–5074.
- (193) Ho, A. L.; Schwartz, G. K.; York, N. *J. Clin. Oncol.* **2011**, *29*, 4581–4583.
- (194) Gu, L.; Shigemasa, K.; Ohama, K. *Int. J. Oncol.* **2004**, *24*, 671–678.
- (195) Thornton, S.; Anand, N.; Purcell, D.; Lee, J. *J. Mol. Med.* **2003**, *81*, 536–548.
- (196) Leclercq, T. M.; Moretti, P. A. B.; Pitson, S. M. *Oncogene* **2011**, *30*, 372–378.
- (197) Huaizheng, L. *Scand. J. Urol. Nephrol.* **2010**, *44*, 223–227.
- (198) Scheiman, J.; Tseng, J.-C.; Zheng, Y.; Meruelo, D. *J. Am. Soc. Gene Cell Ther.* **2010**, *18*, 63–74.
- (199) Bella, A.; Lewis, H.; Phu, J.; Bottrill, A. R.; Mistry, S. C.; Pullar, C. E.; Ryadnov, M. G. *J. Med. Chem.* **2009**, *52*, 7966–7969.
- (200) Pesapane, A. *PhD thesis: Inside the function of the 67 kDa laminin receptor (67LR): a new promising target for cancer drug discovery by structure-based virtual screening*, University of Naples Federico II, 2010.
- (201) Qu, D.; Zhang, Y.; Ma, J.; Guo, K.; Li, R.; Yin, Y.; Cao, X.; Park, D. S. *J. Neurochem.* **2007**, *103*, 408–422.
- (202) Ten Klooster, J. P.; Leeuwen, I. V.; Scheres, N.; Anthony, E. C.; Hordijk, P. L. *EMBO J.* **2007**, *26*, 336–345.
- (203) Dong Wook, K.; Kee Beom, K.; Ji Young, K.; Kyu Sun, L.; Sang Beom, S. *Biochem. Biophys. Res. Commun.* **2010**, *400*, 419–425.
- (204) Madeira, A.; Pommet, J. M.; Prochiantz, A.; Allinquant, B. *FASEB J.* **2005**, *19*, 1905–1907.

- (205) Li, M.; Anthony, M.; Damuni, Z. *J. Biol. Chem.* **1996**, *271*, 11059–11062.
- (206) Christensen, D. J.; Chen, Y.; Oddo, J.; Matta, K. M.; Neil, J.; Davis, E. D.; Volkheimer, A. D.; Lanasa, M. C.; Friedman, D. R.; Goodman, B. K.; Gockerman, J. P.; Diehl, L. F.; de Castro, C. M.; Moore, J. O.; Vitek, M. P.; Weinberg, J. B. *Blood* **2011**, *118*, 4150–4158.
- (207) Mukhopadhyay, A.; Saddoughi, S. A.; Song, P.; Sultan, I.; Ponnusamy, S.; Senkal, C. E.; Snook, C. F.; Arnold, H. K.; Sears, R. C.; Hannun, Y. A.; Ogretmen, B. *FASEB J.* **2009**, *23*, 751–763.
- (208) Fan, Z.; Beresford, P. J.; Zhang, D.; Xu, Z.; Novina, C. D.; Yoshida, A.; Pommier, Y.; Lieberman, J. *Nat. Immunol.* **2003**, *4*, 145–153.
- (209) Kandilci, A.; Grosveld, G. C. *Leukemia* **2005**, *19*, 1439–1445.
- (210) Trinkle-mulcahy, L.; Boulon, S.; Lam, Y. W.; Urcia, R.; Boisvert, F.; Vandermoere, F.; Morrice, N. A.; Swift, S.; Rothbauer, U.; Leonhardt, H.; Lamond, A. *J. Cell Biol.* **2008**, *183*, 223–239.
- (211) Cabaj, J. E.; Hutchinson, J. J.; Zeller, J. R. Preparation of amides of retinoic acid via mixed anhydride and mixed carbonate intermediates. US01221349, 2008.
- (212) Lee, J.; Kang, S.-U.; Kil, M.-J.; Shin, M.; Lim, J.-O.; Choi, H.-K.; Jin, M.-K.; Kim, S. Y.; Kim, S.-E.; Lee, Y.-S.; Min, K.-H.; Kim, Y.-H.; Ha, H.-J.; Tran, R.; Welter, J. D.; Wang, Y.; Szabo, T.; Pearce, L. V.; Lundberg, D. J.; Toth, A.; Pavlyukovets, V. A.; Morgan, M. A.; Blumberg, P. M. *Bioorg. Med. Chem. Lett.* **2005**, *15*, 4136–4142.
- (213) Martini, E.; Norcini, M.; Ghelardini, C.; Manetti, D.; Dei, S.; Guandalini, L.; Melchiorre, M.; Pagella, S.; Scapecchi, S.; Teodori, E.; Romanelli, M. N. *Bioorg. Med. Chem.* **2008**, *16*, 10034–10042.
- (214) Ménard, D.; Niculescu-Duvaz, I.; Dijkstra, H. P.; Niculescu-Duvaz, D.; Suijkerbuijk, B. M. J. M.; Zambon, A.; Nourry, A.; Roman, E.; Davies, L.; Manne, H. a; Friedlos, F.; Kirk, R.; Whittaker, S.; Gill, A.; Taylor, R. D.; Marais, R.; Springer, C. J. *J. Med. Chem.* **2009**, *52*, 3881–3891.
- (215) Bridgeman, E.; Cavill, J. L.; Schofield, D. J.; Wilkins, D. S.; Tomkinson, N. C. O. *Tetrahedron Lett.* **2005**, *46*, 8521–8524.
- (216) Porwal, S.; Chauhan, S. S.; Chauhan, P. M. S.; Shakya, N.; Verma, A.; Gupta, S. *J. Med. Chem.* **2009**, *52*, 5793–5802.
- (217) Chen, Y. K.; Co, E. W.; Guntupalli, P.; Lawson, J. D.; Notz, W. R. L. Oxim Derivatives as HSP90 Inhibitors. WO2009097578A1, 2009.

- (218) Martins, A. F.; Morfin, J.-F.; Kubíčková, A.; Kubíček, V.; Buron, F.; Suzenet, F.; Salerno, M.; Lazar, A. N.; Duyckaerts, C.; Arlicot, N.; Guilloteau, D.; Geraldès, C. F. G. C.; Tóth, E. *ACS Med. Chem. Lett.* **2013**, *4*, 436–440.
- (219) Zhichkin, P. E.; Peterson, L. H.; Beer, C. M.; Rennells, W. M. *J. Org. Chem.* **2008**, *73*, 8954–8959.
- (220) <http://www.schrodinger.com/Maestro/> (Accessed 05.08.14)
- (221) <Http://www.shodex.com/en/da1/09/0201.html> (Accessed 06.09.14)

Appendix A – compound activity in TC32 cells

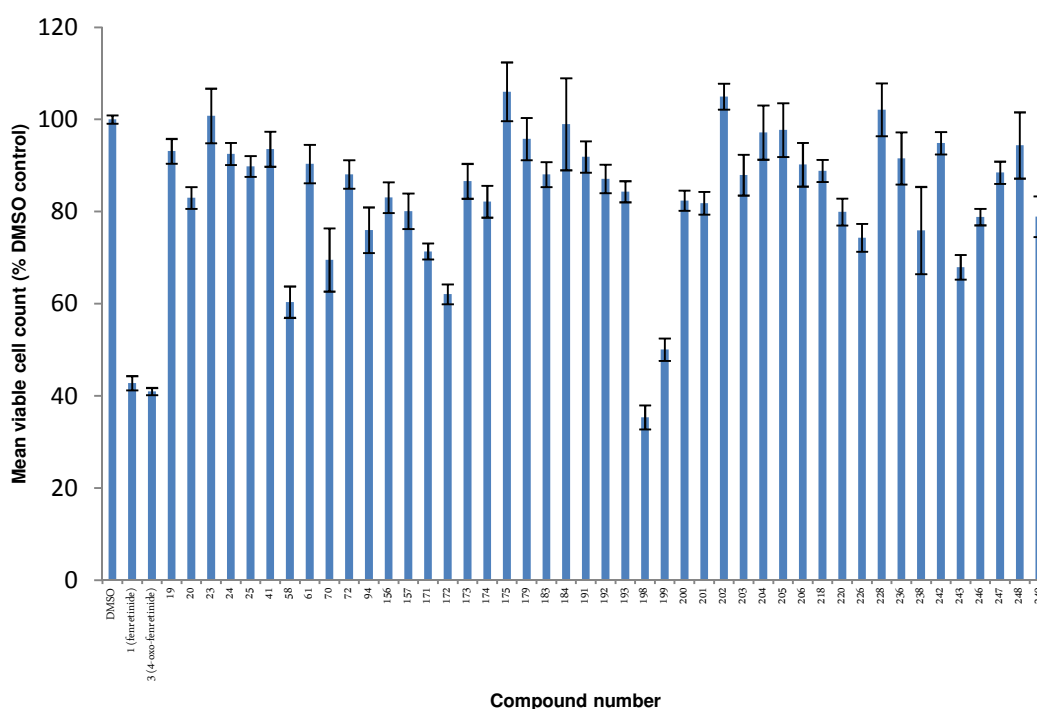


Chart A.1 Effect of the retinoid compounds at 10 μ M on TC32 viable cell number. Viable cell number was counted after treatment of cells for 24 hours. Results are shown as mean \pm SEM, $n \geq 9$.

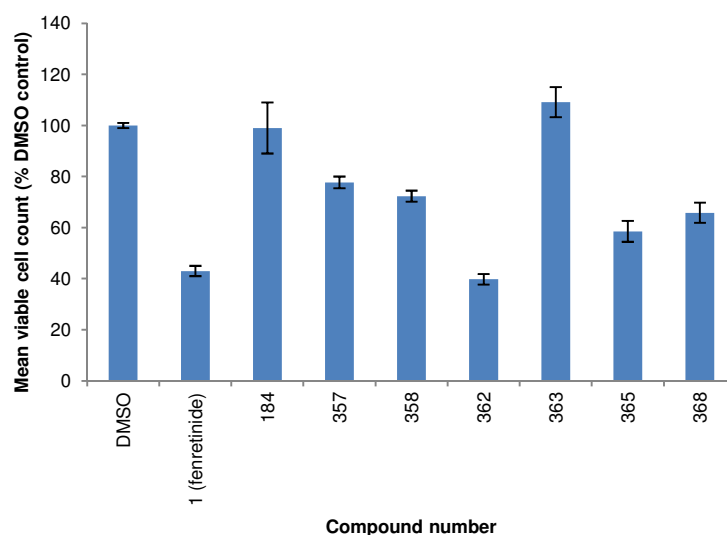


Chart A.2 Effect of the affinity chromatography ligand compounds at 10 μ M on TC32 viable cell number. Viable cell number was counted after treatment of cells for 24 hours. Results are shown as mean \pm SEM, $n \geq 9$.

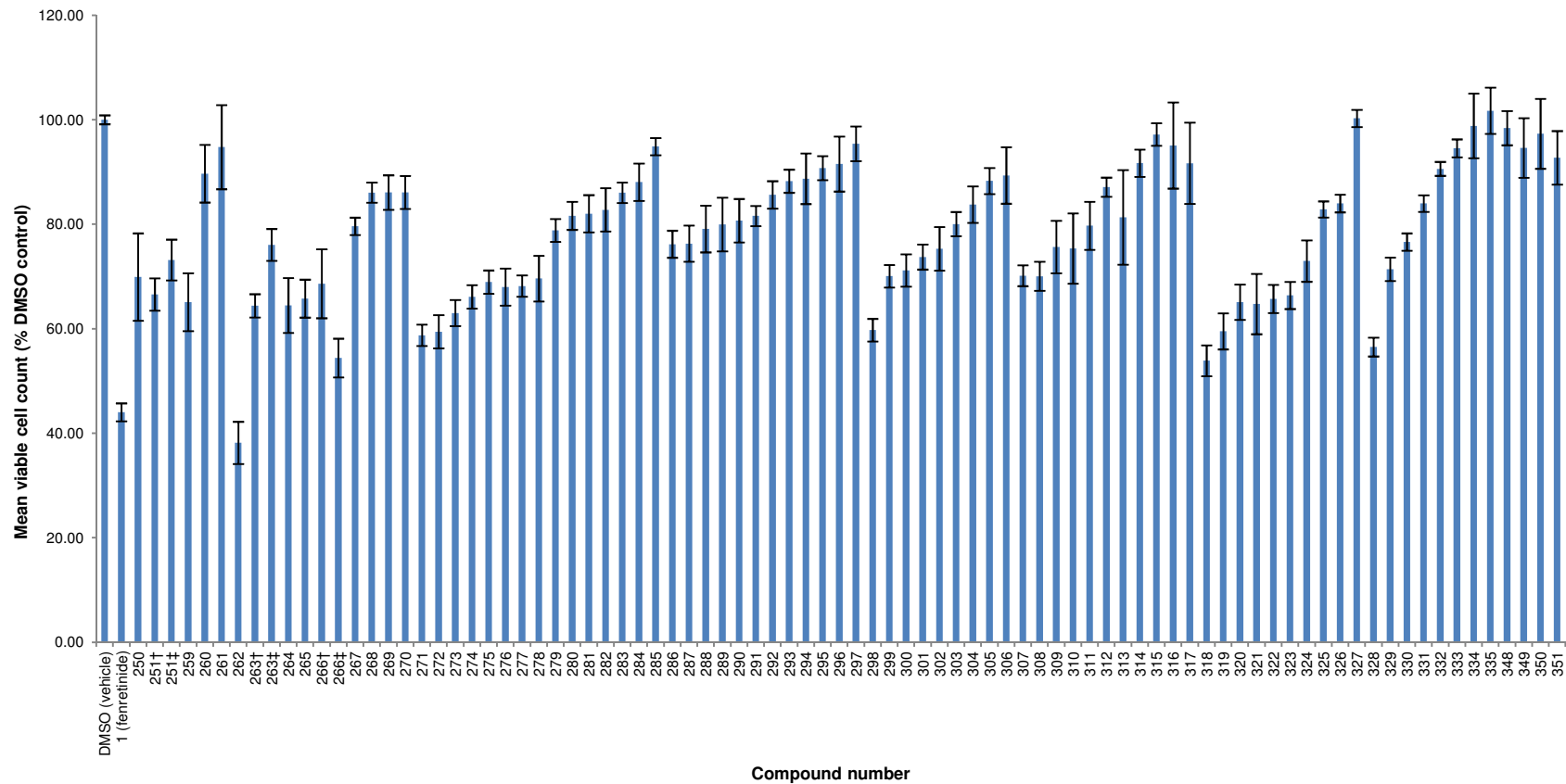


Chart A.3 Effect of the non-retinod compounds at 10 μ M on TC32 viable cell number. Viable cell number was counted after treatment of cells for 24 hours. Results are shown as mean \pm SEM, $n \geq 9$.

Appendix B – concentration response by cell line

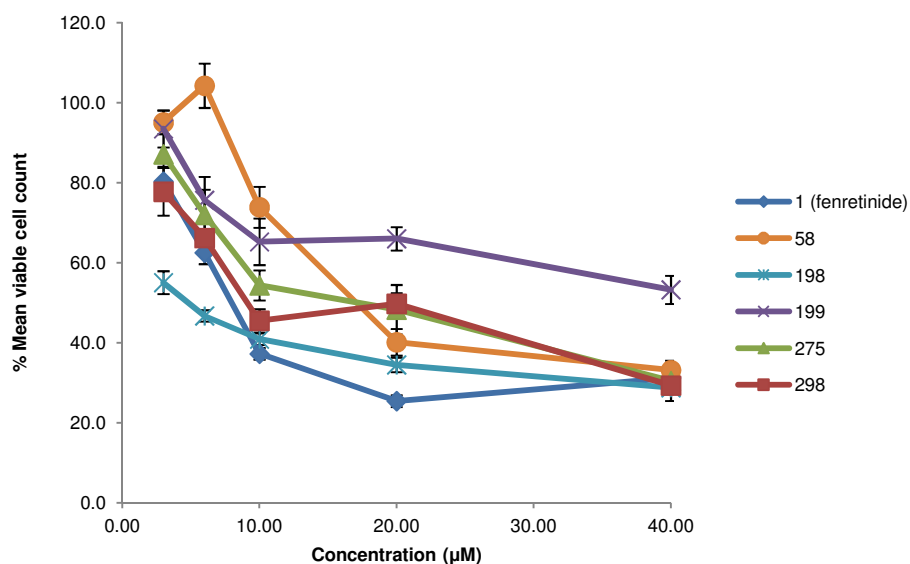


Chart B.1 Cell viability of TC32 ESFT cells treated with 3-10 µM of compounds **1**, **58**, **198**, **199**, **275** and **298** for 24 h (n = 9).

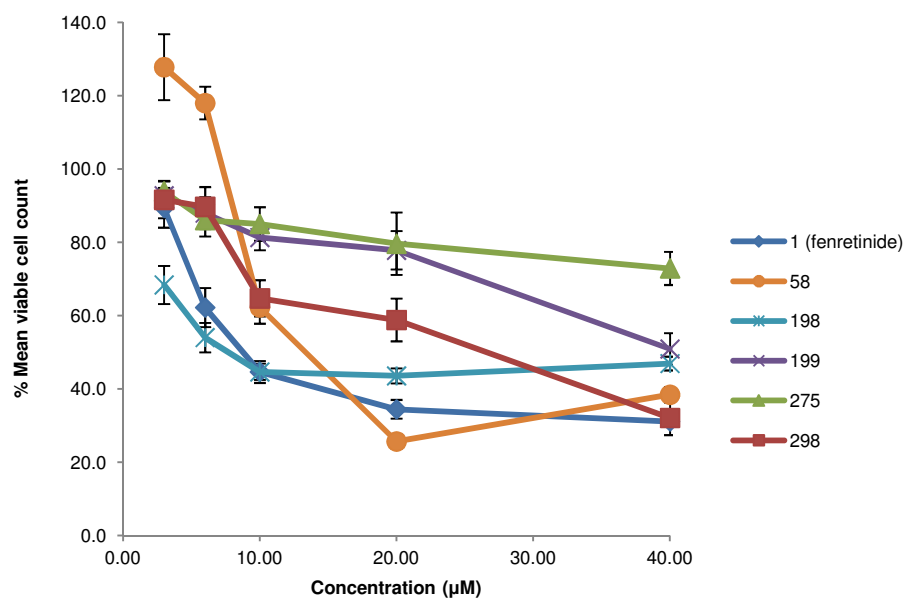


Chart B.2 Cell viability of TTC-466 ESFT cells treated with 3-10 µM of compounds **1**, **58**, **198**, **199**, **275** and **298** for 24 h (n = 9).

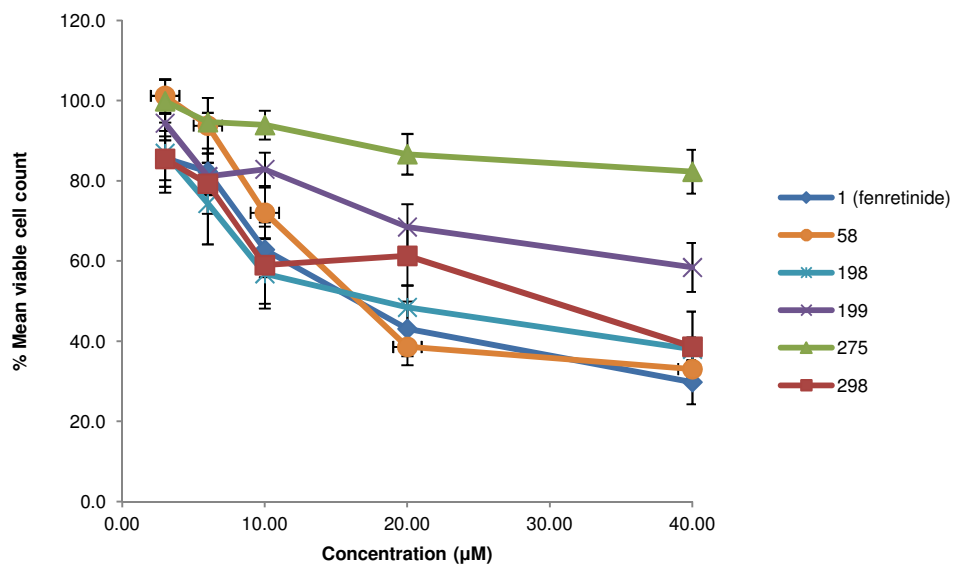


Chart B.3 Cell viability of SK-N-MC neuroblastoma cells treated with 3-10 μM of compounds compounds **1**, **58**, **198**, **199**, **275** and **298** for 24 h (n = 9).

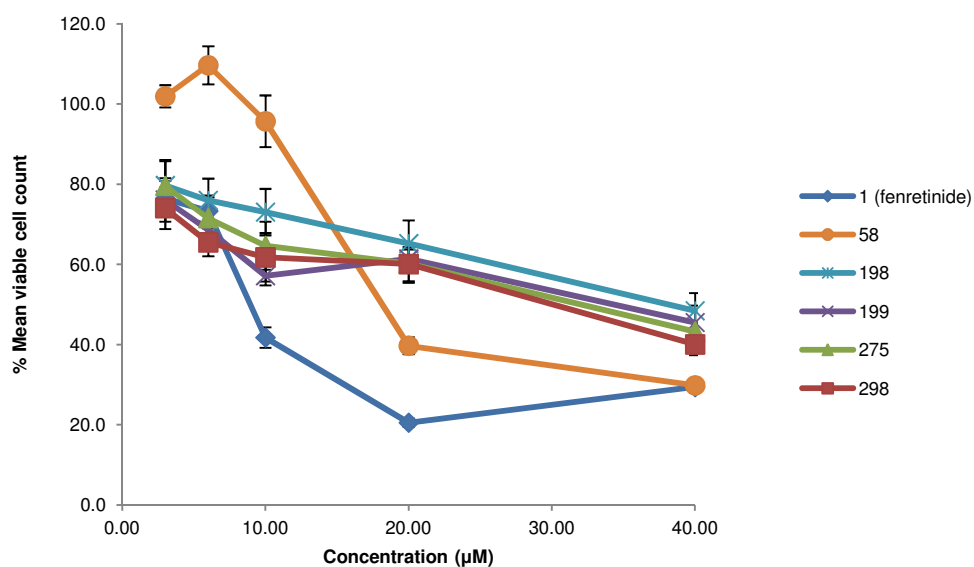


Chart B.4 Cell viability of SK-N-SH neuroblastoma cells treated with 3-10 μM of compounds compounds **1**, **58**, **198**, **199**, **275** and **298** for 24 h (n = 9).

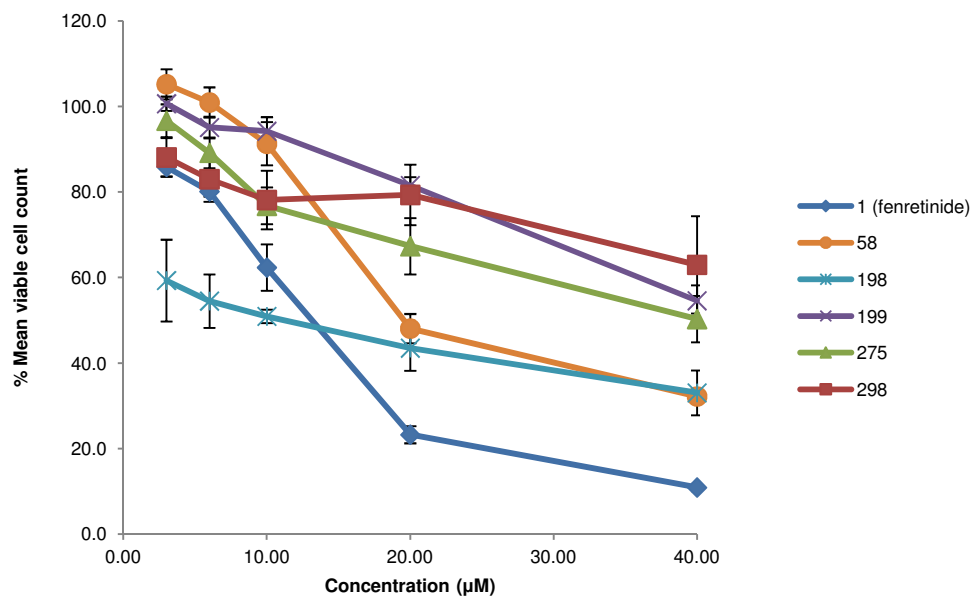


Chart B.5 Cell viability of SHEP-1 neuroblastoma cells treated with 3-10 μM of compounds **1, 58, 198, 199, 275** and **298** for 24 h (n = 9).

Appendix C – mass spectroscopy analysis of binding proteins

Protein Name	Accession*	Number of significant peptides [†]	Score [†]	MW kDa [‡]
Heterogeneous nuclear ribonucleoprotein U (hnRNP U)	HNRPU_HUMAN	3	74	90
Nucleolin	NUCL_HUMAN	6	153	76
Insulin-like growth factor 2 mRNA binding protein1	IF2B1_HUMAN	1	40	63
Tubulin β -chain	TBB5_HUMAN	2	182	50
Ribosomal protein S3	RS3_HUMAN	4	147	27
Acidic leucine rich nuclear phosphoprotein 32 family member A (ANP32A)	AN32A_HUMAN	1	76	29
Ribosomal protein S3A	RS3A_HUMAN	2	56	30
Acidic leucine rich nuclear phosphoprotein 32 family member B (ANP32B)	AN32B_HUMAN	1	53	29
Phosphatase 2A inhibitor (I2PP2A)	SET_HUMAN	2	107	33
Ribosomal protein S5	RS5_HUMAN	1	50	23
Ribosomal protein S9	RS9_HUMAN	1	39	22
Ribosomal protein S14	RS14_HUMAN	2	104	16
Ribosomal protein S25	RS25_HUMAN	2	96	14
Ribosomal protein S16	RS16_HUMAN	3	83	16
Ribosomal protein S10	RS10_HUMAN	2	78	19
Ribosomal protein S19	RS19_HUMAN	2	71	16
Ribosomal protein S18	RS18_HUMAN	2	63	18
Ribosomal protein S20	RS20_HUMAN	1	57	13
Ribosomal protein L22	RL22_HUMAN	1	52	15
Ribosomal protein S13	RS13_HUMAN	1	51	17
Ribosomal protein L12	RL12_HUMAN	1	49	18
Ribosomal protein S23	RS23_HUMAN	1	41	16
Ribosomal protein S17	RS17_HUMAN	1	40	15
Elongation factor 1- α	EF1A1_HUMAN	2	78	50
Ribosomal protein SA	RSSA_HUMAN	3	109	33
Phosphatase 2A inhibitor (I2PP2A)	SET_HUMAN	1	67	33

*The accession is for the UniProt database; [†]the number of significant peptides and score are from Mascot; [‡]the molecular weight (MW) is that of the unmodified mature protein product.

Table C.1 Summary of the 26 proteins isolated (within 10 bands) using affinity chromatography confirmed by mass spectrometry.